Harnessing the metabolic versatility of purple non-sulfur bacteria

Cerruti, M.

DOI
10.4233/uuid:c98876c1-aa83-4c8d-9816-191daf5cc423

Publication date
2022

Document Version
Final published version

Citation (APA)
Cerruti, M. (2022). *Harnessing the metabolic versatility of purple non-sulfur bacteria*. [Dissertation (TU Delft), Delft University of Technology]. https://doi.org/10.4233/uuid:c98876c1-aa83-4c8d-9816-191daf5cc423

Important note
To cite this publication, please use the final published version (if applicable).
Please check the document version above.

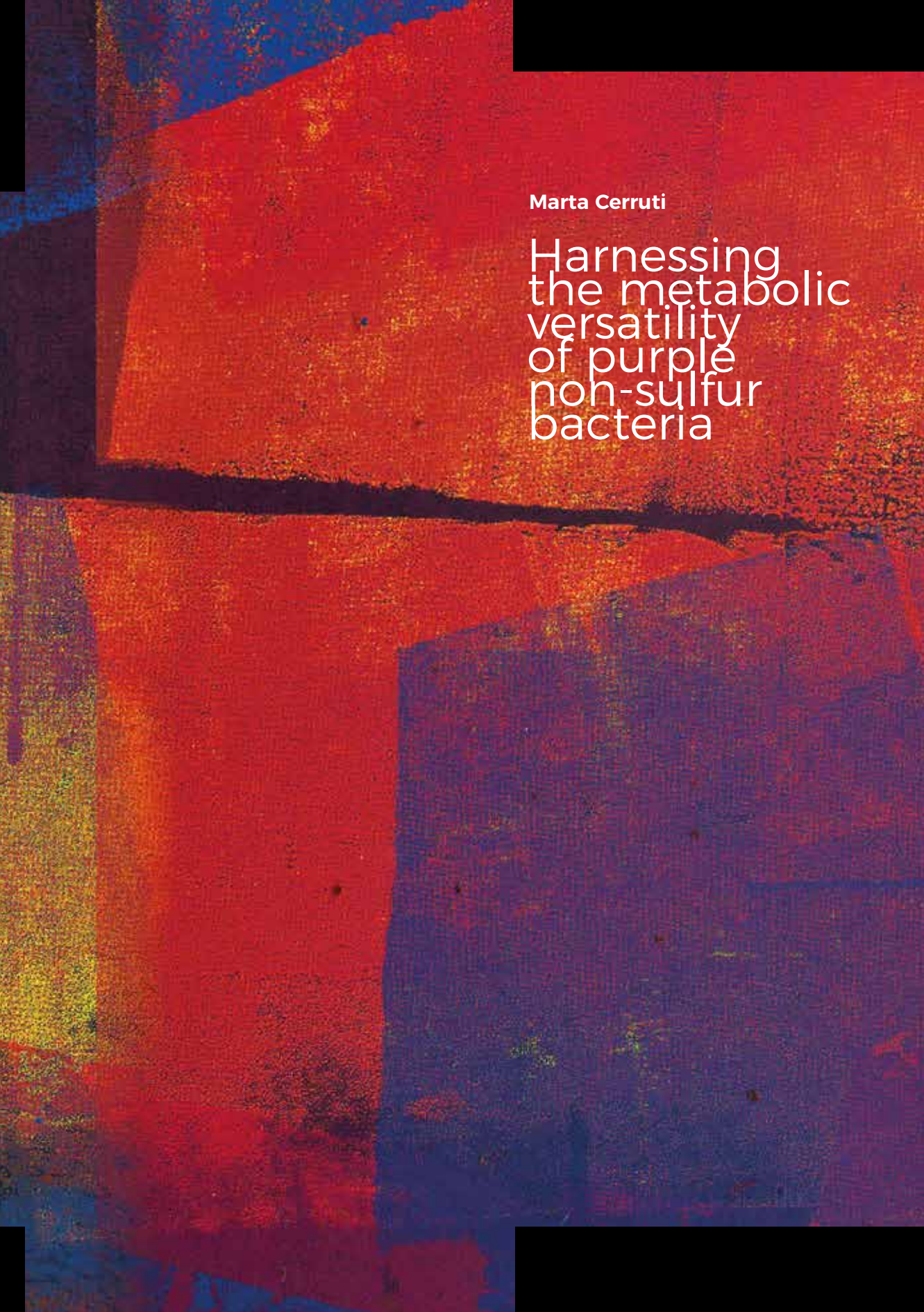

Marta Cerruti

Harnessing the metabolic versatility of purple non-sulfur bacteria

Harnessing the metabolic versatility of purple non-sulfur bacteria

Harnessing the metabolic versatility of purple non-sulfur bacteria

Dissertation
for the purpose of obtaining the degree of doctor
at Delft University of Technology
by the authority of the Rector Magnificus,
Prof.dr.ir. T.H.J.J. van der Hagen,
chair of the Board for Doctorates
To be defended publicly on 17.02.2022, 12:30 o'clock

by
Marta CERRUTI
Master of Science in Plant Biotechnology
Università degli Studi di Torino, Italy

born in Venice, Italy

This dissertation has been approved by the promotors

Promotor: Prof.dr.ir. M.C.M van Loosdrecht
Copromotor: Dr.ir. D.G. Weissbrodt

Composition of the doctoral committee:

Rector Magnificus	Chairperson
Prof. Dr.ir. M.C.M van Loosdrecht	Delft University of Technology, promotor
Dr.ir. D.G. Weissbrodt	Delft University of Technology, co-promotor

Independent members:

Prof.dr. D.G. Allen	University of Toronto, Canada
Prof.dr.ir S.E. Vlaeminck	University of Antwerp, Belgium
Prof.dr. M.J. Barbosa	Wageningen University and Research
Prof.dr.ir F.J.R. Meysman	Delft University of Technology
Dr.ir. R.E.F. Lindeboom	Delft University of Technology
Prof.dr. P.A.S. Daran-Lapujade	Delft University of Technology, reserve member

ISBN 978-94-6384-303-4

Table of content

Propositions

1. A univocal quantitative description of the metabolism of hyper-versatile purple phototrophic bacteria is still a far-away goal.
   (This proposition pertains to this dissertation)

2. A mixed community is always more robust than a pure culture.
   (This proposition pertains to this dissertation)

3. Without a clear understanding of the mechanisms inside the reactor black box, process control is a blind operation.
   (This proposition pertains to this dissertation)

4. Knowledge development, and not self-celebration, should be the main driver in research.

5. Tools to process data are as important as concepts.

6. It's not science *per se* that should be questioned, but methods and interpretations.

7. Coaching spans from micro-managing to advising. Only the latter can be beneficial for both mentor and trainee.

8. Collaborations are the science counterpart of animal mating rituals.

9. Bacterial communities teach us that, with the appropriate environmental conditions, each individual can thrive.

10. 'You might have working hours. Bacteria don't.'

These propositions are regarded as opposable and defendable, and have been approved as such by the promotor Prof.dr.ir. M.C.M. van Loosdrecht and the copromotor Dr.ir. D.G.Weissbrodt

Dai diamanti non nasce niente
dal letame nascono i fior

Fabrizio de Andrè

Summary

A transition to a circular economy is necessary to mitigate the negative effects on the environment of the exploitation and disposal of materials and to achieve society-wide benefits. The current produce-waste-dispose model is slowly changing toward a more sustainable produce-use-recycle-upcycle model. In this context, bio-based processes using microbial mixed cultures are crucial to develop waste-to-resource valorization processes.

Purple phototrophic bacteria (PPB) form a guild of hyper-versatile organisms found in almost all aqueous environments, thriving on infrared light energy, capturing organics by photoorganoheterotrophy, and even recycling CO_2 by photolithoautotrophy. Due to their outstanding metabolic versatility, their organic and nutrient capture ability, and their biomass yields over substrate approaching 1 g CODx g^{-1} CODs, PPB are dedicated organisms to study and use for the development of water resource recovery applications. Despite already 80 years of research on PPB, their physiology still needs to get deciphered, and their environmental biotechnological exploitation is at its infancy.

The aim of this thesis was to study and harness the metabolic versatility of PPB at different levels, from the elucidation of light-driven physiologies in pure cultures to the management of selection phenomena, population dynamics, and distributed metabolic functionalities in mixed cultures. The findings were aggregated to derive to mixed-culture bioprocess application perspectives for capturing organics and nutrients from municipal sewage and agri-food wastewater and producing valuable products, as bioplastics, biohydrogen or photopigments. In this thesis, a comprehensive overview of the potential of PPB for water resource recovery is given. The molecular principles and ecological dynamics governing the PPB metabolism were elucidated with the goal to demonstrate the potential of PPB-based biotechnologies.

In **Chapter 1**, the General Introduction delivers a targeted overview of the purple bacteria, their key metabolic properties, and their implementation potential for water resource recovery. The current European regulations for resource recycling and upgrading are reviewed, with a focus on water and wastewater bodies. A description of the complex metabolism of PPB, along with their potential industrial applications is given. Furthermore, the research questions and research objectives of this thesis are presented.

In **Chapter 2**, *Rhodopseudomonas palustris* was used as model organism to study the physiological responses to light/dark diel energy variations and associated variations in electron sinks. The aim was to elucidate the physiological allocation of electrons derived from organic substrate under light / dark alternation periods. Light is the primary energy source for PPB. In natural environments, it is provided in cycles, alternating with dark periods. This implies a discontinuous energy supply, that can impact the electron distribution in the cells. Redox balance is important for the physiology of PPB, but it has not been addressed in relation to illumination patterns. Under dynamic growth conditions, *Rhodopseudomonas palustris* redirects the electrons in excess toward different routes. Aside biomass, products such as dihydrogen (H_2) and poly-β-hydroxyalkanoates (PHAs) are the main electron sinks. The impact of three different light patterns (24 h continuous infrared illumination, 16h light/8h dark, and 8h light/16h dark) was evaluated in a continuous culture fed with balanced nutrients medium. Under continuous illumination, a stationary state was attained, with a constant growth rate equal to 0.04 h^{-1}. Under dark phases, the biomass was not produced, and acetate, the substrate, accumulated in the reactor. Under light/dark diel cycles, substrate uptake and growth were unbalanced, and *Rhodopseudomonas palustris* first directed the excess of carbon and electrons toward PHA production. Only secondarily, the electron excess was redirected toward H_2 production. A numerical model was used to describe the process dynamics and stoichiometric and kinetic parameters for the conversions. Elucidating the preferential carbon and electron redistribution allows a selective control of the bioproduct formation under dynamic energy conditions.

Due to their high growth yield on substrates, mixed cultures of PPB raise interest for their ability to directly capture organics and nutrients from used aqueous streams by assimilation in their biomass. Prior investigations have been made in diluted cell suspensions with low settling rate, requiring energy-expensive mechanical downstream processing (*e.g.*, membrane filtration or centrifugation) for biomass recovery. The aim of **Chapter 3** was to enrich and produce a concentrated, fast-settling PPB biomass with high nutrient removal capacity in a sequencing batch reactor (SBR). After seeding with a conventional activated sludge inoculum, the microbial community was rapidly enriched with PPB within the first 24 h of operation under infrared light illumination and feeding of an acetate-based synthetic wastewater, and PPB reached up to 90% of the 16S rRNA gene amplicon sequencing dataset. Managing the SBR operational conditions, namely decreasing the hydraulic retention time to 16 h, and increasing the

organic loading rates to 1.3 kg COD d^{-1} m^{-3} stimulated biomass aggregation, settling, and accumulation in the system. Biomass concentration was as high as 3.8 g VSS L^{-1}, 10 times higher than previously reported in literature. Carbon, nitrogen and phosphorous were removed up to 96, 77 and 73 % respectively, reaching the European nutrient discharge limits. The here-examined microbial ecology insights and the aggregation propensity of PPB mixed-cultures can help developing photobiobased processes for water treatment and recovery.

Water resource recovery involves different types of aqueous waste streams. To develop robust PPB-based mixed-culture biorefinery processes, it is necessary to evaluate the impacts of organic streams on the symbiotic / competitive interactions of PPB with other microbial guilds in the engineered community. The aforementioned results highlighted that the supply of infrared light together with acetate as sole carbon source and electron donor preferentially selects for PPB. In carbohydrate-rich wastewaters, fermentative chemoorganoheterotrophic bacteria (FCB) play a key role in sugar dissimilation. The interaction between FCB and PPB has been previously studied in axenic pure cultures or co-cultures. Little is known about their metabolic interactions in open mixed cultures. **Chapter 4** addressed this knowledge gap by assessing the competitive and syntrophic interactions between PPB and FCB. The effects of reactor regimes (batch or continuous) and illumination mode (continuous light or light/dark diel cycles) were studied on glucose conversions and process ecology. Under batch regime, PPB were outcompeted by FCB which displayed a faster maximum growth rate and scavenged the glucose resource, consequently decreasing the pH to 4 in the batch cultures. Under continuous culturing, three main FCB families were enriched to up to 70% (*Enterobacteriaceae, Lachnospiraceae* and *Clostridiaceae*) while the PPB family of *Rhodobacteraceae* accounted for the other 30% of the community. The analysis of the glucose degradation products allowed for the assessment of the syntrophic relationship between FCB and PPB. FCB first fermented glucose into volatile fatty acids and alcohols, and PPB grew on fermentation products. The integration of the effects of reactor regimes and light patterns is crucial in the perspective of designing an efficient anaerobic mixed-culture processes for carbohydrate biorefinery based on associations of PPB and fermentative bacteria.

Light supply is one of the major costs in phototrophic-based technologies for water treatment and bioproduct formation, therefore its effects on microbial physiology need to be carefully estimated. From pure culture studies, it is known that PPB physiology is linked to the light intensity

provided to the cells, and the growth rates increase with the light intensity up to a saturation threshold. Nonetheless, little is known about light intensity effects on PPB mixed cultures. In **Chapter 5** this knowledge gap is addressed, and 9 different light intensities (from 350 to 0 W m^{-2}) were tested on a PPB enrichment under SBR conditions. Under all conditions, PPB were the dominant guild, accounting for more than 70% of the community. Light correlated with a logistic regression to the biomass growth rates, and the half saturation constant was estimated at 10 $\mu mol_{photons}\ s^{-1}\ g_{DW}^{-1}$. It was found that the mass fraction of the photopigments responsible for light harvesting was *ca* 5 times higher at lower light intensities compared to high light intensities, potentially compensating for the lower energy supply. As light is a crucial parameter for phototrophic growth, the assessment of the effects of light intensities on the physiology and microbial ecology of a PPB enrichment paves the way for the development of PPB-based biofactories.

At the end of this book, the main findings of the thesis are summarized in the **Chapter 6**. A perspective on current challenges and future research is given in **Chapter 7**, including applicability of the PPB-based biotechnologies for the treatment different aqueous waste streams, the limitations of light supply and the recovery of high-value products like carotenoids.

Chapter 1

General introduction

Purple bacteria for wastewater resource recovery

1. Wastewater treatment and resource recovery: drivers of the circular economy

1.1 Circular economy principles in the European context

In a linear model of industrial production, the resources are extracted, processed, used, and discarded. To reduce the environmental impact, circular economy principles aim to promote a closed loop for resource exploitation. In this context, the value of the material, resources, products and services is maintained as long as possible, and the waste production is minimized (EEA, 2020).

In 2015, the European Union (EU) adopted the first circular economy action plan, which defined 54 measures to regulate production, consumption, and waste management (European Commission, 2015). The actions aimed to accelerate Europe's transition toward a closed loop of product lifecycle, implementing the recycle and re-use principles. In 2020, the European Union adopted a second action plan, to complete the ongoing tasks and transition toward a regenerative growth model, including waste reduction targets and waste prevention (European Commission, 2020).

The European Green Deal (2019) has the goal to achieve a sustainable EU growth by 2050, setting goals to achieve zero-pollution and protect the natural environment (European Commission, 2019). It describes a set of guidelines to move toward a clean circular economy, reduce the environmental impact and limit ecosystems pollution by improving nutrient management and reducing emissions. The 'Zero Pollution Action Plan for Air, Water and Soil' initiative, included in the European Green Deal, (European Commission, 2021) aims to take measures so that "*Air, water and soil pollution is reduced to levels no longer considered harmful to health and natural ecosystems and that respect the boundaries our planet can cope with, thus creating a toxic-free environment*."

1.2 Water safeguard: a priority for the European Union

Water is one of the most important resources on Earth. It is crucial for the living world, and it sustains public health, development, and economic growth (European Commission, 2010).

Water resources, also in the EU, are increasingly under risk of scarcity and quality deterioration (The European Parliament and the Council, 2020). The safeguard of water resources is one of the European priorities (European Commission, 2018). Along with protective actions of natural

water bodies, a wider re-use of treated wastewater helps reducing this pressure.

In the 2015 action plan for circular economy, the European Commission committed to take actions to promote the use of treated wastewaters, including the development of legislative guidelines for water reuse. Reclaimed treated waters from urban wastewater treatment plants (WWTPs) form a reliable water supply for different purposes, including agricultural applications. The use of treated wastewaters has generally a lower environmental impact compared to other processes such as desalination. It extends the water life cycle and helps preserving water resources (European Commission, 2018).

1.3 Water and wastewater management in the European Union

Clean unpolluted water is crucial for human health and the ecosystem. Agricultural activities and industrial discharges are the principal pollution sources, adding to the domestic sewage emissions. Hazardous substances released in the environment comprehend micropollutants, pesticides, fecal microbes, excess nutrients, and oxygen-consuming substances (organic matter). An excess of nutrients such as carbon, nitrogen, and phosphorus in the water bodies is linked to the eutrophication process. It causes an accelerated growth of algae or plants that disturbs the ecological balance in the waters and the water quality itself. When decaying, algal and plant materials are consumed along with oxygen by microorganisms, therefore depleting the oxygen levels in the water body and hampering aquatic life (Abdel-Raouf et al., 2012; Bartram et al., 2002).
From 1991 onwards, the EU is regulating the wastewater treatment and discharge (European Council, 1991). The water quality objectives set the limits to cumulative pollution. The emission limit values focus on the concentration and loads of pollutants that can be discharged from different sources in the environment. The urban wastewater treatment (UWWT) directive aims to protect waters from adverse waste discharge. To meet the imposed limits, water coming from industrial or municipal sources requires treatment before discharge in the environment (European Council, 1991).

Wastewater treatment incudes different steps to reintroduce clean, unpolluted water in the natural environments. At the forefront of the WWTP, mechanical pre-treatments physically remove large objects from the wastewaters. The primary clarification treatment must reduce by at

least 20% the biochemical oxygen demand (BOD) and 50% the total suspended solids (TSS) (Pescod, 1992).

The UWWT directive stipulates that in agglomerates over 2000 persons equivalents (p.e.), water must be subjected to secondary (or biological) treatment, to substantially reduce soluble organic matter, nitrogen and phosophorus pollution, and further remove suspended solids. In some specific cases, a tertiary, more stringent, treatment can be advised to further remove C, N, P compounds and avoid eutrophication.

Historically, sanitation technologies have been developed to safeguard public health by channeling excreta and removing pathogens. Progressively, with the evolution of environmental protection targets, WWTPs were developed to remove organic matter (C), nitrogen (N) and phosphorus (P). Most efforts made in industrialized regions over the last 50 years have been mainly addressed to design technologies for the removal of these C-N-P macropollutants.

Biological wastewater treatment (BWWT) technologies like activated sludge processes benefit from 100 years of development (Jenkins & Wanner, 2014; Sheik et al., 2014). BWWT takes advantage of the ability of microorganisms to uptake nutrients from the wastewaters and convert them into biomass (Hedaoo et al., 2012).

Control and regulation of biological processes allowed the design of efficient BWWT (Pell & Wörman, 2011). Conventional processes are designed for biological nutrient removal (BNR) in series of tanks where different redox conditions are carefully imposed (*e.g.*, anaerobic-anoxic-aerobic sequences in the A2/O process) to select in the sludge for guilds of microorganisms with metabolisms specialized for the removal of organic matter, nitrogen and phosphorus (Oleszkiewicz & Barnard, 2006). While physicochemical technologies are also used, all nutrients can be removed biologically. Organic matter is typically oxidized by aerobic- or anaerobic-respiring chemoorganoheterotrophic organisms. Nitrogen is removed by association of nitrifiers (that oxidize ammonium into nitrite and nitrate, aerobically) and denitrifiers (that reduce nitrate and nitrite to nitrogen oxides and inert dinitrogen gas using organic matter as electron acceptor) (Fenchel et al., 2012). Phosphorus is taken up in the biomass by polyphosphate-accumulating organisms (PAOs) by alternation of anaerobic and aerobic conditions who simultaneously remove organic matter: in the anaerobic tank they store volatile fatty acids (VFAs) as intracellular poly-β-hydroxyalkanoates (PHAs); in the anoxic or aeration tanks they grow on PHAs using either nitrite/nitrate or dissolved oxygen as terminal electron acceptors, respectively, and store orthophosphates as intracellular polyphosphate; phosphorus therefore ends up in waste sludge (Weissbrodt et al., 2017). These microbial

processes can be assembled in large systems using flocculent activated sludge or intensified with biofilms and granular sludge depending on treatment targets.
The waste sludge derived from these processes was initially simply discharged or incinerated. In more recent times, thanks also to the implementation of circular economy principles, a particular attention has been placed in the valorization of the biomass. Beside the main objectives for public health sanitation and environmental protection, valuable resources can be recovered from used water streams. Anaerobic digestion is already well established since the 1980's for the production of biogas from waste biomass (Lettinga, 1995). Technologies are currently developed to upgrade organics, nutrients and biomass into, *e.g.*, biofuels, biomaterials, fertilizers or food / feed ingredients. WWTPs therefore transition into water resource factories.

2. Phototrophs and their metabolic opportunities for resource protection and recycling

2.1 Phototrophic plasticity: the key for a bio-based circular economy

In parallel to the conventional chemotrophic processes involved in WWTPs, phototrophic systems raise interest in the tertiary WWT (Abdel-Raouf et al., 2012). Phototrophic organisms, like (micro)algae and bacteria, harness the light energy and numerous carbon sources and electron donors / acceptors for biomass growth and bioproducts formation. They use a broad spectrum of inorganic (CO_2) and organic carbon sources, along with numerous nitrogen and phosphorous compounds, promoting a carbon neutral bio-economy (Renuka et al., 2021).
Due to their high nutrient removal abilities, they are used as tertiary WWT. In some cases, their interaction with chemotrophic bacteria have been exploited to improve the WWT performances and reduce the aeration costs (Abdel-Raouf et al., 2012).
Phototrophic systems have been studied for water sanitation since the 1950s (Chu & Phang, 2019). Microalgal systems are primarily used for biofuel production, due to the high lipid content coupled to high growth rates and low production costs (Shin et al., 2018). In WWT, the use of phototrophs has the advantage of removing pathogens and pollutants, nutrient recovery, and energy savings. Microalgal systems have been explored and are currently exploited for simultaneous WWT and biofuel production (Chia et al., 2018). Algal-bacteria consortia have been proposed as efficient processes. Along with established technologies, PPB mixed cultures have gained wide interest for WWT only in the past 5-10 years.

The ability to convert light energy into chemical energy is an evolutionary advantage for phototrophs, that can compete for substrates with heterotrophs under nutrient-limited conditions (Nowicka & Kruk, 2016). In fact, at least part of the energy required for biomass growth is derived from light, and therefore nutrients can be allocated into anabolic reactions to produce biomass and cellular components.
Phototrophs display numerous metabolic types: they are able to use organic and inorganic carbon sources, different electron donors and acceptors, and photons at different wavelengths.
Phototrophs can potentially cover all the possible metabolic modes (Tang et al., 2011). Mixotrophy is common in green microalgae and cyanobacteria, whereas purple bacteria can adapt their metabolism to the environmental conditions. The plasticity of the phototrophic metabolism is a key parameter for the utilization of the resources present in both natural and anthropogenic environments. From an industrial point of view, the phototrophs versatility makes them suitable for a wide range of application. Their applications span from WWT to biofactories for the production of lipids, proteins, biofuels and high-value molecules, such as carotenoids.

2.2 Phototrophy: a metabolism widespread across life domains
Phototrophic metabolisms are widespread along the different life domains, from eukaryotic superior plants and algae to prokaryotic bacteria and archaea. All phototrophs share the ability to capture light photons as energy source to convert it into chemical energy and reducing power through membrane bound complexes (Peretó, 2011). Besides this common trait, phototrophs are diverse organisms with peculiar metabolisms that have found their own niche in diverse environments, both natural and anthropogenic (Stomp et al., 2007).
Three different types of phototrophic metabolism have originated early during the formation of the biosphere. They are known as oxygenic (*i.e.*, cyanobacteria, algae, plants), anoxygenic (e.g., phototrophic green bacteria, purple bacteria and heliobacteria), and rhodopsin-based (e.g., archaea and some bacteria) phototrophs.

The exact evolution of the phototrophic organisms is still uncertain, as microbial phototrophy is dispersed among the three life domains (Eukaryotes, Bacteria and Archaea), with more than 20 diverse and unrelated phyla (Battistuzzi et al., 2004; Heimann & Huerlimann, 2015). The evolutionary evidences displayed by chemical markers, stromatolites fossils and microfossils support different possible origins (Olson et al., 2004). The primordial environment, poor in oxygen, might have selected

for the evolution of anoxygenic phototrophs. Chemosynthetic processes used for carbon fixation were dependent on specific substrates and ran with low efficiencies (Nowicka & Kruk, 2016). Photosynthesis allowed for the retention of energy from the sun, whereas reduced compounds potentially used as electron donors, such as H_2 or H_2S, were available in the oceans (Hamilton et al., 2017).

2.2.1 Rhodopsin-based phototrophic metabolism, a primordial way to harvest energy from light

The simplest phototrophic metabolism is used by archaea and some prokaryotes, utilizing photoactivated rhodopsins. Rhodopsins are a class of membrane-bound, light-driven pumps that harvest light to convert it into ATP, found in prokaryotic organisms and in the visual system of animals (Spudich & Jung, 2005). The prokaryotic rhodopsin pumps ions outside the membranes after light-induced isomerization of the retinal, creating an energy potential used by the ATP-synthase to produce ATP (Bamann et al., 2014; Bryant & Frigaard, 2006). With the advance of new-generation sequencing technologies like metagenomics, rhodopsins have been related to a wide taxonomic distribution. Many of the planktonic prokaryotes present in the photic zones of water surfaces that do not possess a photosynthetic reaction center possess rhodopsin-like systems (Bryant & Frigaard, 2006).

2.2.2 Early anoxygenic phototrophs and the first photosynthesis

The first phototrophs developed around 3.5 billion years ago in an almost oxygen-free environment (Olson, 2006). Reduced compounds as H_2, H_2S, sulfide, were greatly available in the primordial atmosphere. Anoxygenic phototrophs, using light and these reduced compounds as electron donors, synthesized complex organic molecules by reducing CO_2 or simple organic molecules. Anoxygenic phototrophs are unable to use water as an electron donor, and therefore no O_2 is produced as side product (Hanada, 2016).

The wide phylogenetic distribution reflects the environmental adaptability and the hyper-versatile metabolisms (Dubbs & Tabita, 2004) of these organisms, found in saline and non-saline environments across oxygen, sulfide and light gradients (Hallenbeck, 2017b). Members of the anoxygenic phototrophs guild can be found in three prokaryotic groups of green bacteria, purple bacteria and heliobacteria.

2.2.3 Cyanobacteria and the premises of oxygenic photosynthesis

Around 3 to 2.4 billion years ago, cyanobacteria developed the ability to oxidize H_2O, with O_2 formation as side product (Blankenship, 1992). They couple the fixation of CO_2 with the production of O_2, in the in the

widely known process of photosynthesis. It is hypothesized that this event favored the accumulation of oxygen in the atmosphere, contributing to its development (Dismukes et al., 2001). The increasing O_2 concentration both in aquatic and soil environments potentially allowed for the development of increasingly complex organisms, including algae and plants (Dismukes et al., 2001; Sharif et al., 2017). The development of eukaryotes is linked to endosymbiotic events between chemotrophic bacteria and oxygenic phototrophs. The presence of chloroplasts in algae and superior plants proofs this endosymbiosis (Whatley, 1993).

2.3 Niche partitioning along light wavelengths and electron donors

Light, as the main energy source, is a key parameter for niche partitioning and selection mechanisms among phototrophic microorganisms. The light spectrum is distributed unevenly in waters, being influenced by the water depth (Stomp et al., 2007). Underwater, light intensity is diminished due to absorption and scattering phenomena (Gallegos & Moore, 2000), generally described by the Lambert-Beer equations (Abdelrhman, 2017).

$$I_L = I_0 \cdot e^{(-\varepsilon L)} \quad (1)$$

With I_L the irradiance at distance L from the source, I_0 the incident irradiance and ε the extinction coefficient.

Light penetration in water columns is also dependent on the wavelengths (Stomp et al., 2007).

Short wavelengths, like blue light, penetrate deeply in pure water (> 30 m), whereas light with long wavelengths, like infrared light, can only penetrate less than 1 m (Chiang et al., 2011). Microbial photopigments absorb light at different wavelengths, from short wavelengths (*i.e.* carotenoids) to far infrared light (*i.e.* bacteriochlorophylls). This differential light absorption allows niche partitioning across the light spectrum (Cardona et al., 2018).

Photopigments are membrane-bound molecules, that absorb light and start an electrons cascade that ultimately reaches the production of ATP. Primary photopigments absorbing light are (bacterio-) chlorophylls, in the reaction centers of the photosynthetic units. Peripheral to those, carotenoids are accessory photopigments, that have the double function of absorbing light at lower wavelengths and prevent photooxidation (Madigan et al., 2015). Photopigments absorption peaks range between 300 and 1100 nm (Hou, 2014), allowing for a spatial distribution of colorful niches of phototrophs in the aquatic environments (Stomp et al., 2007). In aqueous environments irradiated by infrared light, purple bacteria find their niche.

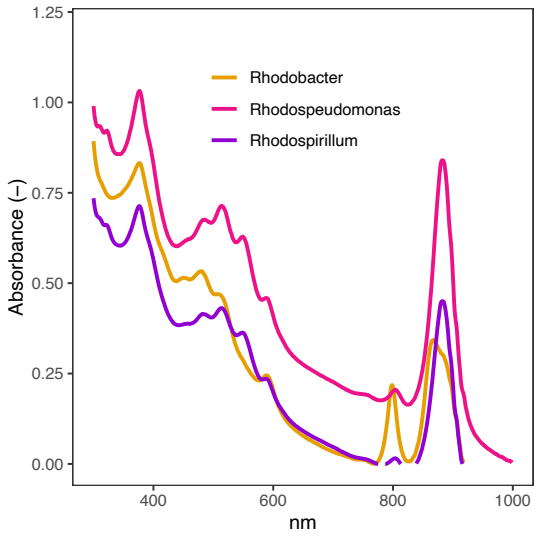

Figure 1 **Whole-cell wavelength spectrum of three PPB species.**
The absorption of light at different wavelengths allows niche partitioning across the light spectrum. Data from wavelength scan of Rhodobacter, Rhodopseudomonas and Rhodospirillum pure cultures isolated from an in-house enrichment.

3. Purple phototrophic bacteria: whole communities in single cells

Purple phototrophic bacteria (PPB) form a guild of hyper-versatile organisms that thrive in ever-changing environments. The first observations of PPB date back to the 1920's, when van Niel, in Delft, discovered them. He was interested by these colorful bacteria (yellow, brown, red, and purple), and their interaction with light. Although representative lineages such as *Rhodobacter*, *Rhodopseudomonas* and *Rhodospirillum* are regrouped under the term PPB, they are not all / always purple *per se*. For instance, *Rhodobacter* relatives can reveal both purple and yellow colors depending on species, phototrophic niche and redox state of the environment in which they grow (Figure 2A). The diverse coloration is given by the photopigments present in the intracellular membranes, in particular carotenoids. The expression of different carotenoids induces a change in bacterial color appearance, which is as well linked to concentration and oxidation state of the carotenoids themselves (Aklujkar & Beatty, 2005).

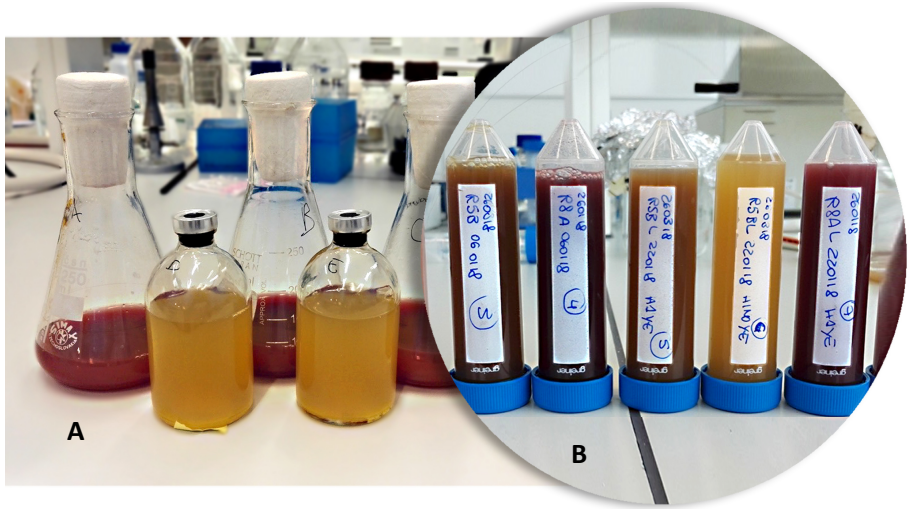

Figure 2 **PPB pure cultures.**

A: Pure cultures of Rhodobacter blasticus grown aerobically (in pink) and anaerobically (in yellow). The color is linked to the oxidation state of the carotenoids present in the membranes;

B: PPB show different coloration depending on the species. This is due to the presence of different types of photopigments, and, in particular, to a different expression of the carotenoid series.

PPB are a major phototrophic guild, that inhabit soils and prevalently aquatic environments. Stimulated by light, they participate in the carbon cycle by both fixing CO_2 and oxidizing organic compounds. Anoxygenic phototrophs, PPB are among the first organisms to have developed on Earth, thanks to their ability to use inorganic compounds as electron donors (Yurkov & Beatty, 1998). Their photosystem is simpler compared to the oxygenic phototrophs, but PPB evolved complex metabolic strategies to find their niche. In nature, they can be found in aquatic environments exposed to light. They are present in sewage, lagoons, waste lagoons and lake or marine waters. Furthermore, they can be found in extremophilic environments, including hypersaline areas, at very low or very high temperature and pH conditions (Madigan, 2003).

More than 50 genera are now classified as PPB, but a univocal definition of the term PPB is not present (Hunter et al., 2009). Traditionally, PPB have been divided into purple sulfur bacteria (PSB) and purple non-sulfur bacteria (PNSB), based on their tolerance to sulfur compounds (van Niel 1944). This classification has later been replaced by molecular studies: 16S rRNA gene sequencing showed that PSB belong to the Gamma proteobacteria phylum, whereas PNSB to the Alpha- and Betaproteobacteria (Imhoff et al., 2005). Metabolically, PSB are primarily photoautotrophs, whereas PNSB are the most abundant photoorganoheterotrophic organisms in nature (Hunter et al., 2009).

Due also to their wide phylogenetic distribution, PPB present metabolic differences, and are probably the most versatile class of organisms know so far. The metabolic versatility has been reported not only between genera, but also in single species. PPB adapt their metabolism based on the environmental conditions, being able to growth phototrophically but also chemotrophically by aerobic and anaerobic respirations and fermentation in the dark, using numerous carbon sources, electron donors and acceptors present in their environment (Schultz & Weaver, 1982; Siefert & Pfennig, 1979). PPB exhibit a variety of ecophysiologies and phenotypes as across cell morphology, motility, salt tolerance, internal membrane structure, lipids content, and photopigments type and disposition. The only common trait PPB share is the cyclic electron transfer process in the photosynthetic membranes.

3.1 Phototrophic machinery and cyclic photophosphorylation in PPB

From his studies on PPB, van Niel discovered that photosynthesis is a light-dependent reaction reducing CO_2 to cellular material (Barker & Hungate, 1990). He generalized the reaction as

$$2H_2A + nCO_2 + light \rightarrow 2A + (CH_2O)_n + H_2O \qquad (2)$$

With A as electron donor.

To capture the light, phototrophs use light-harvesting complexes, placed in a complex of intracellular membranes (Ruivo et al., 2014). Contrary to oxygenic phototrophs, which utilize a linear electron flow to produce ATP and reducing power, PPB convert light energy to chemical energy through a cyclic electron flow (McEwan, 1994).

Light is captured by antenna pigments in the reaction center, embedded in the photosynthetic membranes. It is used to excite the bacteriochlorophylls (Bchl), that becomes a strong electron donor. The excited electrons are transferred through an electron transport chain from low electronegative carriers to high electronegative carriers. They pass from the bacteriochlorophyll to the bacteriopheophytin, to the quinone pool, to the ferredoxin, to the cytochrome c, eventually returning to the reaction center. The electron flow generates a proton motive force. The reduced quinones are oxidized by protons derived from the tricarboxylic acid (TCA) cycle. The protons are transferred to the periplasm. Here, they are used to activate the ATP-synthase and produce ATP. The reducing power (NADH) required for growth is often achieved through a reverse electron transport. In this process, the electrons from the quinone pool are forced against the electrochemical gradient to reduce NAD^+ to NADH through the NADH-dehydrogenase (Madigan et al., 2015).

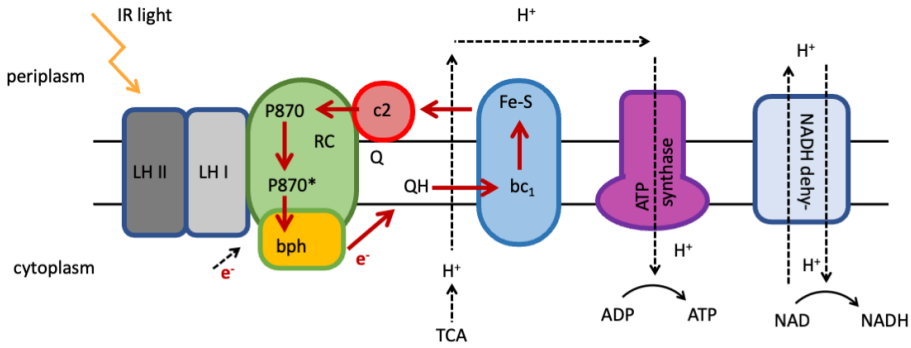

Figure 3 **Schematic representation of the photosynthetic complexes in the membranes and cyclic electron flow in PPB. Photons captured by the bacteriochlorophylls (Bchl) in the Light Harvesting complexes (LH I and II) and used to excite electrons in the Reaction Center (RC). From here, electrons are transferred through the membrane-bound complexes, creating a proton motive force, that activates the ATP synthase.**

3.2 PPB: champions in metabolic versatility

As the name says, PPB are phototrophs, harvesting light from the sun spectrum and converting it to chemical energy. Under anaerobic conditions, and with light as energy source, they can use both organic and inorganic carbon sources. PPB can use several organic compounds as carbon sources, electron donors and electron acceptors, depending on the oxidation state of the electron donor. They can grow both aerobically as chemotrophs or anaerobically as photoheterotrophs. Being able to adapt to several environmental conditions, they are considered champions in metabolic versatility (Nelson & Fraser, 2004). A schematic overview of the possible metabolic modes of PPB is presented in Chapter 3 (Table 1).

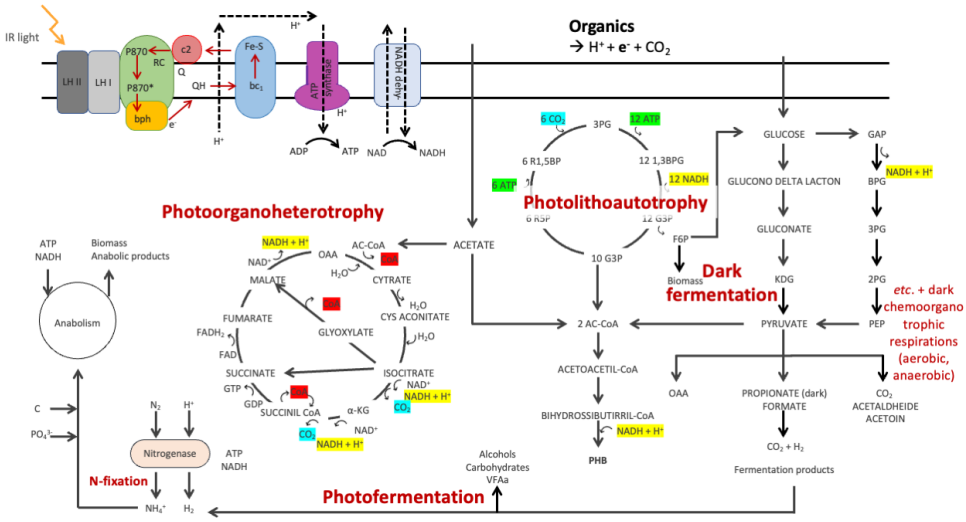

Figure 4 **Schematic of the possible metabolic modes of PPB. Depending on the environmental conditions, PPB can show a photoorganoheterotrophic metabolism, photolithoautotrophic, chemoorganotrophic metabolism, dark and light fermentation.**

3.2.1 Photolithoautotrophic growth

Photolithoautotrophic growth was one of the first to develop, with the use of reduced compounds, such as H_2 or H_2S as electron donors, and biomass as electron acceptor (Nowicka & Kruk, 2016). Opposite to what happen in oxygenic phototrophs, oxygen is not used by PPB as electron acceptor during phototrophic growth. Indeed, phototrophic growth under aerobic conditions is limited, as oxygen inhibits the formation of the photosynthetic complexes (Donohue et al., 1988).

Photosynthetic organisms can concentrate and fix inorganic carbon supplied by dissolved carbon dioxide (CO_2) and bicarbonate (HCO_3^-) in the well-known process called photosynthesis. All phototrophic organisms can grow with photolithoautotrophic metabolism, utilizing different routes for CO_2 fixation. Photolithoautotrophic growth is divided into two steps. In the first light is harvested as previously described to produce ATP and reducing power.

During the second step, in the so-called dark reactions, the inorganic carbon is assimilated and converted / reduced into carbohydrates and complex organic molecules, that can be used to build the cell materials (Madigan et al., 2015).

Five known pathways enable CO_2 fixation, namely the Calvin-Benson cycle (used by eukaryotic and prokaryotic microalgae, heliobacteria, and PPB) (Blankenship et al., 1995), the reductive or reverse tricarboxylic acid (RTCA) cycle (used by green sulfur bacteria) (Tang & Blankenship, 2010), the 3-hydroxypropionate bi-cycle (used by green non-sulfur bacteria) (Shih et al.,

2017), the reductive acetyl-CoA pathway (Tang et al., 2011), and the 3-hydroxypropionate/4-hydroxybutyrate cycle (Thauer, 2007).
The most widely distributed pathway for CO_2 fixation is the Calvin-Benson cycle, used also by PPB. The Calvin-Benson cycle utilizes reducing power and ATP produced in the light reactions to fix CO_2 to carbohydrates, through four major phases: *i*) the carboxylation phase: CO_2 is condensed to a molecule of ribulose bisphosphate (5-C molecule) by the enzyme ribulose bisphosphate carboxylase to form two molecules of 3-phosphogliceric acid (PGA); *ii*) the reduction phase: the PGA is phosphorylated and reduced to glyceraldehyde-3-phosphate; *iii*) in the regeneration phase, the 5-C sugar is reformed, by fixating another molecule of CO_2 to 3 to 7 sugar phosphates; and *iv*) the production phase, where carbohydrates, fatty acids, amino acids and organic acids are synthetized (Richmond, 2003).
In PPB, photolithoautotrophic growth is secondary to photoorganoheterotrophic growth, and can only occur in presence to electron acceptor different from O_2. However, in presence of an excess of electrons, CO_2 fixation can be used as electron sink during photoheterotrophic growth (McKinlay & Harwood, 2010).

3.2.2 Photoorganoheterotrophic growth

The photoorganoheterotrophic metabolism is the preferred growth mode of PPB, allowing them to thrive on carbon and electrons derived from organic compounds. Besides being less widely described than photolithoautotrophy, photoorganoheterotrophy is relatively widespread in natural environments.
Contrary to chemoorganoheterotrophic organisms that need to catabolize a substantial part of the organics to produce ATP, photoorganoheterotrophs derive their energy directly from light. They can therefore grow with high biomass yields over organic substrates, sometimes close to 1 g COD_X g^{-1} COD_S (Alloul et al., 2019). In the photoorganoheterotrophic growth, PPB use organics as electron donors, and, in balanced conditions, biomass as electron acceptor. The electron and carbon sources span from volatile fatty acids (VFAs), to alcohols, to carbohydrates. The terminal electron acceptor is, when an electron imbalance is present, redirected toward other routes (see Chapter 2). In the light, PPB are also able to activate a photofermentative metabolism. In this case, sugar degradation is not coupled with growth, but it is only used as dissipative mechanism with electron redirection toward H_2 formation (Basak et al., 2014).
On top of the photolithoautotrophic growth using CO_2, PPB can grow on other C1 compounds, like methanol, formate and CO. In this case, C1 compounds are oxidized to CO_2, which is then fixed via the Calvin-Benson Cycle (Quayle & Pfennig, 1975; Sahm et al., 1976). The RubisCO enzyme is here used both for carbon fixation and for redox balance, as it allows to use CO_2 as electron acceptor.
Acetate is a volatile fatty acid, often used as a model compound since it can potentially be assimilated by all PPB. Acetate is metabolized through different

pathways, depending on the species. For example, acetate can be used by PPB both as electron donor and electron acceptor (Butow & Dan, 1991) as well as carbon source. As carbon source, it is assimilated by species related to *Rhodopseudomonas* through the glyoxylate cycles (Petushkova et al., 2021), whereas *Rhodobacter* species uses the ethyl-malonyl pathway (Laguna et al., 2011). Alternatively, in species lacking the glyoxylate cycle, the citramalate pathway has been proposed as an alternative pathway (Berg & Ivanovsky, 2009). Other organics, like VFAs or ethanol, are first metabolized to acetyl-CoA and then incorporated into the cellular metabolism through the TCA cycle (Hunter et al., 2009). In PPB metabolism, the TCA cycle is active independently from the carbon source present in the medium, and serves both to catabolic and anabolic reactions. It catalyzes the full oxidation of acetyl-CoA to CO_2, providing reducing equivalents for ATP formation during dark respiratory processes, and at the same time it supplies the biosynthetic pathways with metabolites and reducing power (Petushkova et al., 2019).

3.2.3 Chemotrophic growth

PPB are also capable to grow as chemotrophs when light is absent. The presence of oxygen inhibits at gene-regulation level the formation of the photosynthetic complexes. Under these conditions, PPB can still grow as aerobic chemoorganoheterotrophs, even though with lower growth rates compared to phototrophic metabolism (Madigan et al., 1980). Under dark conditions PPB can ferment sugars (both carbon and electron donors) for biomass formation and biohydrogen production. Growth in the dark is limited, and strictly dependent to the presence of an external source of energy and reducing power (Madigan & Gest, 1979; Petushkova et al., 2021)

4. Environmental biotechnologies fostered by purple phototrophic bacteria

Microorganisms have been used as living factories for centuries, as exemplified by the production of beer and bread. In more recent times, microbial cell factories have been developed growing interest, as workhorses for industrial bioprocesses. The extreme metabolic variability of phototrophs is reflected on the spectrum of compounds that they produce as secondary metabolites under different environmental constrains. Used as electron excess sinks, nutrient storage compounds, or for self-defense, bioproducts from phototrophs attract interests for technology. The main fields of applications include biogas (methane and hydrogen), feedstock additives (with single cell protein production), biopolymers formation (as bioplastics like PHAs) and pharmaceutically interesting compounds (antioxidants and quinones).

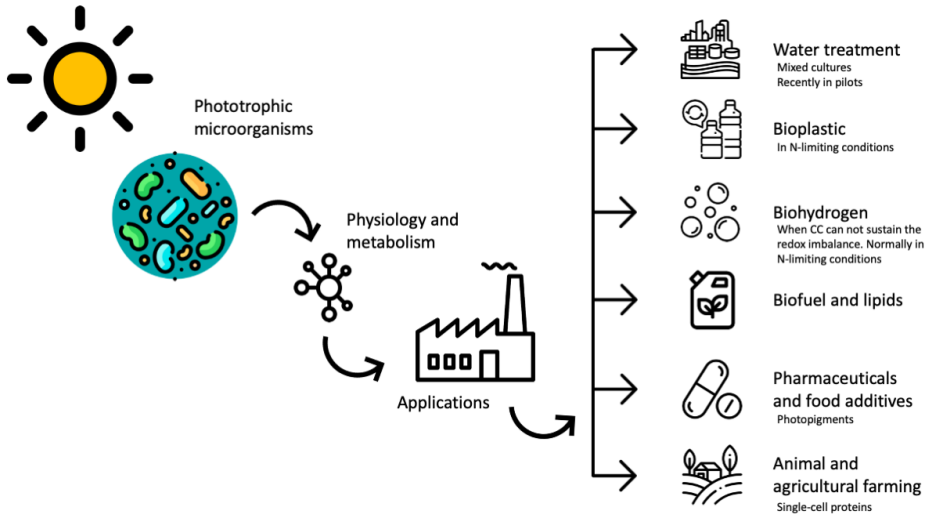

Figure 5: **Understanding the complex metabolism of PPB, from molecular to process scale, allows us to harness its potential, from wastewater treatment to high-value produce production.**

4.1 Biohydrogen

Hydrogen (H_2) is a renewable and clean source of energy. Four major pathways can be harnessed for biological H_2 production: *i*) direct biophotolysis, the simplest and most effective process to produce hydrogen, directly transferring electrons from water to hydrogen-evolving enzymes. It is accompanied by the simultaneous evolution of O_2 and H_2 (Rastegari et al., 2019). *ii*) Indirect biophotolysis, linked to aerobic photosynthesis reactions (Hallenbeck, 2017a). *iii*) Dark fermentation, where H_2 is a side product of carbohydrates fermentation (Abo-Hashesh & Hallenbeck, 2012). *iv*) Photofermentation, performed by PPB under anaerobic light conditions. Short-chain organic acids are used as electron donors, and H_2 is used as electron sink (Androga et al., 2014). Opposite to the dark fermentation, this process does not lead to biomass growth. Two enzymes are responsible for H_2 production in PPB, namely the nitrogenase and hydrogenase enzymes. Nitrogenase is a nitrogen fixing enzyme active under anaerobic conditions (Basak et al., 2014). In presence of nitrogen gas, H_2 production is only secondary to nitrogen fixation, according to the Equation 3

$$N_2 + 8H^+ + 8e^- + 16ATP \rightarrow 2NH_3 + H_2 + 16(ADP + Pi) \quad (3)$$

In absence of N_2, the nitrogenase catalizes the production of hydrogen from protons through an irreversible reaction, as in Equation 4

$$2H^+ + 2e^- + 4ATP \rightarrow H_2 + 4(ADP + Pi) \quad (4)$$

The hydrogenase, instead, catalizes a simple and reversible redox reaction, as in Equation 5

$$2H^+ + 2e^- \leftrightarrow H_2 \quad (5)$$

4.2 Poly-β-hydroxyalkanoates (PHA)

Polyhydroxyalkanoates (PHA) is a group of polyesters produced by microorganisms, stored intracellularly in granules as carbon and reducing equivalents sinks (Madison & Huisman, 1999). They have material properties similar to polypropylene, and find application as petrochemical plastic substitutes (Bugnicourt et al., 2014). PHA have the advantage of being recyclable and biodegradable. Biologically, PHA are produced as reducing power and carbon storage in presence of carbon excess. In PHA producing organisms, PHA can be stored up to 90% of the weight of the cells. In a similar way, PPB can store up to 90% of the dry weight as PHA in pure cultures (Kranz et al., 1997; Sangkharak & Prasertsan, 2007), but the accumulation is dependent on the strain and on the carbon source used. In mixed cultures, it was possible to achieve a maximum of 20% of the dry weight (Luongo et al., 2017).

4.3 Single-cell proteins

Microbial (single-cell) proteins (SCP) are an alternative to increase nutrient content in the animal feed. PPB are an interesting sources of SCP, due to their high protein content, vitamins and photopigments. The use of PPB in shrimp feed has increased the survival and healthiness of the animals. Further applications explore the use of PPB for human consumption in space missions (Chumpol et al., 2018).

4.4 Photopigments

Photopigments are crucial in PPB for light harvest and following energy production. The bacteriochlorophylls are the main light harvesting pigments. They have been proposed as photosensitizers for photodynamic therapy of cancer (Liu et al., 2012; Pantiushenko et al., 2015). Carotenoids, have broad and known utilization ad dyes in food, and as food and feed additives, thanks to their antioxidant properties (Barreiro & Barredo, 2018; Cheng et al., 2020). PPB tune their photopigment content based on light conditions (Liu et al., 2019). PPB utilization as photopigment producers has been explored as animal feed, mainly in combination to SCP production (Chumpol et al., 2018).

5. Closing the loop with purple bacteria: from nutrient removal to production of high-value products from wastewater

Wastewaters can present fluctuating characteristics that influence the substrate consumption abilities of the biological sludges used, including temperature and nutrient (C, N, P) load. Despite the plasticity of the microbial communities, the varying conditions can severely affect their composition and activity, factually reducing the removal of pollutants. PPB, instead, thrive in ever-changing environment. Their ability grow on numerous substrates and electron sources rises interest for high-strength wastewater treatment. Coupled with the possibility to produce industrially interesting compounds, PPB are a promising guild for bio factories.

Wastewater treatment with green phototrophs has been proposed as an efficient process for nutrient capture and biovalorization, in example for lipids and biofuels production. Compared to green phototroph systems, PPB present some advantages: *i*) an hyperversatile metabolism, adaptable to several environmental conditions. When in presence of infrared light, PPB become the dominant community. Laboratory scale experiments showed a stable enrichment above 70% (Hülsen et al., 2016). *ii*) High quantum and carbon yields. The efficiency of photosynthetic conversion of PPB is close to 1 (Sener et al., 2016): this implies that almost all the energy harvested from the photosynthetic complexes can theoretically be converted into chemical energy. Compared to microalgae, in example, PPB show photosynthetic conversion efficiencies 2 times higher (Perrine et al., 2012). (Perrine et al., 2012) *iii*) Similarly, PPB have high biomass yields over their carbon sources, with a theoretical maximum close to 1 $gCOD_x\ gCOD_s^{-1}$ (Alloul et al., 2019). The production of ATP through light-mediated reactions allows the cells to utilize the carbon sources entirely for biomass formation, without having to dissipate a part for energy formation. A higher biomass yield is advisable in biofactories, where the product recovery is dependent on the cell concentration.

Knowledge gaps

1. Electron reallocation in pure cultures

Loads of information is available on the fundamental molecular mechanisms governing the PPB metabolism. Their fascinating complexity has been studied in detail in pure culture systems, and metabolic models have been constructed to clarify and simplify their complexity. Pure culture studies provide a simplification of the genomic and functional potential of the systems. They have the advantage to allow a detailed examination of the metabolism and the responses of the cultures to environmental factors, in example. Despite the numerous studies on

the effects of light cycles on PPB, the internal electron allocation under intermittent energy supply remains puzzling, and the mechanisms that govern the preferential electron flow have not been explained.

2. Light: a central parameter often overlooked

Light, being the energy source for PPB, is of foremost importance. Physiological responses of PPB have primarily been studied under continuous illumination conditions. However, in nature, daily light / dark cycles occur, implying a discontinuous supply of energy. Its effects on the PPB metabolism have been overlooked, and only few studies provide observations on the responses to light / dark cycles. The importance of light to PPB cultures is proven by pure culture studies, as in the case of *Rhodopseudomonas*, where it was possible to correlate growth rates and light intensity (Kuo et al., 2012). However, the effect on mixed cultures is yet to be elucidated. The control of light supply, and its relationship with PPB kinetics, is crucial to design PPB-based WWT processes.

3. Microbial ecology of the PPB black box

The applicability of mixed cultures PPB to WWT has been demonstrated, but often the microbial ecology has been neglected. Mixed-culture systems rely on the metabolic performance of microbial communities, that compete and interact for resources in an ecosystem. However, in environmental biotechnology, microbial communities are often considered as a black box, where kinetics and stoichiometry are used as predominant parameters to define the performances of a process. Understanding the community dynamics, with deeper insights into the microbiological black box, is crucial for a systematic understanding of the observed phenomena. Recent studies focus on the overall performances of PPB-based WWT, but the microbial ecology is overlooked. The principles for an efficient selection and aggregation have not been described. Different carbon and electron inflow streams affect the selection principles and therefore the applicability of PPB to numerous waste streams. Harnessing microbiomes relies on managing the metabolisms of microorganisms selected to perform the conversions of interest. The effects of environmental factors, as nutrient type and load, irradiation intensity and patterns, have been studied in pure cultures. Nonetheless, a microbial community responds differently compared to a pure culture to the same environmental factors. Inter-species interactions, such as cooperation and competitions phenomena, are crucial to understand the microbial complexity and applicability in biobased processes.

Research question

The core research question of this thesis will focus on the fundamental investigation of the metabolism of PNSB in the context of water resource recovery, and is formulated as such:

How can we harness the microbial ecology and metabolic versatility of purple non-sulfur phototrophic bacteria towards water resource recovery and biorefinery?

The thesis will develop around four main research questions:

1. How do PPB respond to redox imbalance and allocate carbon and electrons during light / dark diel cycles?
2. How can we enrich and aggregate PPB in mixed cultures for an intensified capture/removal of nutrients?
3. How are PPB differently selected on fermented (*i.e.*, VFAs) *vs.* fermentable substrates (*i.e.*, carbohydrates/sugars)?
4. What are the effects of decreasing light intensities on the physiology/growth of PPB, community composition, and conversions?

Objectives

With this thesis I aimed to shed light on the microbial ecology principles governing PPB enrichments for wastewater recovery.
In **Chapter 2**, we evaluated the effects of diel light/ dark cycles in the model organisms *Rhodopseudomonas palustris*. We aimed to identify the metabolic drivers for the selective production of PHA or H_2, two major redox sinks for PPB with commercial applications. In **Chapter 3,** a method for PPB enrichment and aggregation was proposed. We coupled a high PPB enrichment to high nutrient removal, so that to comply to the current European law. Depending on the wastewater, the type of carbon and electron source variates. In example, agricultural / food wastes are prevalently composed of sugars. In **Chapter 4** we evaluated the interactions of PPB with fermentative bacteria in glucose-based environment, in regard also to the reactor regimes. PPB convert light energy into chemical energy, factually being able to assimilate carbon sources for biomass growth. In **Chapter 5**, we evaluated the metabolic requirements of a PPB community subjected to a decreased light intensity, to establish a minimum irradiation limit for PPB biomass growth and nutrient removal. The general conclusions of this thesis are given in **Chapter 6**. **Chapter 7** presents an outlook on future research, with a particular focus on the application of PPB mixed communities for wastewater resource recovery.

References

Abdel-Raouf, N., Al-Homaidan, A. A., & Ibraheem, I. B. M. (2012). Microalgae and wastewater treatment. *Saudi Journal of Biological Sciences*, *19*(3), 257–275. https://doi.org/10.1016/j.sjbs.2012.04.005

Abdelrhman, M. A. (2017). Quantifying Contributions to Light Attenuation in Estuaries and Coastal Embayments: Application to Narragansett Bay, Rhode Island. *Estuaries and Coasts*, *40*(4), 994–1012. https://doi.org/10.1007/s12237-016-0206-x

Abo-Hashesh, M., & Hallenbeck, P. C. (2012). Microaerobic dark fermentative hydrogen production by the photosynthetic bacterium, Rhodobacter capsulatus JP91. *International Journal of Low-Carbon Technologies*, *7*(2), 97–103. https://doi.org/10.1093/ijlct/cts011

Aklujkar, M., & Beatty, J. T. (2005). The PufX protein of Rhodobacter capsulatus affects the properties of bacteriochlorophyll a and carotenoid pigments of light-harvesting complex 1. *Archives of Biochemistry and Biophysics*, *443*(1–2), 21–32. https://doi.org/10.1016/j.abb.2005.08.018

Alloul, A., Wuyts, S., Lebeer, S., & Vlaeminck, S. E. (2019). Volatile fatty acids impacting phototrophic growth kinetics of purple bacteria: Paving the way for protein production on fermented wastewater. *Water Research*, *152*, 138–147. https://doi.org/10.1016/j.watres.2018.12.025

Androga, D. D., Sevinç, P., Koku, H., Yücel, M., Gündüz, U., & Eroglu, I. (2014). Optimization of temperature and light intensity for improved photofermentative hydrogen production using Rhodobacter capsulatus DSM 1710. *International Journal of Hydrogen Energy*, *39*(6), 2472–2480. https://doi.org/10.1016/j.ijhydene.2013.11.114

Bamann, C., Bamberg, E., Wachtveitl, J., & Glaubitz, C. (2014). Proteorhodopsin ☆ , ☆☆. *BBA - Bioenergetics*, *1837*, 614–625. https://doi.org/10.1016/j.bbabio.2013.09.010

Barker, H. A., & Hungate, R. E. (1990). *Cornelis Bernardus Van Niel*.

Barreiro, C., & Barredo, J.-L. (2018). Carotenoids Production: A Healthy and Profitable Industry. In *Methods in Molecular Biology* (Vol. 1852, pp. 45–55). https://doi.org/10.1007/978-1-4939-8742-9_2

Bartram, J., Thyssen, N., Gowers, A., Pond, K., Lack, T., Danzon, M., & Jiménez-Beltrán, D. (2002). Water and health in Europe: A joint report from the European Environment Agency and the WHO Regional Office for Europe. *World Health Organization Regional Publications - European Series*, *7*(93).

Basak, N., Jana, A. K., Das, D., & Saikia, D. (2014). Photofermentative molecular biohydrogen production by purple-non-sulfur (PNS) bacteria in various modes: The present progress and future perspective. *International Journal of Hydrogen Energy*, *39*(13), 6853–6871. https://doi.org/10.1016/j.ijhydene.2014.02.093

Battistuzzi, F. U., Feijao, A., & Hedges, S. B. (2004). A genomic timescale of prokaryote evolution: insights into the origin of methanogenesis, phototrophy, and the colonization of land. *BMC Evolutionary Biology*, *4*(1), 44. https://doi.org/10.1186/1471-2148-4-44

Berg, I. A., & Ivanovsky, R. N. (2009). Enzymes of the citramalate cycle in Rhodospirillum rubrum. *Microbiology*, *78*(1), 16–24. https://doi.org/10.1134/S0026261709010032

Blankenship, R. E. (1992). Origin and early evolution of photosynthesis. In *Photosynthesis Research* (Vol. 33). https://link.springer.com/content/pdf/10.1007%2FBF00039173.pdf

Blankenship, R., Madigan, M., & Bauer, C. (1995). *Anoxygenic Photosynthetic Bacteria* (R. E. Blankenship, M. T. Madigan, & C. E. Bauer (Eds.); Vol. 2). Springer Netherlands. https://doi.org/10.1007/0-306-47954-0

Bryant, D. A., & Frigaard, N.-U. (2006). Prokaryotic photosynthesis and phototrophy illuminated. *Review TRENDS in Microbiology*, *14*(11), 488–496. https://doi.org/10.1016/j.tim.2006.09.001

Bugnicourt, E., Cinelli, P., Lazzeri, A., & Alvarez, V. (2014). Polyhydroxyalkanoate (PHA): Review of synthesis, characteristics, processing and potential applications in packaging. *Express Polymer Letters*. https://doi.org/10.3144/expresspolymlett.2014.82

Butow, B., & Dan, T. B. Ben. (1991). Effects of growth conditions of acetate utilization by Rhodopseudomonas palustris isolated from a freshwater lake. *Microbial Ecology*, *22*(1), 317–328. https://doi.org/10.1007/BF02540233

Cardona, T., Shao, S., & Nixon, P. J. (2018). Enhancing photosynthesis in plants: the light reactions. *Essays In Biochemistry*, *62*(1), 85–94. https://doi.org/10.1042/ebc20170015

Cheng, S.-H., Khoo, H. E., Kong, K. W., Prasad, K. N., & Galanakis, C. M. (2020). Extraction of carotenoids and applications. In *Carotenoids:*

Properties, Processing and Applications. Elsevier Inc. https://doi.org/10.1016/b978-0-12-817067-0.00008-7

Chia, S. R., Chew, K. W., Loke Show, P., Yap, Y. J., Ong, H. C., Ling, C., & Chang, J.-S. (2018). *Analysis of Economic and Environmental Aspects of Microalgae Biorefinery for Biofuels Production: A Review*. https://doi.org/10.1002/biot.201700618

Chiang, J. Y., Chen, Y.-C., & Chen, Y.-F. (2011). Underwater Image Enhancement: Using Wavelength Compensation and Image Dehazing (WCID). In J. Blanc-Talon, R. Kleihorst, W. Philips, D. Popescu, & P. Scheunders (Eds.), *Advanced Concepts for Intelligent Vision Systems* (pp. 372–383). Springer Berlin Heidelberg.

Chu, W. L., & Phang, S. M. (2019). Microalgae of Biofuel and for Development Biotechnology Wastewater Treatment. In *Microalgae Biotechnology for Development of Biofuel and Wastewater Treatment*.

Chumpol, S., Kantachote, D., Nitoda, T., & Kanzaki, H. (2018). Administration of purple nonsulfur bacteria as single cell protein by mixing with shrimp feed to enhance growth, immune response and survival in white shrimp (Litopenaeus vannamei) cultivation. *Aquaculture*, *489*(January), 85–95. https://doi.org/10.1016/j.aquaculture.2018.02.009

Dismukes, G. C., Klimov, V. V, Baranov, S. V, Kozlov, Y. N., Dasgupta, J., & Tyryshkin, A. (2001). The origin of atmospheric oxygen on Earth: The innovation of oxygenic photosynthesis. In *PNAS* (Vol. 98, Issue 5). www.pnas.orgcgidoi10.1073pnas.061514798

Donohue, T. J., Kiley, P. J., & Kaplan, S. (1988). The puf operon region of Rhodobacter sphaeroides. In *Photosynthesis Research* (Vol. 19, Issues 1–2, pp. 39–61). https://doi.org/10.1007/BF00114568

Dubbs, J. M., & Tabita, F. R. (2004). Regulators of nonsulfur purple phototrophic bacteria and the interactive control of CO2 assimilation, nitrogen fixation, hydrogen metabolism and energy generation. *FEMS Microbiology Reviews*, *28*(3), 353–376. https://doi.org/10.1016/j.femsre.2004.01.002

EEA. (2020). *Water and agriculture: towards sustainable solutions — European Environment Agency, Report 17/2020* (Issue 17). https://www.eea.europa.eu/publications/water-and-agriculture-towards-sustainable-solutions

European Commission. (2010). Water is for life : How the Water Framework Directive helps safeguard Europe ' s resources. *Reproduction*, 10. https://doi.org/10.2779/83017

European Commission. (2015). *Closing the loop - An EU action plan for the Circular Economy*. https://doi.org/10.1016/0022-4073(67)90036-2

European Commission. (2018). Regulation of the European Parliament and of the Council on minimum requirement for water reuse. *European Commision*, *0169*, 1689–1699.

European Commission. (2019). The European Green Deal. *European Commission*, *53*(9), 24. https://doi.org/10.1017/CBO9781107415324.004

European Commission. (2020). *A new Circular Economy Action Plan For a cleaner and more competitive Europe*. https://doi.org/10.7312/columbia/9780231167352.003.0015

European Commission. (2021). *Pathway to a Healthy Planet for All EU Action Plan: "Towards Zero Pollution for Air, Water and Soil."* https://doi.org/10.1088/1751-8113/44/8/085201

European Council. (1991). The urban waste water treatment directive. *Institution of Water Officers Journal*, *28*(4), 14–15.

Fenchel, T., King, G. M., & Blackburn, T. H. (2012). Bacterial Metabolism. In *Bacterial Biogeochemistry* (pp. 1–34). Elsevier. https://doi.org/10.1016/b978-0-12-415836-8.00001-3

Gallegos, C., & Moore, K. (2000). Factors contributing to water-column light attenuation. In R. Batiuk, P. Bergstrom, M. Kemp, E. Koch, L. Murray, J. Stevenson, R. Bartleson, V. Carter, N. Rybicki, J. Landwehr, & C. Gallegos (Eds.), *Chesapeake Bay Submerged Aquatic Vegetation Water Quality and Habitat-Based Requirements and Restoration Targets: A Second Technical Synthesis* (pp. 16–27). US EPA, Chesapeake Bay Program. https://doi.org/10.13140/RG.2.1.3147.5449

Hallenbeck, P. C. (2017a). Modern topics in the phototrophic prokaryotes: Environmental and applied aspects. In *Modern Topics in the Phototrophic Prokaryotes: Environmental and Applied Aspects*. https://doi.org/10.1007/978-3-319-46261-5

Hallenbeck, P. C. (2017b). Modern Topics in the Phototrophic Prokaryotes: Metabolism, Bioenergetics, and Omics. *Modern Topics in the Phototrophic Prokaryotes: Metabolism, Bioenergetics, and Omics*. https://doi.org/10.1007/978-3-319-51365-2

Hamilton, T. L., Swanner, E., Llirós Dupré, M., Camacho, A., Walter, X. A., Picazo, A., & Zopfi, J. (2017). *Photoferrotrophy: Remains of an Ancient Photosynthesis in Modern Environments*. https://doi.org/10.3389/fmicb.2017.00323

Hanada, S. (2016). Anoxygenic Photosynthesis —A Photochemical Reaction That Does Not Contribute to Oxygen Reproduction—. *Microbes and Environments*. https://doi.org/10.1264/jsme2.ME3101rh

Hedaoo, M. N., Bhole, A. G., Ingole, N. W., & Hung, Y. T. (2012). Biological wastewater treatment. *Handbook of Environment and Waste Management: Air and Water Pollution Control*, 431–473. https://doi.org/10.1142/9789814327701_0012

Heimann, K., & Huerlimann, R. (2015). Microalgal Classification. *Handbook of Marine Microalgae*, 25–41. https://doi.org/10.1016/B978-0-12-800776-1.00003-0

Hou, H. J. M. (2014). *Water Splitting with Sunlight Inspired by Photosynthesis*. *May*.

Hülsen, T., Barry, E. M., Lu, Y., Puyol, D., Keller, J., & Batstone, D. J. (2016). Domestic wastewater treatment with purple phototrophic bacteria using a novel continuous photo anaerobic membrane bioreactor. *Water Research*. https://doi.org/10.1016/j.watres.2016.04.061

Hunter, C. N., Beatty, F. D., Thurnauer, M. C., & Thomas, J. (2009). The Purple Phototrophic Bacteria. In C. N. Hunter, F. Daldal, M. C. Thurnauer, & J. T. Beatty (Eds.), *New York State Journal of Medicine* (Vol. 28, Issue 3). Springer Netherlands. https://doi.org/10.1007/978-1-4020-8815-5

Jenkins, D., & Wanner, J. (2014). Activated Sludge – 100 Years and Counting. *Water Intelligence Online*, *13*. https://doi.org/10.2166/9781780404943

Kranz, R. G., Gabbert, K. K., Locke, T. A., & Madigan, M. T. (1997). Polyhydroxyalkanoate production in Rhodobacter capsulatus: genes, mutants, expression, and physiology. *Applied and Environmental Microbiology*, *63*(8), 3003–3009. https://doi.org/10.1128/AEM.63.8.3003-3009.1997

Kuo, F. S., Chien, Y. H., & Chen, C. J. (2012). Effects of light sources on growth and carotenoid content of photosynthetic bacteria Rhodopseudomonas palustris. *Bioresource Technology*, *113*, 315–318. https://doi.org/10.1016/j.biortech.2012.01.087

Laguna, R., Tabita, F. R., & Alber, B. E. (2011). Acetate-dependent photoheterotrophic growth and the differential requirement for the Calvin–Benson–Bassham reductive pentose phosphate cycle in Rhodobacter sphaeroides and Rhodopseudomonas palustris. *Archives of Microbiology*, *193*(2), 151–154. https://doi.org/10.1007/s00203-010-0652-y

Lettinga, G. (1995). Anaerobic digestion and wastewater treatment systems. *Antonie van Leeuwenhoek*, *67*(1964), 3–28.

Liu, S., Daigger, G. T., Kang, J., & Zhang, G. (2019). Effects of light intensity and photoperiod on pigments production and corresponding key gene expression of Rhodopseudomonas palustris in a photobioreactor system. *Bioresource Technology*, *294*(September), 122172. https://doi.org/10.1016/j.biortech.2019.122172

Liu, T. W. B., Chen, J., Burgess, L., Cao, W., Shi, J., Wilson, B. C., & Zheng, G. (2012). Multimodal Bacteriochlorophyll Theranostic Agent. *Theranostics*, *1*, 354–362. https://doi.org/10.7150/thno/v01p0354

Luongo, V., Ghimire, A., Frunzo, L., Fabbricino, M., d'Antonio, G., Pirozzi, F., & Esposito, G. (2017). Photofermentative production of hydrogen and poly-B-hydroxybutyrate from dark fermentation products. *Bioresource Technology*, *228*, 171–175. https://doi.org/10.1016/j.biortech.2016.12.079

Madigan, M., & Gest, H. (1979). Growth of the photosynthetic bacterium Rhodopseudomonas capsulatus chemoautotrophically in darkness with H2 as the energ source . *Journal of Bacteriology*, *137*(1), 524–530.

Madigan, M. T., Cox, J. C., & Gest, H. (1980). Physiology of dark fermentative growth of Rhodopseudomonas capsulata. *Journal of Bacteriology*, *142*(3), 908–915. https://doi.org/10.1128/jb.142.3.908-915.1980

Madigan, Michael T., Bender, K., Buckley, D., Sattley, M., & Stahl, D. (2015). Brock Biology of Microorganisms. In *Pearson* (Fourtheen, Vol. 1). Pearson. https://doi.org/10.1017/cbo9780511549984.016

Madigan, Michael T. (2003). Anoxygenic phototrophic bacteria from extreme environments. In *Photosynthesis Research* (Vol. 76). https://link.springer.com/content/pdf/10.1023%2FA%3A1024998212684.pdf

Madison, L. L., & Huisman, G. W. (1999). Metabolic Engineering of Poly(3-Hydroxyalkanoates): From DNA to Plastic. *Microbiology and Molecular Biology Reviews*, *63*(1), 21–53. https://doi.org/10.1128/mmbr.63.1.21-53.1999

McEwan, A. G. (1994). Photosynthetic electron transport and anaerobic metabolism in purple non-sulfur phototrophic bacteria. *Antonie van Leeuwenhoek*, *66*(151), 151–164. https://doi.org/10.1007/BF00871637

McKinlay, J. B., & Harwood, C. S. (2010). Carbon dioxide fixation as a central redox cofactor recycling mechanism in bacteria. *Proceedings of the National Academy of Sciences*, *107*(26), 11669–11675. https://doi.org/10.1073/pnas.1006175107

Nelson, K. E., & Fraser, C. M. (2004). Champions of versatility. In *Trends in Microbiology*. https://doi.org/10.1016/j.tim.2004.01.006

Nowicka, B., & Kruk, J. (2016). Powered by light: Phototrophy and photosynthesis in prokaryotes and its evolution. *Microbiological Research*, *186–187*, 99–118. https://doi.org/10.1016/j.micres.2016.04.001

Oleszkiewicz, J. A., & Barnard, J. L. (2006). Nutrient Removal Technology in North America and the European Union: A Review. In *Water Qual. Res. J. Canada* (Vol. 41, Issue 4). https://pdfs.semanticscholar.org/394e/d1efebfb78823bd11f653c6b4b0d75ebb11b.pdf

Olson, J. M. (2006). Photosynthesis in the Archean era. *Photosynthesis Research*, *88*(2), 109–117. https://doi.org/10.1007/s11120-006-9040-5

Olson, J. M., Blankenship, R. E., Hartman, H., Junge, W., Margulis, L., Mathis, P., Mauzerall, D., Meyer, T., Mulkidjanian, A., Nitschke, W., Pierson, B., & Raymond, J. (2004). Thinking about the evolution of photosynthesis. In *Photosynthesis Research* (Vol. 80). https://link.springer.com/content/pdf/10.1023%2FB%3APRES.0000030457.06495.83.pdf

Pantiushenko, I. V., Rudakovskaya, P. G., Starovoytova, A. V., Mikhaylovskaya, A. A., Abakumov, M. A., Kaplan, M. A., Tsygankov, A. A., Majouga, A. G., Grin, M. A., & Mironov, A. F. (2015). Development of bacteriochlorophyll a-based near-infrared photosensitizers conjugated to gold nanoparticles for photodynamic therapy of cancer. *Biochemistry (Moscow)*, *80*(6), 752–762. https://doi.org/10.1134/S0006297915060103

Pell, M., & Wörman, A. (2011). Biological Wastewater Treatment Systems. In *Comprehensive Biotechnology, Second Edition* (Second Edi, Vol. 6). Elsevier B.V. https://doi.org/10.1016/B978-0-08-088504-9.00381-0

Peretó, J. (2011). Phototroph. In M. Gargaud, R. Amils, J. C. Quintanilla, H. J. (Jim) Cleaves, W. M. Irvine, D. L. Pinti, & M. Viso (Eds.), *Encyclopedia of Astrobiology* (p. 1250). Springer Berlin Heidelberg. https://doi.org/10.1007/978-3-642-11274-4_1206

Perrine, Z., Negi, S., & Sayre, R. T. (2012). *Optimization of photosynthetic light energy utilization by microalgae*. https://doi.org/10.1016/j.algal.2012.07.002

Pescod, M. B. (1992). Wastewater treatment and use in agriculture - FAO irrigation and drainage. In *FOOD AND AGRICULTURE ORGANIZATION OF THE UNITED NATIONS Rome* (Vol. 47).

Petushkova, E., Iuzhakov, S., & Tsygankov, A. (2019). Differences in possible TCA cycle replenishing pathways in purple non-sulfur bacteria possessing glyoxylate pathway. *Photosynthesis Research*, *139*(1–3), 523–537. https://doi.org/10.1007/s11120-018-0581-1

Petushkova, E., Mayorova, E., & Tsygankov, A. (2021). TCA cycle replenishing pathways in photosynthetic purple non-sulfur bacteria growing with acetate. *Life*, *11*(7). https://doi.org/10.3390/life11070711

Quayle, J. R., & Pfennig, N. (1975). Utilization of methanol by rhodospirillaceae. *Archives of Microbiology*, *102*(1), 193–198. https://doi.org/10.1007/BF00428368

Rastegari, A. A., Yadav, A. nath, & Gupta, A. (2019). Prospects of Renewable Bioprocessing in Future Energy Systems. In *Biofuels and Biorefineries* (Vol. 10, Issue August). https://doi.org/10.1007/978-3-030-14463-0_13

Renuka, N., Ratha, S. K., Kader, F., Rawat, I., & Bux, F. (2021). Insights into the potential impact of algae-mediated wastewater beneficiation for the circular bioeconomy: A global perspective. *Journal of Environmental Management*, *297*(X), 113257. https://doi.org/10.1016/j.jenvman.2021.113257

Richmond, A. (2003). Handbook of Microalgal Culture. In A. Richmond (Ed.), *Handbook of Microalgal Culture*. Blackwell Publishing Ltd. https://doi.org/10.1002/9780470995280

Ruivo, M., Cartaxana, P., Cardoso, M. I., Tenreiro, A., Tenreiro, R., & Jesus, B. (2014). Extraction and quantification of pigments in aerobic anoxygenic phototrophic bacteria. *Limnology and Oceanography: Methods*. https://doi.org/10.4319/lom.2014.12.338

Sahm, H., Cox, R. B., & Quayle, J. R. (1976). Metabolism of methanol by Rhodopseudomonas acidophila. *Journal of General Microbiology*, *94*(2), 313–322. https://doi.org/10.1099/00221287-94-2-313

Sangkharak, K., & Prasertsan, P. (2007). Optimization of polyhydroxybutyrate production from a wild type and two mutant strains of Rhodobacter sphaeroides using statistical method. *Journal of Biotechnology*, *132*(3), 331–340. https://doi.org/10.1016/j.jbiotec.2007.07.721

Schultz, J. E., & Weaver, P. F. (1982). Fermentation and Anaerobic Respiration by Rhodospirillum rubrum and Rhodopseudomonas capsulata Downloaded from. In *JOURNAL OF BACTERIOLOGY* (Vol. 149, Issue 1). http://jb.asm.org/

Sener, M., Strumpfer, J., Singharoy, A., Hunter, C. N., & Schulten, K. (2016). Overall energy conversion efficiency of a photosynthetic vesicle. *ELife*, *5*(AUGUST). https://doi.org/10.7554/eLife.09541

Sharif, N., Munir, N., Naz, S., Iqbal, R., & Rauf, W. (2017). Chapter 4 - Origin of Algae and Their Plastids. *Algae Based Polymers, Blends, and Composites*, 77–113. https://doi.org/10.1016/B978-0-12-812360-7.00004-5

Sheik, A. R., Muller, E. E. L., Wilmes, P., Clark, K. B., & Zhang, X. (2014). *A hundred years of activated sludge: time for a rethink*. https://doi.org/10.3389/fmicb.2014.00047

Shih, P. M., Ward, L. M., & Fischer, W. W. (2017). Evolution of the 3-hydroxypropionate bicycle and recent transfer of anoxygenic photosynthesis into the Chloroflexi. *Proceedings of the National Academy of Sciences*, *114*(40), 10749–10754. https://doi.org/10.1073/pnas.1710798114

Shin, Y. S., Choi, H. Il, Choi, J. W., Lee, J. S., Sung, Y. J., & Sim, S. J. (2018). Multilateral approach on enhancing economic viability of lipid production from microalgae: A review. *Bioresource Technology*, *258*(January), 335–344. https://doi.org/10.1016/j.biortech.2018.03.002

Siefert, E., & Pfennig, N. (1979). Chemoautotrophic Growth of Rhodopseudomonas Species with Hydrogen and Chemotrophic Utilization of Methanol and Formate. In *Arch. Microbiol* (Vol. 122).

Spudich, J. L., & Jung, K.-H. (2005). *Microbial Rhodopsins: Phylogenetic and Functional Diversity*.http://citeseerx.ist.psu.edu/viewdoc/download?doi=10.1.1.527.9001&rep=rep1&type=pdf

Stomp, M., Huisman, J., Stal, L. J., & Matthijs, H. C. P. (2007). Colorful niches of phototrophic microorganisms shaped by vibrations of the water molecule. *The ISME Journal*, *1*(4), 271–282. https://doi.org/10.1038/ismej.2007.59

Tang, K.-H., & Blankenship, R. E. (2010). Both Forward and Reverse TCA Cycles Operate in Green Sulfur Bacteria * □ S. *THE JOURNAL OF BIOLOGICAL CHEMISTRY*, *285*(46), 35848–35854. https://doi.org/10.1074/jbc.M110.157834

Tang, K.-H. H., Tang, Y. J., Blankenship, R. E., Hanson, T. E., Kappler, U., & Brookings, O. (2011). Carbon Metabolic Pathways in Phototrophic Bacteria and Their Broader Evolutionary Implications. *Frontiers in Microbiology*, *2*(AUG), 165. https://doi.org/10.3389/fmicb.2011.00165

Thauer, R. K. (2007). A fifth pathway of carbon fixation. *Science*, *318*(5857), 1732–1733. https://doi.org/10.1126/science.1152209

The European Parliament and the Council. (2020). Regulation (EU) 2020/741, Minimum requirements for water reuse. *Official Journal of the European Union*, *177*(May 1991), 32–55.

Weissbrodt, D. G., Holliger, C., & Morgenroth, E. (2017). Modeling hydraulic transport and anaerobic uptake by PAOs and GAOs during wastewater feeding in EBPR granular sludge reactors. *Biotechnology and Bioengineering*, *114*(8), 1688–1702. https://doi.org/10.1002/bit.26295

Whatley, J. M. (1993). The Endosymbiotic Origin of Chloroplasts. *International Review of Cytology*, *144*(C), 259–299. https://doi.org/10.1016/S0074-7696(08)61517-X

Yurkov, V. V., & Beatty, J. T. (1998). Aerobic Anoxygenic Phototrophic Bacteria. *Microbiol. Mol. Biol. Rev.*, *62*(3), 695–724. https://doi.org/10.1038/415630a.

Chapter 2

Effects of light/dark diel cycles on electron allocation to PHAs and H_2 in the photoorganoheterotrophic metabolism of *Rhodopseudomonas palustris*

This chapter is deposited in a modified version as preprint with contributions of:
Marta Cerruti, Heleen T. Ouboter, Viktor Chasna, Mark C. M. van Loosdrecht, Cristian Picioreanu, David G. Weissbrodt (2020) Effects of light / dark diel cycles on the photoorganoheterotrophic metabolism of *Rhodopseudomonas palustris* for differential electron allocation to PHAs and H_2, *bioRxiv*, preprint, 2020.08.19.258533.
https://doi.org/10.1101/2020.08.19.258533

Abstract

Purple non-sulfur bacteria (PNSB) are hyperversatile photoorganoheterotrophs that foster organic aqueous waste biorefinery from pure-culture to mixed-culture biotechnologies. Light/dark diel cycles can impact the electron distribution in their metabolism and resulting product formation. For survival and growth, PNSB have developed different mechanisms to allocate excessive electrons under dynamic growth conditions. Products such as dihydrogen (H_2) and intracellular poly-β-hydroxyalkanoates (PHAs) can form alternative electron sinks to biomass formation. Coupling between illumination patterns and redox balancing in the PNSB physiology remained to be uncovered. A controlled continuous culture of *Rhodopseudomonas palustris*, a model PNSB isolated from an in-house enrichment, was fed with an acetate-based balanced nutritive medium and exposed to three irradiance conditions: 24 h continuous infrared illumination, 16 h light/8 h dark, and 8 h light/16 h dark alternations. Durations of light and dark phases over a cycle determined the light energy availability level and attainment of a metabolic stationary state. Under long dark phases, acetate accumulated to levels (ca. 8 C-mM L^{-1}) that were depleted by growth in the light. Under short dark phases, acetate was rapidly consumed in the light with most of phototrophic growth occurring under acetate-limiting conditions. Diel cycles resulted in an imbalance between substrate uptake and biomass growth. *Rhodopseudomonas* shunted the excess of carbon and electron flows first toward PHA production. Only secondarily when PHA storage got saturated, the remaining electron excess was redirected toward H_2. A numerical model was developed to describe dynamics of biomass, nutrients, off-gas compounds (CO_2, H_2) and PHAs during light/dark cycles. Simulations allowed for extracting stoichiometric and kinetic parameters exhibited by *Rhodopseudomonas*. Insights on ecophysiological dynamics of PNSB induced by light/dark diel cycles can help understand, predict and control their functioning in biorefinery processes.

1. Introduction

Purple non-sulfur bacteria (PNSB) form a guild of hyper-versatile anoxygenic phototrophs which establish their niche in the infrared (IR) light wavelength domain (Blankenship et al., 1995). PNSB grow on various organic and inorganic substrates (Alloul et al., 2019), capture nutrients (Cerruti, Stevens, et al., 2020a), and produce biocompounds of interest for the industry and circular economy like fertilizing nutrient-rich biomasses, single-cell proteins for food ingredients, carotenoids antioxidants, intracellular poly-β-hydroxyalkanoates (PHAs) for biodegradable plastics, and dihydrogen (H_2) gas for biofuel (Hülsen et al., 2018; Hustede et al., 1993; Vincenzini et al., 1997; Wang et al., 2017). PNSB foster biorefinery opportunities from pure-culture to co-culture and mixed-culture biotechnologies. *Rhodopseudomonas palustris* is one model PNSB (Madigan & Jung, 2009), widely described and used biotechnologically.

Under light and in presence of organic substrates as carbon and electron sources, PNSB grow photoorganoheterotrophically. In the dark, they can grow chemoorganoheterotrophically on sugars by fermentation (Madigan et al., 1980), or by aerobic or anaerobic respiration when exogenous electron acceptors are supplied (as dissolved oxygen, nitrate, trimethylamine-N-oxide or dimethyl sulfoxide) (Ho Lee et al., 2002; Imhoff, 1995; Madigan et al., 1982).

Light is crucial for phototrophy by providing energy to cells. PNSB capture the photonic energy and couple the light-driven oxidation of the photopigments to an electron transfer through membrane bound-enzymes. The trans-membrane gradient of hydrogen protons (H^+) supports ATP synthesis through cyclic photophosphorylation (Madigan et al., 2015). NADH is mainly produced during catabolic processes. In some cases, a reverse electron flow takes places, and the NADH-dehydrogenase catalyzes the proton transfer from the ubiquinone pool to NAD^+. The control of the redox balance is crucial for cell survival and growth. The ratio between NADH/NAD^+ is important for intracellular redox homeostasis (Green & Paget, 2004). PNSB generate NADH in three different ways (Figure 1), namely: 1) catabolic processes (Laguna et al., 2011); 2) light-driven reactions through the quinone pool (Blankenship et al., 1995); and 3) reverse electron transfer (Dupuis et al., 1998).

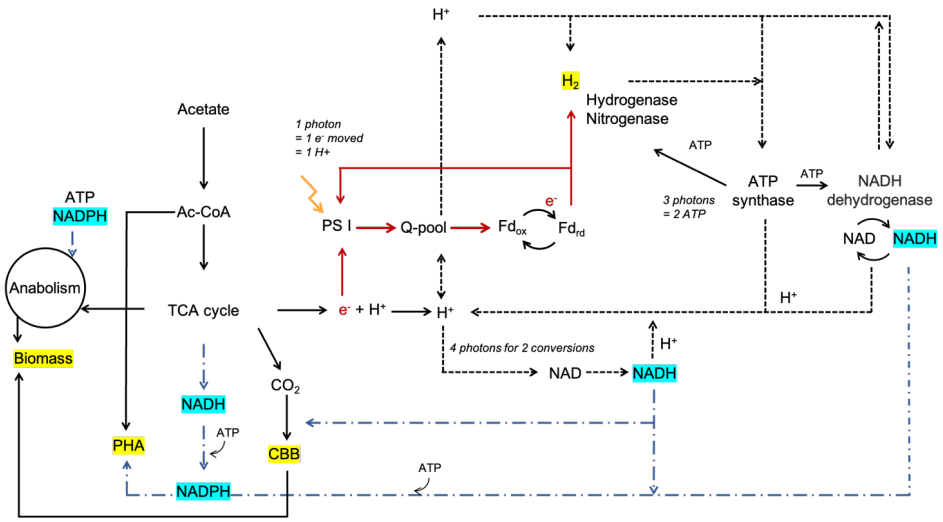

Figure 1. **Schematic representation of the reducing power allocation in Rhodopseudomonas. Red lines: electron flow; Black dashed lines: proton transfer; Blue dotted lines: NADH is normally produced in the catabolic processes, whereas NADPH is used in the anabolic processes, such as poly-hydroxyalkanoate (PHA) formation. Biomass is the primary electron sink in PNSB. PHAs and H_2 are two of the other possible electron sinks.**

To cope with possible redox imbalances, PNSB redistribute the electrons toward different routes (Spero et al., 2016). In *Rhodopseudomonas*, the first and most important electron sink is the biomass itself, that receives the intermediates of the tricarboxylic acid cycle (TCA) and the NADPH produced there (McKinlay & Harwood, 2011). Secondly, the Calvin-Benson-Bassham (CBB) cycle is constitutively active also under photoorganoheterotrophy as central recycling mechanism of redox cofactors coming from the anabolic process (Gordon & McKinlay, 2014; McKinlay & Harwood, 2011). Under photoorganoheterotrophic anaerobic conditions, a surplus of electrons can be disposed through PHA or H_2 production, besides CO_2 fixation (Harwood, 2008). Both these electron sinks are normally produced under nitrogen limitation. H_2 production by PNSB is substantially mediated by nitrogenase (Blankenship et al., 1995). H_2 is a side-product of the dinitrogen fixation process, that can only happen when preferred nitrogen sources like ammonium are depleted (Basak et al., 2014; Kim et al., 1980; Oda et al., 2005). Hydrogenase-mediated H_2 production has been reported in presence of an oxidized organic compound (*i.e.* malate) (Willison et al., 1983). In the environment, numerous bacterial species accumulate PHAs as a means of carbon and electrons storage, conferring them a competitive advantage (Kutralam-Muniasamy et al., 2017). In lab-scale experiments and industrial

processes, to achieve an overproduction, these storage polymers are synthetized when acetyl-CoA and NADPH are in excess but nutrients like nitrogen, sulfur or phosphorus are limiting (Montano-Herrera et al., 2017). Similarly, PNSB can produce PHAs (Hustede et al., 1992) as a means of carbon and electron balance, utilizing the reducing power to build the storage polymers (De Philippis et al., 1992; Haywood et al., 1988). PHA production in PNSB occurs under balanced growth, and it increases under nutrient limitations (Higuchi-Takeuchi et al., 2016). The two processes of H_2 and PHA productions are considered competitive electron dissipation pathways (Hustede et al., 1993; Padovani et al., 2016). However, due to the hyper-versatility of PNSB metabolisms, a univocal response to redox imbalances has not yet been identified.

In natural environments, phototrophs are subjected to diel (*i.e.*, 24-h period) light/dark cycles. Since light is responsible for the production of energy and reducing power, the irradiation patterns impact the cellular physiology. The light and dark cycles impact redox and ATP balance of the cells, subjecting them to metabolic switches. The impact of diel cycles on the metabolic response of PNSB and internal electron allocation patterns remains puzzling. Allocation of reducing power toward the aforementioned routes is known, but mechanisms that govern the preferential electron flow have not been explained yet.

Here, we investigated the effects of diel light/dark cycles on the physiology and electron allocation in PNSB. We used *Rhodopseudomonas palustris* as representative organism isolated from an in-house PNSB enrichment culture implemented for nutrient capture from wastewater (Cerruti, Stevens, et al., 2020). The light/dark dynamic conditions imposed on the acetate-fed continuous culture were hypothesized to influence the organismal physiology by the intermittent supply of the IR light energy source. The process mimicked natural day/night cycles that generate a redox imbalance. Using wet-lab experiments and mathematical modelling, we elucidated the preferential redistribution of carbon and electron flows toward biomass, PHAs and H_2 in function of the lengths of the light and dark periods and of the underlying dynamics in substrate conversions.

2. Material and Methods

2.1 Strain

The *Rhodopseudomonas* strain was isolated by agar colony selection from an in-house PNSB enrichment culture run for nutrient removal from synthetic wastewater (Cerruti, Stevens, et al., 2020a). The isolate was characterized by full-length 16S rRNA gene sequencing. The genomic DNA was extracted using UltraClean® Microbial DNA Isolation Kit (MO BIO Laboratories, Inc., USA), following manufacturer's instructions. The full 16S rRNA gene was amplified by polymerase chain reaction using forward GM3R (5'-AGAGTTTGATCMTGGC-3') and reverse GM4F (5'-TACCTTGTTACGACTT-3') primers (Muyzer et al., 1995), and sequenced for phylogenetic identification by Sanger sequencing (Baseclear, NL). The nucleotide sequence was aligned over the NCBI BLAST database (Altschul et al., 1990), and resulted in a 98.1% identity and query cover with *Rhodopseudomonas palustris.* The amplified sequences are deposited under the accession number (see Supplementary information SUB10460307 rps_chem4E_GM3 OK350353-4).

2.2 Medium

The inflow medium of the continuous cultures was adapted from Cerruti et al. (2020). It consisted of (per liter): 0.914 g $CH_3COONa \cdot 3H_2O$ (13.5 C-mmol L^{-1} and 54 mmol electrons L^{-1} when expressed via degree of reduction or 432 mg COD L^{-1} when expressed as chemical oxygen demand), 0.229 g NH_4Cl (*i.e.*, 4.281 mmol N L^{-1} or 60 mg N-NH_4^+ L^{-1}), 0.014 g KH_2PO_4 and 0.021 g K_2HPO_4 (*i.e.*, 0.223 mmol P L^{-1} or 7 mg P L^{-1}), 0.200 g $MgSO_4 \cdot 7H_2O$, 0.200 g NaCl, 0.050 g $CaCl_2 \cdot 2H_2O$, 1 mL solution of vitamins, 1 mL solution of trace elements, and 4.7 g 4-(2-hydroxyethyl)-1-piperazineethanesulfonic acid (HEPES) used as pH buffer. The medium was autoclaved to assure sterility.

The solution of vitamins was composed of (per liter): 200 mg thiamine–HCl, 500 mg niacin, 300 mg ρ-amino-benzoic acid, 100 mg pyridoxine–HCl, 50 mg biotin and 50 mg vitamin B12.

The solution of trace elements was composed of (per liter): 1100 mg Na EDTA$\cdot 2H_2O$, 2000 mg $FeCl_3 \cdot 6H2O$, 100 mg $ZnCl_2$, 64 mg $MnSO_4 \cdot H_2O$, 100 mg H_3BO_3, 100 mg $CoCl_2 \cdot 6H_2O$, 24 mg $Na_2MoO_4 \cdot 2H_2O$, 16 mg $CuSO_4 \cdot 5H_2O$, 10 mg $NiCl_2 \cdot 6H_2O$ and 5 mg $NaSeO_3$.

The stock solutions of trace elements and vitamins were filtered on 0.22 μm filters (Whatman, USA).

2.3 Reactor setup

Continuous cultures were run to evaluate the influence of the light/dark diel cycles on the physiology of *Rhodopseudomonas palustris*. A 1.5-L continuous-flow stirred-tank reactor (CSTR) with 1.2-L working volume and cylindrical geometry was connected to a programmable logic controller (In-Control and Power unit, Applikon, NL) and operated with stirring at 350 rpm, at pH 7.0 ± 0.5, and a temperature of 30±1 °C during illumination phases and 20°C during dark phases. This temperature pattern resulted from the intermittent switches of the IR light supply. Argon gas (Linde, NL, >99% purity) was sparged continuously in the bulk liquid phase at 120 mL min^{-1} to maintain anaerobic conditions. The use of N_2 gas was avoided since interfering with nitrogenase-mediated H_2 production pathways (Harwood, 2008). The continuous flow rate was set at 0.048 L h^{-1}. It corresponded to a dilution rate of 0.04 h^{-1} chosen based on the growth rate of *Rhodopseudomonas* pure cultures previously measured at 0.11 h^{-1} (data not shown). The biomass was maintained in the CSTR at a low concentration of 0.26 ± 0.05 g dry weight L^{-1} to minimize light shading effects.

The reactor was placed in a shaded hood to tightly control the irradiation patterns. Two halogen floodlight lamps (Handson, NL) were positioned at opposite sides of the reactor diameter. The incident white light spectrum was filtered to supply infrared (IR) light ($\lambda > 700$ nm) using two Black 962 Infrared Transmitting Perspex Acrylic Sheets of 70 x 70 cm (Black Perspex 962, Plasticstockist, UK). The IR light intensity measured at the reactor surface with a pyranometer (CMP3; Kipp & Zonen, NL) was 300 W m^{-2}, enabling non-light-limited conditions in the reactor (Cerruti et al., in prep.). An automatic timer device (Grundig, NL) was used to switch on/off the light at required time sets. Three irradiance conditions were tested: 1) continuous illumination (*i.e.*, 24 h light), 2) 16 h light and 8 h dark cycles, and 3) 8 h light and 16 h dark cycles.

2.4 Analytical methods

The CO_2 and H_2 in the offgas were measured using an online mass spectrometer (Thermofisher, Prima BT Benchtop MS) connected to the bioreactor. The production rates of these components were calculated using the argon gas inflow rate (120 mL h^{-1}).

The biomass concentration was measured from the mixed liquor by absorbance at 660 nm (A_{660}) using a spectrophotometer (Biochrom, Libra S11, USA). A calibration curve was established to correlate A_{660} to dry weight (DW) concentration of biomass: c_X (g DW L^{-1}) = 0.64 A_{660} – 0.06. Biomass dry weight was obtained by taking samples from the mixed liquor, filtering them using 0.45 µm filters (Whatman, USA), and drying them in a 70 °C stove for 72 h (adapted from Lip et al. 2020).

Acetate was measured from the filtrates with a high-performance liquid chromatograph (HPLC) (Waters, 2707, NL) equipped with an Aminex HPX-87H column (BioRad, USA). Analytes were eluted using H_3PO_4 (1.5 mmol L^{-1}, flowrate of 0.6 mL min^{-1}, temperature of 60°C) prior to detections by refraction index (Waters 2414) and UV (210 nm, Waters 484) spectrophotometry.

Concentration of ammonium (as N-NH_4^+) and orthophosphate (as P-PO_4^{3-}) were measured from the filtrates with a discrete analyser (Thermoscientific Gallery, NL) using manufacturer's reagents.

PHA measurements were performed with fluorimetry for high sensitivity on low concentrations of biomass maintained in the reactor. The low biomass concentration did not allow for traditional extractions of PHA and gas chromatographic measurements of monomers. PHAs were stained in the biological samples with Nile red (CAS n. 7385-67-3, Sigma Aldricht), as in (Zuriani et al., 2013). Fluorescence was measured with a microplate reader (1000M pro, Tecan), with excitation at 535 nm and emission at 605 nm.
A calibration curve was used to correlate fluorescent counts to mol fractions of PHAs expressed as hydroxybutyrate (HA) monomer equivalents (C-$mmol_{HB}$ C-$mmol_X^{-1}$) (Supplementary information SI-1). PHA quantifications for the calibration line were performed as in Vermeer et al., (2021).

2.5 Mathematical model

A mathematical model was developed to characterize the behavior of the continuous pure culture of *Rhodopseudomonas* exposed to light/dark cycles. The following assumptions were adopted to build the model structure: (*i*) photoorganoheterotrophic growth was assumed during the light period; (*ii*) under dark, a completely ceased metabolic activity was considered since acetate was the sole carbon source and cannot be metabolized further in absence of light and external electron acceptors. The light-driven growth stoichiometry was defined as in Table 1, with the biomass composition adapted from McKinlay & Harwood (2010).
The growth process was described by a system of balance equations for the relevant substances present in the mixed liquor (Table 2, equations 1-7), namely biomass (C_X), acetate (C_S), ammonium (NH_4^+, C_N), phosphate (PO_4^{3-}, C_P), carbon dioxide (CO_2, C_C), and PHAs as hydroxybutyrate monomer equivalents per mass fraction (HB, C_{PHA}). NH_4^+, PO_4^{3-}, were dissolved in the liquid phase. CO_2 was dissolved in the liquid and the gas phases. Biomass and PHAs were present in the solid phase.

Components i →	**Acetate**	**Ammonium**	**Phosphate**	**Biomass**	**Carbon dioxide**	**PHAs**	**Water**	**Protons**
Abbreviation →	(S)	(N)	(P)	(X)	(C)	(HB)	(W)	(H)
Molecular formula →	CH_3COOH	NH_4^+	PO_3^{4-}	$C_1H_{1.8}O_{0.38}N_{0.18}P_{0.0}$ $_{14}$	CO_2	$C_4H_8O_3$	H_2O	H^+
Units →	C-mol	mol	mol	C-mol	C-mol	C-mol	mol	mol
↓ Microbial processes j								
1) PPB growth on acetate	-0.57125	-0.18	-0.014	1	0.1425	0	0.5335	0.138
Acetate → Biomass	($-Y_{S/X,1} = -1/Y_{X/S,1}$)	($-Y_{N/X,1}$)	($-Y_{P/X,1}$)	fixed	($Y_{C/X,1}$)		($Y_{W/X,1}$)	($Y_{H/X,1}$)
2) Acetate storage as PHAs	-2.25	0	0	0	0.5	1	0.5	0
Acetate → PHA	($-Y_{S/HB,2} = -1/Y_{HB/S,2}$)				($Y_{C/HB,2}$)	fixed	($Y_{W/HB,2}$)	($Y_{H/HB,2}$)
3) PPB growth on PHAs	0	-0.18	-0.014	1	0.0157	-0.254	0.406	0.138
PHA → Biomass		($-Y_{N/X,3}$)	($-Y_{P/X,3}$)	fixed	($Y_{C/X,3}$)	($-Y_{HB/X,3}$)	($Y_{W/X,3}$)	($Y_{H/X,3}$)

Table 1. **Stoichiometric matrix of the mathematical model developed to characterize photoorganoheterotrophic growth and PHA storage by *Rhodopseudomonas palustris* under light/dark diel cycles. According to experimental data, growth was assumed to only occur under periods of illumination with infrared light. Stoichiometric coefficients (ν_{ij}) are expressed as yields normalized per unit of biomass for growth processes and per unit of PHAs (expressed as equivalents of hydroxybutyrate monomers, HB) for the intracellular storage processes.**

Table 2. **Mole balance equations comprising the transport and biokinetic conversion terms of the mathematical model for the photoorganoheterotrophic growth of *Rhodopseudomonas palustris* and intracellular storage.**

Compounds	Mole balance equations	
Biomass	$\frac{dC_X}{dt} = -D \cdot C_X + (\mu_{ace} + \mu_{PHA}) \cdot C_X$	(1)
Acetate	$\frac{dC_S}{dt} = D \cdot (C_{S,in} - C_S) - (q_{S,X} + q_{S,PHA}) \cdot C_X$	(2)
Ammonia	$\frac{dC_N}{dt} = D \cdot (C_{N,in} - C_N) - (q_{N,S} + q_{N,PHA}) \cdot C_X$	(3)
Phosphate	$\frac{dC_P}{dt} = D \cdot (C_{P,in} - C_P) - (q_{P,} + q_{P,PHA}) \cdot C_X$	(4)
CO_2 (aq.)	$\frac{dC_{CO_2}}{dt} = -D \cdot C_{C,L} + q_C \cdot C_X + k_L a_C \cdot (C^*_{C,L} - C_{C,L})$	(5)
CO_2 (gas)	$\frac{dC_{CO_2,gas}}{dt} = -\frac{F_g}{V_g} \cdot C_{C,g} - k_L a \cdot (C^*_{C,L} - C_{C,L}) \cdot \frac{V_L}{V_g}$	(6)
PHAs (HB)	$\frac{dC_{PHA}}{dt} = -D \cdot C_{PHA} + (q_{PHA,S} - q_{PHA,X}) \cdot C_X$	(7)

With C_X the state-variable concentration of biomass in the mixed liquor (C-mmol L^{-1}); t the process time (h); D the dilution rate (h^{-1}); $C_{S,in}$, $C_{N,in}$, $C_{P,in}$ the constant concentrations of dissolved acetate, ammonium and phosphate in the influent ; C_S, C_N, C_P the state-variable concentrations of dissolved acetate, ammonium and phosphate in the bulk liquid; $C_{C,L}$ the state-variable concentration of dissolved CO_2 in the bulk liquid; C_{PHA} the state-variable concentration of PHAs (as hydroxybutyrate monomer equivalents); μ the total growth rate split as growth rates on acetate μ_{ace} (process 1 in Table 1) and on PHAs μ_{PHA} (process 3 in Table 1); q_S the biomass-specific rate of acetate uptake split as acetate uptake for growth ($q_{S,X}$) and for PHA storage ($q_{S,PHA}$).

A mole balance on the gas phase was integrated for CO_2 (Eq. 6): with $C_{C,L}^*$ (mmol CO_2 L^{-1} liquid) the maximum saturation concentration of CO_2 dissolved in the liquid phase, and C_C (mmol CO_2 L^{-1} liquid) the actual concentration of CO_2 dissolved in the liquid phase. The volumetric mass transfer coefficient of CO_2 between the gas and liquid phases (k_La, h^{-1}) was calculated in function of the power input, liquid volume, and gas velocity (see SI-2.1 in Supplementary information). The maximum dissolved CO_2 concentration ($C_{C,L}^*$) was calculated in function of the measured CO_2 concentration in the gas phase ($C_{C,g}$ mmol CO_2 L^{-1} gas), the Henry's coefficient (H_C, mol $L^{-1}atm^{-1}$), the respective temperatures (T) of 20ºC in dark and 30ºC under light, and pressure (1 atm) (SI-2.2).

Parameters and units are described in Table 3.

The liquid flow rate F (L h^{-1}), liquid volume V (L), gas flow rate F_g (L h^{-1}), gas volume V_g (L), and the concentrations of dissolved chemical compounds in the influent ($C_{i,in}$, mmol L^{-1}) were all fixed in the experiments.

Parameter name	Symbol	Value	Units	Source
Stoichiometric parameters				
Biomass yield on acetate	$Y_{X/S}$	1.75	C-mol X · C-mol^{-1} S	Fitted
Biomass yield on PHA (HB)	$Y_{X/HB}$	3.94	C-mol X · C-mol^{-1} HB	Stoichiometry
PHA (HB) yield on acetate	$Y_{HB/S}$	0.44	C-mol HB · C-mol^{-1} S	Stoichiometry
Ammonium yield over biomass	$Y_{N/X}$	0.07	mol N · C-mol^{-1} X	Fitted
Phosphate yield over biomass	$Y_{P/X}$	0.007	mol P · C-mol^{-1} X	Fitted
CO_2 yield on acetate	$Y_{C/S}$	0.24	C-mol CO_2 · C-mol^{-1} S	Fitted
CO_2 yield on HB	$Y_{C/HB}$	0.06	C-mol CO_2 · C-mol^{-1} HB	Stoichiometry
Biokinetic parameters				
Maximum biomass-specific growth rate	μ_{max}	0.15	C-mol X · h^{-1} · C-mol^{-1} X	Fitted
Half-saturation coefficient for acetate	K_S	0.1	C-mmol S · L^{-1}	Lower than in Kaewsuk et al. (2010) (0.3 mM)
Half-saturation coefficient for acetate (growth on HB)	K_{S2}	0.003	C-mmol S · L^{-1}	Arbitrary
Half-saturation coefficient for PHAs (HB)	K_{HB}	0.001	C-mmol HB · L^{-1}	(De Kreuk et al., 2007)
Half-saturation coefficient for ammonium	K_N	0.001	mmol N · L^{-1}	(Wolf et al., 2007)
Half-saturation coefficient for phosphate	K_P	0.003	mmol P · L^{-1}	(Puyol et al., 2017)
Half-saturation coefficient for light	K_I	10	W · m^{-2}	(Prachanurak et al., 2019)
Reactor, transport and light characteristics				
Reactor radius	R	0.055	M	Measured
Liquid volume	V	1.2	L	Measured
Liquid flow rate	F	0.048	L · h^{-1}	Measured
Dilution rate	D	0.04	h^{-1}	$= F/V$
Gas volume	V_g	0.3	L	Measured
Gas flow rate	F_g	7.14	L · h^{-1}	Measured
Inflow acetate concentration	$C_{S,in}$	7	C-mmol S · L^{-1}	Measured
Inflow ammonium concentration	$C_{N,in}$	4.28	mmol N · L^{-1}	Measured
Inflow phosphate concentration	$C_{P,in}$	0.22	mmol P · L^{-1}	Measured
Volumetric mass transfer coefficient of CO_2	k_La	32	h^{-1}	Calculated (SI-1)
Henry coefficient for CO_2	H_C	0.03 (at 30ºC) 0.04 (at 20ºC)	C-mol · L^{-1} · atm^{-1}	(Sander, 2015)
Light intensity at reactor walls	I_0	300	W · m^{-2}	Measured
Light extinction coefficient per biomass concentration	ε	0.1	m^2 · g^{-1}	(Kim et al., 1980)

Table 3. **Stoichiometric and kinetic constants used in the mathematical model describing the photoorganoheterotrophic growth of *Rhodopseudomonas palustris* and intracellular storage. The yields and maximum biomass-specific growth rate were fitted to experimental data. The other parameters were measured during the experiments, calculated or obtained from literature.**

The biomass specific growth rate (μ, h^{-1}) was calculated both in function of acetate (μ_{ace}) and PHAs (μ_{PHA}) (Eq 8-9). They were initially assumed to be limited by the concentrations of multiple chemical compounds and by incident light intensity (I, W m^{-2}). According to liquid phase measurements, acetate and light were the main limiting state variables for biomass growth. Ammonium and phosphate were supplied in excess.

$$\mu_{ace} = \mu_{max} \cdot \frac{C_S}{C_S+K_S} \cdot \frac{C_N}{C_N+K_N} \cdot \frac{C_P}{C_P+K_P} \cdot \frac{I}{I+K_I} \quad (8)$$

$$\mu_{PHA} = \mu_{max} \cdot \frac{C_{HB}}{C_{HB}+K_{HB}} \cdot \frac{C_N}{C_N+K_N} \cdot \frac{C_P}{C_P+K_P} \cdot \frac{I}{I+K_I} \cdot \frac{K_{S,2}}{C_S+K_{S,2}} \quad (9)$$

With μ_{max} defined as the biomass-specific maximum growth rate for *Rhodopseudomonas palustris*.

The volumetric rates of acetate (r_S), ammonium (r_N) and phosphate (r_P) uptake and of CO_2 production (in the gas phase) (r_C) (all in mmol L^{-1} h^{-1}) follow from the overall growth stoichiometric coefficients (*i.e.*, yields) and the biomass growth rate (μ):

$$r_S = -Y_{S/X} \cdot r_X = -\frac{1}{Y_{X/S}} \cdot r_X \quad (10)$$

$$r_N = -Y_{N/X} \cdot r_X \quad (11)$$

$$r_P = -Y_{P/X} \cdot r_X \quad (12)$$

$$r_C = Y_{C/X} \cdot r_X \quad (13)$$

The biomass-specific rates were calculated as:

$$q_{S,X} = \mu_{ace} \cdot \frac{1}{Y_{X/S}} \quad (14)$$

$$q_{S,PHA} = q_{s,max} \cdot \frac{C_S}{C_S+K_{S,2}} \cdot \frac{I}{I+K_I} \quad (15)$$

$$q_{N,S} = \mu_{ace} \cdot Y_{N,S/x} \quad (16)$$

$$q_{N,PHA} = \mu_{PHA} \cdot Y_{N,HB/X} \quad (17)$$

$$q_{P,S} = \mu_S \cdot Y_{P,S/X} \quad (18)$$

$$q_{P,PHA} = \mu_{PHA} \cdot Y_{P,HB/X} \quad (19)$$

$$q_{PHA,X} = \mu_{PHA} \cdot \frac{1}{Y_{X/HB}} \quad (20)$$

$$q_{PHA,S} = Y_{HB/S} \cdot q_{S,HB} \quad (21)$$

$$q_{CO_2} = Y_{1,CO_2/S} \cdot q_{S,HB} + Y_{2,CO_2/S} \cdot q_{S,X} + q_{PHA,S} \cdot Y_{CO_2/HB} \quad (22)$$

The yields of biomass growth on acetate ($Y_{X/S}$) and CO_2 production over biomass production ($Y_{C/X}$) and the biomass-specific maximum growth rate (μ_{max}) were computed by fitting the model outputs to the measurements from the experiment performed with 16 h light / 8 h dark. Additional estimations of μ_{max} were made based on data collected from preliminary batch cultures of the *Rhodopseudomonas* strain incubated at 30°C under IR light with the same cultivation medium as for the reactor, as well as from the CSTR experiments run under continuous illumination and 8 h light / 16 h dark. Overall, an average μ_{max} value of 0.15 ± 0.05 h^{-1} was obtained for this organism under photoorganoheterotrophy. The yields of ammonium consumption ($Y_{N/X}$) and phosphate consumption ($Y_{P/X}$) during biomass growth, and consequently the N and P compositions of the biomass (n_N and n_P, respectively) were determined from the 8 h light / 16 h dark experiment.

Two light sources with resulting IR irradiation intensities I_0 measured at the reactor wall (300 W m^{-2}) were placed at opposite sides next to the reactor. The light intensity decrease away from the reactor wall was assumed to follow the Beer-Lambert attenuation law. Therefore, the total light intensity I_t at a radial position x (m) across the reactor diameter was obtained by summing up the light intensities coming from both sides as following:

$$I_t = I_0 \cdot \left(e^{-\varepsilon \cdot c_X \cdot x} + e^{-\varepsilon \cdot c_X \cdot (2 \cdot R - x)} \right) \quad (23)$$

with R (m) the reactor radius, ε (m^2 g^{-1}) the biomass-specific light attenuation coefficient, and C_X (g m^{-3}) the biomass concentration. We considered that the liquid mixing enabled the cells to be exposed to an average light intensity I (W m^{-2}) computed by integrating eq. 23 over the reactor diameter:

$$I = I_0 \cdot \frac{1 - e^{-2 \cdot \varepsilon \cdot c_X \cdot R}}{\varepsilon \cdot c_X \cdot R} \quad (24)$$

The model was solved in MATLAB (R2018b, Mathworks, Natick, MA, www.mathworks.com) using a stiff solver for the ordinary differential equations system. The initial concentrations were taken to coincide with the measurements. The parameter estimation was performed by a constrained optimization routine minimizing the sum of squares of relative errors between model and experimental data. The fixed model parameters and the fitted parameters are listed in Table 3.

3. Results

The tree IR irradiance regimes were tested in the acetate-fed, anaerobic CSTR targeted and enabled to elucidate the physiology of the PNSB *Rhodopseudomonas palustris*, namely: (i) continuous illumination, (ii) cyclic 16 h light / 8 h dark, and (iii) cyclic 8 h light / 16 h dark. A specific focus was given to carbon and electron allocation to biomass, H_2 and PHA productions. The mathematical model calibrated on the 16 h light / 8 h dark experiment enabled to extract key stoichiometric and kinetic parameters like the biomass production yield on acetate ($Y_{X/S}$), the CO_2 production yield during growth (Y_{CX}), and the maximum biomass-specific growth rate (μ_{max}) (Table 3). The calibrated model was used to predict the behavior of the 8 h light / 16 h dark cycles.

3.1 Biomass production of Rhodopseudomonas palustris

Under continuous illumination, the biomass reached a constant concentration of 12.10 ± 0.44 C-mmol L^{-1}. The outflow of biomass from the reactor corresponded to 88% of the carbon and 99% of the reduction equivalents (COD) provided with the influent. Around 11% of the supplied carbon was recovered as CO_2 (0.112 C-mmol L^{-1}) in the off-gas. HPLC results showed no residual acetate in the bulk liquid at steady state.

Under cyclic operations (Figure 2), the system reached a pseudo-steady-state conditions with similar dynamics in concentrations per light/dark cycle.
In the dark, the biomass did not grow and was washed out of the reactor with the effluent. The biomass wash-out rate ($F / V \cdot C_X$) was very well represented by the numerical model (Figure 2A,B). The corresponding increases in acetate, ammonium and phosphate concentrations during the dark phases matched with the expected change based on the feeding rate. No conversion occurred in the dark.
Under 16-h light periods, the biomass accumulation exceeded the dilution rate ($D = F / V$). An initial growth rate (μ) of 0.15 h^{-1} (assumed to be equivalent to μ_{max} since the reactor experiences a high residual concentration of acetate right after the dark phase) was observed. It reached a steady value ($\mu = D$) of 0.04 h^{-1} after 2 h of exposure to IR light (Figure 2A). The residual acetate concentration

reached a minimal steady value (0.7 ± 0.6 C-mmol L^{-1}) when the biomass growth rate achieved the steady state.

Under shorter 8-h irradiance periods, the biomass growth rate did not reach a stationary state in a cycle, being around 0.1 h^{-1}. Acetate was not depleted at the end of the light phase (Figure 2B). The increase in biomass concentration from 11 C-mmol L^{-1} on the first cycle to 5 C-mmol L^{-1} on the fourth cycle. The growth rate μ during the 8-h light period was approximately 0.12 h^{-1} thus lower than the aforementioned μ_{max}.

The estimated biomass yield on acetate ($Y_{X/S}$) during the photoorganoheterotrophic growth of *Rhodopseudomonas palustris* was 0.88 C-mol X C-mol^{-1} acetate under both irradiance periods of 16 h and 8 h, and matched with the yield measured under 24-h continuous light regime.

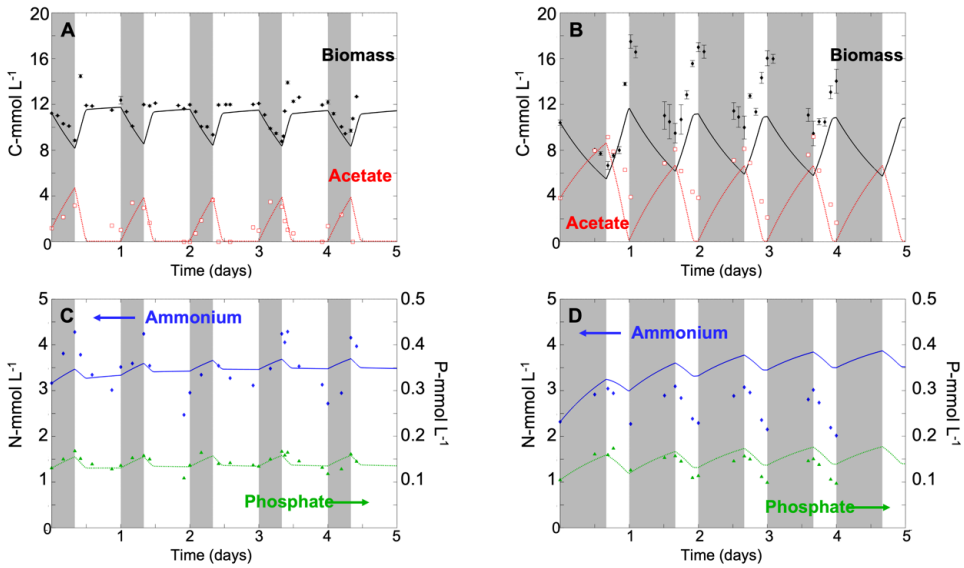

Figure 2. **Dynamics of biomass, acetate, ammonium and phosphate concentrations during light-dark diel cycles in continuous-flow cultures of Rhodopseudomonas palustris: (A and C) 16-h light / 8-h dark regime; (B and D) 8-h light / 16-h dark regime. Gray areas represent the dark periods, white areas the light periods. The measured concentrations of biomass (black circles) and acetate (red open squares) are displayed in panels A and B. The lines display the model simulations. The model was calibrated with the dataset of the 16-h light / 8-h dark and used to predict evolutions under the 8-h light / 16-h dark regime. In the first case, the biomass concentration achieved a stationary state, while acetate reached limiting residual concentrations 2 h after the start of the 16-h light periods. In the second case, the biomass increased without reaching a steady state during the shorter 8-h light periods, while acetate was not fully consumed. The measured concentrations of ammonium (blue diamonds) and phosphate (green triangles) are given in panels C and D, together with the model simulations. Concentrations of N and P were not limiting in any illumination phase.**

3.2 Carbon, nitrogen, and phosphorus assimilation

Under continuous illumination, no residual acetate was detected in the bulk liquid. Under 16 h of light, acetate was almost fully depleted, down to a concentration around 1 C-mmol L^{-1}. This was very well represented by the numerical model. Under 8 h of light, acetate was still present in the bulk liquid in concentrations ranging from 4 to 1.5 C-mmol L^{-1}. In this case, the model overestimated the rate of acetate consumption, *i.e.* predicting acetate depletion at the end of the light phase.

Nitrogen (N) and phosphorus (P) sources were provided in excess, and never became limiting. Under light, ammonium and phosphate were consumed, resulting in a decrease in their concentrations (Figure 2C,D). Under dark, the fed N and P accumulated in the liquid phase since not assimilated by the non-growing biomass. At the end of the dark phase, 3.6 ± 0.6 mmol N L^{-1} and 0.14 ± 0.01 mmol P L^{-1} remained the bulk liquid. N and P dynamics showed irregular behavior under 16 h light (Figure 2C). Therefore, the yields of ammonium ($Y_{N/X}$) and phosphate ($Y_{P/X}$) consumptions during growth were fitted on the 8-h light experiment (Figure 2D). The computed yields ($Y_{N/X}$ = 0.18 mol N C-mol^{-1} X, $Y_{P/X}$ = 0.009 mol P C-mol^{-1} X) were very close to the theoretical yields resulting from the elemental composition of *Rhodopseudomonas* biomass ($Y_{N/X}$ = 0.18 mol N C-mol^{-1} X, $Y_{P/X}$ = 0.014 mol P C-mol^{-1} X) that has been measured by McKinlay & Harwood (2010). With these yields, the N and P dynamics during the 8-h light cycles were well represented by the model: accumulation under dark and consumption by assimilation in the biomass growing under light.

3.3 CO_2 production follows the biomass growth patterns

The CO_2 production rate was constant at 0.075 ± 0.001 mmol h^{-1} during continuous illumination (Figure 3A): the chemostat achieved a stationary operation.

Under 16 h of light, CO_2 emission increased rapidly within the first hour, reaching 0.25 mmol h^{-1}, following the biomass growth rate with acetate uptake (Figure 3B). Once the acetate reached the minimal level, the CO_2 production also decreased to a stable level of 0.07 mmol h^{-1} after the second hour of illumination, reflecting the steady-state operation. The numerical model reproduced the observed trends during light phase, but the residual CO_2 production in the dark phase could not be explained numerically.

Under the 8-h light phases the CO_2 production did not achieve a steady state. In the light phase, the CO_2 production increased with 0.05 to 0.08 mmol h^{-1} during the cycles, reaching a peak after 4 h (0.88 ± 0.013 mmol h^{-1}), which was described qualitatively by the model (Figure 3C). The reason for the discrepancy between model and experimental data is the

larger computed rate of acetate consumption, which leads to a higher CO_2 formation rate in the model results.

In both illumination regimes, the CO_2 production dropped to the same stable value of 0.033 mmol h^{-1} during the dark phase. This residual baseline value of CO_2 in the off-gas under dark periods may relate to the detection limit of the online mass spectrometer (MS) instrument.

3.4 H_2 is produced only during the short light periods

A very low H_2 production was recorded during the continuous illumination with rates of around 0.004 mmol h^{-1} (Figure 3D). Occasionally, unexplained H_2 spikes were recorded, possibly relating to the background noise of the online MS.

During the 16-h light/8-h dark experiment, the emission of hydrogen in the dark was negligible and no specific production pattern was measured in the light (Figure 3E). The very low residual H_2 concentration may relate to an instrumental offset as well.

In contrast, H_2 was produced constantly during the 8-h light periods (Figure 3F), with an increase of 0.02 ± 0.01 mmol h^{-1} per cycle and reaching a maximum of 0.05 mmol h^{-1}. The biomass-specific rate of H_2 production under 8 h of light was 10 times higher (0.156 mmol H_2 h^{-1} g^{-1} DW) than under all other conditions (0.014 mmol H_2 h^{-1} g^{-1} DW). Under continuous illumination, H_2 production corresponded to about 0.008 mmol electrons L^{-1}, *i.e.*, 0.3% of the electrons supplied with the influent.

Under the 16-h light / 8-h dark periods, H_2 production accounted for 0.43 ± 0.28 % (in the light) and 0.33 ± 0.13 % (in the dark) of the electron balances. Under the 16-h dark periods, H_2 contribution made 0.70 ± 0.45 % of the electron balance. Under the 8-h light phases, H_2 made a more important contribution to the electron balance, reaching 2%, *i.e.*, higher than in all other phases (Table 4).

	Component	Acetate		Acetate		Biomass		CO_2	PHAs (as HB)	H_2	Σ out		Carbon balance	Electron balance
	Phase	Influent = Σ in		Effluent		Effluent		Off-gas	Effluent	Off-gas				
	Units	(C-mmol h^{-1})	(e^--mmol h^{-1})	(C-mmol h^{-1})	(e^--mmol h^{-1})	(C-mmol h^{-1})	(e^--mmol h^{-1})	(C-mmol h^{-1})	(e^--mmol h^{-1})	(e^--mmol h^{-1})	(C-mmol h^{-1})	(e^--mmol h^{-1})	(% C)	(% e^-)
	Illumination regime													
1)	24-h continuous light	0.66±0.05	2.69±0.40	<LOD[1]	<LOD[1]	0.58	2.654	0.070±0.001	<LOD[1]	0.008±0.004	0.65	2.662±0.004	**98%**	**99%**
2)	16-h light period	0.66±0.05	2.69±0.40	0.02±0.01	0.52±0.50	0.58±0.03	2.45±0.29	0.08±0.01	0.22±0.06	0.008±0.006	0.75±0.01	3.06±0.32	**115±2%**	**118±16%**
	8-h dark period			0.04±0.02	0.64±0.41	0.50±0.06	2.42±0.21	0.07±0.02	0.16±0.01	0.007±0.002	0.68±0.06	2.79±0.54	**103±9%**	**120±10%**
3)	8-h light period	0.61±0.006	2.44±0.05	0.28±0.03	1.26±0.60	0.57±0.14	2.44±0.60	0.07±0.01	0.28±0.09	0.04±0.02	0.97±0.05	4.03±1.21	**158±8%***	**154±17%***
	16-h dark period			0.19±0.07	0.96±0.46	0.57±0.16	2.84±0.72	0.03±0.002	0.31±0.11	0.02±0.02	0.79±0.15	4.12±1.29	**130±25%***	**158±23%***

Table 4. **Carbon (C-mmol h^{-1}; grey columns) and electron (e-mmol h^{-1}; white columns) balances under the different illumination regimes.**

[1] Limit of detection (LOD)

* The surpassing carbon and electron balances for the third illumination regime can be due to an overestimation of the biomass concentration. The absorbance measurements of biomass might have been influenced by the presence of PHAs inside the cells.

3.5 PHA production follows CO_2 formation under 16 h of light but not under 8 h of light

PHAs were not detectable under continuous illumination.

A PHB peak was detectable in the 16-h light phases, 2 h after the light switch (0.114 ± 0.013 C-mmol HB C-mmol^{-1} X) (Figure 3G), concomitantly to the peak of CO_2 production. The PHAs decreased constantly after the peak, reaching a baseline at 0.063 ± 0.001 C-mmol HB C-mmol^{-1} X. Under the 16-h light / 8-h dark cycles, PHA corresponded on average to 7% of the electron balance, regardless the illumination conditions. The numerical model caught well the PHAs accumulation during the first period of the 16-h light phases, followed by a decrease both under light and under dark conditions.

Under 8-h light / 16-h dark cycles (Figure 3H), PHA production did not present peaks, with an average production of 0.119 ± 0.015 C-mmol HB C-mmol^{-1} X, corresponding to 12% of the electron balance. About 1.7 times more PHAs were detectable in the dark phase of the 8-h light / 16-h dark regime than of the 16-h light / 8-h dark one. The numerical model indicated an oscillation in the PHA production that was not confirmed with experimental data (Figure 3H).

The diel light/dark regimes induced PHA formation. The longer light periods (16 h) generated a typical feast-famine behavior (Montiel Corona et al., 2017). The shorter light periods (8 h) resulted in a higher and more stable PHA content in the cells (Figure 3H).

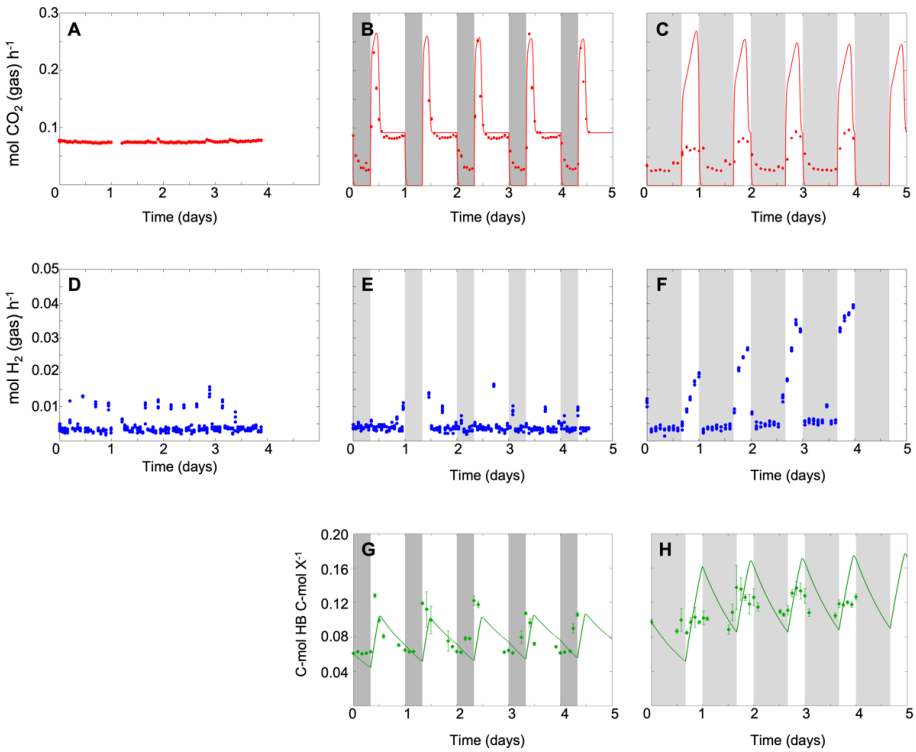

Figure 3. **Dynamics of CO_2, H_2 and PHA during light-dark cycles: (A and D) continuous illumination; (B, E and G) 16-h light / 8-h dark regime; (C, F and H) 8-h light / 16-h dark regime. Gray areas represent the dark periods, white areas the light periods. The measured (red circles) CO_2 production rates are displayed in panels A-C, together with the model simulations for the light/dark cycles (red lines). CO_2 production was constant during continuous illumination, but peaks appeared during light-dark cycles, correlating with the acetate uptake. The measured H_2 production rates (blue circles) are given in panels D-F, but were not modelled since H_2 contributed only to minor fractions of the electron balances. H_2 was produced at a constant low level during continuous illumination and 16-h light cycles. H_2 production significantly increased out of the instrumental noise of the online mass spectrometer during each light period of the 8-h light cycles. PHAs (green diamonds) were indirectly quantified in the light/dark experiments through sensitive fluorimetry measurements calibrated to PHA mol fractions (expressed as hydroxybutyrate, HB) in biomass, and modelled (green lines) (G-H). A PHA peak was measured at the start of each 16-h light phase. Under 8 h of light, PHA contents remained constantly at a higher level during light periods.**

4. Discussion

4.1 Acetate rather than light drives the metabolic responses of Rhodopseudomonas palustris

Light energy source is central for the catabolic processes in PNSB. Organic substrates are used as C-source for biomass synthesis and as electron donors. When no external electron acceptor is present, the difference in degree of reduction between substrate and biomass has to be balanced with internal processes of electron reallocation. The dynamics of the change in N and P concentrations were congruent with assimilation fore biomass formation and their measured yields were close to the elemental composition of *Rhodopseudomonas palustris* biomass ($C_1H_{1.8}O_{0.38}N_{0.18}P_{0.014}$) reported by McKinlay & Harwood (2010). Carbon balances closed for the continuous illumination experiment and for the 16-h light / 8-h dark experiment. This was not the case for the 8-h light / 16-h dark cycles where the over-assessed C-balances seemed to indicate a net production (Table 4). PHA granules that were always present in the cells under 8 h light / 16 h dark may have led to an absorbance overestimation of the biomass present in the reactor. The overestimation of the biomass consequently affected the electron balances as well.

Light/dark cycles occur daily in natural environments. Phototrophic organisms have adapted to cope with imbalances in energy supply. PNSB have higher biomass production under light/dark cycles (Koku et al., 2003; Zhi et al., 2019). H_2 production is increased under discontinuous illumination, following the biomass trend (Li et al., 2011; Wakayama et al., 2000).

Here, the light cycles are important not only for the energy that light provides, but most importantly for the illumination time available for the cultures to metabolize the nutrients. The light intensity at the surface of the reactor was 300 W m^{-2}. Considering the attenuation due to the biomass concentration and the reactor depth, the minimum calculated light available in the reactor was 180 W m^{-2} (Figure SI-3.1 in Supplementary information). Under any given condition, the available light intensity was not limiting the microbial metabolism since always exceeding the half-saturation coefficient for light (K_I) arbitrarily set at 10 W m^{-2} (Prachanurak et al., 2019). PNSB adapt the number and type of photosynthetic unit components based on the different light intensities (Brotosudarmo et al., 2011). However, Imam et al. (2015) have reported that light may be saturating for PNSB growth already from 100 W m^{-2} onward. We can therefore assume that the irradiance intensity used in our study during the light periods did not deeply affect the metabolic state of the cells.

The continuous cultivation system was initially set-up based on the stoichiometric and kinetic parameters derived from anaerobic,

photoorganoheterotrophic batches of the *Rhodopseudomonas palustris* isolate cultivated under the same medium, infrared irradiance and temperature conditions as the CSTR.
In the continuously illuminated chemostat, the biomass reached a steady-state, acetate was limiting (*i.e.*, low residual concentration), and the biomass growth rate equaled to the dilution rate (0.04 h^{-1}). Once the light/dark cycles were applied, a disturbance of the steady state was immediately observed.
Under long (16 h) illumination, the biomass consumed the acetate for growth and after an initial increase of the growth rate the steady-state conditions were restored for the remaining two thirds of the light cycles (with a specific growth rate again equal to the dilution rate).
Longer (16 h) dark periods led to an increased accumulation of acetate in the bulk liquid (twice as high as in the 8 h dark), since acetate was fed twice longer and there was no consumption in the dark. Due to the shorter light (8 h light) periods, acetate was not fully consumed at the end of the light phases. Therefore, acetate was no more growth-rate-limiting and the light period was too short to reach a steady state. The growth rate in the light phase exceeded the value of the imposed dilution rate, leading to a transient accumulation of biomass (Figure 2B).

The modelled biomass dynamics agreed with the measurements, fitting quantitatively the values for the 16-h light experiment, where the exact steady-state values were obtained. When using the same model parameters for the short (8 h) illumination experiment, the calculated amount of biomass formed during the light periods was underestimated. The disagreement may be related to the carbon imbalance reported in Table 4. A longer illumination phase would allow the biomass to reach exactly the same steady state as in the longer light period experiment (Figure SI-3 in Supplementary information) after about 10 h of light and acetate attained the minimum.

The average volumetric rate of acetate consumption was 0.08 C-mol h^{-1} L^{-1} under 16 h of light and 0.15 C-mol h^{-1} L^{-1} under 8 h of light (Figures SI-3.2 in Supplementary information). Initially, the biomass grew at the maximum substrate uptake rate. If the light phase was too short (as in the 8-h light periods), acetate was not fully consumed (residual of 2.5 ± 1.1 C-mmol L^{-1}) and the biomass grew at its maximum growth rate (0.15 h^{-1}).

4.2 The PHA synthesis patterns reflect the metabolic state of the Rhodopseudomonas cells

PHAs can be formed under dynamic conditions or because of imbalance in the degree of reduction between the biomass and carbon source. PHAs constitute carbon, electron and energy stocks for microorganisms surviving dynamic environments (van Aalst-van Leeuwen et al., 1997; Van Loosdrecht et al., 1997). In 24-h continuously irradiated chemostat conditions, carbon was

continuously fed to the cultures and cells did not store PHAs. PHAs synthesis in PNSB has primarily been reported under nitrogen limitation, as an intrinsic mechanism for the redistribution of carbon excess. PHAs accumulation is conventionally reported for PNSB under growth-limiting conditions (Braunegg et al., 1998; Narancic et al., 2016) when the carbon/electron sources are available but the nutrients (such as N, P or S) needed to produce cellular components are limited, resulting in the accumulation of acetyl coenzyme A (acetyl-CoA) in the cells.

During the anabolic reactions, *Rhodopseudomonas* incorporates acetate in the form of acetyl-CoA and releases at the same time the coenzyme A (CoA). In highly active cells, the levels of acetyl-CoA are low, but the levels of CoA are high. In contrast, in non-growing cells, acetyl-CoA is not utilized in anabolic processes and accumulates in the cells (McKinlay et al., 2014). A high acetyl-CoA to CoA ratio and the presence of NADPH are required for the initiation of the PHA pathway (Satoh et al., 2003).

The ratio between carbon sources and other nutrients is important to maintain the balance between substrate uptake rate and growth rate. The composition of the inflow of the CSTR was defined based on the biomass composition of PNSB reported by Puyol et al. (2017): a C:N ratio of 5.68:1 mol C-acetate mol^{-1} $N\text{-}NH_4^+$ was used in the medium. Nitrogen was provided in excess preventing N-limitation imbalance. Consequently, under continuous illumination, no production of PHAs was detected.

After a period of darkness, the biomass was transiently subjected to an excess of light and nutrients (acetate, ammonium, phosphate) resulting in an increased substrate uptake rate. For the first 2 h after switching on the 16-h light phase, the growth rate was close to the previously measured μ_{max} of 0.15 h^{-1}. After 3 h, when acetate became limiting, the growth rate stabilized again at the dilution rate value of 0.04 h^{-1}. When shorter (8 h) light periods were applied, the initial growth rate was around 0.1 h^{-1}. Under both conditions, cells exhibited growth rates close to μ_{max}. This resulted in the production of reducing power, which became in excess, and had to be reallocated. As reported by Kanno et al. (2018), the photosynthetic units are not disassembled in the dark, even under starvation. These are readily available, once the light conditions are restored, to produce ATP and NADH for the biosynthetic processes. This, linked to the prompt availability of the enzymes for PHA formation that are constitutively expressed (Kranz et al., 1997), leads to the immediate production of PHAs. Under 16 h light, a peak of PHB was observed 2 h after the light switch, but it decreased to baseline steady-state levels once the growth rate stabilized again at the dilution rate of 0.04 h^{-1}. The PHB decreased and no H_2 production was observed. Cells reached a maximal capacity of substrate uptake, though not coupled to a

maximal growth rate, similarly to what is described in Krishna & Van Loosdrecht (1999).

Under 8-h light / 16-h dark cycles, acetate was not completely consumed during illumination and increasingly accumulated in the bulk liquid during the dark phases. This resulted in a further imbalance in the redox state of the cells. The redox imbalance generated by the continuous presence of acetate, rather than the illumination conditions alone, led to a more constant production of PHAs. The cells were highly active, with a growth rate close to the maximal growth rate, leading to a low availability of CoA that resulted in PHA formation.

4.3 H_2 production is a secondary pathway of electron dissipation

The H_2 production rates here reported were low compared to other studies that have exposed PNSB to similar light intensities (Imam et al., 2015). However, our experimental conditions were not designed to stimulate H_2 production. H_2 can be produced either via the nitrogenase system, either via the ferredoxin-hydrogenase system. Ammonium is known to inhibit N_2 fixation in photosynthetic bacteria. It also effectively prevents photoproduction of H_2, due to inhibition and inactivation of nitrogenase (Basak et al., 2014). The presence of ammonium in non-limiting amounts in the medium indicated that potentially H_2 production was driven by the hydrogenase rather than by the nitrogenase. The molar C:N ratio (5.7) was 7 times lower than in most other studies on H_2 production (average C:N ratio 40) (Koku et al., 2002). Nonetheless, the H_2 production rate per gram biomass during the 8-h light phases was around 11 times higher than in all other conditions tested here (0.156 *vs.* 0.014 mmol h^{-1} g^{-1} DW). H_2 contribution to the electron balance was therefore 3 to 7 times higher in the 8-h light phases than in all other conditions, indicating that H_2 production acts as further electron dissipation pathway. A similar H_2 production pattern under alternating irradiation in PNSB cultures has been found (Adessi et al., 2012), with H_2 production only during the light phases. H_2 production was not integrated in the numerical model, since H_2 did not contribute significantly to the stoichiometric balance and kinetics (0.87 ± 0.78 % of the electron balance).

The absence of relevant H_2 production during 16 h of light (0.0040 ± 0.0004 mmol H_2 h^{-1} or 0.75 ± 0.01 mmol electrons h^{-1}) and the low but constant H_2 production during 8 h of light (0.025 ± 0.009 mmol H_2 h^{-1} or 0.97 ± 0.05 mmol electrons h^{-1}) indicates that the H_2 sink did not play a major role in the electron redistribution patterns in these experiments.

5. Conclusions

Overall, PNSB are one of the most versatile guilds of microorganisms, whose metabolisms are impacted by dynamics in environmental conditions such as light/dark diel cycles. We elucidated the mechanisms of electron allocation using quantitative biotechnology by involving a continuous culture of the representative PNSB *Rhodopseudomonas palustris* isolated from an in-house enrichment and metabolic modelling.

It can be concluded from this work that:

1. Under light-saturating conditions and continuous-flow reactor regime, durations of light and dark phases in a 24-h diel cycle set the availability of substrate and the achievement of a steady state in the photoorganoheterotrophic metabolism of *Rhodopseudomonas*. Longer dark phases (16 h) result in an excess of substrate available at the start ofthe light phase for biomass growth. Longer light phases (16 h) lead to substrate limitation and steady conditions.
2. Even in actively growing *Rhodopseudomonas* cells, carbon allocation is in place, namely toward PHA production.
3. In growing cells, H_2 production during illumination was a minor electron sink and secondary to PHA production, under the experimental conditions tested.
4. The numerical mathematical model caught the evolution trends in biomass, nutrient and PHAs dynamics measured during the light/dark cycles of different durations (16/8 *vs.* 8/16 h), as well as the CO_2 production and peaks emitted in the 16-h light periods. It allowed for determining stoichiometric and kinetic parameters of *Rhodopseudomonas palustris*.

References

Adessi, A., Torzillo, G., Baccetti, E., & De Philippis, R. (2012). Sustained outdoor H 2 production with Rhodopseudomonas palustris cultures in a 50 L tubular photobioreactor. *International Journal of Hydrogen Energy*, *37*(10), 8840–8849. https://doi.org/10.1016/j.ijhydene.2012.01.081

Alloul, A., Wuyts, S., Lebeer, S., & Vlaeminck, S. E. (2019). Volatile fatty acids impacting phototrophic growth kinetics of purple bacteria: Paving the way for protein production on fermented wastewater. *Water Research*, *152*, 138–147. https://doi.org/10.1016/j.watres.2018.12.025

Altschul, S. F., Gish, W., Miller, W., Myers, E. W., & Lipman, D. J. (1990). Basic local alignment search tool. *Journal of Molecular Biology*, *215*(3), 403–410. https://doi.org/10.1016/S0022-2836(05)80360-2

Basak, N., Jana, A. K., Das, D., & Saikia, D. (2014). Photofermentative molecular biohydrogen production by purple-non-sulfur (PNS) bacteria in various modes: The present progress and future perspective. *International Journal of Hydrogen Energy*, *39*(13), 6853–6871. https://doi.org/10.1016/j.ijhydene.2014.02.093

Blankenship, R., Madigan, M., & Bauer, C. (1995). *Anoxygenic Photosynthetic Bacteria* (R. E. Blankenship, M. T. Madigan, & C. E. Bauer (eds.); Vol. 2). Springer Netherlands. https://doi.org/10.1007/0-306-47954-0

Braunegg, G., Lefebvre, G., & Genser, K. F. (1998). Polyhydroxyalkanoates, biopolyesters from renewable resources: Physiological and engineering aspects. *Journal of Biotechnology*, *65*(2–3), 127–161. https://doi.org/10.1016/S0168-1656(98)00126-6

Brotosudarmo, T. H. P., Collins, A. M., Gall, A., Roszak, A. W., Gardiner, A. T., Blankenship, R. E., & Cogdell, R. J. (2011). The light intensity under which cells are grown controls the type of peripheral light-harvesting complexes that are assembled in a purple photosynthetic bacterium. *Biochemical Journal*, *440*(1), 51–61. https://doi.org/10.1042/BJ20110575

Cerruti, M., Stevens, B., Ebrahimi, S., Alloul, A., Vlaeminck, S. E., & Weissbrodt, D. G. (2020). *Enriching and aggregating purple non-sulfur bacteria in an anaerobic sequencing-batch photobioreactor for nutrient capture from wastewater*. https://doi.org/https://doi.org/10.1101/2020.01.08.899062 .

De Kreuk, M. K., Picioreanu, C., Hosseini, M., Xavier, J. B., & Van Loosdrecht, M. C. M. (2007). Kinetic model of a granular sludge SBR: Influences on nutrient removal. *Biotechnology and Bioengineering*, *97*(4), 801–815. https://doi.org/10.1002/bit.21196

De Philippis, R., Ena, A., Guastiini, M., Sili, C., & Vincenzini, M. (1992). Factors affecting poly-β-hydroxybutyrate accumulation in cyanobacteria and in purple non-sulfur bacteria. *FEMS Microbiology Letters*, *103*(2–4), 187–194. https://doi.org/10.1016/0378-1097(92)90309-C

Dupuis, A., Chevallet, M., Darrouzet, E., Duborjal, H., Lunardi, J., & Issartel, J. P. (1998). The Complex I from Rhodobacter capsulatus. *Biochimica et Biophysica Acta - Bioenergetics*, *1364*(2), 147–165. https://doi.org/10.1016/S0005-2728(98)00025-5

Gordon, G. C., & McKinlay, J. B. (2014). Calvin cycle mutants of photoheterotrophic purple nonsulfur bacteria fail to grow due to an electron imbalance rather than toxic metabolite accumulation. *Journal of Bacteriology*, *196*(6), 1231–1237. https://doi.org/10.1128/JB.01299-13

Green, J., & Paget, M. S. (2004). Bacterial redox sensors. *Nature Reviews Microbiology*, *2*(12), 954–966. https://doi.org/10.1038/nrmicro1022

Harwood, C. S. (2008). Nitrogenase-Catalyzed Hydrogen Production by Purple Nonsulfur Photosynthetic Bacteria. In *Bioenergy* (pp. 259–271). John Wiley & Sons, Ltd. https://doi.org/https://doi.org/10.1128/9781555815547.ch21

Haywood, G. W., Anderson, A. J., Chu, L., & Dawes, E. A. (1988). The role of NADH- and NADPH-linked acetoacetyl-CoA reductases in the poly-3-hydroxybutyrate synthesizing organism Alcaligenes eutrophus. *FEMS Microbiology Letters*, *52*(3), 259–264. https://doi.org/10.1111/j.1574-6968.1988.tb02607.x

Higuchi-Takeuchi, M., Morisaki, K., Toyooka, K., & Numata, K. (2016). Synthesis of high-molecular-weight polyhydroxyalkanoates by marine photosynthetic purple bacteria. *PLoS ONE*, *11*(8). https://doi.org/10.1371/journal.pone.0160981

Ho Lee, T., Park, J. Y., & Park, S. (2002). Growth of Rhodopseudomonas palustris under phototrophic and non-phototrophic conditions and its CO-dependent H2 production. *Biotechnology Letters*, *24*(1), 91–96. https://doi.org/10.1023/A:1013887715895

Hülsen, T., Hsieh, K., Lu, Y., Tait, S., & Batstone, D. J. (2018). Simultaneous treatment and single cell protein production from agri-industrial wastewaters using purple phototrophic bacteria or microalgae – A comparison. *Bioresource Technology*, *254*, 214–223.

https://doi.org/10.1016/j.biortech.2018.01.032
Hustede, E, Steinbiichel, A., & Schlegel, H. G. (1992). Cloning of poly(3-hydroxybutyric acid) synthase genes of Rhodobacter sphaeroides and Rhodospirillum rubrum and heterologous expression in Alcaligenes eutrophus. *FEMS Microbiology Letters*, *93*, 285–291.
Hustede, Eilert, Steinbüchel, A., & Schlegel, H. G. (1993). Relationship between the photoproduction of hydrogen and the accumulation of PHB in non-sulphur purple bacteria. *Applied Microbiology and Biotechnology*, *39*(1), 87–93. https://doi.org/10.1007/BF00166854
Imam, S., Fitzgerald, C. M., Cook, E. M., Donohue, T. J., & Noguera, D. R. (2015). Quantifying the effects of light intensity on bioproduction and maintenance energy during photosynthetic growth of Rhodobacter sphaeroides. *Photosynthesis Research*, *123*(2), 167–182. https://doi.org/10.1007/s11120-014-0061-1
Imhoff, J. F. (1995). Taxonomy and Physiology of Phototrophic Purple Bacteria and Green Sulfur Bacteria. In R. E. Blankenship, M. T. Madigan, & C. E. Bauer (Eds.), *Anoxygenic Photosynthetic Bacteria* (pp. 1–15). Kluwer Academic Publishers. https://doi.org/10.1007/0-306-47954-0_1
Kaewsuk, J., Thorasampan, W., Thanuttamavong, M., & Seo, G. T. (2010). Kinetic development and evaluation of membrane sequencing batch reactor (MSBR) with mixed cultures photosynthetic bacteria for dairy wastewater treatment. *Journal of Environmental Management*, *91*(5), 1161–1168. https://doi.org/10.1016/j.jenvman.2010.01.012
Kanno, N., Matsuura, K., & Haruta, S. (2018). Different metabolomic responses to carbon starvation between light and dark conditions in the purple photosynthetic bacterium, rhodopseudomonas palustris. *Microbes and Environments*, *33*(1), 83–88. https://doi.org/10.1264/jsme2.ME17143
Kim, J. S., Ito, K., & Takahashi, H. (1980). The Relationship between Nitrogenase Activity and Hydrogen Evolution in Rhodopseudomonas palustris. *Agricultural and Biological Chemistry*, *44*(4), 827–833. https://doi.org/10.1271/bbb1961.44.827
Koku, H., Eroglu, I., Gündüz, U., Yücel, M., & Türker, L. (2002). Aspects of the metabolism of hydrogen production by Rhodobacter sphaeroides. *International Journal of Hydrogen Energy*, *27*(11–12), 1315–1329. https://doi.org/10.1016/S0360-3199(02)00127-1
Koku, H., Eroglu, I., Gündüz, U., Yücel, M., & Türker, L. (2003). Kinetics of biological hydrogen production by the photosynthetic bacterium Rhodobacter sphaeroides O.U. 001. *International Journal of Hydrogen Energy*, *28*(4), 381–388. https://doi.org/10.1016/S0360-3199(02)00080-0
Kranz, R. G., Gabbert, K. K., Locke, T. A., & Madigan, M. T. (1997). Polyhydroxyalkanoate production in Rhodobacter capsulatus: genes, mutants, expression, and physiology. *Applied and Environmental Microbiology*, *63*(8), 3003–3009. https://doi.org/10.1128/AEM.63.8.3003-3009.1997
Krishna, C., & Van Loosdrecht, M. C. M. (1999). Effect of temperature on storage polymers and settleability of activated sludge. *Water Research*, *33*(10), 2374–2382. https://doi.org/10.1016/S0043-1354(98)00445-X
Kutralam-Muniasamy, G., Corona-Hernandez, J., Narayanasamy, R.-K., Marsch, R., & Pérez-Guevara, F. (2017). Phylogenetic diversification and developmental implications of poly-(R)-3-hydroxyalkanoate gene cluster assembly in prokaryotes. *FEMS Microbiology Letters*, *364*(13), 1–9. https://doi.org/10.1093/femsle/fnx135
Laguna, R., Tabita, F. R., & Alber, B. E. (2011). Acetate-dependent photoheterotrophic growth and the differential requirement for the Calvin–Benson–Bassham reductive pentose phosphate cycle in Rhodobacter sphaeroides and Rhodopseudomonas palustris. *Archives of Microbiology*, *193*(2), 151–154. https://doi.org/10.1007/s00203-010-0652-y
Li, X., Wang, Y., Zhang, S., Chu, J., Zhang, M., Huang, M., & Zhuang, Y. (2011). Effects of light/dark cycle, mixing pattern and partial pressure of H2 on biohydrogen production by Rhodobacter sphaeroides ZX-5. *Bioresource Technology*, *102*(2), 1142–1148. https://doi.org/10.1016/j.biortech.2010.09.015
Lip, K. Y. F., García-Ríos, E., Costa, C. E., Guillamón, J. M., Domingues, L., Teixeira, J., & van Gulik, W. M. (2020). Selection and subsequent physiological characterization of industrial Saccharomyces cerevisiae strains during continuous growth at sub- and- supra optimal temperatures. *Biotechnology Reports*, *26*, e00462. https://doi.org/10.1016/j.btre.2020.e00462
Madigan, M., Cox, J. C., & Gest, H. (1982). Photopigments in Rhodopseudomonas capsulata cells grown anaerobically in darkness. *Journal of Bacteriology*, *150*(3), 1422–1429. https://doi.org/10.1128/JB.150.3.1422-1429.1982
Madigan, M. T., Cox, J. C., & Gest, H. (1980). Physiology of dark fermentative growth of Rhodopseudomonas capsulata. *Journal of Bacteriology*, *142*(3), 908–915. https://doi.org/10.1128/jb.142.3.908-915.1980
Madigan, Michael T., Bender, K., Buckley, D., Sattley, M., & Stahl, D. (2015). Brock Biology of Microorganisms. In *Pearson* (Fourtheen, Vol. 1). Pearson. https://doi.org/10.1017/cbo9780511549984.016

Madigan, Michael T, & Jung, D. O. (2009). *An Overview of Purple Bacteria: Systematics, Physiology, and Habitats* (pp. 1–15). https://doi.org/10.1007/978-1-4020-8815-5_1

McKinlay, J. B., & Harwood, C. S. (2010). Carbon dioxide fixation as a central redox cofactor recycling mechanism in bacteria. *Proceedings of the National Academy of Sciences*, *107*(26), 11669–11675. https://doi.org/10.1073/pnas.1006175107

McKinlay, J. B., & Harwood, C. S. (2011). Calvin Cycle Flux, Pathway Constraints, and Substrate Oxidation State Together Determine the H 2 Biofuel Yield in Photoheterotrophic Bacteria. *MBio*, *2*(2). https://doi.org/10.1128/mBio.00323-10

McKinlay, J. B., Oda, Y., Rühl, M., Posto, A. L., Sauer, U., & Harwood, C. S. (2014). Non-growing Rhodopseudomonas palustris Increases the Hydrogen Gas Yield from Acetate by Shifting from the Glyoxylate Shunt to the Tricarboxylic Acid Cycle. *Journal of Biological Chemistry*, *289*(4), 1960–1970. https://doi.org/10.1074/jbc.M113.527515

Montano-Herrera, L., Laycock, B., Werker, A., & Pratt, S. (2017). The Evolution of Polymer Composition during PHA Accumulation: The Significance of Reducing Equivalents. *Bioengineering*, *4*(4), 20. https://doi.org/10.3390/bioengineering4010020

Montiel Corona, V., Le Borgne, S., Revah, S., & Morales, M. (2017). Effect of light-dark cycles on hydrogen and poly-β-hydroxybutyrate production by a photoheterotrophic culture and Rhodobacter capsulatus using a dark fermentation effluent as substrate. *Bioresource Technology*, *226*, 238–246. https://doi.org/10.1016/j.biortech.2016.12.021

Muyzer, G., Teske, A., Wirsen, C. O., & Jannasch, H. W. (1995). Phylogenetic relationships of Thiomicrospira species and their identification in deep-sea hydrothermal vent samples by denaturing gradient gel electrophoresis of 16S rDNA fragments. *Archives of Microbiology*, *164*(3), 165–172. https://doi.org/10.1007/BF02529967

Narancic, T., Scollica, E., Kenny, S. T., Gibbons, H., Carr, E., Brennan, L., Cagney, G., Wynne, K., Murphy, C., Raberg, M., Heinrich, D., Steinbüchel, A., & O'Connor, K. E. (2016). Understanding the physiological roles of polyhydroxybutyrate (PHB) in Rhodospirillum rubrum S1 under aerobic chemoheterotrophic conditions. *Applied Microbiology and Biotechnology*, *100*(20), 8901–8912. https://doi.org/10.1007/s00253-016-7711-5

Oda, Y., Samanta, S. K., Rey, F. E., Wu, L., Liu, X., Yan, T., Zhou, J., & Harwood, C. S. (2005). Functional Genomic Analysis of Three Nitrogenase Isozymes in the Photosynthetic Bacterium Rhodopseudomonas palustris. *Journal of Bacteriology*, *187*(22), 7784–7794. https://doi.org/10.1128/JB.187.22.7784-7794.2005

Padovani, G., Carlozzi, P., Seggiani, M., Cinelli, P., Vitolo, S., & Lazzeri, A. (2016). PHB-rich biomass and BioH2 production by means of photosynthetic microorganisms. *Chemical Engineering Transactions*, *49*, 55–60. https://doi.org/10.3303/CET1649010

Prachanurak, P., Chiemchaisri, C., Chiemchaisri, W., & Yamamoto, K. (2019). Modelling of biofilm growth for photosynthetic biomass production in a pipe-overflow recirculation bioreactor. *Biochemical Engineering Journal*, *142*(June 2018), 50–57. https://doi.org/10.1016/j.bej.2018.11.009

Puyol, D., Barry, E. M., Hülsen, T., & Batstone, D. J. (2017). A mechanistic model for anaerobic phototrophs in domestic wastewater applications: Photo-anaerobic model (PAnM). *Water Research*, *116*, 241–253. https://doi.org/10.1016/j.watres.2017.03.022

Sander, R. (2015). Compilation of Henry's law constants (version 4.0) for water as solvent. *Atmospheric Chemistry and Physics*, *15*(8), 4399–4981. https://doi.org/10.5194/acp-15-4399-2015

Satoh, Y., Tajima, K., Tannai, H., & Munekata, M. (2003). Enzyme-Catalyzed Poly(3-Hydroxybutyrate) Synthesis from Acetate with CoA Recycling and NADPH Regeneration in Vitro. *Journal of Bioscience and Bioengineering*, *95*(4), 335–341. https://doi.org/10.1263/jbb.95.335

Spero, A. M., Saheed, I., Daniel, R. N., & Donohuea, T. J. (2016). *Cytochrome Complexes: Evolution, Structures, Energy Transduction, and Signaling* (W. A. Cramer & T. Kallas (eds.); Vol. 41). Springer Netherlands. https://doi.org/10.1007/978-94-017-7481-9

Van Aalst-van Leeuwen, M. A., Pot, M. A., Van Loosdrecht, M. C. M., & Heijnen, J. J. (1997). Kinetic modeling of poly(β-hydroxybutyrate) production and consumption byParacoccus pantotrophus under dynamic substrate supply. *Biotechnology and Bioengineering*, *55*(5), 773–782. https://doi.org/10.1002/(SICI)1097-0290(19970905)55:5<773::AID-BIT7>3.0.CO;2-8

Van Loosdrecht, M. C. M., Pot, M. A., & Heijnen, J. J. (1997). Importance of bacterial storage polymers in bioprocesses. *Water Science and Technology*, *35*(1), 41–47. https://doi.org/10.2166/wst.1997.0008

Vermeer, C. M., Rossi, E., Tamis, J., Jonkers, H. M., & Kleerebezem, R. (2021). From waste to self-healing concrete: A proof-of-concept of a new application for polyhydroxyalkanoate. *Resources, Conservation and Recycling*, *164*. https://doi.org/10.1016/j.resconrec.2020.105206

Vincenzini, M., Marchini, A., Ena, A., & De

Philippis, R. (1997). H2 and poly-β-hydroxybutyrate, two alternative chemicals from purple non sulfur bacteria. *Biotechnology Letters*, *19*(8), 759–762. https://doi.org/10.1023/A:1018336209252

Wakayama, T., Nakada, E., Asada, Y., & Miyake, J. (2000). Effect of Light/Dark Cycle on Bacterial Hydrogen Production by Rhodobacter sphaeroides RV. *Applied Biochemistry and Biotechnology*, *84–86*(1–9), 431–440. https://doi.org/10.1385/ABAB:84-86:1-9:431

Wang, H., Yang, A., Zhang, G., Ma, B., Meng, F., Peng, M., & Wang, H. (2017). Enhancement of carotenoid and bacteriochlorophyll by high salinity stress in photosynthetic bacteria. *International Biodeterioration and Biodegradation*, *121*, 91–96. https://doi.org/10.1016/j.ibiod.2017.03.028

Willison, J. C., Jouanneau, Y., Colbeau, A., & Vignais, P. M. (1983). H2 metabolism in photosynthetic bacteria and relationship to N2 fixation. *Annales de l'Institut Pasteur / Microbiologie*, *134*(1), 115–135. https://doi.org/10.1016/S0769-2609(83)80100-8

Wolf, G., Picioreanu, C., & van Loosdrecht, M. C. M. (2007). Kinetic Modeling of Phototrophic Biofilms: The PHOBIA Model. *Biotechnology and Bioengineering*, *97*, 1064–1079. https://doi.org/10.1002/bit

Zhi, R., Yang, A., Zhang, G., Zhu, Y., Meng, F., & Li, X. (2019). Effects of light-dark cycles on photosynthetic bacteria wastewater treatment and valuable substances production. *Bioresource Technology*, *274*, 496–501. https://doi.org/10.1016/j.biortech.2018.12.021

Zuriani, R., Vigneswari, S., Azizan, M. N. M., Majid, M. I. A., & Amirul, A. A. (2013). A high throughput Nile red fluorescence method for rapid quantification of intracellular bacterial polyhydroxyalkanoates. *Biotechnology and Bioprocess Engineering*, *18*(3), 472–478. https://doi.org/10.1007/s12257-012-0607-z

Supplementary material

Appendix 1: Calibration line translating the PHA contents measured as fluorescent counts per C-mmol biomass into mol fractions of PHAs in the *Rhodopseudomonas* biomass (C-mmol$_{HB}$ C-mmol$_X^{-1}$).

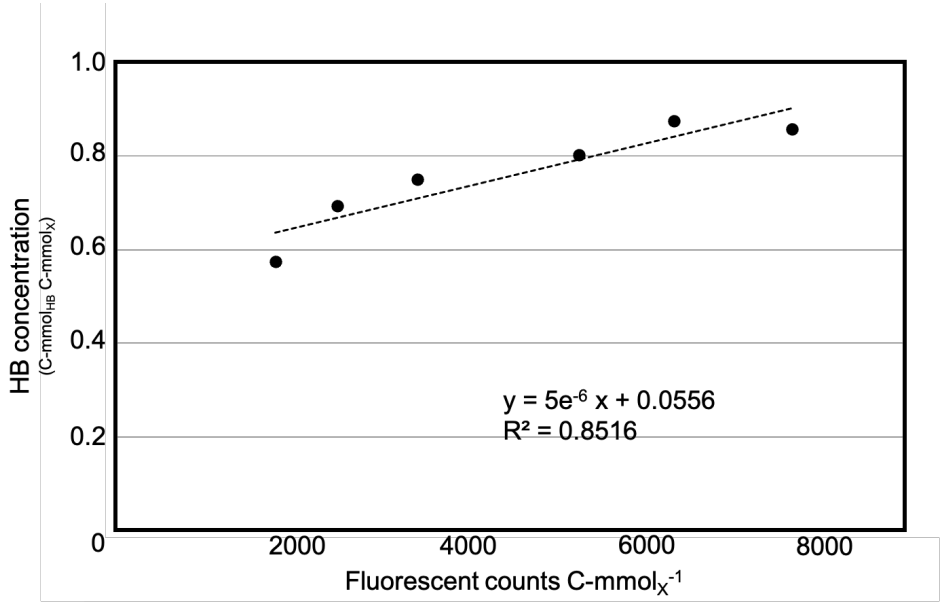

Figure SI-1**: regression between fluorescent counts and C-mol$_{HB}$ C-mol$_X^{-1}$.**

To determine the HB content, *Rhodopseudomonas* was inoculated in the media and cultivated as in Materials and Methods. After one week of incubation, half of the biomass was centrifuged for 15 min at 10000 *x g* and separated from the supernatant. The biomass was re-incubated for one week in the same media but deprived of the nitrogen sources to promote HB accumulation. The other half of the biomass was centrifuged and stored at -20°C until further manipulation after addition of formaldehyde to stop all metabolic activity. To measure the PHA in the cells, the biomass grown in the complete medium was mixed with the one grown under N-limiting conditions in the following ratio:
1:0, 1:1, 1:4, 1:9, 1:18, 0:1 N-limited : non-limited.
For each point of the dilution series, 1 mL of sample was used for Nile-red staining as in the Material and Methods.
All the remaining biomass was freeze-dried and PHAs were quantified according to Vermeer et al., 2021.
The conversion factor between the fluorescent counts g^{-1} DW and the mass fraction mg HB g^{-1} DW was calculated from the regression slope here presented.

Appendix 2: CO_2 solubility

SI-2.1 Estimation of the kLa of gas compounds in the process

The calculation of the volumetric mass transfer coefficient for CO_2 was performed considering the equation for salt solutions (Platas Barradas et al., 2011):

$$k_La\ (s^{-1}) = 0.002 \cdot \left(\frac{P}{V_{liquid}}\right)^{0.7} \cdot u_{gas}^{0.4}$$

where P is the agitation power input (W), V_{liquid} is the bulk liquid volume (m^3), and u_{gas} is the superficial gas velocity ($m \cdot s^{-1}$).

The agitation power input P was calculated through the following equation:

$$P = \rho \cdot N_p \cdot N_i^3 \cdot D_i^5$$

where ρ is the density (kg m^{-3}) of the solution, N_p is the impeller power number, N_i is the impeller rotating speed (s^{-1}), and D_i is the impeller diameter (m).

The power number of the impeller N_p is a function of the impeller type and the Reynolds number Re of the impeller. Re was calculated through the following equation:

$$Re = \frac{\rho N_i D_i^2}{\mu}$$

where μ is the viscosity of the solvent (Pa·s).

Considering the density ρ (997 kg m^{-3}) and viscosity μ of water at 25 °C (0.00089 Pa·s), the Reynolds number Re of the impeller was slightly higher than 10^5 (-). For that Re value and for a 6-blade Rushton turbine impeller, the power number Ni was around 5~6 (-). For the calculations, a power number of 6 was assumed. The diameter of the impeller was around 4 cm and the rotating speed 350 rpm (5.83 s^{-1}). Using those values the power input of the impeller was found equal to 0.101 W.

The superficial gas velocity was calculated by dividing the gas flowrate F (7.14 $L \cdot h^{-1}$) with the surface area A ($= \pi \cdot R^2$). The reactor radius R was 5.5 cm, *i.e.,* 0.055 m. The calculated superficial gas velocity V_g was $2.09 \cdot 10^{-5}$ m s^{-1}.

Using the calculated values of the superficial gas velocity, power input and liquid volume ($1.2 \cdot 10^{-3}$ m^3) the k_La of carbon dioxide was calculated equal to 32 (h^{-1}) through the following equation. The diffusion coefficient used are $1.92 \cdot 10^{-5}$ cm^2 s^{-1}.

$$kLa_x = \frac{kLa_{CO_2}}{\sqrt{\frac{D_{CO_2}}{D_x}}}$$

SI-2.2

The maximum dissolved CO_2 concentration (was calculated in function of the measured CO_2 concentration in the gas phase ($C_{C,g,}$ mmol CO_2 L^{-1} gas), the Henry's coefficient (H_C, mol $L^{-1}atm^{-1}$), the respective temperatures (T) of 20ºC in dark and 30ºC under light, and pressure (1 atm) (SI-2.2).

$$C^*_{C,L} = H_C \cdot 1000 \cdot C_{C,g} \cdot T \cdot R \cdot \frac{1}{101325} \text{ (mol m}^{-3}\text{)}$$

With T the temperature (ºK), R the gas constant (8.314 J mol^{-1} K^{-1}) and H_C the Henry's constant at higher temperature, calculated as

$$H_C = H^{\circ} \cdot \exp\left[\frac{\Delta H}{R} \cdot \left(\frac{1}{T} - \frac{1}{T_0}\right)\right]$$

With H the Henry's constant for CO_2 at 298 K (0.0340 mol L^{-1} atm^{-1}), ΔH the enthalpy of dissolution, and T and T_0 the temperatures.

Appendix 3: Mathematical model simulations

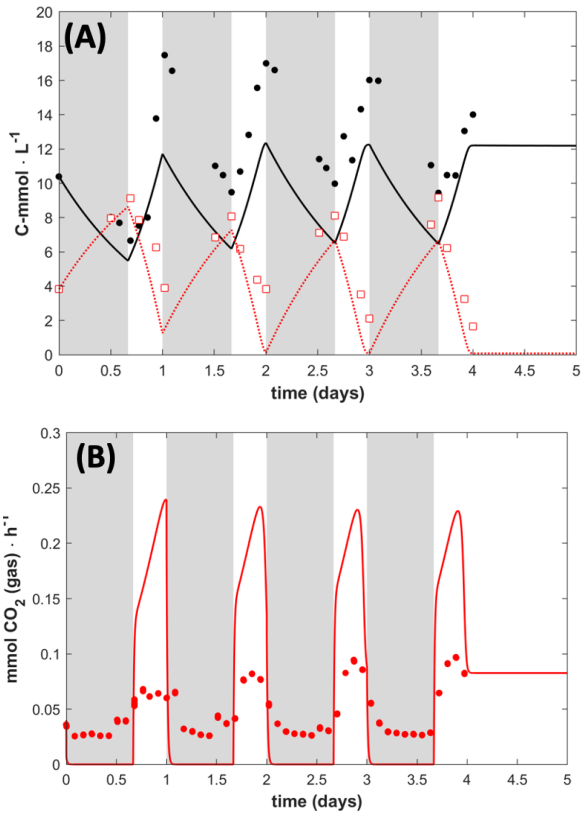

Figure SI-3.1. **Data and simulation with an additional extended light phase after the 8-h light / 16-h dark cycles. (A) Biomass (black circles) and acetate (red open squares) measured concentrations, with lines being the model results. (B) Measured (red circles) and model prediction (line) of the CO_2 production rate A steady state is reached once the concentration of acetate is at its minimum.**

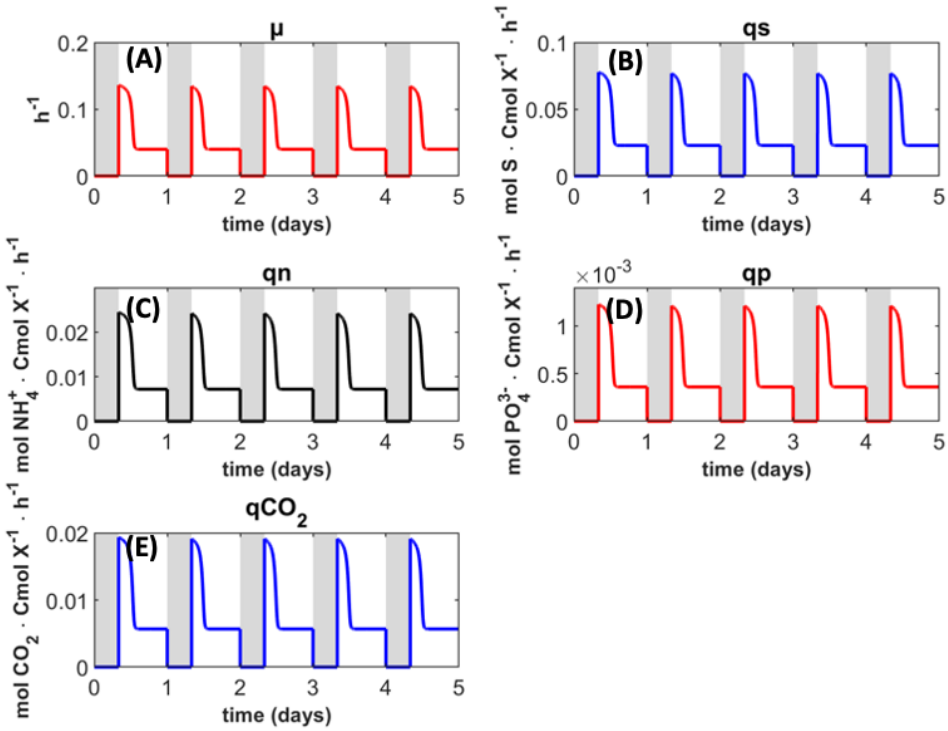

Figure SI-3.2. **Model results for production and uptake rate in the 16 h light / 8 h dark cycles. (A) specific growth rate. (B specific acetate uptake rate. (C) specific ammonium uptake rate. (D) specific phosphate uptake rate. (E) specific CO_2 production rate.**

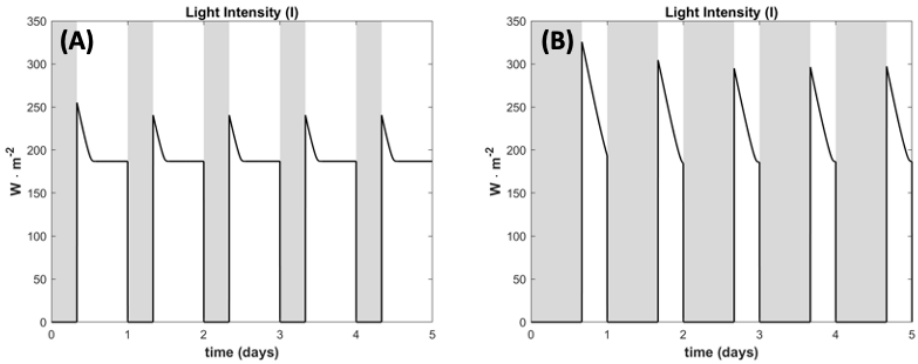

Figure SI-3.3. **Model results for the light intensity inside the reactor. (A) 16 h light / 8 h dark cycles. (B) 8 h light / 16 h dark cycles. Under any given condition light became a limiting factor.**

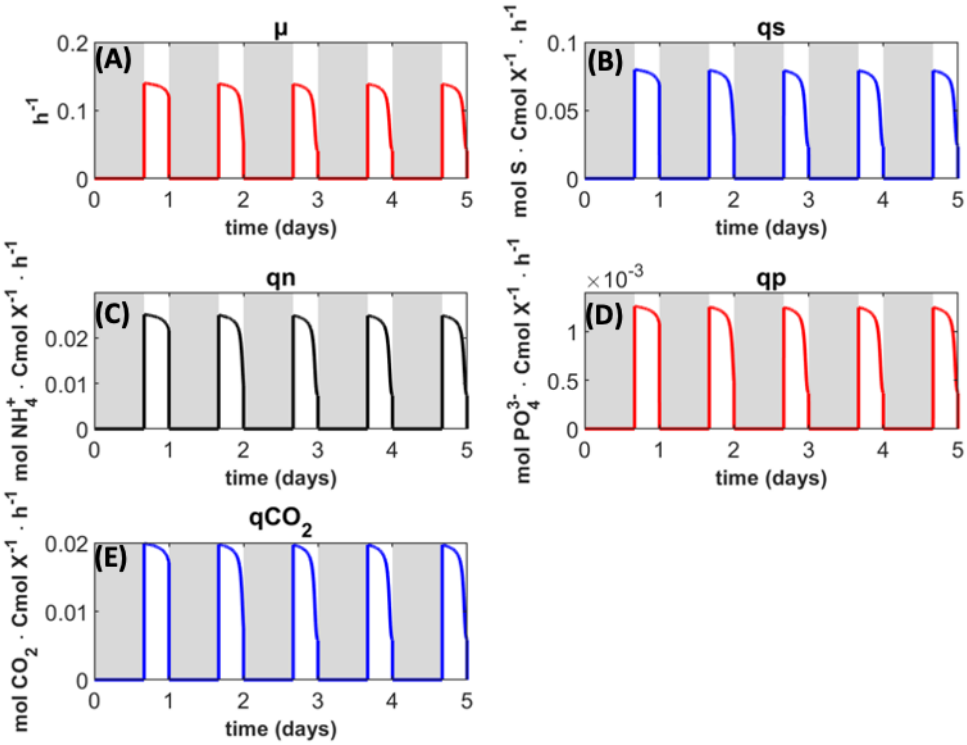

Figure SI-3.4. **Model results for production and uptake rate in the 8 h light / 16 h dark cycles. (A) specific growth rate. (B specific acetate uptake rate. (C) specific ammonium uptake rate. (D) specific phosphate uptake rate. (E) specific CO_2 production rate.**

References SI

Platas Barradas, O., Jandt, U., Da Minh Phan, L., Villanueva, M., Rath, A., Reichl, U., Schräder, E., Scholz, S., Noll, T., Sandig, V., Pörtner, R., & Zeng, A.-P. (2011). Criteria for bioreactor comparison and operation standardisation during process development for mammalian cell culture. *BMC Proceedings*, *5*(S8), P47. https://doi.org/10.1186/1753-6561-5-s8-p47

Vermeer, C. M., Rossi, E., Tamis, J., Jonkers, H. M., & Kleerebezem, R. (2021). From waste to self-healing concrete: A proof-of-concept of a new application for polyhydroxyalkanoate. *Resources, Conservation and Recycling*, *164*. https://doi.org/10.1016/j.resconrec.2020.105206

Chapter 3

Enrichment and aggregation of purple non-sulfur bacteria in a mixed-culture sequencing-batch photobioreactor for biological nutrient removal from wastewater

This chapter is published in a modified version as original research article with contributions of: Marta Cerruti, Berber Stevens, Sirous Ebrahimi, Abbas Alloul, Siegfried E. Vlaeminck, David G. Weissbrodt (2020) Enriching and aggregating purple non-sulfur bacteria in an anaerobic sequencing-batch photobioreactor for nutrient capture from wastewater. *Frontiers in Bioengineering and Biotechnology*, 8, 557234. https://doi.org/10.3389/fbioe.2020.557234

Abstract

Mixed-culture biotechnologies are widely used to capture nutrients from wastewater. Purple non-sulfur bacteria (PNSB), a guild of anoxygenic photomixotrophic organisms, raise interest for their ability to directly assimilate nutrients in the biomass. One challenge targets the aggregation and accumulation of PNSB biomass to separate it from the treated water. Our aim was to enrich and produce a concentrated, fast-settling PNSB biomass with high nutrient removal capacity in a 1.5-L, stirred-tank, acetate-fed, anaerobic sequencing-batch photobioreactor (SBR). PNSB were rapidly enriched after inoculation with activated sludge at 0.1 gVSS L^{-1} in a first batch of 24 h under continuous irradiance of infrared (IR) light (>700 nm) at 375 W m^{-2}, with *Rhodobacter* reaching 54% of amplicon sequencing read counts. SBR operations with decreasing hydraulic retention times (48 to 16 h, *i.e.*, 1 to 3 cycles d^{-1}) and increasing volumetric organic loading rates (0.2 to 1.3 kg COD d^{-1} m^{-3}) stimulated biomass aggregation, settling, and accumulation in the system, reaching as high as 3.8 g VSS L^{-1}. The sludge retention time (SRT) increased freely from 2.5 to 11 d. Acetate, ammonium, and orthophosphate were removed up to 96% at a rate of 1.1 kg COD d^{-1} m^{-3}, 77% at 113 g N d^{-1} m^{-3}, and 73% at 15 g P d^{-1} m^{-3}, respectively, with COD:N:P assimilation ratio of 100:6.7:0.9 m/m/m. SBR regime shifts sequentially selected for *Rhodobacter* (90%) under shorter SRT and non-limiting concentration of acetate during reaction phases, for *Rhodopseudomonas* (70%) under longer SRT and acetate limitation during reaction, and *Blastochloris* (10%) under higher biomass concentrations, underlying competition for substrate and photons in the PNSB guild. With SBR operations we produced a fast-settling PNSB biomass for nutrient capture from wastewater. This provided insights into the microbial ecology of PNSB-based processes for water resource recovery.

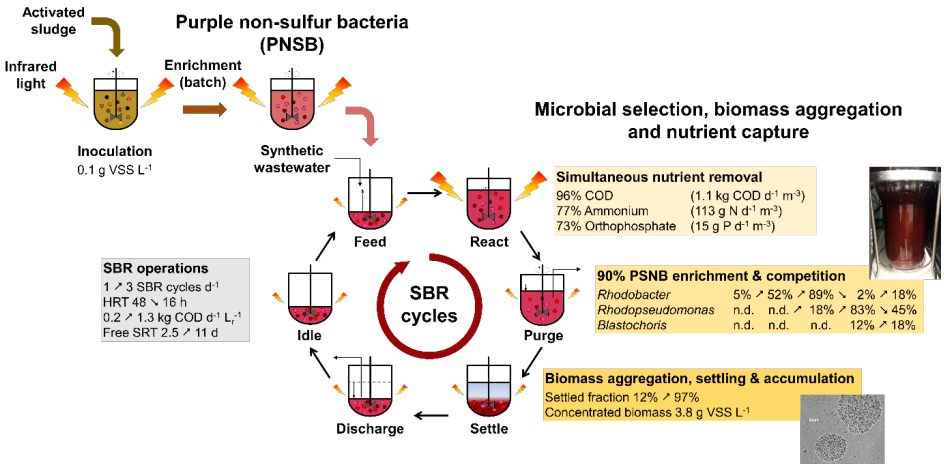

1. Introduction

Biological nutrient removal (BNR) is one of the main goals of wastewater treatment to safeguard aquatic ecosystems from anoxia and eutrophication. Water quality regulations become stricter on the limits of nutrient discharge and removal. European quality criteria target the following residual concentrations and removal of organic matter (125 mg COD_{Tot} L^{-1} and 75% removal; 25 mg BOD_5 L^{-1} and 70-90% removal), nitrogen (10-15 mg N_{Tot} L^{-1}, 70-80% removal), and phosphorus (1-2 mg P_{Tot} L^{-1}, 80% removal) (EUR-Lex, 1991; Guimarães et al., 2018). Besides conventional activated sludge systems, research and innovation target the use of novel microbial processes for water resource recovery (Alloul et al., 2018; Guest et al., 2009; Verstraete & Vlaeminck, 2011) on top of pollution control.

In the resource recovery context, purple non-sulfur bacteria (PNSB) can propel a sustainable treatment by capturing nutrient resources from used water (Daniel Puyol et al., 2017; Verstraete et al., 2016), valorizing waste into biomass, bioenergy, bulk chemicals, and biomaterials. PNSB form an attractive guild of phototrophic organisms with a facultative anaerobic and hyperversatile metabolism that allows them to grow under ever-changing environmental conditions (J.F. Imhoff, 2017; van Niel, 1944). They populate the surface of aquatic environments by absorbing the infrared (IR) spectrum of the sunlight (700-1200 nm) using carotenoids and bacteriochlorophylls, with a competitive advantage in a mixed-culture microbial ecosystem. PNSB can switch between photoorganoheterotrophy, photolithoautotrophy, respiratory or fermentative chemoorgano-heterotrophy, respiratory chemolithoautotrophy, and nitrogen fixation depending on the composition of electron donors and acceptors present in their surroundings (Madigan & Jung, 2009). This enables them to thrive on different pools of electron donors, recycle electrons, achieve redox homeostasis, and grow under alternation of light and dark (McEwan, 1994). PNSB ferment reduced organics into carboxylates in the dark, photoferment them into dihydrogen, or accumulate and condense them as intracellular storage polymers like biopolyesters (*e.g.*, poly-β-hydroxyalkanoates, PHAs) as electron sinks under nutrient limitations (Eilert Hustede et al., 1993). Rediscovering PNSB for ecotechnologies and nutrient capture goes via basic study of their metabolism and selection features from pure to mixed cultures, and eco-design to develop robust, non-axenic, and economically appealing processes (Bryant & Frigaard, 2006).

The potential of PNSB for converting diverse carbon sources such as volatile fatty acids (acetate, malate, butyrate and propionate), sugars or alcohols, has been screened with isolates (Alloul *et al.*, 2019; Madigan & Gest, 1979a; Stoppani *et al.*, 1954), underlying the potential of populations of this guild for water treatment. PNSB can assimilate carbon (C), nitrogen (N), and phosphorus (P) from wastewater at COD:N:P ratio of 100:7:2 versus 100:5:1 m/m/m for

activated sludge, with an elemental formula for purple phototrophic biomass given as $C_1H_{1.8}O_{0.38}N_{0.18}$ (degree of reduction of 4.5 mol e^- C-mol^{-1} X_{PPB}) (D. Puyol et al., 2017). Their photon-capturing and energy-recycling physiology lead PNSB to achieve rapid biomass specific maximum growth rates (μ_{max}) of 1.7 to 5.3 d^{-1} and biomass yields ($Y_{X/COD}$) on organic substrates (expressed as chemical oxygen demand, COD) of 0.6 to 1.2 g COD_X g^{-1} COD_S from mixed to pure cultures (Eroglu et al., 1999; Hülsen et al., 2014), involving additional electron sources from the bulk liquid phase . New-generation biological wastewater treatment processes aim to decrease sludge production and handling, by making use of slow-growing and low-yield microorganisms such as polyphosphate-accumulating and anammox bacteria. In contrast, the use of organisms with a high biomass yield such as PNSB is of definite interest to remove, capture and concentrate carbon, nitrogen and phosphorus nutrient resources out of the wastewater by assimilation into the biomass. The biomass can be then valorized to generate energy through methanization and to produce, *e.g.*, single-cell proteins (*i.e.*, source of microbial proteins), bioplastics via PHAs, and biohydrogen on concentrated streams (Honda et al., 2006; Daniel Puyol et al., 2017).

Technically, one important challenge of photobiotechnologies resides in the limitation of photon supply across the reactor bulk (Pulz, 2001), therefore, many PNSB-based processes have been operated at concentrations below 1 g VSS L^{-1}. Light limitation is often considered *a priori* as a killing factor for the process performance and economics, while such low biomass concentration can remain a drawback for the intensification of volumetric conversions.

Mixed-culture processes are actively investigated to harness the ability of PNSB to treat wastewater (Hülsen et al., 2016; Nakajima et al., 1997; Verstraete et al., 2016), starting from stabilization ponds (Almasi & Pescod, 1996; Freedman et al., 1983). Process configurations involved continuous up-flow system (Driessens et al., 1987), continuous-flow stirred tank reactor (Alloul et al., 2019), tubular reactor (Carlozzi et al., 2006), sequencing batch reactor (SBR) (Chitapornpan et al., 2012; Fradinho et al., 2013), membrane bioreactor (MBR) (Hülsen et al., 2016), and membrane sequencing batch reactor (MSBR) (Kaewsuk et al., 2010). One challenge in the application of PNSB organisms is considered to remain in the solid-liquid (S/L) separation of the biomass from the aqueous stream. Decoupling the hydraulic (HRT) and solid (SRT) retention times is crucial to retain the biomass in the process.

The use of membrane filtration has been recommended because PNSB have been hypothesized to primarily grow in suspension for catching photons and to settle slowly (Chitapornpan et al., 2012). However, membranes are intended to separate biomass from the treated wastewater, but do not foster the formation of a good settling sludge. In the lab, MBRs are used to maintain biomass in

suspension (van der Star et al., 2008). A centrifugation step is still needed after the membrane filtration to efficiently concentrate and harvest the PNSB biomass downstream. Alternatives to MBRs can lead to capital and operational savings, since membrane filtration and fouling relate to substantial pumping energy and maintenance costs besides the use of plastic materials.

Intensification of PNSB-based environmental biotechnologies should be targeted by enhancing the bioaggregation and biofilm-forming ability of the biomass. Although previous works have not tailored SBR regimes to this end (Chitapornpan et al., 2012; Fradinho et al., 2013), the application of substrate gradients via SBR operation can be efficient to stimulate microbial aggregation and biomass accumulation. Granulation of activated sludge biomasses in SBR systems has been the trigger of BNR process intensification (Aqeel et al., 2019; Pronk et al., 2015; M. K. H. Winkler et al., 2018). This should lead to an efficient S/L separation, resulting in lowering costs for downstream processing by potentially reducing the need for ultrafiltration and centrifugation to concentrate the biomass. A SBR design also offers operational flexibility (Wilderer, 1998) to manipulate reactor cycles and loading rates. Although offering less surface-to-volume ratio, the use of simple stirred-tank designs in SBR application can in addition lead to simpler scale-up than flat-sheet, tubular, or membrane-based processes.

Here, we investigated the possibility to develop a mixed-culture biotechnology process based on the enrichment of a concentrated and well-settling PNSB biomass out of activated sludge in a stirred-tank photobioreactor operated under SBR regime and continuously irradiated with IR light. Conditions to enrich and maintain a PNSB mixed culture were elucidated at bench scale, along with microbial competition in the PNSB guild. Biomass growth, aggregation, and composition were analysed along with volumetric rates of C-N-P removal. The here-examined microbial ecology insights and aggregation propensity of the PNSB guild can sustain the development of bioengineering strategies for mixed-culture process development in simple SBR design for wastewater treatment and resource recovery from aqueous nutrient streams.

2. Material and Methods

2.1 Cultivation medium

The composition of the cultivation medium was calculated based on stoichiometric requirements to sustain PNSB growth and complemented with other minerals. It was adapted from Kaewsuk et al. (2010) to meet with C-N-P anabolic requirements of PNSB. The stock solution consisted of (per liter): 0.914 g of $CH_3COONa \cdot 3H_2O$, 0.014 g of KH_2PO_4, 0.021 g of K_2HPO_4, 0.229 g of NH_4Cl, 0.200 g of $MgSO_4 \cdot 7H_2O$, 0.200 g of NaCl, 0.050 g of $CaCl_2 \cdot 2H_2O$, 0.100 g of yeast extract, 1 mL of vitamin solution, and 1 mL of trace metal so-

lution. The vitamin solution contained (per liter) 200 mg of thiamine–HCl, 500 mg of niacin, 300 mg of ρ-amino-benzoic acid, 100 mg of pyridoxine–HCl, 50 mg of biotin, and 50 mg of vitamin B12. The trace metal solution contained (per liter) 1100 mg of EDTA–2Na·2H_2O, 2000 mg of FeCl3·6H_2O, 100 mg of ZnCl2, 64 mg of $MnSO_4$·H_2O, 100 mg of H_3BO_3, 100 mg of $CoCl_2$·6H_2O, 24 mg of Na_2MoO_4·2H_2O, 16 mg of $CuSO_4$·5H_2O, 10 mg of $NiCl_2$·6H_2O, and 5 mg of $NaSeO_3$. Carbon sources (acetate) were separated from nitrogen and phosphate sources to avoid contaminations.

2.2 Anaerobic, sequencing-batch, photobioreactor setup

The PNSB enrichment was performed in a 1.5-L cylindrical, single-wall, glass, stirred-tank reactor (Applikon Biotechnology, Netherlands) (Figure 1.A). The reactor was inoculated at 0.1 g VSS L^{-1} of flocculent activated sludge taken from the BNR WWTP Harnaschpolder (the Netherlands) after washing the sludge with the cultivation medium 3 times. The reactor operated for 6 months under SBR regime at controlled temperature of 30 ± 1 °C and pH of 7.0 ± 1.0 on the cultivation medium.

To select for purple phototrophs and to avoid the proliferation of green phototrophs, the reactor was placed in a dark fume hood providing only IR light. A white light source was beamed with two halogen lamps (120 W, Breedstraler, GAMMA, Netherlands) placed at the side of the reactor and filtered for IR wavelengths (>700 nm) with two filter sheets (Black Perspex 962, Plasticstockist, UK) placed in front of the lamps. Irradiance was measured at the reactor surface with a pyranometer (CMP3, Kipp & Zonen, Netherlands) and set at a relatively high value of 375 W m^{-2} to promote PNSB enrichment and biomass growth.

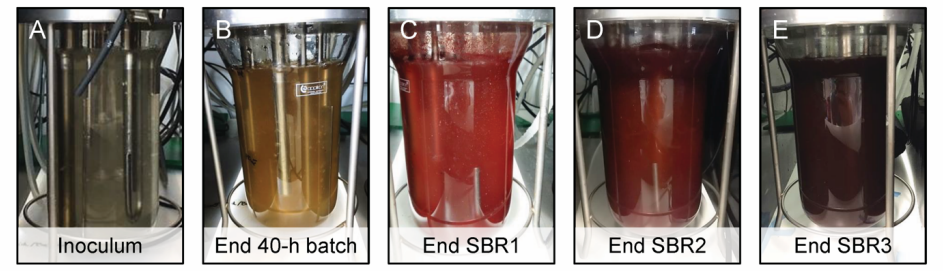

Figure 1. **Stirred-tank photobioreactor enriched in PNSB. The reactor was inoculated at 0.1 g VSS L^{-1} with BNR activated sludge. One initial batch of 40 h was used to activate the biomass and test the enrichment of PNSB prior to switching to SBR operation over 5 months.**

2.3 Anaerobic, sequencing-batch, photobioreactor operation

After a first 40-h period under batch regime to check for the selection of PNSB, the system was switched to an SBR regime, consisting of discharge, idle, feed and settling phases (Figure 1.B). Different cycle timings and HRT, reaction phase length, and COD loading rates were tested as followed in three operational modes. In *SBR1*, 24 cycles of 24 h each were applied (*i.e.*, 24 days of experiment), consisting of: biomass settling (3 h) effluent withdrawal (5 min), influent feeding (5 min), and reaction (20.75 h). In *SBR2*, the total length of the cycles was decreased 3-fold and set at 8 h. The reaction phase was shortened to 4.75 h, while all the other phases were maintained. The reactor was operated over 205 cycles. In *SBR3*, the cycle composition was maintained as in SBR2, while the COD concentration was doubled from 430 to 860 mg COD_{Ac} L^{-1} in the influent to prevent COD-limitations along the reaction phase. All SBRs were operated at a volume exchange ratio of 50%. The stepwise adaptation of the SBR operations from 1 to 3 cycles day^{-1} resulted in HRTs from 48 h (SBR1) to 16 h (SBR2 and SBR3) and in volumetric organic loading rates (OLRs) of 0.215 (SBR1) to 0.645 (SBR2) and 1.290 (SBR3) kg COD d^{-1} m^{-3} (Table 1). The sludge retention time (SRT) was let freely evolve across the SBR operations without controlled purge of the biomass, with median values ranging from 1.5 to 11 d as calculated from eq. 2 in Supplementary material 1, as a result of biomass accumulation.

The pH of the mixed liquor was controlled at 7.0 ± 1.0 by automatic addition of HCl or NaOH at 1 mol L^{-1} each. The bulk liquid was sparged with argon gas (quality 99.999%) to maintain anaerobic conditions, while continuously stirring at 378 rpm (potentiostat ADI 1012, Applikon, the Netherlands) during the reaction phase.

Table 1. **Operational conditions of the three SBR regimes across the experimental period. SBR1 was run with a 24-h cycle composed of 20.75 h of reaction time and with 257 ± 54 mg COD L^{-1} in the bulk liquid phase after feeding. In SBR2, the total cycle length was shortened to 8 h, with a reaction time of 4.75 h. In SBR3, the initial COD concentration was doubled compared to the first two SBRs. All SBRs were run at a volume exchange ratio of 50%.**

Process parameters	Units	SBR1	SBR2	SBR3
SBR cycles				
Number of SBR cycles per day	(-)	1	3	3
Reaction phase length per cycle	(h)	20.75	4.75	4.75
Discharge, idle, feeding phases lengths	(min)	5	5	5
Settling phase length	(h)	3	3	3
Retention times				
Hydraulic retention time (HRT)	(h)	48	16	16
Sludge retention time (SRT) [1]	(d)	1.5	7.2	10.6
Loadings				
Volumetric organic loading rate (OLR)	(g COD d^{-1} L_r^{-1})	0.215	0.645	1.29
C:N:P ratio in the influent	(m / m / m)	100 : 35.8 : 3.8	100 : 35.8 : 4.2	100 : 11.2 : 1.7
Measured initial concentrations in the bulk liquid phase at the beginning of reaction phases				
Acetate	(mg COD L^{-1})	257 ± 54	232 ± 18	443 ± 76
Ammonium	(mg N-NH_4^+ L^{-1})	92 ± 21	83 ± 16	49 ± 17
Orthophosphate	(mg P-PO_4^{3+} L^{-1})	9.7 ± 1.3	9.9 ± 3.3	7.7 ± 1.1

[1] The sludge retention time (SRT) was let freely evolve over the experimental period. The reactor was operated without purge of biomass. The SRT increased as a result of biomass accumulation in the reactor. The median value over each SBR period is provided. The distributions of SRT are displayed in Figure 2 and detailed evolutions in Supplementatry material 3.

2.4 Analytical methods to measure growth and nutrient consumptions

2.4.1 Measurements of biomass growth and nutrient concentrations

Biomass growth was monitored spectrophotometrically by absorbance at a wavelength of 660 nm (DR3900, Hach, Germany) 4-5 times a week (Supple-mentary material 2), and gravimetrically by quantifying the concentration of volatile suspended solids (VSS) as described in experimental methods for wastewater treatment (van Loosdrecht et al., 2016). For the 40-batch and SBR1, absorbance measurements were adequate since the biomass was low in concentration and in suspension.

For SBR2 and SBR3, the biomass aggregated and VSS measurements were much more accurate.
The consumption of the dissolved nutrients was monitored by sampling the mixed liquor at the beginning and end of the reaction phase, after centrifugation (5 min, 17000 x g) and filtration of the supernatant on 0.45-µm filters (Millex-HV, PVDF, Germany). The concentrations of COD, ammonium (as $N\text{-}NH_4^+$) and orthophosphate (as $P\text{-}PO_4^{3-}$) were measured by colorimetric assays (LCK kits no. 114/614/COD, 302/303/ammonium, 348/350/phosphate; Hach-Lange, Dusseldorf, Germany) followed by spectrophotometry (DR3900, Hach, Germany). The COD colorimetric method measured all oxidizable substances (here notably acetate, yeast extract, and EDTA from the trace element solution). As technical control, samples were measured in triplicates and the relative standard deviation was 0.5 - 1.9%.

2.4.2 Computations of microbial conversions and extraction of growth parameters

All symbols and equations used to compute microbial conversions and extraction of growth parameters are available in Supplementary material 1.
In short, the average percentage of removal (η_S, %), total rate of nutrient removal (R_S, kg S d^{-1}), apparent volumetric rate of removal of nutrients (r_S, kg S d^{-1} m^{-3}), and apparent growth rate (μ_{max}, d^{-1}) were calculated using mass balances over the C-N-P nutrients and biomass at a volumetric exchange ratio (VER) of 50%. Measurements of nutrients were performed at the beginning and end of the batch reaction phases of the SBR. Influent concentrations were back-calculated using the VER. The concentrations of nutrients in the effluent were assumed identical as at the end of the reaction phase.

Basic kinetic and stoichiometric parameters for microbial conversions and growth were assessed from nutrient consumptions and biomass production profiles using Aquasim (Reichert, 1994). A mathematical model was constructed using mass balances for substrate consumption and biomass production, and fitted to the experimental data. The maximum biomass-specific rate of acetate consumption ($q_{S,max}$, kg S d^{-1} kg X), maximum yield of biomass production on substrate ($Y_{X/S,max}$, kg X kg^{-1} S), and maintenance rate on substrate (m_S, kg S d^{-1} kg X) were derived by parameter fit from the Herbert-Pirt relation of substrate allocation for growth and maintenance. The biomass-specific maximum rate of growth (μ_{max}, d^{-1}) was computed from the relation between $q_{S,max}$ and $Y_{X/S,max}$, assuming the maintenance rate negligible compared to the maximum growth rate during the exponential phase of the batch reaction period.

2.5 Analysis of biomass and microbial community compositions

2.5.1 Light microscopy analysis of microbial morphotypes and bioaggregates

Microbial morphotypes present in the enrichment were visually observed by phase contrast microscopy (Axioplan 2, Zeiss, Germany).

2.5.2 Wavelength scan analysis of pigment content in the PNSB-enriched biomass

The evolution of the biomass contents in bacteriochlorophyll a (BChl a) and carotenoids in the biomass was used as a proxy for tracking the PNSB enrichment in the mixed liquor. Measurements were performed by wavelength scan over the visible and near-infrared spectrum from 400 to 1000 nm (DR3900, Hach, Germany). A focus was attributed to absorbance peaks between 800-900 nm (BChl a) and 400-600 nm (carotenoids).

2.5.3 V3-V4 16S rRNA gene amplicon sequencing of bacterial community compositions

Genomic DNA was extracted from biomass samples throughout the duration of the experiment, using UltraClean Microbial Isolation kits (MOBIO laboratories, Inc., USA) following manufacturer's instructions, and stored at -20 °C. The concentrations and qualities of the DNA extracts were measured by Qbit3 fluorimeter (Thermofisher Scientific, USA), according to manufacturer's instructions. The DNA extracts were sent to Novogene (China) for amplicon sequencing. The V3-V4 regions of the 16S rRNA gene were amplified by polymerase chain reaction (PCR) using the set of forward V3-V4 forward 341f (5'-CCTACGGGAGGCAGCAG
-3') and reverse 806r (5'- GGACTACHVGGGTWTCTAAT-3') primers (Takahashi *et al*., 2014). The amplicon sequencing libraries were pooled and sequenced in an Illumina paired-end platform. After sequencing, the raw read were quality filtered, chimeric sequences were removed and OTUs were generated on the base of ≥ 97% identity. Subsequently, microbial community analysis was performed by Novogene using Mothur & Qiime software (V1.7.0). For phylogenetical determination the most recent SSURef database from SILVA (http://www.arb-silva.de/) was used. Relative abundances of OTUs were reported as % total sequencing reads count.

3. Results

3.1 High and simultaneous removal of C-N-P nutrients was achieved in the PNSB-enriched, mixed-culture, stirred-tank SBR

The nutrient removal performances achieved by the PNSB-based process from SBR1 to SBR2 and SBR3 regimes are displayed in Figure 2 and Table 2. The detailed dynamics in nutrient and biomass concentrations and compositions are provided in Supplementary material 3.

3.1.2 Nutrient removing activities were detected during the initial batch

During the first 40 h of batch used to activate the biomass, nutrients were removed at 98 % COD (as acetate), 52 % N-NH_4^+, and 60% P-PO_4^{3-} (Figure 2.A). These related to apparent volumetric removal rates of 0.190 ± 0.048 kg COD d^{-1} m^{-3}, 21.5 ± 8.6 g N d^{-1} m^{-3}, and 2.5 ± 0.5 mg P d^{-1} m^3 (Figure 2.B). The COD:N:P consumption ratio was 100:7.5:0.12 (m/m/m) in this batch.

3.1.3 A complete removal of acetate was achieved across all SBR operation modes

During SBR1, the average percentage of removal of the biodegradable COD was 96%, with an average volumetric consumption rate of 0.220 ± 0.060 kg COD d^{-1} m^{-3}. During SBR2, 96% of the COD was removed as well at a 4-fold higher rate of 0.891 ± 0.235 kg COD d^{-1} m^{-3}. The carbon was fully removed over the first hour of the reaction phase, resulting in remaining 3.75 h of substrate limitation. During SBR3, the COD load in the influent was doubled, and as a result, no nutrient limitation occurred during the reaction phase. COD remained highly removed at 91%, with a volumetric removal rate of 1.08 ± 0.32 kg d^{-1} m^{-3}.

3.1.4 A maximum of 85% of ammonium and 74% of phosphate was removed from the inflow

The ammonium removal rates increased from 26 ± 13 g N-NH_4^+ d^{-1} m^{-3} in SBR1 to 83.4 ± 35 g N d^{-1} m^{-3} during SBR2, and 113.3 ± 62 g N d^{-1} m^{-3} during SBR3. Average N-removal percentages evolved from 53% to 44% and 77% of the ammonium load across the three SBRs, respectively. Removal rates of orthophosphate increased from 3.0 ± 0.7 g P-PO_4^{3-} d^{-1} m^{-3} of SBR1 to 10.7 ± 4.5 g P d^{-1} m^{-3} in SBR2 and 15.2 ± 4.6 g P d^{-1} m^{-3} in SBR3, with average P-removal percentages of 57, 45 and 73% per cycle, respectively. Under the non-limiting COD conditions of SBR3, the acetate, ammonium, and orthophosphate were released at median concentrations of 43 (min = 17; 1st-3rd quartile = 28-62) mg COD L_{Eff}^{-1}, 10 (2; 8-13) mg N-NH_4^+ L_{Eff}^{-1}, and 2.0 (0.4; 1.7-2.9) mg P-PO_4^{3-} L_{Eff}^{-1}, *i.e.*, close to European discharge criteria.

Thus, the average apparent COD:N:P assimilation ratio evolved from 100:7.5:0.12 in the batch to 100:9.2:1.2 (SBR1-2) under COD-limitation and 100:6.7:0.9 (SBR3) under non-COD-limitation. Across and beyond the experimental period, the intrinsic kinetics and stoichiometry of the PNSB-enriched biomass ranged with a biomass specific maximum growth rate (μ_{max}) of 0.96-2.16 d^{-1} and a maximum yield of biomass production on substrate ($Y_{X/COD,max}$) of 0.21-0.74 g VSS g^{-1} CODs, respectively. This related to a yield value of 0.34-1.19 g CODx g^{-1} CODs when using a theoretical elemental composition of $C_1H_{1.8}O_{0.38}N_{0.18}$ (1.607 g CODx g^{-1} VSS) for purple phototrophic bacteria (D. Puyol et al., 2017). The maximum biomass specific consumption of acetate

($q_{COD,max}$) ranged from 0.03-0.78 kg CODs h^{-1} kg^{-1} VSS. These measurements were performed directly during SBR cycles at the actual concentration of the biomass present in the system. More accurate measurements and derivation of these physiological parameters can be performed at diluted initial concentrations of PNSB biomass to prevent nutrient and light limitations during batch tests.

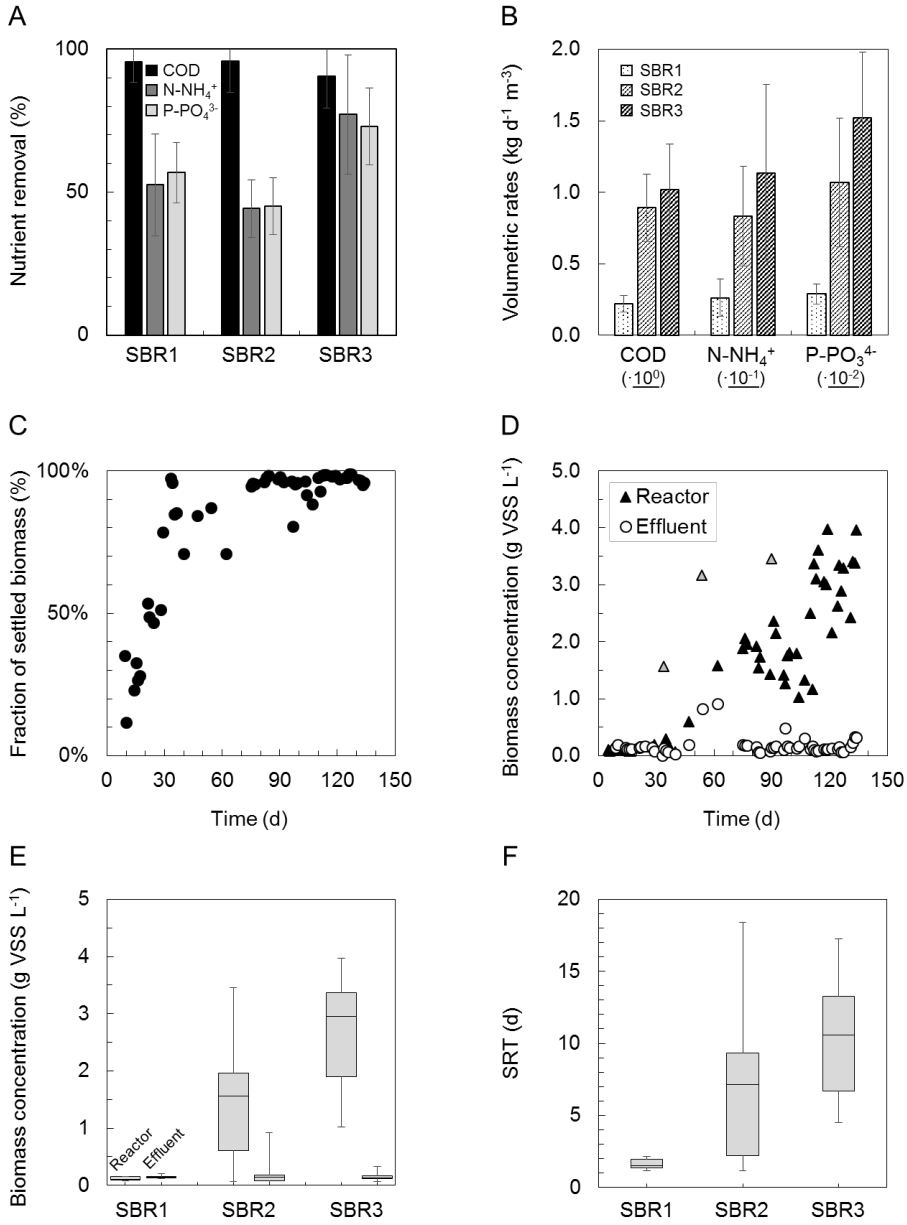

Figure 2. **Nutrient removal and biomass characteristics across SBR operations in the mixed-culture PNSB photobioreactor. A: Increases in COD, ammonium, and orthophosphate nutrient removal percentages from SBR1 to SBR3. On average, 95% of the COD was removed during all operational states. N-NH_4^+ and P-PO_4^{3-} reached 77% and 73% of removal from the synthetic influent. B: Gradual increases in volumetric rates of C-N-P nutrient removals from SBR1 to SBR3. C: Increase in the fraction of mixed-liquor biomass that settled in the bioreactor along SBR1 (days 3-30), SBR2 (days 30-100), and SBR3 (days 100-135) after inoculation with BNR activated sludge and a first batch of 40 h. D: Accumulation of biomass in the photobioreactor from SBR1 to SBR2 and SBR3. The grey triangles relate to cleanings and resuspensions of the wall biofilm in the biosystem. They indicate the total amount of biomass that accumulated in the reactor. E: Distributions of biomass concentrations in the reactor at the end of the reaction phase and in the effluent after settling. The settling ability of the biomass increased steadily during SBR operations. The residual biomass concentration in suspension at the end of the settling phase in SBR3 was 10 times lower than the concentration in the mixed liquor during reaction time, displaying the well-settling property of the PNSB-enriched biomass. F: The SRT was let freely evolve in the reactor, increasing from median values of 2 d (SBR1) to 7.5 d (SBR2) and 11 d (SBR3) along with biomass accumulation.**

Table 2. **Nutrient removal by the PNSB-enriched biomass in SBR1, SBR2, and SBR3 presented as averages and maximal values of removal rates and removal percentages. Residual concentration and removal percentages for COD met with European legislation limits for all SBRs (averages above 90% removal, with residues close to 60 mg COD L^{-1}). Ammonium and orthophosphate were removed up to 77% and 73%, respectively, with residual concentrations reaching 11 mg N-NH_4^+ L^{-1} and 2 mg P-PO_4^{3-} L^{-1}.**

Chemical parameter	Units	SBR1	SBR2	SBR3
Organic matter (as COD)				
Volumetric removal rates	(kg d^{-1} m^{-3})	0.220 ± 0.056	0.891 ± 0.235	1.019 ± 0.318
Removal percentage	(%)	96 ± 7	96 ± 11	91 ± 11
Maximal volumetric removal rates	(kg d^{-1} m^{-3})	0.387	1.488	2.437
Maximal removal percentage	(%)	100	100	98
Average residual concentrations	(mg L^{-1})	67 ± 25	62 ± 32	61 ± 6
Ammonium (as N-NH_4^+)				
Volumetric removal rates	(g d^{-1} m^{-3})	26 ± 13	83 ± 35	113 ± 62
Removal percentage	(%)	53 ± 18	44 ± 10	77 ± 21
Maximal volumetric removal rates	(g d^{-1} m^{-3})	52	159	65
Maximal removal percentage	(%)	83	60	94
Average residual concentrations	(mg L^{-1})	39 ± 16	39 ± 6	11 ± 7
Orthophosphate (as P-PO_4^{3-})				
Volumetric removal rates	(g d^{-1} m^{-3})	3 ± 1	11 ± 5	15 ± 5
Removal percentage	(%)	60 ± 11	45 ± 10	73 ± 14
Maximal volumetric removal rates	(g d^{-1} m^{-3})	5	18	25
Maximal removal percentage	(%)	91	59	95
Average residual concentrations	(mg L^{-1})	4 ± 1	5 ± 1	2 ± 1

3.1.5 Kinetic and stoichiometric parameters of microbial growth

The maximum biomass specific rate of substrate consumption ($q_{S,max}$), the yield of biomass growth of substrate consumption ($Y_{X/S}$) and the maximum biomass specific growth rate (μ_{max}) were obtained by parameter fit to batch evolutions of acetate and biomass during selected reaction phases of the SBRs (Table 3). Under the conditions of the initial batch and of SBR1 (*i.e.*, long HRT of 48 h, low OLR of 0.215 kg COD d^{-1} m^{-3}, very low biomass concentration of 0.1 g VSS L^{-1}, and low SRT of 1.5 d), the highly-enriched PNSB biomass displayed a high $q_{S,max}$ between 5.8-13.7 g COD_S d^{-1} g^{-1} VSS on which it maximized its growth rate: μ_{max} (2.16-3.36 d^{-1}) was substantial, ranging between values reported in literature for mixed cultures and pure cultures of PNSB. The biomass thus developed at a relatively low yield $Y_{X/S,\ max}$ (0.23-0.39 g VSS g^{-1} COD_S). The maintenance rate (m_s) was estimated to 0.72 g COD_S d^{-1} g^{-1} VSS. Under the conditions of SBR2 and SBR3 (*i.e.*, 3-times lower HRTs, 3 to 6-times higher OLRs, 16 to 30-times higher biomass concentrations, and 5 to 7-times longer SRTs), the biomass consumed acetate at a 3 to 8-fold lower $q_{S,max}$ (1.8-2.2 g COD_S d^{-1} g^{-1} VSS). The maximum growth rate and yield values could not be extracted from the data collected from the reactions phases at high biomass concentration (low sensitivity of absorbance and VSS measurements to detect changes). More accurate estimates are obtained with batch tests conducted with a diluted concentration of biomass.

Table 3. **Observed physiological parameters of the biomass of the PNSB mixed culture extracted from the reaction periods of the initial batch and the three SBR periods, and comparison with literature data obtained from pure-culture and mixed-culture PNSB systems. The values are given based on measured COD units for the acetate substrate and absorbance-calibrated VSS units for the biomass. The elemental formula for purple phototrophic bacteria C1H1.8O0.38N0.18 (4.5 mol e- C-mol-1, 36 g COD C-mol-1, 22.4 g VSS C-mol-1, 1.607 g CODX g-1 VSS) (D. Puyol et al., 2017) may be used for conversion of VSS in to COD units.**

System	$q_{S,max}$ (g COD_S d^{-1} g^{-1} VSS)	$Y_{X/S,max}$ (g VSS g^{-1} COD_S)	μ_{max} (d^{-1})
PNSB pure cultures	n.a.	0.98-1.23 [a]	5.28 [a]
PNSB mixed culture	n.a.	0.23-0.63 [b]	0.72-1.68 [b]
Initial batch	5.76	0.39	2.16
SBR1 [c]	13.68 ± 5.04	0.23 ± 0.02	3.36 ± 1.4
SBR2 [c]	1.76 ± 0.91	n.a. [d]	n.a. [d]
SBR3 [c]	2.22 ± 0.79	n.a. [d]	n.a. [d]

[a] Taken from literature (Eroglu et al., 1999; Jih, 1998)

[b] Taken from literature (Hülsen et al., 2016; Hülsen et al., 2014; Kaewsuk et al., 2010; Puyol et al., 2017)

[c] Average values collected over different cycles monitored over SBR1 (cycles 11, 17), SBR2 (cycles 21, 145, 166), and SBR3 (cycles 10, 31, 49, 91).

[d] High biomass concentrations in the system. VSS and absorbance measurement are no sensitive enough to detect growth over reaction period. External batches with diluted biomass should be performed to this end.

3.2 SBR operations enhanced the settling ability and accumulation of the PNSB biomass

The settling ability of the PNSB biomass increased across enrichment SBR operations, leading to substantial accumulation of biomass in the system from 0.1 (SBR1) to 1.6 (SBR2) to 3.0 (SBR3) g VSS L^{-1} as median values (Figure 2.C-D). The enhancement of the settling ability was measured by comparing these biomass concentrations present in the mixed liquor at the end of the reaction phase with the concentrations in the effluent after the settling phase which was for all SBRs as low as 0.13-0.15 g VSS L_{Eff}^{-1} (Figure 2.C-D). The fraction of settled biomass increased across SBR1 from 12% to 53% of the VSS present in the mixed liquors at the end of reaction phases, reached 96% by end of SBR2, and remained high at 97±3% over SBR3 (Figure 2.C). The total rates of biomass accumulation calculated over the full settling period of 3 h increased from 0.02±0.01 (SBR1) to 0.69±0.46 (SBR2) and 1.30±0.45 (SBR3) g VSS h^{-1}, or from 0.02±0.01 to 0.46±0.31 and 0.87±0.30 kg VSS h^{-1} m^{-3}, respectively, when translated into volumetric rates. At the beginning of SBR1, the full 3 h period was required to settle the suspended biomass. At the end of SBR3, most of the 5.9 g VSS of biomass that aggregated and accumulated in the system settled in about 10 min (*i.e.*, 35 gVSS h^{-1} or 24 kg VSS h^{-1} m^{-3} effectively). This high settling rate obtained on SBR3 corresponds to a sedimentation G-flux of solids of 4.7 kg h^{-1} m^{-2}. This displayed the well-settling property of the aggregated PNSB biomass. It underlined potential for considerably shortening the settling phase and SBR cycle length in order to increase the daily loading of the system.

The fraction of VSS in the TSS remained relatively high with 85% (SBR1) to 93% (SBR2) to 80% (SBR3) as median values, *i.e.*, corresponding to a fraction of inorganic suspended solids (ISS) between 7-20%. During SBR3 a period at lower VSS fraction with values below 60% and higher ISS fraction (>40%) was detected between days 97-117, underlying potential accumulation of inorganics, *e.g.*, as intracellular polyphosphate (not measured), during nutrient assimilation in the biomass.

The SRT was let to increase freely, without controlled purge of biomass, as a result of the enhancement of settling properties of the biomass: it rose from 2 d in SBR1 to 7 d in SBR2 and 11 d in SBR3 as median values (Figure 2.D). Strategies can be tested to control the SRT at specific values on the range between, *e.g.*, 3-10 days, depending on nutrient capture and biomass production targets.

The PNSB enrichment process could be easily be tracked visually with the gradual increase in the purple color intensity in the bioreactor (Figure 3.A-D).

3.3 Microscopy images showed an increasing size in microbial aggregates

After inoculation with flocculent activated sludge, phase-contrast microscopy imaging revealed the presence of dense aggregates already in SBR1 formed by the PNSB biomass (Figure 3.E-G). Some cells clustered in flower-shaped aggregates, in a way comparable to the typical morphotype of *Rhodopseudomonas*. Other rod-shaped cells were present, putatively belonging to *Rhodobacter* and *Blastochloris* genera. The size of the aggregates increased from 50 to 150 µm during the operational time along with the better settling abilities of the biomass.

3.4 Wavelength scans highlighted the enrichment of carotenoid and bacteriochlorophyll pigments in the biomass and a shift in predominant populations in the PNSB guild

Carotenoids and bacteriochlorophylls, and their increase along the enrichment of the PNSB biomass, were detected by the presence of absorbance peaks at wavelengths between 450-500 nm and between 800-900 nm. The wavelength scan data presented in Figure 3.H are normalized by the biomass concentrations, expressed as absorbance units at 660 nm. Peaks at 800 nm and 850 nm were already present at the end of the initial batch phase, and persisted during SBR1. At the end of SBR2, the absorbance peaks shifted to higher wavelengths of 805 nm and 865 nm. During SBR3, another peak was detected at 1000 nm that is characteristic for the genus *Blastochloris*. This suggested a shift in predominant microbial populations harbouring different types of pigments in the PNSB guild across the mixed-culture enrichment process.

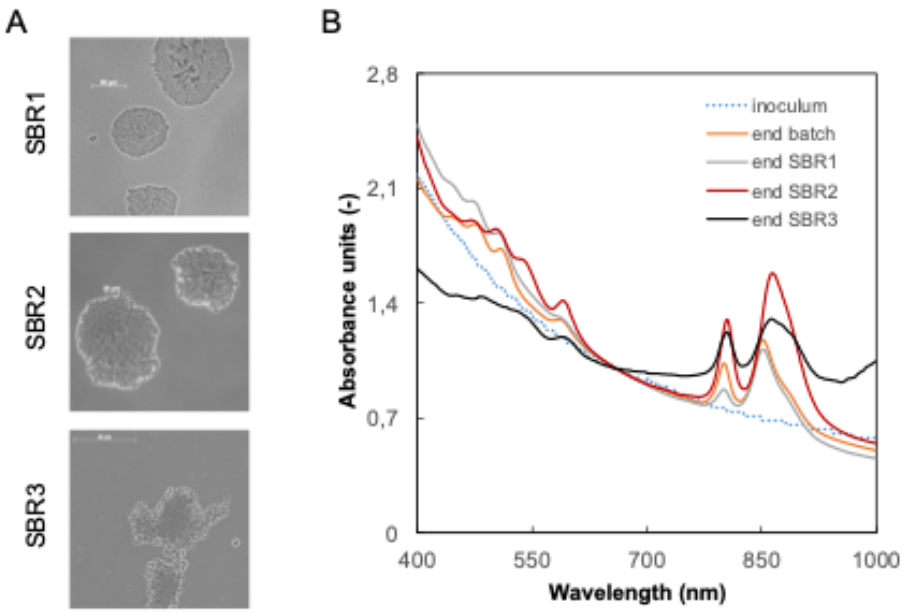

Figure 3. **Evolution of the pigmentation and aggregative characteristics of the PNSB-enriched biomass. A: Phase-contrast microscopy images of the aggregates present in SBR1 to SBR3. The size of the aggregates increased during time along with increased settling abilities of the biomass. B: Wavelength scans of intact cultures, normalized for the biomass content (at 660 nm). The presence of PNSB was tracked at peaks around 800-900 nm (Bchl a) and 400-500 nm (carotenoids). After the initial batch phase of 40 h, the peaks typical for PNSB pigments were present, and persisted in the biomass until the end of SBR3.**

3.5 Amplicon sequencing revealed selection shifts from Rhodobacter to Rhodopseudomonas and Blastochloris genera within the guild of PNSB

The composition of the bacterial community of the mixed culture and underlying shifts in predominant populations were analysed by V3-V4 16S rRNA gene amplicon sequencing. The times series of PNSB populations are displayed in Figure 4. The detailed times series of the full set of identified genera across the sequencing dataset is given in Supplementary material 5.

The BNR activated sludge inoculum presented a diversity of genera, with *Rhodobacter* as the main PNSB detected at 4% of the sequencing read counts. The typical populations of the BNR sludge like ammonium oxidizer (*Nitrosomonas*), nitrite oxidizer (*Nitrospira*), denitrifier (*Zoogloea*), polyphosphate- ("*Candidatus* Accumulibacter") and glycogen-accumulating ("*Ca.* Competibacter") organisms got rapidely outcompeted right after start-up of the first batch under PNSB-selective conditions (Supplementary material 5).

At the end of the 40-h batch phase, *Rhodobacter* reached a relative abundance of 52%. At the end of the first cycle of SBR1, a high-grade enrichment of 90% of *Rhodobacter* was obtained. Around the 10th cycle of SBR1 (10 days), the genus *Rhodopseudomonas* got enriched at 15%, and reached 50% at the end of the 23rd cycle (23 days after inoculum). The compositions of the communities of the mixed liquor and of the biofilm that developed on the walls of the reactor during the 13th cycle revealed that *Rhodopseudomonas* (55%) was outcompeting *Rhodobacter* (5%) in the biofilm, while *Rhodobacter* (60%) was more enriched than *Rhodopseudomonas* (10%) in the mixed liquor. Then, *Rhodobacter* decreased constantly from cycle to cycle, while *Rhodopseudomonas* progressively took the lead in the flocculent biomass as well.

After 18 cycles of SBR2 (*i.e.*, 4.5 and 22.5 days from the starts of SBR2 and SBR1, respectively), *Rhodopseudomonas* became dominant (70%), outcompeting *Rhodobacter* (17%) in the enrichment culture. Interestingly, after 20 days of SBR2, the genus *Blastochloris*, also an affiliate of the PNSB guild, got selected, while the relative abundance of *Rhodopseudomonas* decreased to 60% at the end of SBR2. In SBR3, *Blastochloris* reached 10% of the bacterial community dataset.

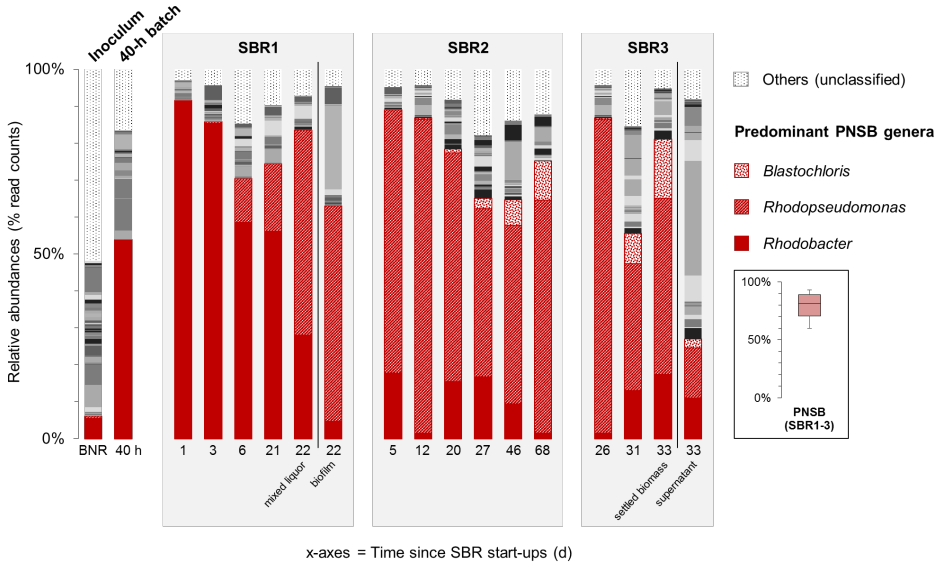

Figure 4. **Time series of V3-V4 16S rRNA gene amplicon sequencing of bacterial community compositions in the PNSB-enriched mixed-culture process along SBR regime shifts. After inoculating the reactor with BNR activated sludge ("BNR"), a first PNSB genus Rhodobacter was initially enriched during the first 40-h batch ("40 h") and early SBR1 period. The second PNSB genus Rhodopseudomonas was predominantly selected across operations of SBR2 and SBR3. The third PNSB genus Blastochloris popped up by end of SBR2 and SBR3. The PNSB guild remained predominant in the biomass across the process with an average total relative abundance of sequencing reads affiliated to known PNSB above 60% of the total community dataset (median = 81%; min-max = 60-93%). In SBR1, both the mixed liquor and the wall biofilm were sampled on day 22 and sequenced. In SBR3, both the settled biomass and s were sampled on day 33 after settling, and sequenced. The full set of genera is given in Supplementary material 5.**

4. Discussion

4.1 A high-grade enrichment of a concentrated, well-settling PNSB biomass can be obtained under SBR regime

The enrichment of PNSB has often been successful, while most PNSB mixed cultures reported so far have mainly been in membrane systems (Hülsen et al., 2016). Here, we successfully enriched a mixed culture of PNSB out of activated sludge under traditional SBR regime in a stirred-tank system without the use of a membrane module to separate the biomass and the bulk liquid phase. This went by using the natural propensity of PNSB to form biofilms and bioaggregates. SBR regimes result in substrate gradients across reactor operation from high concentrations at the beginning of the cycle to low residual concentrations at the end. Such substrate gradients are known to promote the bioaggregation of microorganisms (Aqeel et al., 2019; Pronk et al., 2015; M. K. H. Winkler et al., 2018).

Promotion of bioaggregation of PNSB is key for a good S/L separation and accumulation of biomass in the system. One important outcome of this study highlighted that aggregation of PNSB can be stimulated under SBR regime to intensify the volumetric conversions and to facilitate downstream processing. After inoculation at 0.1 g VSS L^{-1}, a high concentration of a PNSB-enriched biomass of up to a maximum of 4.0 g VSS L^{-1} was obtained in SBR3. The good settling ability of the PNSB biomass obtained under this regime resulted in the emission of less than 5% of the mixed liquor biomass in the effluent of SBR3, as low as 0.1 g VSS L^{-1}. Interestingly, Driessens et al. (Driessens et al., 1987) have early reported the flocculation and good sedimentation (G-flux of 7-9 kg h^{-1} m^{-2} comparable to well-flocculated activated sludge) of *Rhodobacter capsulatus* in an upflow continuous photobioreactor operated under loading rates of 2.5-5.0 kg C d^{-1} m^{-3} (as calcium lactate; *i.e.*, 6.7-13.3 kg COD d^{-1} m^{-3}) and 0.5-1.0 kg N d^{-1} m^{-3} (as ammonium) with 87% C and N assimilation in the biomass (3.3-4.2 g VSS L^{-1}). The PNSB-enriched biomass during SBR3 displayed a high sedimentation G-flux of 4.7 kg h^{-1} m^{-2} relatively close to the values reached by Driessens et al. (Driessens et al., 1987) under highly concentrated loading rates 5 to 10-fold higher than used here (max. 1.3 kg COD d^{-1} m^{-3} in SBR3). Collectively, this comparison sustains that PNSB can be aggregated for a higher accumulation and retention of biomass to intensify nutrient conversions.

In the PNSB mixed culture, the HRT was initially set high to 48 h (*i.e.*, 1 cycle d^{-1} at a volume exchange ratio of 50%) to maintain biomass during start-up, prior to decreasing it to 16 h (3 cycles d^{-1}) from SBR2 onward. This value was in the range of the HRTs of 8-24 h that have been used in the operation of continuous photo anaerobic membrane bioreactor (PAnMBR) to enrich for purple phototrophic bacteria (PPB) at bench (Hülsen et al., 2016). It was also in

the range of traditional SBRs operated with conventional activated sludge (Mace & Mata-Alvarez, 2002). An operation at 4 cycles d^{-1} may be foreseen. Decreasing the settling phase length would lead to selectively retain the biomass fraction with higher settling property, with granulation potentialities. This is a typical approach to form a granular sludge out of flocculent activated sludge (Merle K. de Kreuk & van Loosdrecht, 2006; Lochmatter & Holliger, 2014; M. K. H. Winkler et al., 2018).

The settling ability increased along the SBR operation, with a settled biomass fraction raising from 12% (SBR1) to 97% (SBR2-3). Amplicon sequencing revealed that the settled biomass accounted for a 3-fold higher relative abundance of PNSB (80% as sum of *Rhodobacter*, *Rhodopseudomonas*, and *Blastochloris*) than the non-settled biomass (25%) (Figure 4). Together with the phase-contrast microscopy measurements, this highlighted that PNSB are capable of forming bioaggregates with good settling properties. Such increased settling ability links to a more efficient separation of the PNSB biomass from the treated bulk liquid, thus facilitating the downstream processing to recover and valorize the PNSB biomass rich in nutrients for biorefinery purposes.

4.2 A high, simultaneous removal of C-N-P nutrients was achieved by the PNSB biomass

High performances of organic matter (96% COD removal at a volumetric rate of 1.1 kg COD d^{-1} m^{-3}), ammonium (77% N-removal at 113 g N d^{-1} m^{-3}), and orthophosphate (73% P-removal at 15 g P d^{-1} m^{-3}) removal were obtained under operation with a single anaerobic reaction phase using the PNSB process. Conventionally, a sequence of anaerobic, anoxic, and aerobic conditions is needed for full BNR in activated sludge or granular sludge (Barnard & Abraham, 2006; Merle K. de Kreuk et al., 2005). The main difference relies that with PNSB single organisms can remove all nutrients by assimilation into the biomass by making use of photonic energy. BNR activated sludges make use of different microbial guilds of nitrifiers, denitrifiers, polyphosphate- and glycogen-accumulating organisms among others to remove all nutrients biologically. In activated sludge or granular sludge SBRs, the different redox conditions should be alternated to this end. Hence, this PNSB SBR process is a very interesting compact alternative to conventional BNR systems, that enables an enhanced removal of all nutrients in a single reaction phase by managing one single predominant microbial guild, thus simplifying considerably the microbial resource management.

With the PNSB biomass, the SBR process becomes simpler in terms of sequencing operation by feeding, anaerobic reaction, settling, and withdrawal. In practice, a fill/draw phase can be envisioned in function of the settling properties of the PNSB biomass. This can result in a SBR system operated by alternation of fil/draw and reaction phases only. Energy-wise, aeration is not

needed in a PNSB process, resulting in possible electricity savings. In the case of sunlight use, electricity savings will be substantial. The tank will have to be equipped with light filters to supply IR light and select for PNSB as predominant phototrophs in the mixed culture. The irradiance of 375 W m^{-2} applied in this bench-scale photoSBR is high versus of practical operation window. Sunny regions of Europe are typically characterized by an annual average sunlight irradiance of 150 W m^{-2} (Posten, 2009). Nonetheless, light can be provided synthetically in photobioreactors using, *e.g.*, immersed LED devices. In the case of 'artificial' supply of IR light, *e.g.*, with LEDs, the process economics will have to be balanced with the electrical power needed to provide the irradiance needed to run the process. Biofilm formation on light-emitting tubes or light-emitting floating carriers will necessitate periodical cleaning to remediate shading, such as conventionally done for the maintenance of sensors used for process monitoring and control. The aim of this study was not to optimize the reactor design. Further thermoeconomical analysis will have to be conducted to determine the optimum irradiance to supply. This is analogical to the comparison of stirring performances in bench-scale reactors versus full-scale systems. There is room to study PNSB processes at different illumination intensities and their impact on the system responses such as enrichment grades, biomass concentrations, aggregation levels, and nutrient removal performances. Recent studies published on purple phototrophic bacteria have involved irradiances of *ca*. 50 W m^{-2} (Hülsen et al., 2016; D. Puyol et al., 2017) which is about 8-times lower than the one used here at bench. However, no study has yet come with clear information on irradiance cutoffs and light patterns related to the microbial performance of PNSB in the mixed-culture and the economics of pilot and full-scale PNSB processes.

The volumetric removal rate of up to 1.1 kg COD d^{-1} m^{-3} achieved under the operation of SBR3 is comparable to the ranges of 0.8-2.5 kg COD d^{-1} m^{-3} reported for the PAnMBR (Hülsen et al., 2016), 0.2-1.4 kg COD d^{-1} m^{-3} for a continuous-flow stirred-tank reactor without separation of PNSB biomass (Alloul et al., 2019), and 1.2-3.2 kg COD d^{-1} m^{-3} for conventional BNR activated sludge processes (Tchobanoglous *et al*., 2003). It was nonetheless higher compared to aeration reactors, anaerobic ponds, and oxidation ditches (Tchobanoglous *et al*., 2003). Further enhancement of the COD loading rate and removal rate will be achieved by decreasing the SBR cycle time.

The difference in COD:N:P assimilation ratio between SBR1-2 (100:9.2:1.2 m/m/m) and SBR3 (100:6.7:0.9) resulted from the doubling of the acetate load in the influent. These COD:N:P assimilation ratios were in the range of ratios of 100:5.1-7.1:0.9-1.8 that have been characterized during growth of purple phototrophic bacteria (Hülsen *et al*., 2016a; Puyol *et al*., 2017b). As comparison basis, a COD-N-P assimilation ratio of 100:5:1 is theoretically used for activated sludge (Henze et al., 2000).

The oscillating periods of higher ISS content (>40%) in the PNSB biomass during SBR3 may underlie an interesting accumulation of inorganics in the biomass, *e.g.*, as intracellular polyphosphate. Similar ISS fractions of 30-40% have been widely detected in biomasses engineered for an enhanced biological phosphorus removal (EBPR) (Weissbrodt et al., 2014). Ecophysiological elucidation of PNSB populations for phosphorus removal is of scientific and technological interests.

4.3 Acetate and wavelength gradients can trigger microbial selection in the PNSB guild

Phototrophic organisms are widespread in natural and anthropogenic environments. In the 16S rRNA gene amplicon sequencing analysis of the flocculating activated sludge here used as inoculum, around 4% of the total reads was reported to belong to the genus *Rhodobacter*, and sequences corresponding to *Rhodopseudomonas* genus were also detected, highlighting the presence of PNSB in conventional sludges. Potentially, due to their versatile metabolism, different genera of PNSB can be constitutively present in activated sludges. Phototrophs derive the energy for their metabolism from the conversion of photons energy to chemical energy. The lack of requirements of substrate utilization to generate energy and external electron acceptors to catabolize acetate give to phototropic organisms a selective advantage over general chemotrophic organisms. PNSB absorb light in the IR spectrum to generate energy. The extensive IR irradiation along with a continuous stirring of the system led to the penetration of the light in the reactor, providing a selective pressure for the enrichment of PNSB. Spectrophotometric measurements of the biomass by wavelength scans from 300 to 900 nm revealed absorbance peaks characteristics for carotenoids and bacteriochlorophylls in PNSB. Peaks at 805 and 850 nm are typical for bacteriochlorophylls detected *in vivo* from cells of *Rhodopseudomonas capsulata* (Michael T Madigan & Gest, 1979), whereas a peak around 865 nm is typical for *Rhodobacter* (Zubova et al., 2005). These peaks were detected across the whole experimental period, indicating the presence and selection of PNSB organisms in the process. Pigments are excellent biomarkers of phototrophic populations, and provide specificity to distinguish between them (Stomp et al., 2007). Wavelength scan analyses are therefore very efficient for a rapid measurement (at min level) of the selection of PNSB.

The 16S rRNA gene amplicon sequencing analysis provided insights at higher resolution on the composition of the PNSB guild and underlying selection phenomena. Amplicon sequencing revealed a consistent enrichment of PNSB after already the first 40 h of batch. The initial enrichment of *Rhodobacter* followed by selection of *Rhodopseudomonas* and then *Blastochloris* can be

explained by competition phenomena across substrate and wavelength gradients between these genera inside the guild of PNSB.

Okubo & Hiraishi (2007) have reported a preferential selection of *Rhodobacter* under high acetate concentration (5-20 mmol L^{-1}, *i.e.*, 320-1280 mg CODs L^{-1}) due to its low affinity for acetate, while *Rhodopseudomonas* was enriched at lower concentrations (0.5 – 1 mmol L^{-1}, *i.e.*, 32-64 mg CODs L^{-1}). The initial 40-h batch was fully loaded with acetate across the whole reaction period, making this condition favourable to select for *Rhodobacter*. Instead, *Rhodopseudomonas* harbours a higher affinity (*i.e.*, lower affinity constant K_s of 0.11 mM for *Rhodopseudomonas vs* 0.23 mM for *Rhodobacter*) (Okubo & Hiraishi, 2007) for acetate, enabling this population to grow more efficiently than *Rhodobacter* under acetate-limited conditions. During SBR1 and SBR2, the carbon source became progressively depleted after 1.5 h of reaction phase, leaving other 2.5 h of starvation period at low residual acetate concentration. This provided *Rhodopseudomonas* with a competitive advantage for growth.

The competition between *Rhodobacter* and *Rhodopseudomonas* may also be governed by their growth rate and thus the SRT in the system. Populations of *Rhodobacter* have displayed a higher maximum growth rate (1.8-2.2 d^{-1} in an enrichment and 2.3-3.8 d^{-1} with isolates) about 2.6 times faster than *Rhodopseudomonas* on VFA (Alloul et al., 2019). Batch regimes primarily select on growth rate: organisms deploy their maximum growth rate across most of a batch period during which substrate concentrations are mostly not limiting (Rombouts et al., 2019a). The organism with the highest growth rate that can be activated under the actual operation conditions is therefore preferentially selected. This underlay the selection for *Rhodobacter* first prior to the progressive establishment of *Rhodopseudomonas* along the progressive increase in SRT. Light availability can also be accounted as responsible for the selective enrichment of *Rhodobacter* or *Rhodopseudomonas*. As mentioned, bacteriochlorophylls from *Rhodobacter* and *Rhodopseudomonas* absorb at different wavelengths (800-850 *vs*. 865 nm respectively). At the beginning of the operation, the biomass concentration in the reactor was lower compared to following phases (*i.e.*, SBR3). The initial higher availability of light at shorter wavelengths can have led to the selection of *Rhodobacter*, and similarly, the shadowing effect of the biomass can have acted as a natural filter, resulting in the selection of *Rhodopseudomonas*.
The genus *Blastochloris*, which appeared during SBR3, harbours bacteriochloropyll b (BChl b) instead of BChl a in *Rhodobacter* and *Rhodopseudomonas*. BChl b absorbs lower photonic energy at higher wavelengths (1020-1030 nm) (Hoogewerf et al., 2003) and can, therefore, interestingly survive at higher cell densities (here, around 1.5 g VSS L^{-1}) with lower light penetration in the bulk liquid. Absorbance of the incident IR light increased across reactor operation with the development of a biofilm dominated by *Rhodopseudomonas* on the reactor wall and with a high concentration of

PNSB biomass of up to 3.8 g VSS L^{-1} that accumulated in the reactor. According to the Beer-Lambert law, the accumulation of *Rhodobacter and Rhodopseudomonas* in the reactor and wall biofilm resulted in the absorbance of the higher-energy wavelengths in the 800-850 nm range of the IR light supplied, thus acting as wavelength filter. The lower-energy wavelengths not absorbed by *Rhodobacter* or *Rhodopseudomonas* were still available in the bulk-liquid, where *Blastochloris* could have absorbed them. The conjunction of the relatively high irradiance of 375 W m^{-2} and high SRT of 11 d were likely favorable for *Blastochloris* selection. Physiological characterization of this genus is needed in order to better predict its competition with other members of the diverse PNSB guild like *Rhodobacter* and *Rhodopseudomonas* among others.

Overall, substrate gradients, light gradients, biofilm formation, and bioaggregation were identified as factors that triggered population selection and dynamics in the PNSB enrichment. Different lineages therefore act *de concert* inside the guild of PNSB, providing metabolic redundancy and process resilience in the case of regime shifts in the process.

4.4 PNSB mixed cultures from bench toward process development

The development of a lab-scale SBR system enriched for PNSB opens the doors for a possible upscaling of the process. A high nutrient capture was coupled with the production of a PNSB-rich biomass. Such biomass can be valorized for, *e.g.*, proteins or PHAs productions (Alloul et al., 2018; Honda et al., 2006; Hülsen et al., 2018b). The high settling ability of the biomass allows an easier solid-liquid separation of the latter from the treated water either in a compact external settler or directly in the SBR tank. This provides a definite downstream processing advantage over suspended biomass. It also overcomes the use of membrane filtration modules. The SBR regime resulted in the efficient aggregation of PNSB, underlying an enhanced settling ability and accumulation of biomass in the system. The SRT is an important process variable to control toward a stable bioprocess (Morgenroth & Wilderer, 1999). This becomes even more important in the perspective of harnessing the phosphorus removal capability of the PNSB biomass: cells saturated with phosphorus have to be effectively removed from the system such as conventionally performed by purge of excess sludge to maintain robust activated sludge or granular sludge processes operated for EBPR (Barnard & Abraham, 2006; Weissbrodt et al., 2013). The growth rate and affinity for the substrate are further important parameter to manage the selection of PNSB populations in either batch or continuous-flow reactor regimes, respectively. Similarly, light irradiance is a key operational variable since it constitutes the primary energy source for PNSB. Light penetration and distribution are directly linked to the reactor geometry. In surface water ecosystems, IR light photons are typically consumed over the first 30 cm depth. Following the Beer-Lambert law, the absorbance of

light will substantially increase with the biomass concentration. Shallow reactor systems can be opportune. SBR regimes can easily be transferred from stirred-tank to any reactor design, like raceway systems (or also known as carrousel plants) currently under investigation for green and purple phototrophic mixed-culture processes (Alloul et al., submitted). The application of substrate gradients via SBR or plug-flow reactor configurations can foster biomass aggregation to sustain efficient S/L separation for biomass recovery on top of nutrient capture.

5. Conclusions

We investigated at bench the possibility to establish a mixed-culture PNSB process for nutrient capture from wastewater in a photobioreactor operated as a traditional simple and flexible stirred-tank SBR. This work led to the following three main conclusions:

SBR process conditions stimulated aggregation and accumulation (as high as 3.8 g VSS L^{-1}) of a PNSB-enriched mixed culture in a fast-settling biomass that removed all nutrients biologically in a single reaction stage. The formation of compact aggregates facilitated S/L separation.

Nutrient removal was substantial by assimilation in the biomass, reaching simultaneously 96% of organic matter at 1.1 kg COD d^{-1} m^{-3}, 77% of ammonium at 113 g N d^{-1} m^{-3}, and 73% of orthophosphate at 15 g P d^{-1} m^{-3}, *i.e.*, comparable to BNR activated sludge processes. Under non-COD-limiting conditions, the process reached the nutrient discharge limits set by the European Union.

The PNSB guild accounted for as high as 90% of the bacterial community of the sludge (*i.e.*, amplicon sequencing dataset), enabling a simple management of the microbial resource. A sequential selection between the genera *Rhodobacter*, *Rhodopseudomonas*, and *Blastochloris* was detected inside PNSB, allowing for functional redundancy in the microbiome and highlighting the microbial ecology of PNSB populations across light wavelengths.. Next investigations should elucidate competition phenomena along growth rates, substrate affinities, and wavelength gradients across the mixed liquor.

For engineering practice, process analysis should cover the technological and economical aspects related to light supply in the bioreactor. Besides wastewater treatment, the value of the PNSB-based mixed-culture SBR process will reside in opportunities for water and resource recovery by valorization of the retained, concentrated, and nutrient-rich PNSB biomass.

References

Alloul, A., Ganigué, R., Spiller, M., Meerburg, F., Cagnetta, C., Rabaey, K., & Vlaeminck, S. E. (2018). Capture–Ferment–Upgrade: A Three-Step Approach for the Valorization of Sewage Organics as Commodities. *Environmental Science & Technology*, *52*(12), 6729–6742. https://doi.org/10.1021/acs.est.7b05712

Alloul, A., Wuyts, S., Lebeer, S., & Vlaeminck, S. E. (2019). Volatile fatty acids impacting phototrophic growth kinetics of purple bacteria: Paving the way for protein production on fermented wastewater. *Water Research*, *152*, 138–147. https://doi.org/10.1016/j.watres.2018.12.025

Almasi, A., & Pescod, M. B. (1996). Wastewater treatment mechanisms in anoxic stabilization ponds. *Water Science and Technology*, *33*(7), 125–132. https://doi.org/10.1016/0273-1223(96)00347-2

Aqeel, H., Weissbrodt, D. G., Cerruti, M., Wolfaardt, G. M., Wilén, B. M., & Liss, S. N. (2019). Drivers of bioaggregation from flocs to biofilms and granular sludge. In *Environmental Science: Water Research and Technology* (Vol. 5, Issue 12, pp. 2072–2089). https://doi.org/10.1039/c9ew00450e

Barnard, J. L., & Abraham, K. (2006). Key features of successful BNR operation. *Water Science and Technology*, *53*(12), 1–9. https://doi.org/10.2166/wst.2006.400

Bryant, D. A., & Frigaard, N.-U. (2006). Prokaryotic photosynthesis and phototrophy illuminated. *Review TRENDS in Microbiology*, *14*(11), 488–496. https://doi.org/10.1016/j.tim.2006.09.001

Carlozzi, P., Pushparaj, B., Degl'Innocenti, A., & Capperucci, A. (2006). Growth characteristics of Rhodopseudomonas palustris cultured outdoors, in an underwater tubular photobioreactor, and investigation on photosynthetic efficiency. *Applied Microbiology and Biotechnology*, *73*(4), 789–795. https://doi.org/10.1007/s00253-006-0550-z

Chitapornpan, S., Chiemchaisri, C., Chiemchaisri, W., Honda, R., Yamamoto, K., S. Chitapornpan, C. Chiemchaisri, W. Chiemchaisri, R. H., & and K. Yamamoto. (2012). Photosynthetic bacteria production from food processing wastewater in sequencing batch and membrane photo-bioreactors. *Water Science and Technology*, *65*(3), 504–512. https://doi.org/10.2166/wst.2012.740

de Kreuk, M. K., Heijnen, J. J., & van Loosdrecht, M. C. M. (2005). Simultaneous COD, nitrogen, and phosphate removal by aerobic granular sludge. *Biotechnology and Bioengineering*, *90*(6), 761–769. https://doi.org/10.1002/bit.20470

de Kreuk, M. K., & van Loosdrecht, M. C. M. (2006). Formation of aerobic granules with domestic sewage. *Journal of Environmental Engineering*, *132*(6), 694–697. https://doi.org/10.1061/(ASCE)0733-9372(2006)132:6(694)

Driessens, K., Liessens, J., Masduki, S., Verstraete, W., Nelis, H., & De Leenheer, A. (1987). Production of Rhodobacter capsulatus ATCC 23782 with short residence time in a continuous flow photobioreactor. *Process Biochemistry*, *22*(6), 160–164.

Eroglu, nci, Aslan, K., Gündüz, U., Yücel, M., & Türker, L. (1999). Substrate consumption rates for hydrogen production by Rhodobacter sphaeroidesin a column photobioreactor. *Progress in Industrial Microbiology*, *35*(C), 103–113. https://doi.org/10.1016/S0079-6352(99)80104-0

EUR-Lex. (1991). Council Directive 91/271/EEC of 21 May 1991 concerning urban waste-water treatment. *Official Journal of the European Communities*.

Fradinho, J. C., Domingos, J. M. B., Carvalho, G., Oehmen, A., & Reis, M. A. M. (2013). Polyhydroxyalkanoates production by a mixed photosynthetic consortium of bacteria and algae. *Bioresource Technology*, *132*, 146–153. https://doi.org/10.1016/j.biortech.2013.01.050

Freedman, D., Koopman, B., & Lincoln, E. P. (1983). Chemical and biological flocculation of purple sulphur bacteria in anaerobic lagoon effluent. *Journal of Agricultural Engineering Research*,

28(2), 115–125. https://doi.org/10.1016/0021-8634(83)90081-1

Guest, J. S., Skerlos, S. J., Barnard, J. L., Beck, M. B., Daigger, G. T., Hilger, H., Jackson, S. J., Karvazy, K., Kelly, L., Macpherson, L., Mihelcic, J. R., Pramanik, A., Raskin, L., Van Loosdrecht, M. C. M., Yeh, D., & Love, N. G. (2009). A new planning and design paradigm to achieve sustainable resource recovery from wastewater. *Environmental Science and Technology*, *43*(16), 6126–6130. https://doi.org/10.1021/es9010515

Guimarães, L. B., Wagner, J., Akaboci, T. R. V., Daudt, G. C., Nielsen, P. H., van Loosdrecht, M. C. M., Weissbrodt, D. G., & da Costa, R. H. R. (2018). Elucidating performance failures in use of granular sludge for nutrient removal from domestic wastewater in a warm coastal climate region. *Environmental Technology (United Kingdom)*, *0*(0), 1–16. https://doi.org/10.1080/09593330.2018.1551938

Henze, M., Gujer, W., Mino, T., & van Loosdrecht, M. C. M. (2000). *Activated sludge models ASM1, ASM2, ASM2d and ASM3*. IWA Publishing.

Honda, R., Fukushi, K., & Yamamoto, K. (2006). Optimization of wastewater feeding for single-cell protein production in an anaerobic wastewater treatment process utilizing purple non-sulfur bacteria in mixed culture condition. *Journal of Biotechnology*, *125*, 565–573. https://doi.org/10.1016/j.jbiotec.2006.03.022

Hoogewerf, G. J., Jung, D. O., & Madigan, M. T. (2003). Evidence for limited species diversity of bacteriochlorophyll b-containing purple nonsulfur anoxygenic phototrophs in freshwater habitats. *FEMS Microbiology Letters*, *218*(2), 359–364. https://doi.org/10.1016/S0378-1097(02)01195-3

Hülsen, T., Barry, E. M., Lu, Y., Puyol, D., Keller, J., & Batstone, D. J. (2016). Domestic wastewater treatment with purple phototrophic bacteria using a novel continuous photo anaerobic membrane bioreactor. *Water Research*. https://doi.org/10.1016/j.watres.2016.04.061

Hülsen, T., Batstone, D. J., & Keller, J. (2014). Phototrophic bacteria for nutrient recovery from domestic wastewater. *Water Research*, *50*, 18–26. https://doi.org/10.1016/j.watres.2013.10.051

Hülsen, T., Hsieh, K., Lu, Y., Tait, S., & Batstone, D. J. (2018). Simultaneous treatment and single cell protein production from agri-industrial wastewaters using purple phototrophic bacteria or microalgae – A comparison. *Bioresource Technology*, *254*, 214–223. https://doi.org/10.1016/j.biortech.2018.01.032

Hustede, E., Steinbüchel, A., & Schlegel, H. G. (1993). Relationship between the photoproduction of hydrogen and the accumulation of PHB in non-sulphur purple bacteria. *Applied Microbiology and Biotechnology*, *39*(1), 87–93. https://doi.org/10.1007/BF00166854

Imhoff, J. F. (2017). Diversity of anaerobic anoxygenic phototrophic purple bacteria. In *Modern Topics in the Phototrophic Prokaryotes: Environmental and Applied Aspects* (pp. 47–85). https://doi.org/10.1007/978-3-319-46261-5_2

Kaewsuk, J., Thorasampan, W., Thanuttamavong, M., & Seo, G. T. (2010). Kinetic development and evaluation of membrane sequencing batch reactor (MSBR) with mixed cultures photosynthetic bacteria for dairy wastewater treatment. *Journal of Environmental Management*, *91*(5), 1161–1168. https://doi.org/10.1016/j.jenvman.2010.01.012

Lochmatter, S., & Holliger, C. (2014). Optimization of operation conditions for the startup of aerobic granular sludge reactors biologically removing carbon, nitrogen, and phosphorous. *Water Research*, *59*, 58–70. https://doi.org/10.1016/j.watres.2014.04.011

Mace, S., & Mata-Alvarez, J. (2002). Utilization of SBR technology for wastewater treatment: An overview. *Industrial and Engineering Chemistry Research*, *41*(23), 5539–5553. https://doi.org/10.1021/ie0201821

Madigan, M. T., & Gest, H. (1979). Growth of the Photosynthetic Bacterium Rhodopseudomonas capsulata Chemoautotrophically in Darkness with H2 as the Energy Source. In *JOURNAL OF BACTERIOLOGY* (Vol. 137, Issue 1). http://www.psbiosystem.it/pdf/jbacter00284-0544.pdf

Madigan, M. T., & Jung, D. O. (2009). *An Overview of Purple Bacteria: Systematics, Physiology, and Habitats* (pp. 1–15). https://doi.org/10.1007/978-1-4020-8815-5_1

McEwan, A. G. (1994). Photosynthetic electron transport and anaerobic metabolism in purple non-sulfur phototrophic bacteria. *Antonie van Leeuwenhoek*, *66*(151), 151–164. https://doi.org/10.1007/BF00871637

Morgenroth, E., & Wilderer, P. A. (1999). Controlled biomass removal — The key parameter to achieve enhanced biological phosphorus removal in biofilm systems. *Water Science and Technology*, *39*(7), 33–40. https://doi.org/10.1016/S0273-1223(99)00147-X

Nakajima, F., Kamiko, N., & Yamamoto, K. (1997). Organic wastewater treatment without greenhouse gas emission by photosynthetic bacteria. *Water Science and Technology*, *35*(8), 285–291. https://doi.org/10.1016/S0273-1223(97)00178-9

Okubo, Y., & Hiraishi, A. (2007). Population Dynamics and Acetate Utilization Kinetics of Two Different Species of Phototrophic Purple Nonsulfur Bacteria in a Continuous Co-culture System. *Microbes Environ*, *22*(1), 82–87. http://wwwsoc.nii.ac.jp/jsme2/

Posten, C. (2009). Design principles of photo-bioreactors for cultivation of microalgae. *Engineering in Life Sciences*, *9*(3), 165–177. https://doi.org/10.1002/elsc.200900003

Pronk, M., Abbas, B., Al-zuhairy, S. H. K., Kraan, R., Kleerebezem, R., & van Loosdrecht, M. C. M. (2015). Effect and behaviour of different substrates in relation to the formation of aerobic granular sludge. *Applied Microbiology and Biotechnology*, *99*(12), 5257–5268. https://doi.org/10.1007/s00253-014-6358-3

Pulz. (2001). *Photobioreactors: production systems for phototrophic microorganisms* https://link.springer.com/content/pdf/10.1007%2Fs002530100702.pdf

Puyol, D., Barry, E. M., Hülsen, T., & Batstone, D. J. (2017). A mechanistic model for anaerobic phototrophs in domestic wastewater applications: Photo-anaerobic model (PAnM). *Water Research*, *116*, 241–253. https://doi.org/10.1016/j.watres.2017.03.022

Puyol, Daniel, Batstone, D. J., Hülsen, T., Astals, S., Peces, M., & Krömer, J. O. (2017). Resource recovery from wastewater by biological technologies: Opportunities, challenges, and prospects. *Frontiers in Microbiology*, *7*(JAN), 1–23. https://doi.org/10.3389/fmicb.2016.02106

Reichert, P. (1994). Aquasim - A tool for simulation and data analysis of aquatic systems. *Water Science and Technology*, *30*(2), 21–30. https://doi.org/10.2166/wst.1994.0025

Rombouts, J. L., Mos, G., Weissbrodt, D. G., Kleerebezem, R., & Van Loosdrecht, M. C. M. (2019). Diversity and metabolism of xylose and glucose fermenting microbial communities in sequencing batch or continuous culturing. *FEMS Microbiology Ecology*, *95*(2), 233. https://doi.org/10.1093/femsec/fiy233

Shyue Koong Chang, & Schonfeld, P. M. (1991). Wastewater Engineering Treatment and Reuse. In *Transportation Research Part B* (4th ed. /, Vol. 25, Issue 6). McGraw-Hill. https://doi.org/10.1016/0191-2615(91)90038-K

Stomp, M., Huisman, J., Stal, L. J., & Matthijs, H. C. P. (2007). Colorful niches of phototrophic microorganisms shaped by vibrations of the water molecule. *The ISME Journal*, *1*(4), 271–282. https://doi.org/10.1038/ismej.2007.59

Stoppani, A. 0 M., Fuller, R. C., & Calvin, A. M., 2017. *Carbon dioxide fixation by Rhodopseudomonas capsulatus* https://www.ncbi.nlm.nih.gov/pmc/articles/PMC357574/pdf/jbacter00543-0027.pdf

Takahashi, S., Tomita, J., Nishioka, K., Hisada, T., & Nishijima, M. (2014). Development of a prokaryotic universal primer for simultaneous analysis of Bacteria and Archaea using next-generation sequencing. *PLoS ONE*, *9*(8). https://doi.org/10.1371/journal.pone.0105592

van der Star, W. R. L., Miclea, A. I., van Dongen, U. G. J. M., Muyzer, G., Picioreanu, C., & van Loosdrecht, M. C. M. (2008). The membrane bioreactor: A novel tool to grow anammox bacteria as free cells. *Biotechnology and Bioengineering*. https://doi.org/10.1002/bit.21891

van Niel, C. B. (1944). The culture, general physiology, morphology, and classification of the non-sulfur purple and brown bacteria. *Bacteriological Reviews*, *8*(1), 1–118. https://doi.org/10.1128/MMBR.8.1.1-118.1944

Verstraete, W., Clauwaert, P., & Vlaeminck, S. E. (2016).

Used water and nutrients: Recovery perspectives in a "*panta rhei*" context. *Bioresource Technology*, *215*, 199–208. https://doi.org/10.1016/j.biortech.2016.04.094

Verstraete, W., & Vlaeminck, S. E. (2011). ZeroWasteWater: Short-cycling of wastewater resources for sustainable cities of the future. *International Journal of Sustainable Development and World Ecology*. https://doi.org/10.1080/13504509.2011.570804

Weissbrodt, D. G., Maillard, J., Brovelli, A., Chabrelie, A., May, J., & Holliger, C. (2014). Multilevel correlations in the biological phosphorus removal process: From bacterial enrichment to conductivity-based metabolic batch tests and polyphosphatase assays. *Biotechnology and Bioengineering*, *111*(12), 2421–2435. https://doi.org/10.1002/bit.25320

Weissbrodt, D. G., Schneiter, G. S., Fürbringer, J.-M., & Holliger, C. (2013). Identification of trigger factors selecting for polyphosphate- and glycogen-accumulating organisms in aerobic granular sludge sequencing batch reactors. *Water Research*, *47*(19), 7006–7018. https://doi.org/10.1016/j.watres.2013.08.043

Wilderer, P. A. (1998). *Sequencing Batch Reactor Technology: Concept and Design*.

Winkler, M. K. H., Meunier, C., Henriet, O., Mahillon, J., Suárez-Ojeda, M. E., Del Moro, G., De Sanctis, M., Di Iaconi, C., & Weissbrodt, D. G. (2018). An integrative review of granular sludge for the biological removal of nutrients and recalcitrant organic matter from wastewater. *Chemical Engineering Journal*, *336*, 489–502. https://doi.org/10.1016/j.cej.2017.12.026

Zubova, S. V., Melzer, M., & Prokhorenko, I. R. (2005). Effect of environmental factors on the composition of lipopolysaccharides released from the *Rhodobacter capsulatus* cell wall. *Izvestiya Akademii Nauk Seriya Biologicheskaya*, *2*, 168–173.

Supplementary material

Supplementary material 1: Symbols and Equations

Table SM1.1. **Symbols used in calculation and model computation formula. Substrate concentrations were expressed in COD (organic matter), N-NH_4^+ (ammonium), and P-PO_4^{3-} (orthophosphate) based units. Biomass concentrations were expressed in COD based units.**

Symbols	Units	Definition
C_S	kg S m^{-3} or mg S L^{-1}	Concentration of substrate in the reactor (state variable)
$C_{S,inf}$	kg S m^{-3} or mg S L^{-1}	Concentration of substrate in the influent
$C_{S,0}$	kg S m^{-3} or mg S L^{-1}	Concentration of substrate at beginning of reaction phase
$C_{S,end}$	kg S m^{-3} or mg S L^{-1}	Concentration of substrate at end of reaction phase
$C_{S,eff}$	kg S m^{-3} or mg S L^{-1}	Concentration of substrate in the effluent
C_X	kg X m^{-3} or mg X L^{-1}	Concentration of biomass in the reactor (state variable)
$C_{X,eff}$	kg X m^{-3} or mg X L^{-1}	Concentration of biomass in the effluent
HRT	d or h	Hydraulic retention time
K_S	kg S m^{-3} or mg S L^{-1}	Half-saturation affinity constant for substrate
m_S	kg S d^{-1} kg^{-1} X	Biomass maintenance rate
M_S	kg S	Mass of substrate
M_X	kg X	Mass of biomass
μ or q_X	kg X d^{-1} kg^{-1} X = d^{-1}	Biomass specific growth rate
N_{cycles}	cycles d^{-1}	Number of SBR cycles per day
η_S	%	Percentage of nutrient removal
q_S	kg S d^{-1} kg^{-1} X	Biomass specific rate of substrate consumption
$Q_{inf} = Q_{eff} = Q$	m^3 $cycle^{-1}$ or L $cycle^{-1}$	Volume of influent fed and effluent withdrawn per SBR cycle
Q_{sample}	m^3 $cycle^{-1}$ or mL $cycle^{-1}$	Volume of mixed liquor samples collected during reaction phase
Q_{purge}	m^3 $cycle^{-1}$ or mL $cycle^{-1}$	Volume of mixed liquor purged at the end of reaction phase (Q_{purge} = 0 if SRT let freely evolve)
r_S	kg S d^{-1} m^{-3}	Apparent volumetric rate of nutrient removal
R_S	kg S d^{-1}	Total rate of nutrient removal
SRT	d	Sludge retention time
t	d or h	Time
t_{cycle}	h or d	SBR cycle time length
V	m^3 or L	Volume
V_{inf}	m^3 or L	Volume of influent
V_r	m^3 or L	Working volume of the reactor
V_{eff}	m^3 or L	Volume of effluent
VER	%	Volume exchange ratio

Table SM1.2. **Equations used in calculations and model computations. Definitions and units of symbols are available in Table SM2.1 above.**

Hydraulic retention time in a SBR, HRT (d or h)

$$HRT = \frac{V_r}{Q_{inf}\, N_{cycles}} \qquad \text{(eq. 1)}$$

Sludge retention time in a SBR, SRT (d)

$$SRT = \frac{C_x\, V_r}{(Q_{eff}\, C_{x,eff} + Q_{purge}\, C_x + Q_{sample}\, C_x)\, N_{cycles}} \qquad \text{(eq. 2)}$$

Apparent volumetric rate of nutrient removal, r_S (kg S d^{-1} m^{-3})

$$rs = \frac{(Cs,\inf Qinf - Cs,eff\ Qeff)\ Ncycles}{Vr} = \frac{(Cs,\inf - Cs,eff)\ Q\ Ncycles}{Vr} \equiv \frac{Cs,0 - Cs,end}{tcycle} \qquad \text{(eq. 3)}$$

with:

$$Cs,0 = Cs,\inf \frac{Vinf}{Vr} + Cs,end \frac{Vr - Vinf}{Vr} = Cs,\inf VER - Cs,end\ (1 - VER)$$

$$Cs,inf = Cs,0 \frac{1}{VER} - Cs,end \frac{1 - VER}{VER}$$

$$Cs,eff = Cs,end$$

$$VER = \frac{Vinf}{Vr} = \frac{Veff}{Vr}$$

Percentage of nutrient removal, η_S (%)

$$\eta s = \frac{Cs,inf - Cs,eff}{Cs,inf} 100 = \left(1 - \frac{Cs,eff}{Cs,inf}\right) 100 = \frac{Cs,0 - Cs,end}{Cs,0 - Cs,end\ (1 - VER)} 100 \qquad \text{(eq. 4)}$$

Total rate of nutrient removal, R_S (kg S d^{-1})

$$|\ Rs\ | = \frac{dMs}{dt} = Vr\ \frac{dCs}{dt} = Vr\ rs \qquad \text{(eq. 5)}$$

Substrate consumption balance during a batch phase (at constant V_r)

$$\frac{dC_s}{d_t} = q_s\, C_x = q_{s,max}\ \frac{C_s}{C_s + K_s}\ C_x \qquad \text{(eq. 6)}$$

Biomass production balance during a batch phase (at constant V_r)

$$\frac{dC_x}{d_t} = \mu\, C_x = (q_s - m_s)\, Y_{sx,max}\; C_x = \quad \text{(eq. 7)}$$

$$(q_{s,max}\; \frac{C_s}{C_s + K_s} - m_s)\, Y_{sx,max}\, C_x$$

Herbert-Pitt equation for substrate allocation for growth and maintenance

Biomass specific rates of substrate consumption, q_s (kg S d^{-1} kg^{-1} X)
Biomass specific growth rate, μ (kg X d^{-1} kg^{-1} X = d^{-1})
Biomass maintenance rate, m_s (kg S d^{-1} kg^{-1} X)

$$q_s = \frac{1}{Y_{x/s}}\mu + m_s \qquad \text{or} \qquad \mu = (q_s - m_s)\, Y_{x/s} \quad \text{(eq. 8)}$$

$$\mu_{max} = (q_{s,max} - m_s)\, Y_{x/s} \approx q_{s,max}\, Y_{x/s} \quad \text{with } q_{s,max} \gg m_s \quad \text{(eq. 9)}$$

Supplementary material 2

Correlation between VSS and absorbance measurements

The correlation between the absorbance measurement and the VSS concentration of the PNSB-enriched biomass is described in Figure SM1.1 hereafter. It displays the experimental data of three measurement series with the linear regression line. Such a correlation analysis should checked on regular basis across a long-term experimental period in function of the composition of the biomass. It should also be done for every new experiment, since the content of pigments and of intracellular storage compounds of the PNSB biomass can vary from case to case, based on environmental conditions tested. Absorbance measurements of biomass are mainly applicable with biomass in suspension and at relatively low concentrations. It was mainly valid here for the first 40-h batch period and SBR1. As soon as biomass aggregates, traditional gravimetry measurements via TSS, ISS and VSS as described in standard methods are more effective. This was applied on SBR2 and SBR3. One should nonetheless keep in mind that gravimetry measurements do not differentiate cells and organic intracellular polymers such as PHAs.

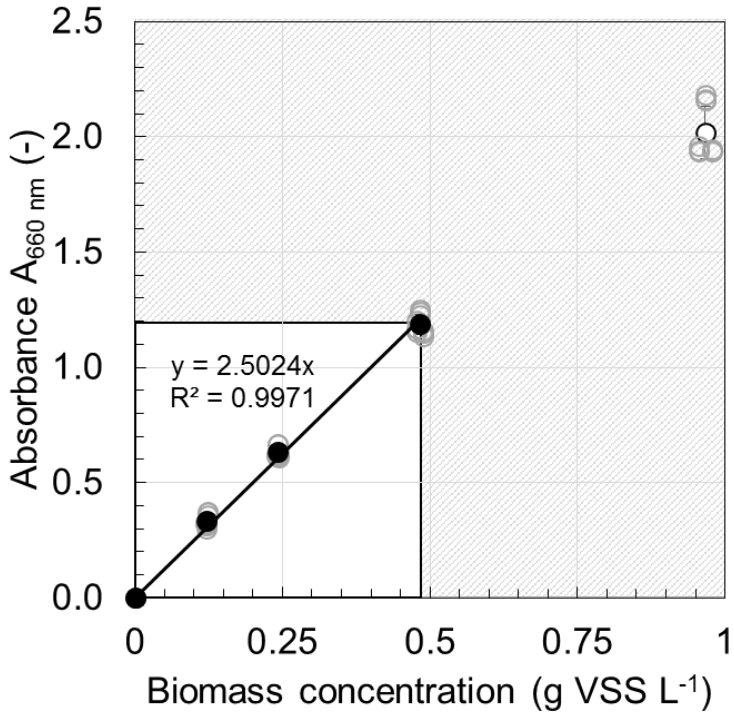

Figure SM2.1. **Correlation between the absorbance at 660 nm and the VSS concentration of the PNSB-enriched biomass, based on dilution series of mixed liquor taken from the reactor (2×, 4×, 8×, 16× diluted). The linear regression of serie 1 is y = 0.3995x, serie 2 is y = 0.3856 x and serie 3 is y = 0.4124 x. For absorbance measurements, mixed-liquor samples were diluted to fit in the range from 0.2-1.2 absorbance units. On this abosrbance window the correlation to VSS was considered as linear. Absorbance data were mainly accurate measurements for the 40-h batch and SBR1 where the biomass was low concentrated and in suspension. In SBR2 and SBR3, the biomass aggregated and VSS measurements were much more accurate.**

Supplementary material 3

Dynamics of nutrient and biomass concentration and composition

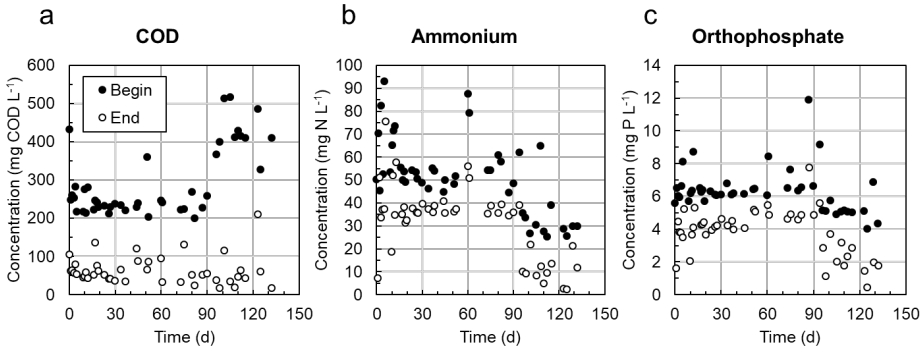

Figure SM3.1. **Evolutions of COD (A), ammonium (B) and orthophosphate (C) removal across SBR1 (1st month), SBR2 (2nd-3rd months), SBR3 (4th-5th months). Concentrations at begin (black dots) and end (white dots) of the reaction phases of the SBRs are displayed. While acetate was fully removed, the remaining COD primarily related to EDTA present in the medium (ca. 50 mg COD L^{-1}).**

Supplementary material 4

Parameter fit in Aquasim along the 40-h batch and SBRs 1-3

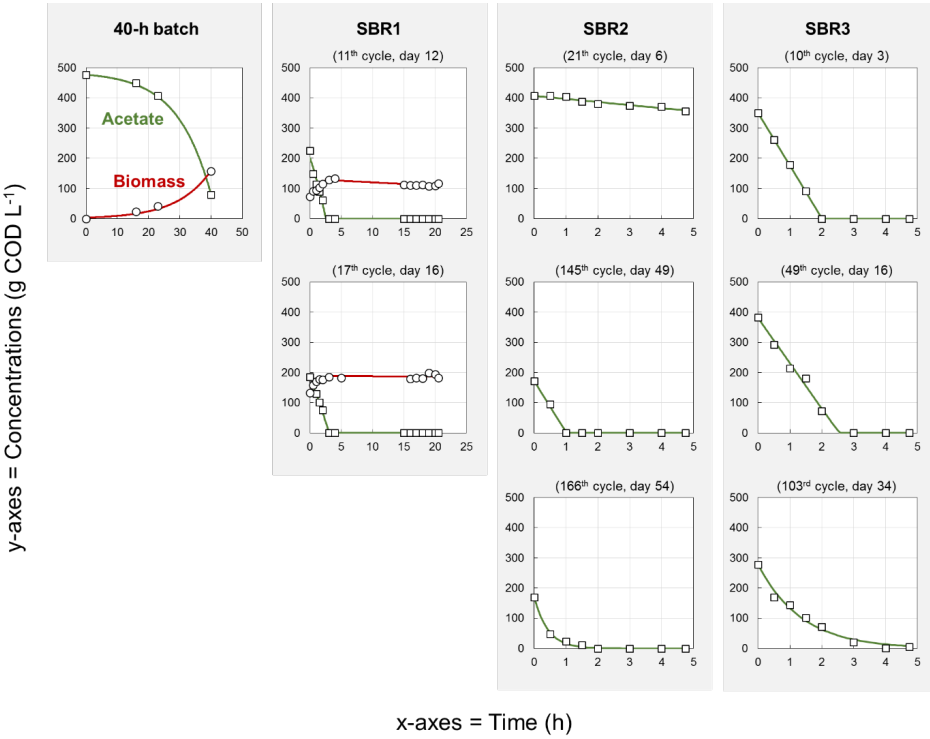

Figure SM4.1. **Conversion dynamics during the 40-h batch and during the batch reaction phase of selected cycles in SBR1, SBR2, and SBR3 used for the computation of basic kinetic and stoichiometric parameters. Experimental data of biomass growth and COD depletion are displayed with the fitted Aquasim model along the batch reaction phase.**

Chapter 4

Syntrophy between fermentative and purple phototrophic bacteria to treat and valorize carbohydrate-based wastewater

This chapter is deposited in a modified version as preprint with contributions of: Marta Cerruti, Guillaume Crosset-Perrotin, Mythili Ananth, Julius Laurens Rombouts and David G. Weissbrodt 2021. Syntrophy between fermentative and purple phototrophic bacteria for carbohydrate-based wastewater treatment. *bioRxiv*, preprint, 2021.05.13.444055.
https://doi.org/10.1101/2021.05.13.444055

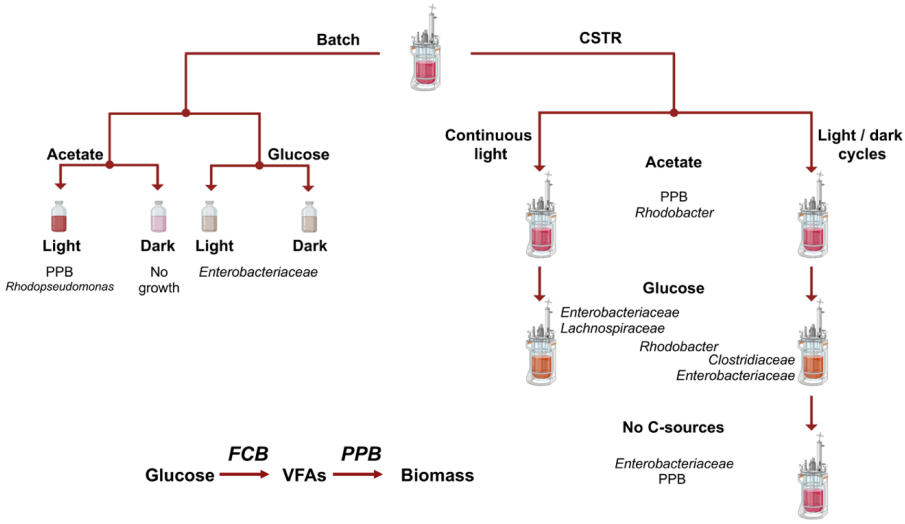
Batch
CSTR
Acetate
Glucose
Light
Dark
Light
Dark
PPB
Rhodopseudomonas
No
growth
Enterobacteriaceae
Continuous
light
Light / dark
cycles
Acetate
PPB
Rhodobacter
Glucose
Enterobacteriaceae
Lachnospiraceae
Rhodobacter
Clostridiaceae
Enterobacteriaceae
No C-sources
Enterobacteriaceae
PPB
Glucose
FCB
VFAs
PPB
Biomass

Abstract

Fermentative chemoorganoheterotrophic bacteria (FCB) and purple photoorganoheterotrophic bacteria (PPB) are two interesting microbial guilds to process carbohydrate-rich wastewaters. Their interaction has been studied in axenic pure cultures or co-cultures. Little is known about their metabolic interactions in mixed cultures. We aimed to harness the competitive and syntrophic interactions between FCB and PPB in mixed cultures. We studied the effect of reactor regimes (batch or chemostat) and illumination modes (continuous irradiation with infrared light, dark, or light/dark diel cycles) on glucose conversions and the ecology of the process. In batch, FCB (>80% of sequencing read counts) outcompeted PPB, under both dark and continuous infrared light conditions. In chemostat under continuous and alternating irradiance, three FCB populations of *Enterobacteriaceae, Lachnospiraceae* and *Clostridiaceae* were enriched (>70%), while *Rhodobacteraceae* relatives of PPB made 30% of the community. Fermentation products generated from glucose were linked to the dominant FCB. Continuous culturing at a dilution rate of 0.04 h^{-1} helped maintain FCB and PPB in syntrophy: FCB first fermented glucose into volatile fatty acids and alcohols, and PPB grew on fermentation products. Direct supply of carboxylates like acetate under infrared light selectively enriched for PPB (60%) independent of reactor regimes. Engineering the association between FCB- and PPB-based can help treat and valorize carbohydrate-based aqueous waste feedstocks.

1. Introduction

In nature, microorganisms have evolved to occupy diverse functional niches (Deines et al., 2020). They form metabolic associations to grow under nutrient-limiting conditions (Pearman et al., 2008). Wastewater treatment plants (WWTPs) use microbial communities to remove relatively high concentrations of organics (from 200-500 mg COD L^{-1} in municipal wastewater treatment to 30-50 g COD L^{-1} in anaerobic digestion) and other nitrogenous and phosphorous nutrients. WWTPs deal with complex compositions of organic matter like cellulose and undigested fibers from food. In agri-food industrial wastewaters, most of organics are derived from simple carbohydrates (*e.g.*, glucose, fructose or xylose) and polymeric sugars such as starch, cellulose and lignocellulosic derivates (Ghosh et al., 2017).

The wastewater treatment sector transitions to develop bioprocesses that combine nutrient removal with bioproduct valorization. Environmental biotechnologies involving mixed cultures are studied to treat and valorize nutrient-rich wastewaters by unravelling the biochemical mechanisms that can drive microbial conversions and products formations (Kleerebezem & Van Loosdrecht, 2007). The efficiency of mixed-culture processes is based on proper selection of microbial guilds needed to metabolize the wastes.

Two guilds across chemo- and photoorganoheterotrophic groups are particularly attractive to process carbohydrate- and carboxylate-rich feedstocks, namely fermentative chemoorganoheterotrophic bacteria (FCB) and purple phototrophic bacteria (PPB).

FCB like *Clostridium*, *Enterobacter*, *Lactobacillus* degrade carbohydrates through fermentation pathways, producing a spectrum of valuable compounds such as carboxylates (*e.g.*, volatile fatty acids – VFAs, lactic acid), ethanol and H_2. Their microbial niches are harnessed in non-axenic mixed-culture fermentation processes to valorize, *e.g.*, lignocellulosic sugars into targeted fermentation products like lactate or ethanol (Rombouts et al., 2020).

PPB like *Rhodobacter*, *Rhodopseudomonas*, *Rhodospirillum* are versatile microorganisms, involving a diversity of phototrophic and chemotrophic metabolisms depending on environmental and physiological conditions (Table 1). They grow preferentially as photoorganoheterotrophs, harvesting their energy from infrared (IR) light and using a variety of carbon sources from carboxylates to carbohydrates to alcohols (Puyol et al., 2017). PPB can also grow as chemotrophs using organic or inorganic substrates (Hunter et al., 2009). As photoorganoheterotrophs, they can achieve high biomass yields up to 1 g COD_X g^{-1} COD_S (Puyol & Batstone, 2017). PPB can thus be exploited to valorize anabolic products like biomass, single-cell proteins used in animal/human feed, or industrially relevant compounds like carotenoids. PPB can also photoferment, coupling glucose degradation to H_2 production.

Metabolism	**Energy source** (photo-/chemo-)	**Electron donors** (organo-/litho-)	**Oxidized e-donors**	**Carbon source** (hetero-/auto-)	**Electron acceptors**	**Reduced e-acceptors**
Under light conditions						
Anoxygenic photoorganoheterotrophy	Light photons	Reduced organic	Oxidized organic, CO_2	Organic	Endogenous compound, CO_2 fixation	Biomass
Anoxygenic photolithoautotrophy	Light photons	Reduced inorganic H_2 H_2S Fe^{2+} NO_2^-	Oxidized inorganic H_2O SO_4^{2-} Fe^{3+} NO_3^-	Inorganic (CO_2)	Endogenous compound, CO_2 fixation	Biomass
Oxygenic photolithoautotrophy	Light photons	H_2O	O_2	Inorganic (CO_2)	Endogenous compound, CO_2 fixation	Biomass
Photofermentation (not growth associated)	Light photons	Excess electrons energized from substrate	-	-	H^+	H_2
Under dark conditions						
Aerobic-respiring chemoorganoheterotrophy	Chemical redox reaction by aerobic respiration	Reduced organic	CO_2	Organic	O_2	H_2O Biomass
Anaerobic-respiring chemoorganoheterotrophy	Chemical redox reaction by anaerobic respiration	Reduced organic	CO_2	Organic	NO_3^- SO_4^{2-}	N_2 S^0, HS^-, H_2S Biomass
Fermentative chemoorganoheterotrophy	Chemical redox reaction by fermentation	Reduced organic (*e.g.*, fermentable sugars)	Pyruvate or CO_2	Organic	Endogenous compound	Fermentation products (*e.g.*, acetate, H_2), Biomass

Table 1. **Metabolic versatility of purple phototrophic bacteria (PPB). PPB can grow by combining a diversity of substrates and redox conditions. PPB grow primarily as photoorganoheterotrophs using VFAs as preferential carbon sources. but they are able to grow also on glucose with low growth rates. The metabolisms targeted in this study for the conversion of glucose by combination of fermentation and photoorganoheterotrophy are highlighted in grey.**

Combinations of fermentative chemoorganoheterotrophy, photoorganoheterotrophy and photofermentation processes have been investigated to degrade, convert and valorize carbohydrates in different configurations using pure cultures and synthetic co-cultures of FCB and PPB. First, a two-stage process of dark fermentation and photoorganoheterotrophy has been carried in two separate reactors. In the upstream unit, a pure culture of FCB degrade carbohydrates into VFAs that are fed in the downstream unit to produce a PPB biomass in pure culture (Ghimire et al., 2015). Second, in a single-stage dark fermentation process, a pure culture of PPB has been used to convert glucose and other organics into H_2. This has necessitated longer contact times compared to the two-stage fermentation process and the requirement of a pre-sterilized feed stream and axenic environment (Abo-Hashesh & Hallenbeck, 2012). Third, in single-stage dark- and photo-fermentation process, attempts have been made to co-cultivate defined FCB and PPB to simultaneously degrade carbohydrates and convert the produced VFAs to biomass (Rai & Singh, 2016). Despite the advantages of this synthetic co-culture approach for lower investment and operation costs compared to two-stage fermentation process, it still requires an axenic environment that impacts process economics. Open mixed-culture biotechnologies associating FCB and PPB can become beneficial to treat and valorize carbohydrate-based wastewaters. Compared to traditional industrial biotechnologies, open mixed cultures do not require sterilization of the inflow and tank, therefore substantially reducing the costs (Kleerebezem & Van Loosdrecht, 2007). Based on ecological principles, microorganisms can be selected to specifically target substrate degradation, bioproduct valorization or both.
Little is known about the selection phenomena and community dynamics in open mixed cultures of FCB and PPB, and the impact of substrate composition, environmental conditions, and reactor regimes thereof. Competition and metabolic interactions between these microbial guilds have not been unraveled yet. One can also wonder whether PPB, due to their wide metabolic versatility, could be selectively enriched in a carbohydrate-fed mixed culture to complete the full network of metabolisms from glucose fermentation to photoorganoheterotrophy, or whether FCB would more efficiently ferment glucose, prior to supplying fermentation products for the PPB to grow.

Here, we evaluated the ecological association of PPB and FCB in carbohydrate-fed mixed cultures. We addressed the selection mechanisms, competitive and syntrophic interactions of the two microbial guilds across reactor regimes (batch, chemostat) and IR light irradiance patterns (continuous light, continuous dark, dark/light alternation) using either glucose or acetate as model carbohydrate and carboxylate substrates, respectively, that harbor the same degree of reduction (4 mol e^- C-mol^{-1}). With these microbial ecology insights, we tested the treatment of a carbohydrate-rich synthetic wastewater in a

continuous single-stage mixed-culture process assembling FCB and PPB in syntrophy, by ecological engineering.

2. Material and methods

To evaluate microbial competition between PPB and fermenters, two mixed-culture bioreactor regimes (batch and continuous culturing), two substrates with the same degree of reduction per carbon mole (acetate and glucose), and three light patterns (continuous illumination, continuous dark, and light / dark alternation in a 16 h / 8 h sequence) were applied. The reactor performances were measured by kinetic and stoichiometry endpoints (rates, yields). Microbial selection and community dynamics were tracked by 16S amplicon sequencing. The experimental design is shown in Table 2.

Table 2. **Combinations of operational conditions tested to address selection, competition, and interaction mechanisms between FCB and PPB.**

Reactor regime	**Organic substrate**	**Illumination**	**Input concentration of organic matter (gCOD L^{-1})**
Batch	Acetate	Continuous	10
Batch	Acetate	No (dark)	10
Batch	Glucose	Continuous	10
Batch	Glucose	No (dark)	10
CSTR	Acetate	Continuous	5 / 10
CSTR	Glucose	Continuous	5
CSTR	Acetate	16h light / 8h dark	10
CSTR	Glucose	16h light / 8h dark	10
CSTR	No carbon sources	16h light / 8h dark	-

2.1 Composition of cultivation media

Under all conditions, the cultures were provided with a mineral medium composed as in Cerruti et al. (2020). The cultivation medium was buffered at pH 7.0 with 4-(2-hydroxyethyl)-1piperazineethanesulfonic acid (HEPES) at 4 g L^{-1}. Sodium acetate and glucose were used as carbon sources, in a concentration of 5 or 10 g COD L^{-1} depending on experimental conditions (Table 2), mimicking concentrations of moderately loaded agri-food wastewaters. Acetate was provided as $C_2H_3O_2Na \cdot 3H_2O$ (18.28 g L^{-1}) and glucose as $C_6H_{12}O_6 \cdot H_2O$ (9.68 g L^{-1}).

2.2 Batch operational conditions

Batch tests were first operated to study the competition of PPB and FCB in discontinuous mode. PPB biomass from an in-house enrichment culture grown and maintained in a sequencing batch reactor (SBR) (Cerruti et al., 2020) was used to inoculate 100-ml anaerobic batch bottles. The cultures were flushed with 99% argon gas to maintain anaerobic conditions (Linde, NL, >99% purity). Every batch bottle was duplicated. Half of the batch bottles were exposed to dark. The other half were exposed to IR light (> 700 nm) supplied by a halogen lamp (white light) with a power of 120 W whose wavelengths below 700 nm were filtered out by two Black 962 Infrared Transmitting Perspex Acrylic Sheets (Black Perspex 962, Plasticstocktist, UK). Every batch was incubated in a closed shaker (Certomat® BS1, Sartorius Stedim Biotech, Germany) at 30±1 °C in the dark and at 37±1 °C under IR light: these temperature differences originated from the heat emitted from the lamps. The flasks were agitated at 170 rpm. The cultures were fed with 10 g COD L^{-1} of either glucose or acetate.

2.3 Continuous culturing conditions

Competition and syntrophy of FCB and PPB under continuous culturing were tested and tuned in a 2.5-L single-wall, continuous-flow stirred-tank reactor (CSTR) with 2 L of working volume connected to a controller system (In-Control and Power units, Applikon, Netherlands). The pH was controlled at 7.0 with NaOH at 0.25 mol L^{-1} and HCl 1 mol L^{-1}. The temperature was maintained at 30°C with a finger-type heat exchanger connected to a thermostat (WK 500, Lauda, Germany).

Similar to the batches, the reactor was irradiated from two opposite sides with two incandescent halogen lights of 120 W filtered to select for IR wavelengths λ > 700 nm using Black Perspex 962 sheets (Plasticstocktist, UK) to promote PPB growth. An effective incident light intensity of 270 W m^{-2} was measured on the reactor wall with a pyranometer (CMP3, Kipp & Zonen, The Netherlands).

The reactor was inoculated with an in-house PPB enrichment, and started under batch mode. After 48 h it was switched to continuous mode. To enrich for PPB, the dilution rate was set to 0.04 h^{-1}, *i.e.*, less than half of the biomass-specific

maximum growth rate (μ_{max}) of the representative PPB genus *Rhodopseudomonas* (0.15 h^{-1}) (Cerruti et al., 2020).
Four combinations of energy patterns and carbon sources were then tested in the mixed-culture CSTR: (*i*) continuous light with acetate, (*ii*) continuous light with glucose, (*iii*) 16/8 h light/dark alternation cycles with acetate, and (*iv*) 16/8 h light/dark alternation cycles with glucose. Light/dark alternation was controlled with an automatic switch time controller (GAMMA, The Netherlands).
After 3 months of continuous cultivation, the carbon source feed was stopped, while phosphate and nitrogen sources were maintained for a period of 4 days (*ca*. 4.5 hydraulic retention times – HRTs), in order to test/confirm the hypothesis that PPB can grow on fermentation products produced by FCB.

2.4 On-line mass spectrometry analysis of off-gas composition

The off-gas of all CSTR experiments was connected to a mass spectrometer (Thermofisher, Prima BT Benchtop MS) which was used to measure on-line the production rates of CO_2 and H_2 (used in the simulations).

2.5 Sampling of mixed liquors for biomass and liquid phase analyses

All mixed liquor samples were collected in 2-mL Eppendorf tubes, centrifuged at 10000 x *g* for 3 min. The biomass pellet was separated from the supernatant and stored at -20°C until further analysis. The supernatant was filtered with 0.2 µm filters (Whatman, US), and stored at -20°C until further analysis. From the batch cultures, the samples were collected every 24 h. From the CSTR, 5 to 9 samples were collected for each condition along the experiments.

2.6 Measurement of biomass concentrations

Biomass concentrations were measured over the time course of the batch and continuous reactors by spectrophotometry (Biochrom, Libra S11, US) through absorbance at 660 nm (A_{660}). A calibration curve was established to correlate A_{660} to the concentration of volatile suspended solids (VSS): c(g VSS L^{-1}) = 0.61 A_{660} (-). The VSS concentrations were measured by taking samples from the mixed liquor, filtering them using 0.2 µm filters (Whatman, 435 USA), drying the wet filters at 105 °C in a stove for 24 h, prior to incinerating the dried filters at 550 °C in an oven for 2 h, and weighted.

2.7 Wavelength scans of biomass samples to rapidly track PPB selection

Wavelength scan of biomass samples were done using a spectrophotometer (DR3900, Hach, Germany) to evaluate the presence of the typical PPB photopigments (carotenoids at 400-500 nm and bacteriochlorophyll at ca 850 nm). Absorbance profiles were measured at each wavelength between 320 nm and 999 nm.

2.8 Amplicon sequencing analysis of bacterial community compositions

Genomic DNA was extracted using DNeasy Powersoil microbial extraction kits (Qiagen, Hilden, Germany) accordingly to manufacturer's instructions. The DNA extracts were quantified by fluorometry (Qubit; Thermofisher, US), and stored at -20°C (pending analysis) and transferred at -80°C for long-term storage. The compositions of the bacterial communities of the mixed liquors were characterized from the DNA extracts by V3-V4 16S rRNA gene-based amplicon sequencing as detailed in Cerruti et al. (2020). Aliquots of the DNA extracts were submitted to Novogene (UK) for library preparation and amplicon sequencing. The fastq files of the sequencing datasets provided from Novogene were analysed with the QIIME2 pipeline (Bolyen et al., 2019), using the Greengenes database. The sequences were deposited in the online database NCBI under the Bioproject code ID PRJNA759396.

2.9 Chromatography analysis of substrate conversions and fermentation products

The depletion of substrates (acetate and glucose) and the formation of fermentation products (succinate, propionate, formate, lactate, acetate, butyrate) were monitored using high-performance liquid chromatography (HPLC) (Waters, 2707, NL) equipped with an Aminex HPX-87H separation column (BioRad, USA) maintained at 60°C. The H_3PO_4 (1.5 mmol L^{-1}) eluent was supplied at a flowrate of 0.6 mL min^{-1}. The compounds were detected by refraction index (Waters 2414, US) and UV (210 nm, Waters 2489, US). Ethanol was quantified through gas-chromatography as in Rombouts et al. (2019).

2.10 Solver for pathway utilization prediction

Based on the observed yields, a mathematical simulation was used to evaluate the contribution of the fermentative and phototrophic pathways to the carbon metabolism. The model was constructed in Microsoft Excel 16.48 minimizing the residual sum of squares (SSQ) error between modelled and measured yields:

$$\min(SSQ) = \min\left(\sqrt{\sum_{i=1}^{n} \frac{(\hat{y}_i - y_i)^2}{n}}\right) \quad (1)$$

where $\hat{y}_i$ is the modelled yield value and y_i is the measured yield value, and n is the amount of metabolic compounds that are considered.

The fermentation products yields (observed yields) were calculated as

$$y_i = Y_{p/s} = \frac{q_p}{q_s} \quad (2)$$

With q_p and q_s the biomass specific rates.

The solver estimated the contribution of the singular pathways (Table 3) to the overall metabolism as fractions. The modelled yields were estimated by summing the products between the pathway fractions and their stoichiometric coefficients. The process was automatically reiterated to minimize the SSQ between the observed and the estimated yields through the Generalized Reduced Gradient (GRG) Nonlinear solver available in Excel. The pathways that were used in the model varied per enrichment, depending on the microbial community structure, assuming only the activity of relevant catabolic and anabolic pathways. To simulate the carbon metabolism in batch enrichments the equations 1.1-1.9 were used. To simulate the pathways used in the CSTRs, reactions 1.10-1.11 were also added (Table 3). The model output indicated, as percentage, the contribution of the individual pathways to the total carbon, oxygen, hydrogen and electrons metabolism. The flux distribution of the different pathways predicted from the model is represented a semi-quantitative way in Figure 4.

Reactions	Pathways	Glucose $C_6H_{12}O_6$	Ethanol C_2H_6O	Acetate $C_2H_3O_2$	Propionate $C_3H_5O_2$	Lactate $C_3H_5O_3$	Butyrate $C_4H_7O_2$	Succinate $C_4H_4O_4$	Formate CH_2O_2	Hydrogen H_2	Carbon dioxide CO_2	Biomass FCB $CH_{1.8}O_{0.5}$	Biomass PPB	Protons H^+	Water H_2O
1.1)	Glucose → Biomass + CO_2	-1.00	0.00	0.00	0.00	0.00	0.00	0.00	0.00	-0.10	2.00	4.00	0.00	5.00	0.00
1.2)	Glucose → Ethanol + CO_2	-1.00	2.00	0.00	0.00	0.00	0.00	0.00	0.00	0.00	2.00	0.00	0.00	0.00	0.00
1.3)	Glucose + → Acetate + Ethanol + CO_2	-1.00	1.00	1.00	0.00	0.00	0.00	0.00	2.00	0.00	0.00	0.00	0.00	1.00	-1.00
1.4)	Glucose → Butyrate + CO_2	-1.00	0.00	0.00	0.00	0.00	1.20	0.00	0.00	0.00	1.20	0.00	0.00	1.20	1.20
1.5)	Glucose → Succinate	-1.00	0.00	0.00	0.00	0.00	0.00	1.71	0.00	0.00	-0.86	0.00	0.00	3.43	0.86
1.6)	Glucose → Lactate	-1.00	0.00	0.00	0.00	2.00	0.00	0.00	0.00	0.00	0.00	0.00	0.00	2.00	0.00
1.7)	Lactate → Acetate + Propionate + CO_2	0.00	0.00	1.00	2.00	-3.00	0.00	0.00	0.00	0.00	1.00	0.00	0.00	0.00	1.00
1.8)	Formate → CO_2 + H_2	0.00	0.00	0.00	0.00	0.00	0.00	0.00	-1.00	1.00	1.00	0.00	0.00	0.00	0.00
1.9)	Acetate → Biomass + CO_2	0.00	0.00	-1.00	0.00	0.00	0.00	0.00	0.00	-0.02	1.00	0.00	1.00	2.00	-0.38
1.1)	CO_2 + H_2O → Biomass + H_2	0.00	0.00	0.00	0.00	0.00	0.00	0.00	0.00	0.00	-1.00	1.00	1,00	-5.00	1.60

Table 3. **Stoichiometric matrix of the putative reactions included in the numerical model of metabolic reactions along FCB and PPB pathways. The reactions 1.1-1.9 were used to evaluate the contribution of each pathway under batch conditions. The reactions 1.10 and 1.11 were included in the simulation of the CSTRs.**

3. Results & Discussion

The batch and continuous reactor experiments revealed key insights into the microbial community assembly principles that govern the selection, competition and interaction of FCB and PPB in open mixed cultures in function of organic substrates, light patterns, and reactor regimes.

3.1 Selection and competition of PPB and FCB in batch cultures

3.1.1 In mixed-culture batches, PPB were selectively enriched on acetate and IR light

In batches, the acetate-fed cultures grew only when subjected to light, reaching a biomass concentration of 1 g VSS L^{-1} at a biomass specific growth rate (μ) of 0.0411 ± 0.0007 h^{-1} and with a yield of biomass on substrate ($Y_{X/S}$) of 0.60 ± 0.09 C-$mmol_X$ C-$mmol_S^{-1}$. Little growth was reported in the six days of cultivation for the acetate cultures in the dark (μ = 0.006 h^{-1}).

The inocula of the batches originated from a PPB in-house enrichment culture operated and maintained as SBR in parallel to the experiments. The inoculum seeded in the acetate-fed batches presented a relative abundance above 60% (*vs.* total amplicon sequencing read counts) of the purple non-sulfur genus *Rhodopseudomonas*. In the acetate-fed batches, *Rhodopseudomonas* sp. reached as high as 80% of the total community after 6 days of cultivation under IR light. Despite the low growth, chemoorganoheterotrophs of the family of the *Moraxellaceae* showed the highest relative abundance (80%) in the little biomass obtained on acetate in the dark (Figure 1A).

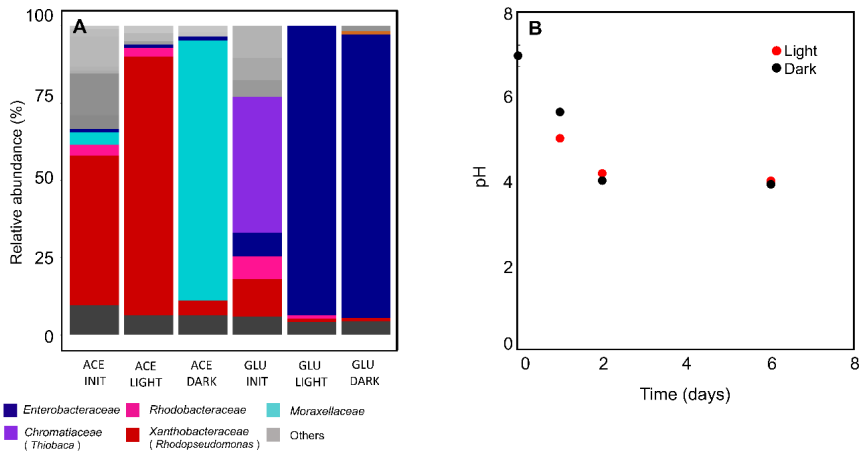

Figure 1. **A: Microbial community composition in batches. PPB are dominant at the beginning of the cultivation (ACE INIT and GLU INIT). After 6 days of cultivation under acetate feed, PPB were dominant under light conditions (ACE LIGHT). Under acetate-dark conditions there was little grow from the genus Moraxellaceae. Under glucose feed, independently of the light conditions, the family Enterobacteriaceae was dominant. B: pH evolution in the glucose-fed batches. Both under light and under dark conditions the pH dropped to 4 in the first 2 days of incubation.**

Acetate is one of the preferred substrates for PPB (Blankenship et al., 1995). It is assimilated into biomass by many PPB species, through the tricarboxylic acids cycle (Pechter et al., 2016). Acetate and IR light selected for *Rhodopseudomonas*, belonging to the *Xanthobacteraceae* family, under acetate and light conditions. Among the PPB, *Rhodopseudomonas* has the highest biomass-specific maximum growth rate (μ_{max}) on acetate (0.15 h^{-1}) (Cerruti et al., 2020) and therefore was predominant at the end of the batch cultivation. The growth rate in the acetate-fed cultures in the dark was 7 times lower than under light; the biomass concentration after 6 days was 270 times lower in the dark than under light. In the dark, acetate can only be assimilated by PPB in presence of suitable electron acceptors (*e.g.*, S^0 or SO_4^{2-}) in order to produce ATP for growth (Madigan et al., 1982). In the batches, little external electron acceptor was present in the medium (3 mmol SO_4^{2-} L^{-1}).

3.1.2 In mixed-culture batches, FCB outcompeted PPB on glucose, independent of light supply

In the glucose-fed batches, higher biomass concentration (1 g VSS L^{-1}) and growth rate (μ of 0.070 ± 0.001 h^{-1}) were reached in the dark than in the light (0.4 g VSS L^{-1}; 0.020 ± 0.002 h^{-1}).

The inoculum of the glucose-fed batches was dominated by the purple sulfur genus *Thiobaca*, due to an unexpected variation of the microbial community composition in the parent reactor. In the glucose-based batches, the genus of *Enterobacter* was predominant (>90%) both under light and dark (Figure 1A).

The *Enterobacteriaceae* family is widely predominant in anaerobic environments in the presence of non-limiting concentration of monomeric carbohydrates, such as glucose (Wijffels et al., 2003). Rombouts et al. (2019) reported an enrichment of 75% of the genus *Enterobacter* in a glucose-fed SBR, in nutrient, temperature and pH conditions similar to the one here presented.

pH was not controlled in batch cultivations. During glucose fermentations, pH dropped to 4 within 48 h, despite the presence of the HEPES buffer (Figure 1B).

3.1.3 Ethanol was the main fermentation product in glucose-fed batches

In irradiated acetate-fed batches, acetate was fully depleted after 6 days of incubation.

In glucose-fed batches, the biomass yields on glucose were 0.052 ± 0.002 C-$mmol_X$ C-$mmol_S^{-1}$ under light and 0.134 ± 0.011 C-$mmol_X$ C-$mmol_S^{-1}$ in the dark (Figure 2).

After 6 days of dark batch fermentations, ethanol was the main fermentation product with a yield of 0.20 ± 0.10 C-mmol$_{et}$ C-mmol$_S^{-1}$, followed by succinate (0.07 ± 0.03 C-mmol$_{succ}$ C-mmol$_S^{-1}$) and acetate (0.03 ± 0.01 C-mmol$_{ace}$ C-mmol$_S^{-1}$).
In the irradiated glucose-fed batches, 30% of the initial glucose was still present in the reaction broth after 6 days, and carbon balances could not be properly closed (>90% recovery). Ethanol was the main fermentation product (0.10 ± 0.07 C-mmol$_{et}$ C-mmol$_S^{-1}$), followed by lactate (0.05 C-mmol$_{lac}$ C-mmol$_S^{-1}$) and succinate (0.04 ± 0.02 C-mmol$_{succ}$ C-mmol$_S^{-1}$).

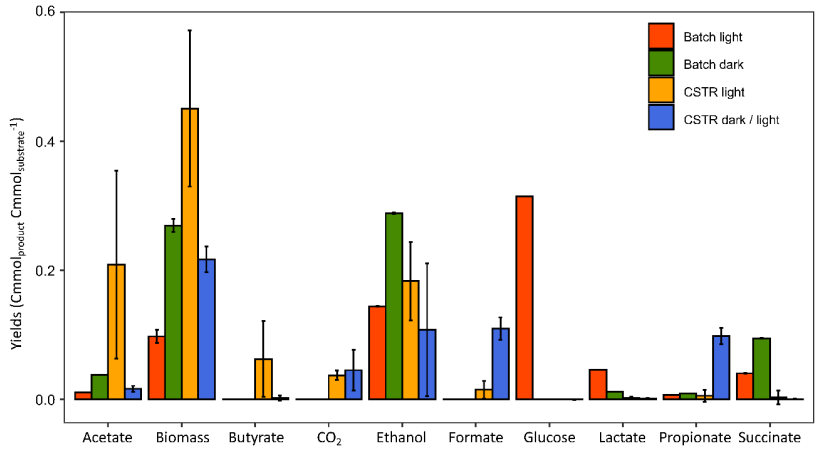

Figure 2. **Yields of the glucose-fed cultures. Under batch conditions, the main fermentation products were ethanol and succinate. Under light conditions, glucose was not fully depleted. Under CSTR conditions, the main fermentation products were ethanol, formate and acetate.**

A solver enabled to evaluate the theoretical contribution of 8 putative glucose fermentation pathways to the overall carbon and electron balances. In batches, the phototrophic pathways were not included in the simulation, since the relative abundance of PPB was very low (~1%), being outcompeted by FCB with glucose (Figure 1A). The predicted contribution of the individual pathways to the overall yields of the batches under light and dark were comparable. In batches, the dominant metabolic pathway was identified as homo-ethanol production from glucose (Table 3, Eq. 1.2). This catabolism is associated with the fermentative *Enterobacteriaceae* (Jang et al., 2017).

Wavelength scans are commonly used as an indirect measure to rapidly check for the presence/selection of PPB in the cultures, since photopigments absorb photons with specific wavelengths. Absorbance peaks around 400-500 nm represent the carotenoids series, and the peaks around 850 nm the bacteriochlorophyll a (bchl a) (Stomp et al., 2007). In the acetate-based irradiated batches, the aforementioned peaks were clearly detected at 450 nm

for carotenoids and 800-850 nm for bchl a. In the acetate-fed dark batches, almost no growth was reported within the 6 days of incubation but peak for photopigments was detected at 800 and 850 nm. No photopigment characteristic peaks were detected in the spectra of the biomasses cultivated in both the dark and irradiated glucose-fed batches, (Figure 3A/B).
Overall, in anaerobic batches, PPB are predominantly selected with acetate and IR light. FCB outcompete PPB on glucose independent of light or dark conditions.

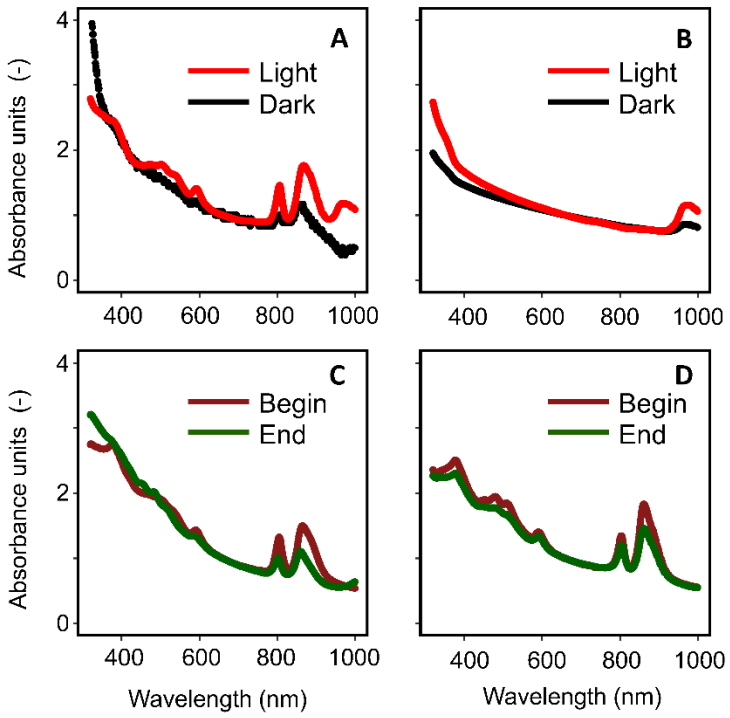

Figure 3. **Wavelength scan from 300 to 1000 nm. Absorbance units normalized for the biomass concentration (as A.U. at 660nm). A: acetate-fed batches. The typical PPB peaks (at ca 850 nm) were clearly visible under light conditions. B: glucose-fed batches. No peak was present. C: continuous light glucose-fed CSTR. The presence of PPB was confirmed by the presence of their typical peaks. D: dark / light glucose-fed CSTR. The presence of PPB was confirmed by the presence of their typical peaks.**

3.1.4 Fermentative Enterobacteriaceae were enriched in batches because of higher growth rates

In batch, μ_{max} is a key factor driving selection mechanisms in substrate-rich environments (Winkler et al., 2017), if no significant intermediate storage of substrate is displayed. FCB populations of the genus *Enterobacter* present a μ_{max} of 0.45-0.80 h^{-1} in mineral medium conditions with moderate sugar concentrations (<10 g_{COD} L^{-1}) (Rombouts et al., 2019). When fermenting

carbohydrates like glucose in pure culture, *Rhodopseudomonas capsulata* grows at a μ_{max} of 0.014 h^{-1} (Conrad & Schlegel, 1978). In batches, where the substrate is not limiting across most of the conversion time, the organisms with higher substrate uptakes rates get selected above organisms with high biomass yields (Rombouts et al 2019). According to the Herbert-Pirt relation, when the substrate uptake is directly coupled with growth, the organisms with the highest growth rate dominate. Using these studies, the genus *Enterobacter* is estimated to exhibit a μ_{max} about 32 times higher than *Rhodopseudomonas* on glucose, making FCB successful to outcompete PPB for glucose in batch.

In both irradiated and dark glucose-fed batches, populations of the family of *Enterobacteriaceae* were enriched (>90%). *Enterobacteriaceae* relatives ferment sugars through either the Embden-Meyerhof pathway or the pentose phosphate pathway, with a net production of ethanol (Jang et al., 2017). Ethanol can be used as substrate for growth by PPB, but with a strict pH regulation at 7.0 (Inui et al., 1995). Because of the production of lactate (pKa = 3.8) – a major byproduct of the glucose fermentation pathway to ethanol (Converti & Perego, 2002) – and insufficient pH buffering, the pH dropped to 4.0 within the first 2 days of glucose fermentation (Figure 1B). FCB can still grow at low pH such as below 5.5 (Tsuji et al., 1982). PPB grow instead in a pH range between 6.5 and 9.0, with an optimum at 7.0 (Pfennig, 1977). The low pH (pH = 4.0) resulting in the glucose-fed batches may have prevented PPB to grow on alcohols and VFAs produced by *Enterobacter*, explaining their low relative abundance (~ 1%). We postulate that with a strict pH control of the batch cultures to 7.0, PPB should be able to grow on fermentation products of FCB.

The genus *Enterobacter* can grow in a range of temperatures between 20 and 45°C (Gill & Suisted, 1978), with an optimum growth at 40°C (Tanisho, 1998). The temperature differences reported here for the batches incubated under dark (30°C) and light (37°C) (*i.e.*, *ca*. 7°C difference, resulting from the heat emitted by the lamps) should not have substantially affected its specific growth rates. On the other hand, light irradiance has been used as a method to prevent the proliferation of fermentative organisms (Gwynne & Gallagher, 2018). Since the illuminated cultures were supplied with IR light, although less energetic than white light, we postulate an inhibitory action on FCB, possibly explaining the 3.5-times lower growth rates measured under light than in the dark. The effective inhibition mode of action of photons on cellular and molecular level remains to be elucidated by future works.

3.2 Unravelling the selection and syntrophy of FCB and PPB in continuous cultures

Under continuous-flow regime, four different light and substrate conditions were imposed, namely: (i) acetate under light; (ii) acetate under dark/light cycles; (iii) glucose under light; and (iv) glucose under dark/light cycles. The pH was controlled at 7.0 to favor the enrichment of PPB.

3.2.1 Ethanol was the main fermentation product in the glucose-fed CSTR as well

In glucose-fed CSTRs, the biomass yield over glucose was 0.22 ± 0.02 C-$mmol_X$ C-$mmol_S^{-1}$ under continuous illumination and 0.45 ± 0.12 C-$mmol_X$ C-$mmol_S^{-1}$ under dark/light cycles. Ethanol was the main fermentation product (0.18 ± 0.06 under continuous light and 0.11 ± 0.10 C-$mmol_{et}$ C-$mmol_S^{-1}$ under dark/light cycles). In the continuously irradiated CSTR, acetate (0.21 ± 0.15 C-$mmol_{ace}$ C-$mmol_S^{-1}$) and butyrate (0.06 ± 0.05 C-$mmol_{but}$ C-$mmol_S^{-1}$) were also produced. In the dark/light CSTR, formate (0.11 ± 0.01 C-$mmol_{form}$ C-$mmol_S^{-1}$) and butyrate (0.10 ± 0.01 C-$mmol_{but}$ C-$mmol_S^{-1}$) were present in the fermentation product spectrum (Figure 2).

In CSTR, assimilation of acetate by photoorganohetrotrophy and CO_2 fixation (photosynthesis) by photolithoautotrophy were added to the solver matrix to evaluate the contribution of PPB to the total carbon and electron balances. Under all CSTR conditions, the major fermentation pathway involved fermentation of glucose through acetyl-CoA (Figure 4), up to 83% under continuous illumination and 55% under dark/light cycles. In the continuously irradiated CSTR, the solver estimated a high contribution of the photolithoautotrophic pathway enabling PPB to recycle CO_2 as extra carbon source, and of the photoheterotrophic pathway under dark/light cycles.

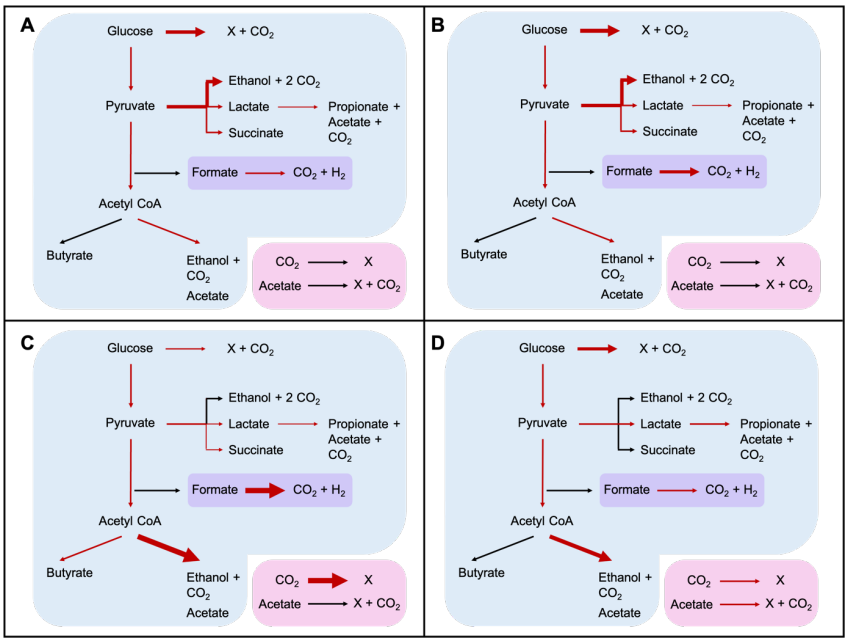

Figure 4. **Pathways involved under the different reactor regimes. The thickness of the arrows represents the predicted yield toward a specific metabolic route, based on the calculations of the solver. The reactions with the blue background are performed by FCB.**

The reaction with the purple background is performed by both FCB and PPB. The reactions with the pink background are performed by PPB. A: batch conditions with continuous illumination. B: batch conditions in the dark. C: CSTR under continuous illumination. D: CSTR conditions under light / dark cycles. Under batch conditions the pathways used were mainly directed toward biomass and ethanol production. Under CSTR ethanol was the main fermentation product, but the production of propionate, succinate and lactate was predicted. The phototrophic pathways were not included for the batch conditions but were included in the carbon and electron balance of the CSTRs. The conversion of lactate and acetate to butyrate (1.9 of Table 3) was not included in the diagram as the solver predicted 0% flux through it under all conditions.

3.2.2 PPB were enriched in the acetate-fed CSTR

In the continuously illuminated CSTR fed with acetate, PPB formed the dominant guild (68 ± 21 %) (Figure 5). The genus *Rhodopseudomonas* was predominant at the beginning of the CSTR (65%). Its relative abundance decreased to 40% after one week of cultivation (8.5 HRTs), while the genus *Rhodobacter* got concomitantly enriched (from 13 to 23%). *Rhodobacter* was further enriched once the dark/light cycles were applied, reaching 65% after 15.6 HRTs, while *Rhodopseudomonas* remained stable below 10%.

3.2.3 FCB were enriched in the glucose-fed CSTR

In the CSTR, FCB accounted above 50% under glucose feed, regardless of the light condition. In CSTR, dark/light cycles impacted the selection of FCB. Under continuous illumination, the family of *Lachnospiraceae* was predominant (around 30 %, with a peak at 75%), followed by the family of *Enterobacteriaceae* (15%) (Figure 5). Under dark/light cycles, *Enterobacteriaceae* (32 ± 17 %) and *Clostridiaceae* (18 ± 15 %) relatives were predominant.

Rhodobacter was the only PPB to significantly persist in the glucose-fed CSTR (19.5 ± 14 %) (Figure 5) independently of the illumination regime. The persistence of PPB in the glucose-fed CSTRs was further proven by the wavelength scan. Peaks for carotenoids (400-450 nm) and bacteriochlorphyll a (800 and 850 nm) photopigments were identified for both the continuous illumination and dark/light cycles (Figure 3C/D).

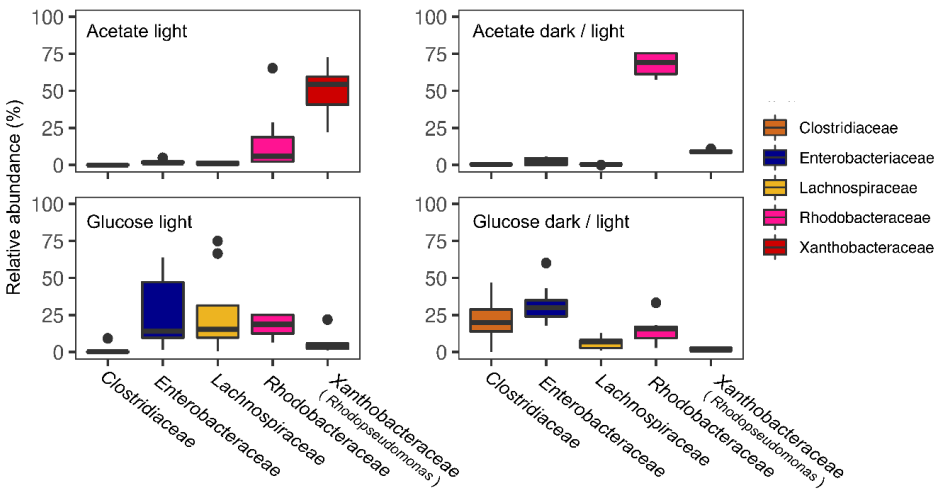

Figure 5. **Relative abundance of five representative families under CSTR conditions based on 16s rRNA gene amplicon sequencing analysis.. Under acetate conditions, PPB were dominant community, with a shift from Rhodopseudomonas under continuous illumination to Rhodobacter under light / dark conditions. Under glucose feed, the FCB were dominant, especially the genera Enterobacteriaceae and Lachnospiraceae.**

3.2.4 The microbial composition of the fermentative guild defined the spectrum of fermentation products

Clostridiaceae, *Enterobacteri*aceae and *Lachnospiraceae* relatives are all able to ferment glucose. They compete for glucose through different fermentation pathways (Grimmler et al., 2011; Horiuchi et al., 2002). *Lachnospiraceae* and *Clostridiaceae* are phylogenetically and morphologically heterogeneous families belonging to the phylum of *Firmicutes* (De Vos et al., 2005). Glucose fermentation through acetyl-CoA is typical of *Clostridiaceae* (Aristilde et al., 2015). In human gut microbiota, they contribute to sugar fermentation to lactate and short-chain fatty acids production (Venegas et al., 2019). Butyrate was produced only in the CSTR under continuous illumination (0.06 ± 0.05 C-mmol C-mmol$_S^{-1}$). The *Lachnospiraceae* and *Clostridiaceae* families ferment glucose into primarily butyrate, acetate and ethanol (Rombouts et al., 2019b; Temudo et al., 2008). Butyrate is produced through the butyril-CoA dehydrogenase gene, responsible for the conversion of crotonyl-CoA to butyryl-CoA and the butyryl-CoA:acetyl-CoA transferase (Venegas et al., 2019). According to the NCBI database (NCBI, 2021), the gene encoding for this enzyme is present in the phylum of *Firmicutes* that comprises *Clostridiaceae* and *Lachnospiraceae* relatives, but not in the proteobacterial family of the *Enterobacteriaceae*, explaining the absence of butyrate in the glucose-fed batches.

In the dark/light CSTR, the relatively high production of propionate (0.10 ± 0.01 C-mmol C-mmol$_S^{-1}$, *i.e.*, 17 times higher than under continuous

illumination) can be linked to the abundance of *Clostridiaceae*, which are propionate producers (Johns, 1952). *Clostridium* species can present a μ_{max} of 0.25 h^{-1} (Gomez-Flores et al., 2015) with primary fermentation products including ethanol, butyrate, acetate and propionate (Lamed et al., 1988). *Clostridium beijerincki* decreases its H_2 production when exposed to light intensities above 200 W m^{-2}, with a shift from a preferential production of butyric acid to acetic acid (Zagrodnik & Laniecki, 2016). Continuous illumination in the CSTR might have inhibited *Clostridiaceae* and selected for other *Firmicutes* like *Lachnospiraceae*.

Formate and propionate production was 10 times higher under dark/light conditions compared to continuous illumination. Acetate production was instead 12 times lower under dark/light cycles compared to continuous illumination (Figure 2). This may link to a higher relative abundance of *Enterobacteriaceae* relatives under dark/light cycles (31%) compared to the continuous illumination (18%) (Figure 5). *Enterobacteriaceae* present a μ_{max} between 0.5-1 h^{-1} (Khanna et al., 2012; Martens et al., 1999) and are known to ferment sugars to primarily ethanol, with lactate and acetate as major byproducts (Converti & Perego, 2002).

3.2.5 PPB metabolized the fermentation products released by FCB

After 3 months of CSTR operation, we tested the hypothesis that PPB grow on the fermentation products of FCB. Glucose supply in the feed was stopped while nitrogen and phosphate were still provided over 4 days (*i.e.*, 4.5 HRTs). Along the 4 days of operation, the relative abundance of the PPB shifted from 10 to 50% (Figure 6A). The biomass concentration sharply decreased already 2 h after stopping the glucose feed, from 80 C-$mmol_X$ L^{-1} and stabilizing at a concentration of 15.7 ± 2 C-$mmol_X$ L^{-1}. Butyrate, ethanol, formate, lactate, propionate and succinate were washed out of the system at the imposed dilution rate (0.04 h^{-1}). Acetate was depleted in 50 h, *i.e.*, 4 times faster than the theoretical washout rate (Figure 6B). In absence of glucose as carbon source, the highly active fermentative organisms were not growing. The increase in the PPB relative abundance proved their interaction with FCB, showing that PPB utilize VFAs as preferred substrate and can selectively grow on FCB fermentation products.

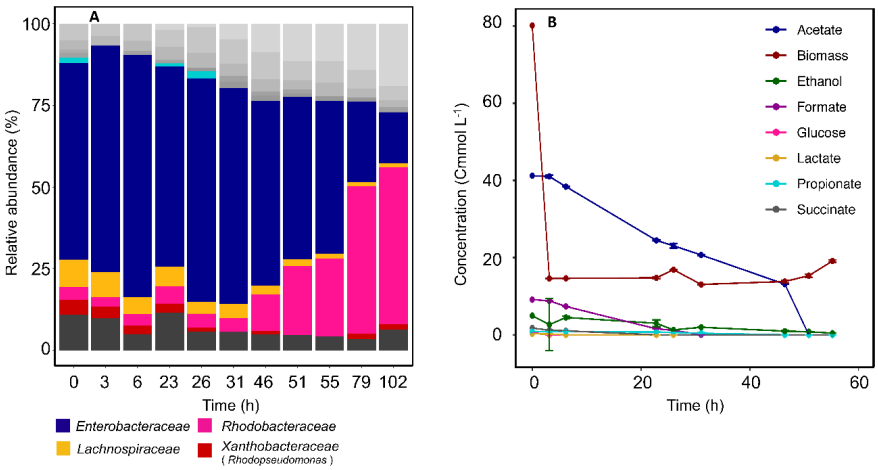

Figure 6. **A: Microbial composition after the stop to the glucose feed. Over time, the FCB relative abundance decreased over time, while the Rhodobacteraceae increased. B: Fermentation products concentration after the glucose feed-stop. After 55 h all the fermentation products were depleted.**

3.3 Metabolic strategies for tuning the microbial assembly of FCB and PPB

Microorganisms use a combination of adaptive reactions to coexist with other organisms. Based on the adaptation techniques, two major types of organisms can be identified (Andrews & Harris, 1986), namely r- and K-strategists. The r-strategists show high growth and conversion rates, in low-populated and resources-rich environments. K-strategists thrive in highly populated environments, where the resources are limited. They exhibit lower growth rates but high substrate conversion yields.

Under the different reactor regimes, the microbial communities followed this postulate. *Enterobacteriaceae* were predominant under non-limiting conditions (batches) and can be classified as r-organisms. *Clostridiaceae* and *Lachnospiraceae* showed high growth rates in nutrient-limiting environments (chemostat) and can be classified as K-strategists. Among the PPB guild, *Xanthobacteraceae* like *Rhodopseuodmonas* showed a high-rate behavior, dominating in substrate-rich environments. *Rhodobacteraceae* showed high efficiency typical of K-organisms, being able to survive to nutrient-limited environments, as the CSTRs (Table 4).

Substrates	Maximum growth rate μ_{max} (h^{-1})				
	Fermentative chemoorganoheterotrophic bacteria (FCB)			Purple photoorganoheterotrophic bacteria (PPB)	
	Enterobacteriaceae	*Lachnospiraceae*	*Clostridiaceae*	*Rhodopseudomonas*	*Rhodobacter*
Glucose	0.3 – 1 *(Hasona et al., 2004; Khanna et al., 2012)*	0.3 (Soto-Martin et al., 2020)	0.25 (Gomez-Flores et al., 2015)	0.014 (Conrad & Schlegel, 1978)	0.1 (Imam et al., 2011)
Acetate	-	-	-	0.15 (Cerruti et al., 2020)	0.05 (Kopf & Newman, 2012)
Selection strategy	r-strategist (on glucose)	K-strategist (on glucose)	K-strategist (on glucose)	r-strategist (on acetate)	K-strategist (on acetate)

Table 4. **Reported maximum growth rates of the main FCB and PPB in the systems under glucose and acetate feed and adaptation strategies.**

Kinetic parameters define the microbial selection mechanisms in CSTRs (Kuenen, 2019). In the CSTRs, the dilution rate set to retain PPB in the system was relatively low (0.04 h^{-1}) compared to the maximum growth rates of the fermentative organisms (0.5-1 h^{-1}). In a continuous culture, the substrate (here glucose) is the limiting compound, and the organisms with higher affinity for it get predominant (Andrews & Harris, 1986). Within the guild of FCB, *Clostridiaceae* and *Lachnospiaraceae* are expected to harbor a lower affinity constant (K_s), outcompeting *Enterobacteriaceae.* The controlled

pH (7.0) and appropriate dilution rate (0.04 h^{-1}) sustained the persistence of PPB. Notably, *Rhodobacteraceae* were enriched in the glucose-fed CSTRs regardless the illumination conditions. We propose here a syntrophic association of FCB and PPB for glucose conversion toward CO_2 and biomass (**Figure 4**). Glucose was first converted into acetate, ethanol, formate and lactate, and lactate was further transformed into acetate and propionate. All the fermentation products can be potentially used by PPB for growth.

3.3.1 Syntrophic associations between FCB and PPB

The syntrophy between FCB and PPB is not only important at an ecological level but can also be exploited for wastewater treatment. FCB are used to treat food and agricultural wastes, to degrade sugars and produce biofuels as bioethanol and hydrogen gas, or carboxylates like VFAs (L. Li et al., 2015; Thapa et al., 2019). PPB, thanks to high biomass yields (Alloul et al., 2018), harbor a major industrial potential for the production of antioxidants and single-cell proteins.

3.3.2 Advantages of single-sludge and two-sludge processes for the treatment and valorization of carbohydrate-based aqueous feedstocks by FCB and PPB

The single-step bioprocess implemented here by combining the metabolisms of FCB and PPB in one single sludge can help to simultaneously treat carbohydrate-rich wastewaters, factually removing the organic pollutants, and enriching organisms with high industrial potential (*i.e.* for single cell proteins and photopigments production). An integrated single-stage process combining fermentation and photoorganoheterotrophy allows to treat carbohydrates in only one tank, therefore minimizing capital and operating expenditures. The illumination conditions did not affect the syntrophy between FCB and PPB. A discontinuous illumination can further reduce the operational costs compared to a continuously irradiated system (Qin et al., 2018). Understanding interactions between the FCB and PPB will help design efficient processes for carbohydrates-based wastewater treatment and valorization, in example toward single cell proteins production. If the aim is to maximize and valorize the PPB biomass, a two-sludge process can be efficient to first ferment carbohydrates in a first tank selecting for FCB and supply the fermentation products (whose spectrum can be engineered by mastering the selection of fermentative microbial niches) to a subsequent photoorganoheterotrophic compartment to select for, *e.g.*, an edible PPB biomass, both tanks being operated as selective open mixed cultures.

4. Conclusions

We elucidated the competitive and syntrophic phenomena between FCB and PPB in mixed culture. FCB degrade glucose into VFAs, lactate and ethanol. Acetate was preferentially assimilated into biomass by PPB. Combination of acetate and IR light supply selectively enriches for PPB. The operational conditions are crucial to establish an interaction between FCB and PPB guilds. FCB are more efficient, fast-growing fermenters than the metabolically versatile PPB. In glucose-fed batches, FCB outcompeted PPB under the action of both faster growth rate and pH drop. In glucose-fed CSTRs, PPB got enriched up to 30% in syntrophic association with FCB. An appropriate dilution rate (0.04 h^{-1}) and pH regulation to 7.0 enabled to enrich PPB in glucose-rich environments by enabling their metabolic coupling with FCB.

References

Abo-Hashesh, M., & Hallenbeck, P. C. (2012). Microaerobic dark fermentative hydrogen production by the photosynthetic bacterium, Rhodobacter capsulatus JP91. *International Journal of Low-Carbon Technologies*, *7*(2), 97–103. https://doi.org/10.1093/ijlct/cts011

Alloul, A., Ganigué, R., Spiller, M., Meerburg, F., Cagnetta, C., Rabaey, K., & Vlaeminck, S. E. (2018). Capture–Ferment–Upgrade: A Three-Step Approach for the Valorization of Sewage Organics as Commodities. *Environmental Science & Technology*, *52*(12), 6729–6742. https://doi.org/10.1021/acs.est.7b05712

Andrews, J. H., & Harris, R. F. (1986). *r- and K-Selection and Microbial Ecology* (pp. 99–147). https://doi.org/10.1007/978-1-4757-0611-6_3

Aristilde, L., Lewis, I. A., Park, J. O., & Rabinowitz, J. D. (2015). Hierarchy in pentose sugar metabolism in Clostridium acetobutylicum. *Applied and Environmental Microbiology*, *81*(4), 1452–1462.
https://doi.org/10.1128/AEM.03199-14

Blankenship, R., Madigan, M., & Bauer, C. (1995). *Anoxygenic Photosynthetic Bacteria* (R. E. Blankenship, M. T. Madigan, & C. E. Bauer (Eds.); Vol. 2). Springer Netherlands. https://doi.org/10.1007/0-306-47954-0

Bolyen, E., Rideout, J. R., Dillon, M. R., Bokulich, N. A., Abnet, C. C., Al-Ghalith, G. A., Alexander, H., Alm, E. J., Arumugam, M., Asnicar, F., Bai, Y., Bisanz, J. E., Bittinger, K., Brejnrod, A., Brislawn, C. J., Brown, C. T., Callahan, B. J., Caraballo-Rodríguez, A. M., Chase, J., … Caporaso, J. G. (2019). Reproducible, interactive, scalable and extensible microbiome data science using QIIME 2. *Nature Biotechnology*, *37*(8), 852–857. https://doi.org/10.1038/s41587-019-0209-9

Cerruti, M., Ouboter, H. T., Chasna, V., van Loosdrecht, M. C. M., Picioreanu, C., & Weissbrodt, D. G. (2020). Effects of light / dark diel cycles on the photoorganoheterotrophic metabolism of Rhodopseudomonas palustris for differential electron allocation to PHAs and H2. *BioRxiv*.
https://doi.org/10.1101/2020.08.19.258533

Cerruti, M., Stevens, B., Ebrahimi, S., Alloul, A., Vlaeminck, S. E., & Weissbrodt, D. G. (2020). *Enriching and aggregating purple non-sulfur bacteria in an anaerobic sequencing-batch photobioreactor for nutrient capture from wastewater*. https://doi.org/https://doi.org/10.1101/2020.01.08.899062 .

Conrad, R., & Schlegel, H. G. (1978). Regulation of Glucose, Fructose and Sucrose Catabolism in Rhodopseudomonas capsulata. *Journal of General Microbiology*, *105*(2), 315–322. https://doi.org/10.1099/00221287-105-2-315

Converti, A., & Perego, P. (2002). Use of carbon and energy balances in the study of the anaerobic metabolism of Enterobacter aerogenes at variable starting glucose concentrations. *Applied Microbiology and Biotechnology*, *59*(2–3), 303–309. https://doi.org/10.1007/s00253-002-1009-5

Deines, P., Hammerschmidt, K., & Bosch, T. C. G. (2020). Exploring the Niche Concept in a Simple Metaorganism. *Frontiers in Microbiology*, *11*. https://doi.org/10.3389/fmicb.2020.01942

Ghimire, A., Frunzo, L., Pirozzi, F., Trably, E., Escudie, R., Lens, P. N. L., & Esposito, G. (2015). A review on dark fermentative biohydrogen production from organic biomass: Process parameters and use of by-products. *Applied Energy*, *144*, 73–95. https://doi.org/10.1016/j.apenergy.2015.01.045

Ghosh, S., Dairkee, U. K., Chowdhury, R., & Bhattacharya, P. (2017). Hydrogen from food processing wastes via photofermentation using Purple Non-sulfur Bacteria (PNSB) – A review. *Energy Conversion and Management*, *141*, 299–314. https://doi.org/10.1016/j.enconman.2016.09.001

Gill, C. O., & Suisted, J. R. (1978). The effects of temperature and growth rate on the proportion of unsaturated fatty acids in bacterial lipids. *Journal of General Microbiology*, *104*(1), 31–36.
https://doi.org/10.1099/00221287-104-1-31

Gomez-Flores, M., Nakhla, G., & Hafez, H. (2015). Microbial kinetics of Clostridium termitidis on cellobiose and glucose for biohydrogen production. *Biotechnology Letters*, *37*(10), 1965–1971.
https://doi.org/10.1007/s10529-015-1891-4

Grimmler, C., Janssen, H., Krauße, D., Fischer, R. J., Bahl, H., Dürre, P., Liebl, W., & Ehrenreich, A. (2011). Genome-wide gene expression analysis of the switch between acidogenesis and solventogenesis in continuous cultures of Clostridium acetobutylicum. *Journal of Molecular Microbiology and Biotechnology*, *20*(1), 1–15. https://doi.org/10.1159/000320973

Gwynne, P. J., & Gallagher, M. P. (2018). Light as a

Broad-Spectrum Antimicrobial. *Frontiers in Microbiology*, *9*(FEB). https://doi.org/10.3389/fmicb.2018.00119

Hasona, A., Kim, Y., Healy, F. G., Ingram, L. O., & Shanmugam, K. T. (2004). Pyruvate Formate Lyase and Acetate Kinase Are Essential for Anaerobic Growth of Escherichia coli on Xylose †. *JOURNAL OF BACTERIOLOGY*, *186*(22), 7593–7600. https://doi.org/10.1128/JB.186.22.7593-7600.2004

Horiuchi, J. I., Shimizu, T., Tada, K., Kanno, T., & Kobayashi, M. (2002). Selective production of organic acids in anaerobic acid reactor by pH control. *Bioresource Technology*, *82*(3), 209–213. https://doi.org/10.1016/S0960-8524(01)00195-X

Hunter, C. N., Beatty, F. D., Thurnauer, M. C., & Thomas, J. (2009). The Purple Phototrophic Bacteria. In C. N. Hunter, F. Daldal, M. C. Thurnauer, & J. T. Beatty (Eds.), *New York State Journal of Medicine* (Vol. 28, Issue 3). Springer Netherlands. https://doi.org/10.1007/978-1-4020-8815-5

Imam, S., Yilmaz, S., Sohmen, U., Gorzalski, A. S., Reed, J. L., Noguera, D. R., & Donohue, T. J. (2011). IRsp1095: A genome-scale reconstruction of the Rhodobacter sphaeroides metabolic network. *BMC Systems Biology*, *5*(July). https://doi.org/10.1186/1752-0509-5-116

Inui, M., Momma, K., Matoba, R., Ikuta, M., Yamagata, H., & Yukawa, H. (1995). Characterization of alcohol-assimilating photosynthetic purple non-sulfur bacteria and cloning of molecular chaperones from a purple non-sulfur bacterium. *Energy Conversion and Management*, *36*(6–9), 767–770. https://doi.org/10.1016/0196-8904(95)00117-V

Jang, J. W., Jung, H. M., Im, D. K., Jung, M. Y., & Oh, M. K. (2017). Pathway engineering of Enterobacter aerogenes to improve acetoin production by reducing by-products formation. *Enzyme and Microbial Technology*, *106*, 114–118. https://doi.org/10.1016/j.enzmictec.2017.07.009

Johns, A. T. (1952). The Mechanism of Propionic Acid Formation by Clostridium propionicum. *Journal of General Microbiology*, *6*(1–2), 123–127. https://doi.org/10.1099/00221287-6-1-2-123

Khanna, N., Kumar, K., Todi, S., & Das, D. (2012). Characteristics of cured and wild strains of Enterobacter cloacae IIT-BT 08 for the improvement of biohydrogen production. *International Journal of Hydrogen Energy*, *37*(16), 11666–11676. https://doi.org/10.1016/j.ijhydene.2012.05.051

Kleerebezem, R., & Van Loosdrecht, M. C. M. (2007). Mixed culture biotechnology for bioenergy production. *Current Opinion in Biotechnology*, *18*(3), 207–212. https://doi.org/10.1016/j.copbio.2007.05.001

Kopf, S. H., & Newman, D. K. (2012). Photomixotrophic growth of Rhodobacter capsulatus SB1003 on ferrous iron. *Geobiology*, *10*(3), 216–222. https://doi.org/10.1111/j.1472-4669.2011.00313.x

Kuenen, J. G. (2019). Continuous Cultures (Chemostats). In *Reference Module in Biomedical Sciences* (pp. 743–761). Elsevier. https://doi.org/10.1016/B978-0-12-801238-3.02490-9

Lamed, R. J., Lobos, J. H., & Su, T. M. (1988). Effects of Stirring and Hydrogen on Fermentation Products of Clostridium thermocellum. In *Applied and Environmental microbiology* (Vol. 54, Issue 5). http://aem.asm.org/

Li, L., Li, K., Wang, Y., Chen, C., Xu, Y., Zhang, L., Han, B., Gao, C., Tao, F., Ma, C., & Xu, P. (2015). Metabolic engineering of Enterobacter cloacae for high-yield production of enantiopure (2R,3R)-2,3-butanediol from lignocellulose-derived sugars. *Metabolic Engineering*, *28*, 19–27. https://doi.org/10.1016/j.ymben.2014.11.010

Madigan, M., Cox, J. C., & Gest, H. (1982). Photopigments in Rhodopseudomonas capsulata cells grown anaerobically in darkness. *Journal of Bacteriology*, *150*(3), 1422–1429. https://doi.org/10.1128/JB.150.3.1422-1429.1982

Martens, D. E., Béal, C., Malakar, P., Zwietering, M. H., & Van 'T Riet, K. (1999). Modelling the interactions between Lactobacillus curvatus and Enterobacter cloacae: I. Individual growth kinetics. *International Journal of Food Microbiology*, *51*(1), 53–65. https://doi.org/10.1016/S0168-1605(99)00095-1

NCBI. (n.d.). *Gene [Internet]. Bethesda (MD): National Library of Medicine (US), National Center for Biotechnology Information; 2004 –*

https://www.ncbi.nlm.nih.gov/gene/No Title.

Okubo, Y., Futamata, H., & Hiraishi, A. (2005). Distribution and Capacity for Utilization of Lower Fatty Acids of Phototrophic Purple Nonsulfur Bacteria in Wastewater Environments. *Microbes and Environments*, *20*(3), 135–143. https://doi.org/10.1264/jsme2.20.135

Pearman, P. B., Guisan, A., Broennimann, O., & Randin, C. F. (2008). Niche dynamics in space and time. In *Trends in Ecology and Evolution* (Vol. 23, Issue 3, pp. 149–158).

https://doi.org/10.1016/j.tree.2007.11.005
Pechter, K. B., Gallagher, L., Pyles, H., Manoil, C. S., & Harwood, C. S. (2016). Essential genome of the metabolically versatile alphaproteobacterium Rhodopseudomonas palustris. *Journal of Bacteriology*. https://doi.org/10.1128/JB.00771-15
Pfennig, N. (1977). Phototrophic green and purple bacteria: a comparative, systematic survey. In *Annual review of microbiology* (Vol. 31, pp. 275–290). https://doi.org/10.1146/annurev.mi.31.100177.001423
Puyol, D., Barry, E. M., Hülsen, T., & Batstone, D. J. (2017). A mechanistic model for anaerobic phototrophs in domestic wastewater applications: Photo-anaerobic model (PAnM). *Water Research*, *116*, 241–253. https://doi.org/10.1016/j.watres.2017.03.022
Puyol, Daniel, & Batstone, D. J. (2017). Editorial: Resource Recovery from Wastewater by Biological Technologies. *Frontiers in Microbiology*, *8*, 998. https://doi.org/10.3389/fmicb.2017.00998
Qin, C., Lei, Y., & Wu, J. (2018). Light/dark cycle enhancement and energy consumption of tubular microalgal photobioreactors with discrete double inclined ribs. *Bioresources and Bioprocessing*, *5*(1). https://doi.org/10.1186/s40643-018-0214-8
Rai, P. K., & Singh, S. P. (2016). Integrated dark- and photo-fermentation: Recent advances and provisions for improvement. *International Journal of Hydrogen Energy*, *41*(44), 19957–19971.
https://doi.org/10.1016/j.ijhydene.2016.08.084
Rombouts, J. L., Kranendonk, E. M. M., Regueira, A., Weissbrodt, D. G., Kleerebezem, R., & Loosdrecht, M. C. M. (2020). Selecting for lactic acid producing and utilising bacteria in anaerobic enrichment cultures. *Biotechnology and Bioengineering*, *117*(5), 1281–1293. https://doi.org/10.1002/bit.27301
Rombouts, J. L., Mos, G., Weissbrodt, D. G., Kleerebezem, R., & Van Loosdrecht, M. C. M. (2019a). Diversity and metabolism of xylose and glucose fermenting microbial communities in sequencing batch or continuous culturing. *FEMS Microbiology Ecology*, *95*(2), 233. https://doi.org/10.1093/femsec/fiy233
Rombouts, J. L., Mos, G., Weissbrodt, D. G., Kleerebezem, R., & Van Loosdrecht, M. C. M. (2019b). The impact of mixtures of xylose and glucose on the microbial diversity and fermentative metabolism of sequencing-batch or continuous enrichment cultures. *FEMS Microbiology Ecology*, *95*, 112.
https://doi.org/10.1093/femsec/fiz112
Soto-Martin, E. C., Warnke, I., Farquharson, F. M., Christodoulou, M., Horgan, G., Derrien, M., Faurie, J.-M., Flint, H. J., Duncan, S. H., & Louis, P. (2020). *Vitamin Biosynthesis by Human Gut Butyrate-Producing Bacteria and Cross-Feeding in Synthetic Microbial Communities*. https://doi.org/10.1128/mBio.00886-20
Stomp, M., Huisman, J., Stal, L. J., & Matthijs, H. C. P. (2007). Colorful niches of phototrophic microorganisms shaped by vibrations of the water molecule. *The ISME Journal*, *1*(4), 271–282. https://doi.org/10.1038/ismej.2007.59
Tanisho, S. (1998). Hydrogen Production by Facultative Anaerobe Enterobacter aerogenes. In O. R. Zaborsky, J. R. Benemann, T. Matsunaga, J. Miyake, & A. San Pietro (Eds.), *BioHydrogen* (pp. 273–279). Springer US. https://doi.org/10.1007/978-0-585-35132-2_35
Temudo, M. F., Muyzer, G., Kleerebezem, R., & Van Loosdrecht, M. C. M. (2008). Diversity of microbial communities in open mixed culture fermentations: Impact of the pH and carbon source. *Applied Microbiology and Biotechnology*, *80*(6), 1121–1130. https://doi.org/10.1007/s00253-008-1669-x
Thapa, L. P., Lee, S. J., Park, C., & Kim, S. W. (2019). Metabolic engineering of Enterobacter aerogenes to improve the production of 2,3-butanediol. *Biochemical Engineering Journal*, *143*, 169–178. https://doi.org/10.1016/j.bej.2018.12.019
Tsuji, A., Kaneko, Y., Takahashi, K., Ogawa, M., & Goto, S. (1982). The Effects of Temperature and pH on the Growth of Eight Enteric and Nine Glucose Non-Fermenting Species of Gram-Negative Rods. *Microbiology and Immunology*, *26*(1), 15–24. https://doi.org/10.1111/j.1348-0421.1982.tb00149.x
Venegas, D. P., De La Fuente, M. K., Landskron, G., González, M. J., Quera, R., Dijkstra, G., Harmsen, H. J. M., Faber, K. N., & Hermoso, M. A. (2019). Short chain fatty acids (SCFAs)mediated gut epithelial and immune regulation and its relevance for inflammatory bowel diseases. In *Frontiers in Immunology* (Vol. 10, Issue MAR, p. 277). Frontiers Media S.A. https://doi.org/10.3389/fimmu.2019.00277
Vos, P., Garrity, G., Jones, D., Krieg, N. R., Ludwig, W., Rainey, F. A., Schleifer, K.-H., & Whitman, W. B. (2005). Bergey's Manual® of Systematic Bacteriology. In D. J. Brenner, N. R. Krieg, & J. T. Staley (Eds.), *Bergey's Manual® of Systematic Bacteriology*. Springer US. https://doi.org/10.1007/0-387-29298-5

Wijffels, R. H., Barten, H., & Reith, R. H. (2003). *Bio-methane and bio-hydrogen : status and perspectives of biological methane and hydrogen production* (J. H. Reith & R. H. Wijffels (Eds.)). Dutch Biological Hydrogen Foundation.

Winkler, M.-K. H., Boets, P., Hahne, B., Goethals, P., & Volcke, E. I. P. (2017). Effect of the dilution rate on microbial competition: r-strategist can win over k-strategist at low substrate concentration. *PLOS ONE*, *12*(3), e0172785. https://doi.org/10.1371/journal.pone.0172785

Zagrodnik, R., & Laniecki, M. (2016). An unexpected negative influence of light intensity on hydrogen production by dark fermentative bacteria Clostridium beijerinckii. Bioresource Technology, 200, 1039–1043. https://doi.org/10.1016/j.biortech.2015.10.049

Supplementary material 1

Off-gas analysis of CO_2 production rate

The CO_2 partial pressure in the off-gas of the CSTR was monitored to evaluate the growth state of the biomass. For PPB, CO_2 production is a side product of acetate assimilation (Sadaie et al., 1997).

In acetate-fed CSTRs, CO_2 production was constant under continuous illumination (0.0111 ± 0.0004 C-mmol$_{CO2}$ C-mmol$_S^{-1}$) (Figure S1/A). When dark / light cycles were applied, the CO_2 production decreased to 0 C-mmol h^{-1} during the 8 h dark periods and increased again to 0.3 C-mmol h^{-1} during the 16 h light phases (Figure S1/B). The CO_2 production during the light phases indicated that acetate was continuously assimilated, whereas the sudden decrease during the dark periods (1/3 less within the first hour of dark) indicated that the metabolic activity was switched off. An oscillation in the CO_2 production rate was already observed in *Rhodopseudomonas* pure cultures under CSTR (Cerruti et al., 2020). In both cases, when the substrate was provided in excess, PPB grew with a growth rate close to μ_{max} (0.1 h^{-1}) during the light periods. In the dark, PPB halted their metabolic activity.

Both under continuous illumination and dark/light cycles, a change in CO_2 production was observed 24-48 h after the switch from acetate feed to glucose feed. In the CSTR under continuous illumination, a peak of CO_2 production reached 1.2 C-mmol h^{-1} 24 h (ca 1 HRT) after the switch to the glucose feed and stabilized at 0.6 C-mmol h^{-1} 2 days later (Figure S1/A). Under light / dark cycles a peak of CO_2 production (up to 5.6 C-mmol h^{-1}) was observed after two full cycles (3.8 HRTs from the glucose switch). After 8 HRTs from the switch to the glucose feed, the CO_2 production rate presented oscillations between light and dark periods. The CO_2 production rate increased of 0.5 C-mmol h^{-1} at the beginning of the light phase and it decreased of 0.4 C-mmol h^{-1} in every dark period (Figure S1/B). This behavior was observed for 8 HRTs, until the pH dropped to 2 due to a technical failure.

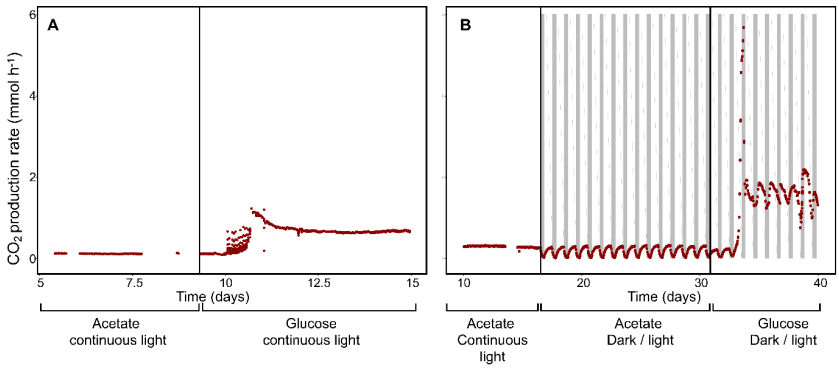

Figure S-1. A: **CO_2 production rates under acetate-fed and glucose-fed CSTR continuous light conditions. An increase of ca 1 mmol h^{-1} was observed 3 days after the switch to glucose feed, and then stabilized. B: CO_2 production rates under acetate continuous light, acetate dark / light and glucose dark / light conditions. Under acetate continuous illumination CO_2 was produced at constant rate. Under acetate dark / light CO_2 was produced only during the light periods. Under glucose dark / light conditions, a peak in production rate was observed after 3 days from the switch to the glucose-feed. The production rates increased during dark periods and decreased during light periods.**

Supplementary material 2

Detailed amplicon sequencing analysis of the four CSTR conditions

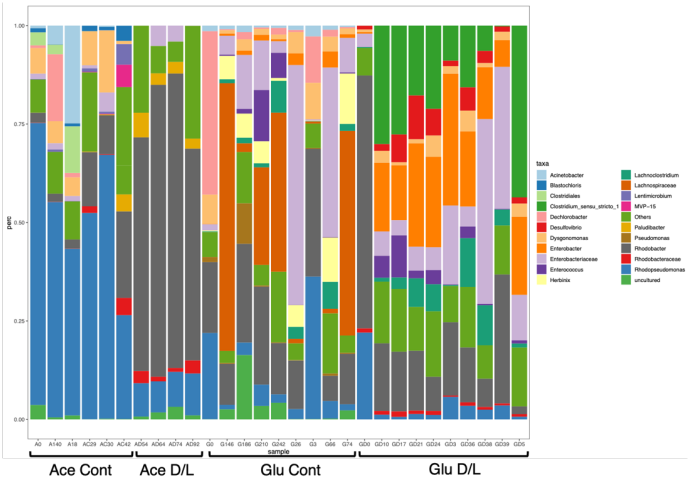

Figure SI-2: **Relative abundance of the microbial genera analysed. During the acetate-fed CSTR under continuous illumination, Rhodopseudomonas was the dominant genus. Once the light/dark cycles were applied, the community shifted toward toward the genus Rhodobacter. Under glucose-fed CSTR, the FCB of the genera Lachnoclostridium, Clostridium and Enterobacter were dominant.**

Supplementary material 3

Product yields in glucose-fed batches and CSTRS

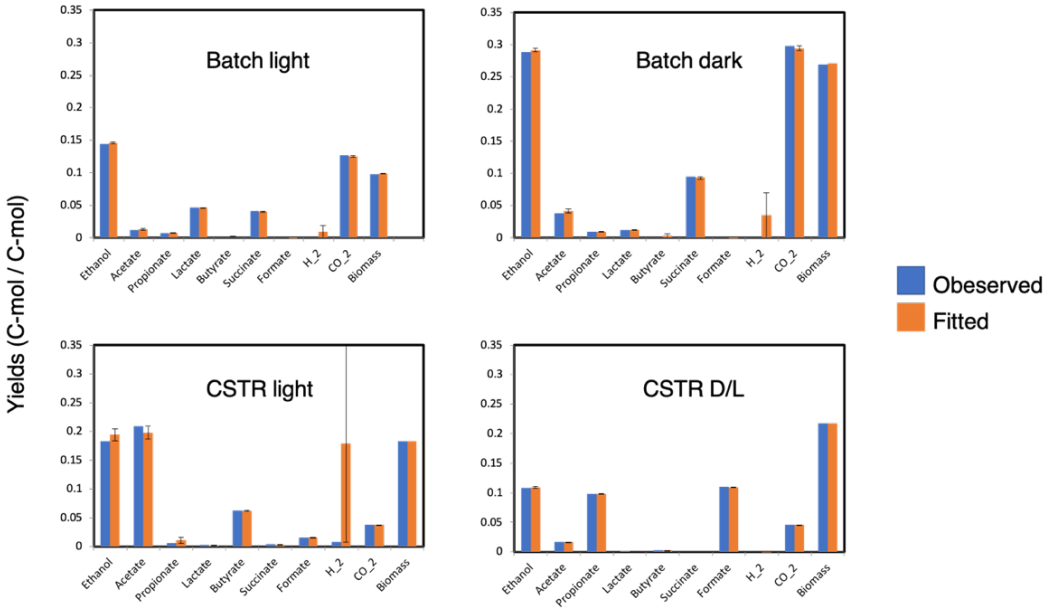

Figure SI-3: **Observed and calculated yields of product formations on glucose (C-mol / C-mol) for the mixed-culture batches and CSTRs. The calculated yields were obtained by fitting the metabolic model built based on the reactions in Table 3 by minimizing the sum of squares according to Equation 1 provided in the article.**

Chapter 5

Effect of light intensities on growth and photopigment content of a mixed culture of purple phototrophic bacteria

This chapter will be deposited in a modified version as preprint with contributions of: Marta Cerruti, Jeong-Hoon Kim, Martin Pabst, Mark C. M. van Loosdrecht and David G. Weissbrodt

Abstract

Purple bacteria (PPB) are a guild of phototrophic organisms that thrive on aquatic environments in presence of infrared (IR) light. PPB are metabolically hyper-versatile, but they use the photoheterotrophic metabolism as preferential growth mode. Photons captured from infrared light (IR) are essential in the PPB metabolism for the providence of cellular bioenergy. Thanks to their hyper versatile metabolism and high biomass yields over substrate, PPB are promising candidate for recovery of resources from wastewater. Photopigments like bacteriochlorophylls and carotenoids are high-value compounds that can be recovered from PPB biomass. Light is a pivotal parameter to control and design PPB-based recovery facilities. So far, impact of light intensity has only been studied in pure cultures of PPB, showing that light is a limiting factor for cell growth. However, the effects of light intensities on the PPB physiology and selection in mixed cultures remain unclear. Furthermore, the enzymatic mechanisms governing the adaptation strategies to different levels of photonic energy have not been elucidated.

Here, we studied the effect of IR light irradiance ranging from 0 to 350 W m^{-2} on a PPB enrichment under anaerobic sequencing batch reactor regime fed with acetate as electron donor and carbon source. Higher irradiance resulted in higher growth and carbon removal. An empirical mathematical model allowed relating the growth rate of PPB to irradiance. The cellular concentration in bacteriochlorophyll a, the pigment responsible for light harvesting, and the carotenoids, the accessory pigments, was higher (6 mg_{bchl} g_{DW}^{-1} and 3 $mg_{lycopenel}$ g_{DW}^{-1}) at an incident light of 30 W m^{-2}.

Amplicon sequencing revealed that the PPB remain dominant under all conditions (>80%), even in the absence of light. The metaproteomic analysis revealed that PPB adapt to light intensity by modulating the enzymes responsible for energy capture through the phototrophic complexes, in particular regulating the cytochrome formation and the oxidative phosphorylation pathways. The results provide in-depth phylogenetic and metabolic information on the light irradiance impacts on PPB to sustain the design of light-driven, anaerobic mixed-culture PPB processes for wastewater treatment of wastewater and the valorization of bioproducts like pigments.

Keywords: Anaerobic wastewater treatment, water resource recovery, PPB, irradiance effects

1. Introduction

Biological wastewater treatment is an established technique to treat polluted waters before discharge in the environment or re-use. Several microbial processes have been harnessed to achieve biological nutrient removal (BNR) and recovery of resources embedded in the wastewater *e.g.*, conventional activated sludge, biofilm systems, granular sludge, anaerobic processes, and phototrophic systems (Pell & Wörman, 2006). Within latest incentives to reach circular economy goals, technologies are developed to capture nutrients and valorize the microbial biomass (Guest et al., 2009; Kehrein et al., 2020)

Purple phototrophic bacteria (PPB) obtain increasing interest for wastewater treatment combined with capture of nutrients into a valuable biomass (Alloul et al., 2018; Hülsen et al., 2018b; D. Puyol et al., 2019). These anoxygenic photoorganoheterotrophs can use numerous organic and inorganic substrates as carbon and/or electron sources, growing with biomass yields over substrate close to unity by thriving on light energy (Capson-Tojo et al., 2020). PPB biomasses can be valorized for biogas and bioplastic productions, as fertilizer, and feed additive. Central to their phototrophic metabolism, PPB synthetize photopigments to capture the light and produce cellular energy (Yurkov & Beatty, 1998). Bacteriochlorophylls and carotenoids, placed in the intracellular membranes, harvest light. Bacteriochlorophylls present high quantum yields: almost all the energy from the photons is transferred and used for chemical energy production (Wraight & Clayton, 1974). Carotenoids are accessory pigments, that transfer light to the reaction centers and protect the cells from photooxidation damage (Cerullo et al., 2003). Both types of photopigments can find industrial applications. Bacteriochlorophylls can for instance be used as biomarkers in drug development (Pantiushenko et al., 2015). Carotenoids of natural and artificial synthesis, are used as food additives and food dyes (Cardoso et al., 2017).

Artificial light supply accounts for one of the major costs in photobiosystems (Blanken et al., 2013), and therefore its effects on the microbial bioprocess need to be carefully estimated. In their growth physiology, phototrophic organisms can face three main regimes driven by light intensity, namely: light limitation (growth linked to light intensity), and light saturation (Carvalho et al., 2011). PPB responses to light variations have been extensively studied in pure cultures and membrane extracts (Imam et al., 2015; Kuo et al., 2012). They adapt the number and disposition of the light harvesting complexes to the environmental conditions (Jackson et al., 2012; Muzziotti et al., 2017). The growth rates of PPB are as well dependent on light intensity (Katsuda et al., 2004), increasing with irradiance up to a saturation threshold (325 µmol photons s^{-1} m^{-2} for purple

sulfur bacteria and at around 60 µmol photons s^{-1} m^{-2} for purple non-sulfur bacteria) (Ritchie, 2013; Ritchie & Mekjinda, 2015).
Light is attenuated by the biomass and by the specific photopigment content (Lee et al., 2015). Shading effects have a substantial impact on the light available for the cells to grow, factually decreasing it. These effects are often neglected in PPB studies, where only the incident light is measured. An efficient growth of PPB in mixed culture and nutrient removal was achieved at low light intensities (1.4 W m^{-2}, or 11 µmol photons s^{-1} m^{-2} of IR light) (Dalaei et al., 2020), but the minimum quantum requirement (the minimal irradiance necessary for growth) and the 'affinity constant for light', are not reported for PPB. Despite the pivotal importance of light for PPB growth, little is known about the PPB microbial community structure and robustness under light variations.
Here, we evaluated the effect of 9 different light intensities from 350 to 0 W m^{-2} on the PPB community structure and growth kinetics, along with photopigment content. Using this wide range of light intensities, we evaluated the growth limits of a PPB enrichment, linked to photopigment content and enzymatic functionality. The knowledge developed on PPB community adaptation strategies to variations in energy supply will help develop PPB-based technologies for water resource recovery.

2. Material and methods

2.1 Reactor setup and operational conditions

A 2.5-L sequencing batch photobioreactor with 2.0-L working volume connected to a controller system (In-Control and Power units, Applikon, Netherlands) was used to cultivate the PPB enrichment on an acetate-based synthetic wastewater. The photobioreactor consisted of a cylindrically shaped vessel with a curved bottom made of borosilicate glass (transmittance ≥ 90% in the wavelength range of the filtered light (Xia et al., 2017)). Temperature was controlled at 30° C through a finger-type heat exchanger connected to a thermostat (WK 500, Lauda, Germany). Argon gas (99% purity, Linde, NL) was continuously sparged in the reactor (excluding the settling phase) to ensure anaerobic conditions. Uniform mixing was provided with a custom-made anchor stirrer. Silicon blades were attached to the anchor stirrer to wipe the inner surface of the reactor and minimize biofilm growth on the reactor surface which can severely interfere the penetration of light into the reactor. Residual biofilm growth on probes and stirrer was removed once a week.
The system was operated in a continuously-illuminated sequencing batch reactor (SBR) mode with an 8-h cycle composed of 5 min of feed, 281 min of reaction, 4 min of purging of mixed liquor, 210 min of settling, 5 min of discharge of the supernatant, 5 minutes of idle. The purge volume was adjusted based on the

conditions to maintain an SRT of 31 h. The volume exchange ratio was set to 50% of the working volume.

The cultures were provided with a synthetic wastewater medium composed of (per L): 0.914 g $C_2H_3O_2 \cdot 3H_2O$, 0.14 g KH_2PO_4, 0.21 g K_2HPO_4, 1 g NH_4Cl, 2 g $MgSO_4 \cdot 7H_2O$, 1 g $CaCl_2 \cdot 2H_2O$, 1 g NaCl, as well as 2 mL of trace elements and 2 mL of vitamins solutions. The stock solution of vitamins was composed of 200 mg thiamine–HCl, 500 mg niacin, 300 mg ρ-amino-benzoic acid, 100 mg pyridoxine–HCl, 50 mg biotin and 50 mg vitamin B12 per liter. The trace elements solution was made of (per L): 1100 mg $Na_2EDTA \cdot 2\ H_2O$, 2000 mg $FeCl_3 \cdot 6\ H_2O$, 100 mg $ZnCl_2$, 64 mg $MnSO_4 \cdot H_2O$, 100 mg H_3BO_3, 100 mg $CoCl_2 \cdot 6\ H_2O$, 24 mg $Na_2MoO_4 \cdot 2\ H_2O$, 16 mg $CuSO_4 \cdot 5\ H_2O$, 10 mg $NiCl_2 \cdot 6\ H_2O$ and 5 mg $NaSeO_3$. The cultivation medium was buffered at pH 7.0 with 4 g L^{-1} 4-(2-hydroxyethyl)-1-piperazineethanesulfonic acid (HEPES).

The SBR was started with an in-house mother mixed culture of PPB maintained under non-limiting IR light at 350 W m^{-2} (Cerruti, Stevens, et al., 2020a). The experiments at high irradiances (350, 264, 175 and 87 W m^{-2}) and the experiments at low irradiances (30, 15, 7, 3 and 0 W m^{-2}) were subsequently performed in two different periods over the year. Between these two sets of experiments the SBR was maintained at 350 W m^{-2}, for a period of 4 months.

2.2 Infrared light irradiance and measurements

The photobioreactor was placed in a dark hood to prevent external light penetration. Light was provided from two opposite sides of the reactor with halogen lamps (Philips Plusline ES 120W R7S 230V, Philips, NL), filtered through two Black 962 Infrared Transmitting Perspex Acrylic Sheets (Black Perspex 962, Plasticstocktist, UK) for supplying infrared (IR) wavelengths (λ) > 700 nm to promote PPB growth. A dimmer was used to tune the light intensity to nominal setpoints (GAMMA, NL). Incident IR light intensity at the surface of the reactor was measured with a pyranometer (CMP3; Kipp & Zonen, NL). To evaluate the effects of different light intensities, the biomass was subjected to 9 different incident light conditions: 350, 264, 175, 87, 30, 15, 7, 3 and 0 W m^{-2}. To convert the measured light intensity (W m^{-2}) to photon flux (µmol photons s^{-1} m^{-2}), the average of the photon flux per wavelength was used. To calculate it, the equation (1) was used:

$$\Phi = \frac{I \cdot \lambda \cdot 10^6}{N \cdot h \cdot c} = \frac{\mu mol\ photons}{m^2 \cdot s} \qquad (1)$$

with Φ photon flux (µmol photons s^{-1} m^{-2}), I irradiance (W m^{-2}, *i.e.*, J s^{-1} m^{-2}), λ wavelength (m), N Avogadro number ($6.02 \cdot 10^{23}$ photons $mole^{-1}$), h Planck's constant ($6.63 \cdot 10^{-34}$ J s), c speed of light ($2.88 \cdot 10^8$ m s^{-1}).

The emission spectrum of the filtered light is presented in Supplementary material 1.

2.3 Specific light supply rate

The specific light supply rate (rEX) defines the amount of light available per gram of biomass. It was calculated as in (Sforza et al., 2015)

$$rEX = \frac{PFD \cdot A}{X_{av} \cdot V} \quad (2)$$

with PFD the photon flux (µmol photons m^{-2} s^{-1}), A the irradiated surface (calculated from the reactor geometry) (m^2), X_{av} the average biomass concentration in the cycles for each condition (g L^{-1}), V the reactor working volume (L). The correlation between incident light and rEX is presented in Supplementary material 2.

2.4 Sample collection

Each light condition was maintained for 14 days (10.8 STRs). Samples for community composition analysis, photopigment concentration and acetate removal were collected from day 10-11 to day 14 after the beginning of a new light intensity condition, corresponding to 7.7 to 10.8 SRTs from the beginning of the new phase.

2.5 Measurement of biomass concentration

The biomass concentrations in the mixed liquor obtained at the different IR-light irradiances were measured by spectrophotometry (Biochrom, Libra S11, US) through absorbance at 660 nm (Abs_{660}). A calibration curve was established to correlate Abs_{660} to the biomass concentration (g VSS): $c = 1.4 \cdot Abs_{660}$. Volatile suspended solids were measured as in standard methods (Water Environment Federation, 1999).

2.6 Analysis of bacterial community compositions by amplicon sequencing

The compositions of the bacterial communities present in the mixed liquors under the different IR light irradiances were characterized from the biomass samples by V3-V4 16S rRNA gene-based amplicon sequencing as detailed in Cerruti et al., 2020. The DNA extracts were sent to Novogene (UK) for library preparation and amplicon sequencing using an Illumina 600N sequencer. The fastq files provided by Novogene were analysed with the QIIME2 pipeline (Bolyen et al., 2019). The sequencing results are at NCBI database under the Bi-oProject number ID PRJNA799236.

2.7 Extraction and analysis of photopigments

Bacteriochlorophyll and carotenoid photopigments were extracted and their mass fractions quantified and compared from the PPB biomasses obtained at the different IR light irradiances.

2.7.1 Photopigments extraction

Prior to pigments extraction, biomass was freeze-dried for 12 h at -50 °C and at a pressure of 0.05 mbar, to remove water from the pellets and facilitate polar solvents penetration.

Hexane / methanol / water in proportions of 2:1:1 (v:v:v) were used to extract the photopigments. Hexane and methanol were mixed and pre-chilled at 4°C overnight. 1200 µl of this solution were added to the biomass in a cold and dark environment. The cells were vortexed with intermittent cooling on ice to promote the extraction of non-polar compounds. Once completely resuspended, the cells were incubated in ice for 5 min. Water was added to promote the separation of the photopigments (non-polar) from cells debris, and the samples were centrifuged for 5 min at 17000 x g, resulting in two separate phases. The upper phase, non-polar, consisting of methanol and hexane, was collected for spectrophotometric quantification of the photopigments.

2.7.2 Quantification of photopigments

Concentration of the photopigments in the samples was calculated according to the Lambert-Beer equation

$$A = \varepsilon_\lambda \cdot C_p \cdot D \qquad (3)$$

Where A is the measured absorbance at the peak wavelength (lycopene = 473 nm, bchl = 776 nm), ε_λ the molar absorption coefficient (lycopene = 1.72*10^5 M^{-1} $g_{photopigment}^{-1}$, bchl = 6*10^4 M^{-1} $g_{photopigment}^{-1}$ (Bóna-Lovász et al., 2013)) of the compound at specific wavelength λ, Cp is the molar concentration of the photopigment and D is the pathlength of light (0.5 cm).

To calculate the photopigment mass fraction, the photopigments molar concentration was divided by the bacterial mass before the extraction and multiplied for the final volume of solvent (hexane) used for the elution

2.8 Calculation of growth kinetic and stoichiometric parameters

Growth rate

Biomass specific growth rates μ (h^{-1}) were calculated from the mixed culture as:

$$\mu = ln(\frac{X_1}{X_0}) \cdot \frac{1}{T_1 - T_0} \qquad (4)$$

with X_0 and X_1 the biomass concentration at the beginning and at the end of the reaction phase, respectively, and T_0 and T_1 the beginning of the reaction phase and end of the growth period, respectively.

The growth rates were fitted to the light intensity with a generic logistic function (Eq. 5) through the lsqcurvefit function of MATLAB (R2018b, Mathworks, Natick, MA, www.mathworks.com). It is a nonlinear least-square solver that finds the coefficients that best fit a given nonlinear function.

$$y = \frac{a}{1+ e^{(-b(x-c))}} \quad (5)$$

2.9 Metaproteomic analysis

High-resolution analysis of the metaproteome of the mixed culture was performed on selected biomass samples collected at the end of the experimental periods at incident irradiances of 350, 87 and 15 W m^{-2} to evaluate the differences in pathway expression. The protein extraction followed by shotgun metaproteomic analysis, pre-filtering, sequence randomisation, Unipept submission and compositional analysis is described in detail in (Kleikamp et al., 2021).

The area of the peak for each protein was normalized for the total area of each sample, and expressed as its percentage. A statistical analysis was carried on the samples triplicates using Rstudio (RStudio Team (2020). http://www.rstudio.com/). The 87 W m^{-2} condition was used as reference point. The protein average and the foldchange was calculated. A t-test was used to evaluate the significance in protein expression difference between the three conditions. Proteins with a p-value below 0.05 were marked as significantly differently expressed, comparing 350 W m^{-2} *vs* 87 W m^{-2} conditions and 15 W m^{-2} *vs* 87 W m^{-2} conditions. Proteins with a p-value < 0.05 and a $\log_2$-fold-change > 0.5 or < -0.5 were considered over- or underexpressed compared to the reference set (87 W m^{-2}) , respectively.

The UniProt accession identifiers were translated to KEGG IDs through BlastKOALA (BlastKOALA, https://www.kegg.jp/blastkoala/) server. Protein classification was done according to the KEGG database. A manual classification of the entries not represented in the KEGG database was further performed.

3. Results

3.1 Biomass growth and acetate consumption

Incident IR light intensities supplied at the surface of the anaerobic sequencing batch photobioreactor impacted biomass growth and nutrient capture by the PPB mixed culture. Under high light intensities of 350 and 264 W m^{-2}, the biomass reached a concentration plateau of 2.8 ± 0.2 g_{DW} L^{-1} (Table 1) within the first 70 min of cycle operation (Figure 1A). At medium light intensities of 175 and 87 W m^{-2}, the biomass grew to lower concentrations and continuously during the 4 h of cycle operation. At lower light intensities of 30 – 0 W m^{-2}, the biomass growth was almost negligible (Figure 1A).

Conversion-wise, at high light intensities (350 W m^{-2}), acetate was fully depleted within the first hour of reaction (Figure 1B). At 264 and 175 W m^{-2}, acetate reached a residual concentration of 0.05 ± 0.06 mmol L^{-1} and 0.04 ± 0.10 mmol L^{-1} at the end of the reaction phase (Table 1). At 87 W m^{-2}, acetate was linearly decreasing over the 4 h of incubation, reaching a final concentration 0.27 ± 0.05 mmol L^{-1}. At 30 W m^{-2}, at the end of the incubation time 2.34 ± 2.02 mmol L^{-1} of acetate was present at the end of the reaction phase. At the end of the reaction phase of the low light (15-0 W m^{-2}) conditions acetate was still present (3.10 ± 0.6 mmol L^{-1}).

	Condition ($W\ m^{-2}$)								
	0	**3**	**7**	**15**	**30**	**87**	**175**	**264**	**350**
Biomass* ($g_{DW}\ L^{-1}$)	0.09±0.02	0.15±0.01	0.75±0.05	0.61±0.06	1.28±0.02	2.04±0.11	2.37±0.06	2.65±0.04	2.94±0.48
Acetate* ($mmol\ L^{-1}$)	3.79±0.68	3.28±0.36	3.00±1.33	2.34±2.02	1.37±0.49	0.27±0.05	0.04±0.10	0.05±0.06	BDL[+]
Growth rate (h^{-1})	0.03±0.03	0.01±0.01	0.01±0.01	0.02±0.01	0.01±0.01	0.02±0.00	0.10±0.01	0.18±0.03	0.22±0.05

Table 1: **Biomass and acetate concentration at the end of the reaction phase and specific growth rates calculated for each condition**

*Concentration measured at the end of the reaction phase.
[+]BDL: below detection limit
Values are presented as average of the four cycles recorded and corresponding standard deviations.

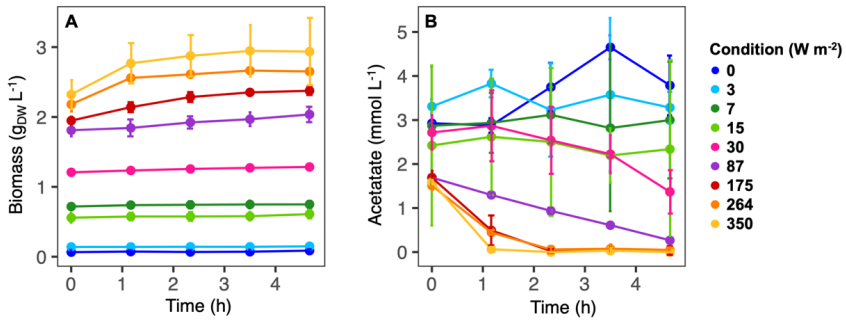

Figure 1: **Biomass (A) and acetate (B) concentration along the SBR cycles. Values are expressed as the average value for each time point. Samples were collected for three cycles. At high light intensities (350-87 W m^{-2}) acetate was fully consumed at the end of the reaction cycles. At low light intensity (30-0 W m^{-2}) acetate was still present at the end of the reaction phase and biomass growth was negligible.**

3.2 Biomass growth rates followed a logistic distribution

The growth rates decreased with the light intensity, from 0.22 ± 0.05 h^{-1} at 350 W m^{-2} to 0.03 ± 0.01 h^{-1} at 87 W m^{-2} to 0.008 ± 0.006 h^{-1} at 3 W m^{-2}. The growth rates followed a logistic distribution, both considering the specific light supply rate (rEX) (Figure 2A) and the incident light (Figure 2B). It was possible to identify two conditions: acetate- and light- limited conditions. Considering the specific light supply rate, the cultures which had no acetate at the end of the reaction phase were acetate-limited and had a rEX above 10 $\mu mol_{photons}$ s^{-1} g_{DW}^{-1}, corresponding to an incident light of 87 W m^{-2}. Below 10 $\mu mol_{photons}$ s^{-1} g_{DW}^{-1} the cultures were light limited, and growth was reduced compared to the higher irradiances. The logistic curve (Eq. 5) fitted through the data allowed to identify three parameters: *a*, corresponding to the maximum growth rate ($\mu_{max,}$ h^{-1}), *b*, a correction factor, and *c*, corresponding to a 'half saturation constant' for light. The factor *a* was identified at 0.24 and 0.22 h^{-1} for the rEX and the incident light curvess respectively. The factor *c*, at 34 $\mu mol_{photons}$ s^{-1} g_{DW}^{-1} in the rEX fit and 189 W m^{-2} in the incident light fit. In Eq. 5, *x* was defined as the light intensity (both as rEX and as incident irradiance), and *y* the specific growth rate.

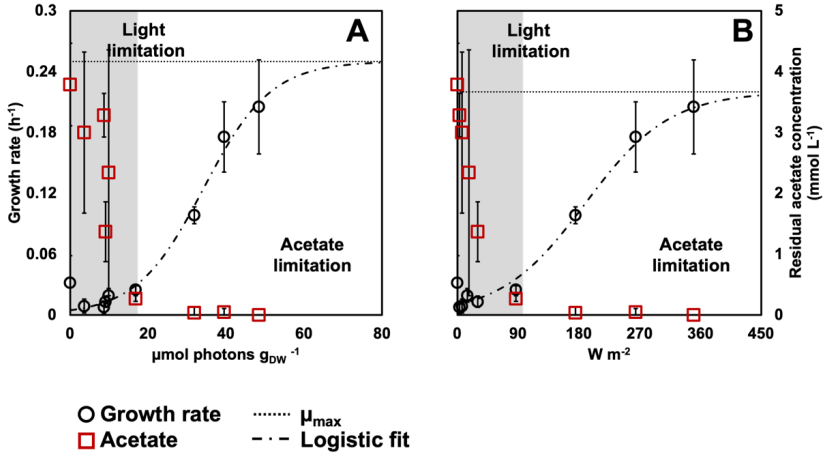

Figure 2: **Biomass growth rates (black circles) and acetate concentration (red squares) in relation to rEX (A) and incident light intensity (B). The growth rates fitted a logistic regression (dashed line), that allowed to identify the μ_{max} for the PPB enrichments (dotted line). Based on the acetate concentration at the end of the reaction phase, an acetate- and a light-limited condition were identified.**

3.3 Community composition

The taxonomic compositions of the bacterial communities obtained under the different irradiance treatments were measured by 16S rRNA gene amplicon sequencing. PPB were highly enriched, accounting for 81 ± 9 % of the total reads under all irradiance conditions, except under dark conditions (*i.e.*, 0 W m^{-2}) (Figure 3A) . Under dark conditions, the PPB enrichment decreased to 40%, while the genus *Dechloromonas* increased to 22%. Uncultured genera of the family of the *Rikenellaceae* accounted for 8%. The metaproteomic analysis confirmed the amplicon sequencing data. In the three samples analysed by metaproteomics (350, 87 and 15 W m^{-2}), more than 75 % of the proteins were assigned to genera belonging to the PPB guild, namely *Rhodopseudomonas*, *Rhodobacter*, *Blastochloris*, *Thiobaca* (Figure 3B).

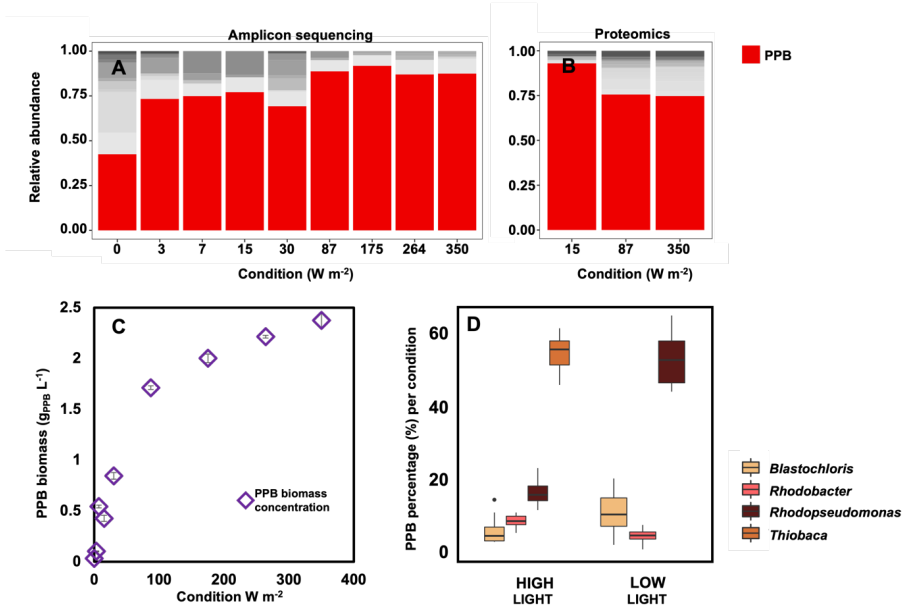

Figure 3: **A: amplicon sequencing results for community composition. PPB genera (Blastochloris, Rhodobacter, Rhodopseudomonas and Thiobaca, red bars) were the dominant guild under all condition, accounting for ca 70% of the total community, excluding under dark condition. B: metaproteomic analysis of the community composition for selected samples. These results confirmed the amplicon sequencing results. C: PPB concentration in the bulk liquid increased with the increase of incident light intensity. D: Distribution of the main PPB genera based on amplicon sequencing results under high (350-87 W m^{-2}) and low (30-0 W m^{-2}) conditions. Notably, the genus Thiobaca was present only under high light conditions.**

The concentration of PPB in the bulk liquid decreased with the decrease of the incident light, from 2.38 ± 0.07 g_{PPB} L^{-1} at 350 W m^{-2} to 0.03 ± 0.00 g_{PPB} L^{-1} under dark conditions (Figure 3C).

Among the PPB, *Thiobaca* was the dominant organism at high light intensities (350-87 W m^{-2}), with a relative abundance of 56± 6%. *Rhodopseudomonas* and *Blastochloris* reached a relative abundance of 17 ± 4 % of 7 ± 4%. Under low light conditions (30-3 W m^{-2}) *Rhodopseudomonas* and *Blastochloris* were the dominant populations, with 54 ± 8 % 12 ± 6 % respectively. The genus *Thiobaca* was not detectable under these conditions (Figure 3D.) These differences might be attributed to the different inocula in the reactor under high and light irradiation, as explained later.

3.4 Photopigment mass fraction

Wavelength scans between 320 and 1100 nm were recorded to determine the photopigment content in the whole cells of the biomass and in the pigments extract. Peaks in the wavelengths of the bacteriochlorophylls (800-900 nm) and carotenoids (between 400-500 nm) were detected under all conditions, including under dark, both in the extract and in the whole cells (Figure 4A/B). In the whole cells, under high light conditions (350-87 W m^{-2}) two peaks were detected at 800 and 890 nm, corresponding to the bacteriochlorophylls (bchl). At low light intensities (30-0 W m^{-2}), the bchl peaks were detectable at 805 and 866 nm. In the carotenoid area, peaks were detected at 322 and 370 nm under all conditions (Figure 4A).
In the extracts, the peaks for bchl were detected at 776 nm under all conditions. In the carotenoids area, peaks were present at 511, 475, 446 and 389 nm (Figure 4B). The bchl mass fraction at low light intensities (3.8 ± 1.7 mg g_{DW}^{-1} at 0-30 W m^{-2}) was about 4.6 times higher than under high irradiance (0.8 ±0.2 mg g_{DW}^{-1} at 87-350 W m^{-2}) . Similarly, the representative carotenoid (lycopene) showed a higher concentration at lower light intensities, with a maximum of about 3 mg g_{DW}^{-1} at 30 W m^{-2} (Figure 4C).

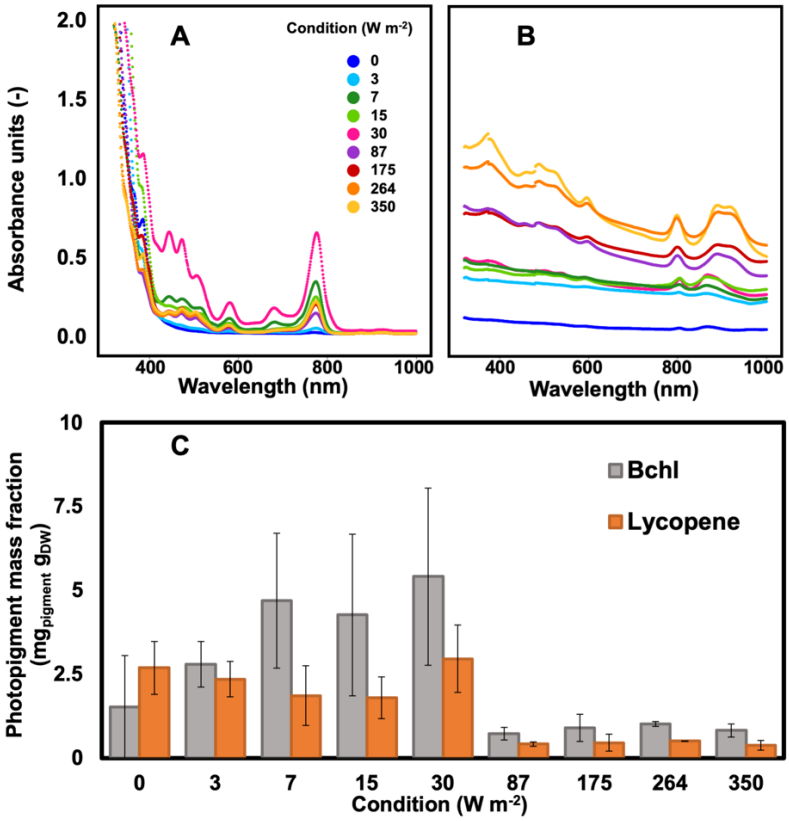

Figure 4: **A: Wavelength scan of PPB photopigments extract resuspended in hexane. The highest absorption peak was visible at 30 W m^{-2}. B: Wavelength scan of PPB whole cells. The Absorption peaks in the bchl area shifted when changing high and low light intensities. C: The photopigments (bchl and lycopene) concentration in the cells was higher at lower light intensities compared to high light intensities.**

3.5 Metaproteomics analysis

The metaproteomic analysis identified 1471 proteins. The complete metaprote-omic profile of the analysed samples is presented in Supplementary material 4. A number of 1099 of the proteins (75% of the total) belonged to the four main PPB genera identified in the amplicon sequencing analysis, namely *Thiobaca*, *Rhodopseudomonas*, *Rhodobacter* and *Blastochloris*. Under all conditions, the most abundant proteins belonged to the phototropic machinery (reaction center proteins and cytochromes) and carbon metabolism. Following KEGG classification, the proteins for the phototrophic machinery ac-counted for 22.5 ± 0.7 % of the total PPB proteins. The proteins of the reaction center (log_2-foldchange = 0.97 ± 4.61) and the light harvesting complexes (log_2-foldchange = 3.58 ± 2.52) were significantly more expressed in the 15 W m^{-2} condition compared to the 87 W m^{-2} condition. In contrast with the results of the photopigments extraction, proteins involved in the photopigment formation were under-expressed at 15 W m^{-2} compared to the 87 W m^{-2} condition. At high light intensities (350 W m^{-2}), proteins involved in phototrophic carbon fixation (log_2-foldchange = 0.09 ± 1.88) and oxidative phosphorylation were more expressed compared to the 87 W m^{-2} condition. In the carbon metabolism, at 15 W m^{-2} proteins involved in PHA metabolism were overexpressed compared to the 87 W m^{-2} (log_2-foldchange = 0.84 ± 4). Similarly, also the enzyme involved in the glyoxylate cycle, with a log_2-foldchange of 0.61± 2.75 were overexpressed. At 350 W m^{-2}, no significant difference was reported in the expression of the carbon metabolism enzymes compared to the 87 W m^{-2} condition.

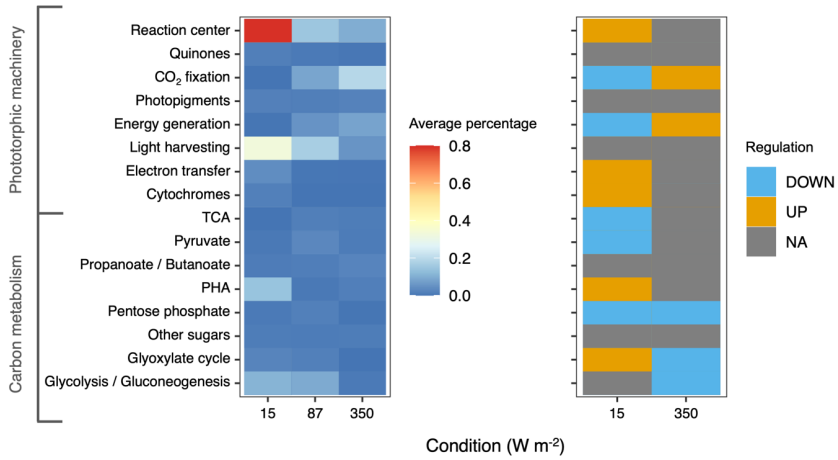

Figure 5**: A: Heatmap representing the average percentage of the protein expressed in each metabolic category based on KEGG classification. The heatmaps represents only carbon metabolism and phototrophic pathways. B: Differential regulation of the different pathways under 15 and 350 W m^{-2} compared to the 87 W m^{-2} condition. Oxidative phosphorylation and photosynthesis pathways were upregulated in the 350 W m^{-2} condition and downregulated in the 15 W m^{-2} conditions compared to the 87 W m^{-2} condition.**

4. Discussion

4.1 Photopigments content was inversely proportional to light intensity

For phototrophic organisms, energy is derived by light. Based on the irradiation conditions, PPB adapt the number and disposition of photopigments in their membranes to maximize the light harvest (Brotosudarmo et al., 2011; Gardiner et al., 1993). In line with previous observations (S. Liu et al., 2019), we report an increase in photopigment content (both bacteriochlorophylls and carotenoids) with a decrease of light intensity. In fact, bacteriochlorophyll and carotenoids mass fraction was respectively 4.6 and 10 times higher under low light conditions compared to high light conditions. The variation in the photopigment content of the biomass can be attributed to different factors. The decrease of photopigments is an acclimatization strategy to high light intensities. Muzziotti et al., 2016 report that *Rhodopseudomonas* increases the bacteriochlorophyll mass fraction by a factor 6 and the carotenoids mass fraction by a factor 2.5 when light intensity changes from 250 to 1500 $\mu mol_{phtotons}$ m^{-2} s^{-1} (corresponding to *ca* 33 and 190 W m^{-2}) under anaerobic conditions. By reducing the antenna size and consequently the amount of light absorbed, PPB protect the cells from photodamage induced by high light intensities (Bayon-Vicente et al., 2020; Muzziotti et al., 2017). Furthermore, the phototrophic growth is linked to the photopigment content and activation state of the reaction centers, that harvest

light and convert it into chemical energy (Saikin et al., 2014). To compensate for the lower energy supply, PPB increased the mass fraction of photopigments.
The variation in photopigment mass fraction might also be linked to the taxonomic composition of the enrichment. The microbial community was different in the two experimental set-ups (high and low light intensities, Figure 3D). At low light intensities, the community was enriched for the genus *Rhodopseudomonas*. At high light intensities, instead, the most abundant genus was *Thiobaca*. Each organism has a different distribution of the photopigment, both spatial and of type (Bullough et al., 2009; Timpmann et al., 2014). To maximize the efficiency of energy capture, PPB combine protein and pigments in the light-harvesting complexes and reaction center (Fixen et al., 2016). The differences in protein binding of the pigments influence the stability of the complexes (Mizoguchi et al., 2012), and potentially have affected the extraction yields in our enrichments. However, the taxonomic difference between *Thiobaca* and *Rhodopseudomonas* cannot be interpreted as a selection mechanism caused by light irradiance, such as explained in the next section.

4.2 PPB were enriched under all conditions

PPB formed the dominant guild under all conditions, confirming the possibility to efficiently enrich them on acetate as electron donor and carbon source and with IR light as energy source (Alloul et al., 2019; Cerruti et al., 2020). The supply of IR light selectively enriches for PPB and prevents the growth of other phototrophs, such as green / blue phototrophic organisms that extract their energy on other wavelengths. This prevents formation of oxygen and ensures all organic matter is available for the PPB. The PPB enrichment was confirmed both at genetic (amplicon sequencing) and functional level (metaproteomics).
The taxonomic variation from a *Thiobaca*- to a *Rhodopseudomonas*-dominant community was due to the inoculum rather than to a light effect. The low light conditions were applied to the same parent reactor 4 months after the high light conditions. The predominance of the genus *Rhodopseudomonas* at high light intensities (> 300 W m^{-2}) was repeatedly reported in other SBR systems (Cerruti et al., 2020, Cerruti et al, in preparation). In a batch system, the selective pressure is determined by the growth rates (Winkler et al., 2017). No information is currently available for the growth kinetics of *Thiobaca*. Pure cultures of *Rhodopseudomonas* present higher growth rates (μ_{max} = 0.15 h^{-1} (Cerruti, Ouboter, et al., 2020)) compared to other PPB pure cultures like *Rhodobacter* or *Blastochloris* under acetate feed (0.10 and ca 0.03 h^{-1} respectively) and was therefore predominant under SBR conditions (LaClair, 2006; Zavala et al., 2019). We were not able to detect what did cause the presence of *Thiobaca* in the initial mother culture. Potentially, the competition between purple sulfur bacteria (*Thiobaca*) and purple non-sulfur bacteria (*Rhodopseudomonas*, *Rhodobacter*, *Blastochloris*) might be linked to the

accumulation of sulfur compounds (not measured in this study). Competition phenomena between PNSB and PSB should be further researched in the future.

The PPB enrichment was stable under all IR light intensities, with a relative abundance above 75%, except for the dark condition (0 W m^{-2}). In presence of IR-light, PPB show relatively high growth rates, ranging between 0.03 and 0.3 h^{-1} (Alloul et al., 2019). Few organisms can grow under anaerobic conditions with acetate as sole carbon and electron source, since acetate is already a fermentation product. Acetoclastic organisms, like the slow-growing methanogenic archaea, present a μ_{max} of 0.004-0.013 h^{-1} (Kotsyurbenko et al., 2019). In the reactor, the SRT was controlled at 31 h, implying that the minimum growth rate to be retained in the bulk liquid was set to 0.03 h^{-1}. The taxonomic analyses showed that no methanogens were detected both at 16S rRNA gene level and at protein level. Under dark anaerobic conditions, PPB cannot grow on acetate without external electron acceptors (Yen & Marrs, 1977), which were not present in the cultivation medium. Possibly, the high relative abundance of PPB under dark conditions can be attributed to the biomass retention during the settling phase. The chemotrophic growth of *Dechloromonas* (present at 22 % under dark conditions) explains the apparent higher growth rates measured for the biomass under dark condition compared to other low light intensities. Under low-light conditions, the growth rates were almost equal to the SRT (0.03 h^{-1}). Iasimone et al., 2018 report an increase in the length of the lag phase with the decrease of light intensity. Possibly, at low light intensities the PPB enrichment was still in the lag phase. An increase of the reaction length might lead to a biomass increase, and consequently higher carbon uptake and photopigment recovery.

4.3 Enzymatic expression changed with light intensity

In the proteomic analysis, it emerged that at low light conditions the proteins responsible for the light harvest were overexpressed compared to higher light intensities. These results match the hypothesis that, with lower irradiances, cells require to produce more light harvesting complexes to be able to sustain the energy requirements. Interestingly, the proteins for the formation of accessory pigments were expressed under all conditions at the same level.

Enzymes involved in the electron transport chain and ATP generation were overexpressed at high light intensities, similarly to what reported for microalgae (Toyoshima et al., 2019). The higher ATP production rate can have enhanced the carbon fixation (photosynthesis) pathway, whose enzymes were overexpressed at high light conditions (350 W m^{-2}). In fact, the Calvin-Benson-Bassham cycle is a known mechanism of electron reallocation (McKinlay & Harwood, 2010). The energy-expensive CO_2 fixation regulates the redox balance by increasing the fixation rates when an excess of ATP is produced through the electron transport chain (Alsiyabi et al., 2019). Poly-hydroxyalkanoates

(PHA) formation in PPB is usually linked to redox stress conditions (Bayon-Vicente et al., 2020; Cerruti et al., 2020). The enzymes linked to the PHA granules were upregulated in the low light condition (15 W m^{-2}), namely proteins belonging to the phasin family. However, enzymes for PHA formation were not detected. The function of the phasin proteins under this condition is unclear.
The high standard deviations reported for the log2-foldchange can be attributed to the microbial community composition. For example, at low light intensities, where *Rhodopseudomonas* was the most abundant genus, 284 proteins belonging to *Rhodopseudomonas* were over-expressed compared to the 87 W m^{-2} condition, 58 were not significantly different and only 17 were downregulated. The opposite was reported for *Thiobaca* (the most abundant genus at high light intensities): only 2 of its proteins were upregulated at low light conditions, whereas 268 were downregulated and 32 not significantly different.
The over-expression of the glyoxylate cycle enzymes in the 15 W m^{-2} condition can also be linked to the community composition. Carbon metabolism in PPB is specie-specific, meaning that the different organisms use different pathways to catabolize acetate. For instance, the genus *Rhodopseudomonas* utilizes the glyoxylate shunt to metabolize the acetate (Albers & Gottschalk, 1976), whereas *Rhodobacter* uses the EMC pathway (Alber et al., 2006). An enrichment of *Rhodopseudomonas* in the reactor can explain an enrichment of the glyoxylate cycle proteins at low light intensities.

4.4 Growth rates are dependent to light availability

Numerous kinetics models have been constructed to correlate the growth rates of phototrophic organisms to light intensity and substrate availability (Lee et al., 2015). Light and nutrients are complementary factors contributing to growth kinetics of phototrophs. Under light-saturating conditions, concentrations of the limiting substrate (within electron donor and C-P-N nutrients), defines the growth rates, as described by the Monod model (Doran, 2013). Under nutrient-saturating conditions, growth rates are instead controlled by light intensity. At light saturation level, the maximum growth rate is achieved (Undurraga et al., 2016). Above this point, growth is inhibited (photoinhibition). Below the saturation level, growth is light-limited. At present, the definition of a univocal kinetic model for phototrophic growth is not possible, as numerous factors influence the growth rates (Lee et al., 2015). Furthermore, the kinetic parameters to define saturation and inhibition constants are species-specific (Huesemann et al., 2013), further complicating the task.
For the PPB biomass growth two conditions were found, light limited and acetate limited growth. At high light intensities (350-175 W m^{-2}), the complete depletion of the carbon source corresponded to the stop of the biomass growth, indicating that the acetate was the limiting compound. Under these conditions, the biomass grew with a growth rate close to the calculated μ_{max} (0.10-0.22 h^{-1}). At low light intensities, the biomass displayed growth rates almost 8 times lower

than under high irradiance. The presence of acetate at the end of the reaction phase suggested that the culture was light-limited. In our study, the biomass growth rates could be approximated by a logistic expression. The logistic function has been used for more than one century in ecology to describe the growth of populations (Kendrick & Kesava Pai, 1911; Verhulst, 1838). More recently, it has been used to describe the growth of some PPB (Eroğlu et al., 2004; Eroğlu et al., 2008; Koku et al., 2003). In the logistic model, the growth of a population is described in terms of intrinsic rate of increase, or μ_{max}, and the carrying capacity. In our study, the fitted μ_{max} was 0.22-0.25 h^{-1}, in the range of the reported μ_{max} for PPB (Hunter et al., 2009). The carrying capacity was defined at a rEX of 10 $\mu mol_{photons}\ s^{-1}\ g_{DW}^{-1}$, or an incident light of 87 W m^{-2}. These values can be considered as the half saturation constant for light (K_L). The (K_L) of the rEX is particularly important for process design, as it allows to determine the limit for biomass growth. Our result suggests that light is governing all the other metabolic processes, by providing energy to the cells, and an ATP balance would be required to further sustain this hypothesis. ATP production and consumption in PPB have been described in metabolic models (Golomysova et al., 2010), but an accurate measurement of the ATP produced by PPB per photon absorbed has not yet been reported.

4.5 Light intensity impacted PPB systems

In phototrophic systems, light provides energy to the cells, that use it for growth. To design a phototrophs-based process, it is necessary to accurately manage the light attenuation, as it impacts the reactor performances. The Lambert-Beer equation describes the light attenuation due to biomass concentration and photopigment content, but it is lacking the refraction and scattering component. On the other hand, the specific light supply rate describes how much light each gram of cell can experience but does not consider the optical effects. Numerous models have been developed to link nutrients and light availability to the biomass kinetic parameter (reviewed in Lee et al., 2015). These models are based on pure culture studies, and do not consider the interactions, as competition, mutualism or synthrophysm, between organisms in a community.

In the PPB enrichment, we found that the specific growth rates were correlated to the light intensity available for the cells through a logistic regression. The data fitting provided insights on the kinetic parameters of the PPB culture, as the limit for photoinhibition phenomena (μ_{max} = 0.25 h^{-1} at 80 $\mu mol_{photons}\ s^{-1}\ g_{DW}^{-1}$) and the half saturation constant for light (K_L= 10 $\mu mol_{photons}\ s^{-1}\ g_{DW}^{-1}$). Growth kinetic models are needed to understand PPB growth and therefore to optimize the cultivation condition. For scale-up purposes, mathematical modelling proves to be a useful tool to predict the microbial behavior. Future research should address a multivariate predictive analysis of the kinetic parameters of PPB enrichments.

5. Conclusions

PPB form a complex microbial guild, whose metabolism is primarily photoheterotrophic. By changing the incident light, we elucidated the mechanisms of adaptation of a PPB community to variation in energy supply. Our findings contribute to paving the way for PPB-based bioprocesses.

We can conclude that:

The PPB guild was enriched above 70% of the total community under all conditions in presence of IR light. In the dark, it was still dominant, but only at 40%.

PPB growth can be either nutrient-limited or light-limited. At a flux rate (rEX) above 10 $\mu mol_{photons}\ s^{-1}\ g_{DW}^{-1}$, the enrichment was acetate-limited. Below this point it was light limited. Notably, this value is important for process design.

PPB growth rates fitted a logistic function. This allowed to identify the maximum growth rate ($\mu_{max} = 0.25\ h^{-1}$) and the half saturation constant for light ($K_L = \mu mol_{photons}\ s^{-1}\ g_{DW}^{-1}$)

Photopigment mass fraction was *ca* 5 times higher at low light intensities compared to high light intensities. This can be due both to physiological responses and to community composition.

PPB adapted their enzymatic expression to respond to the light stress. At low light intensities the proteins involved in light-harvesting processes were more expressed, whereas at high light intensities PPB activated the mechanisms for stress response.

References

Alber, B. E., Spanheimer, R., Ebenau-Jehle, C., & Fuchs, G. (2006). Study of an alternate glyoxylate cycle for acetate assimilation by Rhodobacter sphaeroides. *Molecular Microbiology*, *61*(2), 297–309. https://doi.org/10.1111/j.1365-2958.2006.05238.x

Albers, H., & Gottschalk, G. (1976). Acetate Metabolism in Rhodopseudomonas gelatinosa and Several Other Rhodospirillaceae. *Arch. Microbiol*, *111*(1–2), 45–49. https://doi.org/10.1007/BF00446548

Alloul, A., Ganigué, R., Spiller, M., Meerburg, F., Cagnetta, C., Rabaey, K., & Vlaeminck, S. E. (2018). Capture–Ferment–Upgrade: A Three-Step Approach for the Valorization of Sewage Organics as Commodities. *Environmental Science & Technology*, *52*(12), 6729–6742. https://doi.org/10.1021/acs.est.7b05712

Alloul, A., Wuyts, S., Lebeer, S., & Vlaeminck, S. E. (2019). Volatile fatty acids impacting phototrophic growth kinetics of purple bacteria: Paving the way for protein production on fermented wastewater. *Water Research*, *152*, 138–147. https://doi.org/10.1016/j.watres.2018.12.025

Alsiyabi, A., Immethun, C. M., & Saha, R. (2019). Modeling the Interplay between Photosynthesis, CO2 Fixation, and the Quinone Pool in a Purple Non-Sulfur Bacterium. *Scientific Reports*, *9*(1), 1–9. https://doi.org/10.1038/s41598-019-49079-z

Bayon-Vicente, G., Wattiez, R., & Leroy, B. (2020). Global Proteomic Analysis Reveals High Light Intensity Adaptation Strategies and Polyhydroxyalkanoate Production in Rhodospirillum rubrum Cultivated With Acetate as Carbon Source. *Frontiers in Microbiology*, *11*, 464. https://doi.org/10.3389/fmicb.2020.00464

Blanken, W., Cuaresma, M., Wijffels, R. H., & Janssen, M. (2013). Cultivation of microalgae on artificial light comes at a cost. In *Algal Research* (Vol. 2, Issue 4, pp. 333–340). https://doi.org/10.1016/j.algal.2013.09.004

blastKOALA, https://www.kegg.jp/blastkoala/. (n.d.).

Bolyen, E., Rideout, J. R., Dillon, M. R., Bokulich, N. A., Abnet, C. C., Al-Ghalith, G. A., Alexander, H., Alm, E. J., Arumugam, M., Asnicar, F., Bai, Y., Bisanz, J. E., Bittinger, K., Brejnrod, A., Brislawn, C. J., Brown, C. T., Callahan, B. J., Caraballo-Rodríguez, A. M., Chase, J., … Caporaso, J. G. (2019). Reproducible, interactive, scalable and extensible microbiome data science using QIIME 2. *Nature Biotechnology*, *37*(8), 852–857. https://doi.org/10.1038/s41587-019-0209-9

Bóna-Lovász, J., Bóna, A., Ederer, M., Sawodny, O., & Ghosh, R. (2013). A Rapid Method for the Extraction and Analysis of Carotenoids and Other Hydrophobic Substances Suitable for Systems Biology Studies with Photosynthetic Bacteria. *Metabolites*, *3*(4), 912–930. https://doi.org/10.3390/metabo3040912

Brotosudarmo, T. H. P., Collins, A. M., Gall, A., Roszak, A. W., Gardiner, A. T., Blankenship, R. E., & Cogdell, R. J. (2011). The light intensity under which cells are grown controls the type of peripheral light-harvesting complexes that are assembled in a purple photosynthetic bacterium. *Biochemical Journal*, *440*(1), 51–61. https://doi.org/10.1042/BJ20110575

Bullough, P. A., Qian, P., & Hunter, C. N. (2009). Reaction Center-Light-Harvesting Core Complexes of Purple Bacteria. In C. N. Hunter, F. Daldal, M. C. Thurnauer, & J. T. Beatty (Eds.), *The Purple Phototrophic Bacteria* (pp. 155–179). Springer Netherlands. https://doi.org/10.1007/978-1-4020-8815-5_9

Capson-Tojo, G., Batstone, D. J., Grassino, M., Vlaeminck, S. E., Puyol, D., Verstraete, W., Kleerebezem, R., Oehmen, A., Ghimire, A., Pikaar, I., Lema, J. M., & Hülsen, T. (2020). Purple phototrophic bacteria for resource recovery: Challenges and opportunities. *Biotechnology Advances*, *43*(March), 107567. https://doi.org/10.1016/j.biotechadv.2020.107567

Cardoso, L. A. C., Karp, S. G., Vendruscolo, F., Kanno, K. Y. F., Zoz, L. I. C., & Carvalho, J. C. (2017). Biotechnological Production of Carotenoids and Their Applications in Food and Pharmaceutical Products. *Carotenoids*. https://doi.org/10.5772/67725

Carvalho, A. P., Silva, S. O., Baptista, J. M., & Malcata, F. X. (2011). Light requirements in microalgal photobioreactors: An overview of biophotonic aspects. *Applied Microbiology and Biotechnology*, *89*(5), 1275–1288. https://doi.org/10.1007/s00253-010-3047-8

Cerruti, M., Ouboter, H. T., Chasna, V., van Loosdrecht, M. C. M., Picioreanu, C., & Weissbrodt, D. G. (2020). Effects of light / dark diel cycles on the photoorganoheterotrophic metabolism of Rhodopseudomonas palustris for differential electron allocation to PHAs and H2. *BioRxiv*. https://doi.org/10.1101/2020.08.19.258533

Cerruti, M., Stevens, B., Ebrahimi, S., Alloul, A., Vlaeminck, S. E., & Weissbrodt, D. G. (2020a). *Enriching and aggregating purple non-sulfur bacteria in an anaerobic sequencing-batch photobioreactor for nutrient capture from wastewater*. https://doi.org/https://doi.org/10.1101/2020.01.08.899062 .

Cerruti, M., Stevens, B., Ebrahimi, S., Alloul, A., Vlaeminck, S. E., & Weissbrodt, D. G. (2020b). Enrichment and Aggregation of Purple Non-sulfur Bacteria in a Mixed-Culture Sequencing-Batch Photobioreactor for Biological Nutrient Removal From Wastewater. *Frontiers in Bioengineering and Biotechnology*, *8*. https://doi.org/10.3389/fbioe.2020.557234

Cerullo, G., Polli, D., Lanzani, G., De Silvestri, S., Hashimoto, H., & Cogdell, R. J. (2003). Photosynthetic light-harvesting by carotenoids: detection of an intermediate excited state. *2003 European Quantum Electronics Conference. EQEC 2003 (IEEE Cat No.03TH8665)*, *298*(December), 169. https://doi.org/10.1109/EQEC.2003.1314026

Dalaei, P., Bahreini, G., Nakhla, G., Santoro, D., Batstone, D., & Hülsen, T. (2020). Municipal wastewater treatment by purple phototropic bacteria at low infrared irradiances using a photo-anaerobic membrane bioreactor. *Water Research*, *173*, 115535. https://doi.org/10.1016/j.watres.2020.115535

Doran, P. M. (2013). *Chapter 12 - Homogeneous Reactions* (P. M. B. T.-B. E. P. (Second E. Doran (Ed.); pp. 599–703). Academic Press. https://doi.org/https://doi.org/10.1016/B978-0-12-220851-5.00012-5

Eroğlu, E., Gündüz, U., Yücel, M., Türker, L., & Eroğlu, I. (2004). Photobiological hydrogen production by using olive mill wastewater as a sole substrate source. *International Journal of Hydrogen Energy*, *29*(2), 163–171. https://doi.org/10.1016/S0360-3199(03)00110-1

Eroğlu, I., Tabanoğlu, A., Gündüz, U., Eroğlu, E., & Yücel, M. (2008). Hydrogen production by Rhodobacter sphaeroides O.U.001 in a flat plate solar bioreactor. *International Journal of Hydrogen Energy*, *33*(2), 531–541. https://doi.org/10.1016/j.ijhydene.2007.09.025

Fixen, K. R., Oda, Y., & Harwood, C. S. (2016). Clades of Photosynthetic Bacteria Belonging to the Genus Rhodopseudomonas Show Marked Diversity in Light-Harvesting Antenna Complex Gene Composition and Expression . *MSystems*, *1*(1), 1–12. https://doi.org/10.1128/msystems.00006-15

Gardiner, A. T., Cogdell, R. J., & Takaichi, S. (1993). The effect of growth conditions on the light-harvesting apparatus in Rhodopseudomonas acidophila. In *Photosynthesis Research* (Vol. 38). Kluwer Academic Publishers.

Golomysova, A., Gomelsky, M., & Ivanov, P. S. (2010). Flux balance analysis of photoheterotrophic growth of purple nonsulfur bacteria relevant to biohydrogen production. *International Journal of Hydrogen Energy*, *35*(23), 12751–12760. https://doi.org/10.1016/J.IJHYDENE.2010.08.133

Guest, J. S., Skerlos, S. J., Barnard, J. L., Beck, M. B., Daigger, G. T., Hilger, H., Jackson, S. J., Karvazy, K., Kelly, L., Macpherson, L., Mihelcic, J. R., Pramanik, A., Raskin, L., Van Loosdrecht, M. C. M., Yeh, D., & Love, N. G. (2009). A new planning and design paradigm to achieve sustainable resource recovery from wastewater. *Environmental Science and Technology*, *43*(16), 6126–6130. https://doi.org/10.1021/es9010515

Huesemann, M. H., Van Wagenen, J., Miller, T., Chavis, A., Hobbs, S., & Crowe, B. (2013).

A screening model to predict microalgae biomass growth in photobioreactors and raceway ponds. *Biotechnology and Bioengineering*, *110*(6), 1583–1594. https://doi.org/10.1002/bit.24814

Hülsen, T., Hsieh, K., Lu, Y., Tait, S., & Batstone, D. J. (2018). Simultaneous treatment and single cell protein production from agri-industrial wastewaters using purple phototrophic bacteria or microalgae – A comparison. *Bioresource Technology*, *254*, 214–223. https://doi.org/10.1016/j.biortech.2018.01.032

Hunter, C. N., Beatty, F. D., Thurnauer, M. C., & Thomas, J. (2009). The Purple Phototrophic Bacteria. In C. N. Hunter, F. Daldal, M. C. Thurnauer, & J. T. Beatty (Eds.), *New York State Journal of Medicine* (Vol. 28, Issue 3). Springer Netherlands. https://doi.org/10.1007/978-1-4020-8815-5

Iasimone, F., Panico, A., De Felice, V., Fantasma, F., Iorizzi, M., & Pirozzi, F. (2018). Effect of light intensity and nutrients supply on microalgae cultivated in urban wastewater: Biomass production, lipids accumulation and settleability characteristics. In *Journal of Environmental Management* (Vol. 223, pp. 1078–1085). https://doi.org/10.1016/j.jenvman.2018.07.024

Imam, S., Fitzgerald, C. M., Cook, E. M., Donohue, T. J., & Noguera, D. R. (2015). Quantifying the effects of light intensity on bioproduction and maintenance energy during photosynthetic growth of Rhodobacter sphaeroides. *Photosynthesis Research*, *123*(2), 167–182. https://doi.org/10.1007/s11120-014-0061-1

Jackson, P. J., Lewis, H. J., Tucker, J. D., Hunter, C. N., & Dickman, M. J. (2012). Quantitative proteomic analysis of intracytoplasmic membrane development in Rhodobacter sphaeroides. *Molecular Microbiology*, *84*(6), 1062–1078.

Katsuda, T., Yegani, R., Fujii, N., Igarashi, K., Yoshimura, S., & Katoh, S. (2004). Effects of light intensity distribution on growth of Rhodobacter capsulatus. *Biotechnology Progress*, *20*(3), 998–1000. https://doi.org/10.1021/bp030063w

Kehrein, P., Van Loosdrecht, M., Osseweijer, P., Garfí, M., Dewulf, J., & Posada, J. (2020). A critical review of resource recovery from municipal wastewater treatment plants-market supply potentials, technologies and bottlenecks. *Environmental Science: Water Research and Technology*, *6*(4), 877–910. https://doi.org/10.1039/c9ew00905a

Kendrick, A. G. M., & Kesava Pai, M. (1911). The rate of Multiplication of Micro-organisms . *Proceedings of the Royal Society of Edinburgh*.

Kleikamp, H. B. C., Pronk, M., Tugui, C., Guedes da Silva, L., Abbas, B., Lin, Y. M., van Loosdrecht, M. C. M., & Pabst, M. (2021). Database-independent de novo metaproteomics of complex microbial communities. *Cell Systems*, *12*(5), 375-383.e5. https://doi.org/10.1016/j.cels.2021.04.003

Koku, H., Eroglu, I., Gündüz, U., Yücel, M., & Türker, L. (2003). Kinetics of biological hydrogen production by the photosynthetic bacterium Rhodobacter sphaeroides O.U. 001. *International Journal of Hydrogen Energy*, *28*(4), 381–388. https://doi.org/10.1016/S0360-3199(02)00080-0

Kotsyurbenko, O. R., Glagolev, M. V., Merkel, A. Y., Sabrekov, A. F., & Terentieva, I. E. (2019). Methanogenesis in Soils, Wetlands, and Peat. In *Biogenesis of Hydrocarbons*. https://doi.org/10.1007/978-3-319-78108-2_9

Kuo, F. S., Chien, Y. H., & Chen, C. J. (2012). Effects of light sources on growth and carotenoid content of photosynthetic bacteria Rhodopseudomonas palustris. *Bioresource Technology*, *113*, 315–318. https://doi.org/10.1016/j.biortech.2012.01.087

LaClair, D. D. (2006). Optimization and characterization of the growth of the photosynthetic bacterium Blastochloris viridis and a brief survey of its potential as a remediative tool. *Optimization and Characterization of the Growth of the Photosynthetic Bacterium Blastochloris Viridis and a Brief Survey of Its Potential as a Remediative Tool*.

Lee, E., Jalalizadeh, M., & Zhang, Q. (2015). Growth kinetic models for microalgae cultivation: A review. *Algal Research*, *12*, 497–512.

https://doi.org/10.1016/j.algal.2015.10.004
Liu, S., Daigger, G. T., Kang, J., & Zhang, G. (2019). Effects of light intensity and photoperiod on pigments production and corresponding key gene expression of Rhodopseudomonas palustris in a photobioreactor system. *Bioresource Technology*, *294*(September), 122172. https://doi.org/10.1016/j.biortech.2019.122172
McKinlay, J. B., & Harwood, C. S. (2010). Carbon dioxide fixation as a central redox cofactor recycling mechanism in bacteria. *Proceedings of the National Academy of Sciences*, *107*(26), 11669–11675. https://doi.org/10.1073/pnas.1006175107
Mizoguchi, T., Isaji, M., Harada, J., & Tamiaki, H. (2012). Isolation and pigment composition of the reaction centers from purple photosynthetic bacterium Rhodopseudomonas palustris species. *Biochimica et Biophysica Acta - Bioenergetics*, *1817*(3), 395–400. https://doi.org/10.1016/j.bbabio.2011.12.001
Muzziotti, D., Adessi, A., Faraloni, C., Torzillo, G., & De Philippis, R. (2016). H2 production in Rhodopseudomonas palustris as a way to cope with high light intensities. *Research in Microbiology*. https://doi.org/10.1016/j.resmic.2016.02.003
Muzziotti, D., Adessi, A., Faraloni, C., Torzillo, G., & De Philippis, R. (2017). Acclimation strategy of Rhodopseudomonas palustris to high light irradiance. *Microbiological Research*, *197*, 49–55. https://doi.org/10.1016/j.micres.2017.01.007
Pantiushenko, I. V., Rudakovskaya, P. G., Starovoytova, A. V., Mikhaylovskaya, A. A., Abakumov, M. A., Kaplan, M. A., Tsygankov, A. A., Majouga, A. G., Grin, M. A., & Mironov, A. F. (2015). Development of bacteriochlorophyll a-based near-infrared photosensitizers conjugated to gold nanoparticles for photodynamic therapy of cancer. *Biochemistry (Moscow)*, *80*(6), 752–762. https://doi.org/10.1134/S0006297915060103
Pell, M., & Wörman, A. (2006). Biological Wastewater Treatment Systems. *Journal of Comparative Physiology A*, *192*, 270–279.
Puyol, D., Monsalvo, V. M., Marin, E., Rogalla, F., Melero, J. A., Martínez, F., Hülsen, T., & Batstone, D. J. (2019). Purple phototrophic bacteria as a platform to create the next generation of wastewater treatment plants: Energy and resource recovery. In *Wastewater Treatment Residues as Resources for Biorefinery Products and Biofuels* (pp. 255–280). Elsevier. https://doi.org/10.1016/B978-0-12-816204-0.00012-6
Ritchie, R. J. (2013). The use of solar radiation by the photosynthetic bacterium, rhodopseudomonas palustris: Model simulation of conditions found in a shallow pond or a flatbed reactor. *Photochemistry and Photobiology*, *89*(5), 1143–1162. https://doi.org/10.1111/php.12124
Ritchie, R. J., & Mekjinda, N. (2015). Measurement of photosynthesis using PAM technology in a purple sulfur bacterium thermochromatium tepidum (Chromatiaceae). *Photochemistry and Photobiology*, *91*(2), 350–358. https://doi.org/10.1111/php.12413
RStudio Team (2020). RStudio: Integrated Development for R. RStudio, PBC, Boston, MA URL http://www.rstudio.com/. (n.d.).
Saikin, S. K., Khin, Y., Huh, J., Hannout, M., Wang, Y., Zare, F., Aspuru-Guzik, A., & Tang, J. K.-H. (2014). Chromatic acclimation and population dynamics of green sulfur bacteria grown with spectrally tailored light. *Scientific Reports*, *4*(1), 5057. https://doi.org/10.1038/srep05057
Sforza, E., Calvaruso, C., Meneghesso, A., Morosinotto, T., & Bertucco, A. (2015). Effect of specific light supply rate on photosynthetic efficiency of Nannochloropsis salina in a continuous flat plate photobioreactor. *Applied Microbiology and Biotechnology*, *99*(19), 8309–8318. https://doi.org/10.1007/s00253-015-6876-7
Timpmann, K., Chenchiliyan, M., Jalviste, E., Timney, J. A., Hunter, C. N., & Freiberg, A. (2014). *Efficiency of light harvesting in a photosynthetic bacterium adapted to different levels of light*. *1837*(10), 1835–1846. https://doi.org/10.1016/j.bbabio.2014.06.007
Toyoshima, M., Sakata, M., Ohnishi, K., Tokumaru, Y., Kato, Y., Tokutsu, R., Sakamoto, W., Minagawa, J., Matsuda, F., & Shimizu, H. (2019). Targeted proteome analysis of microalgae under high-light conditions by optimized protein extraction of photosynthetic organisms. In *Journal of*

Bioscience and Bioengineering (Vol. 127, Issue 3, pp. 394–402). https://doi.org/10.1016/j.jbiosc.2018.09.001

Undurraga, D., Poirrier, P., & Chamy, R. (2016). Microalgae growth kinetic model based on the PSII quantum yield and its utilization in the operational curves construction. *Algal Research*, *17*, 330–340. https://doi.org/10.1016/j.algal.2016.05.020

Verhulst, P. F. (1838). Notice sur la loi que la population poursuit dans son accroissement. *Correspondance Mathé- Matique et Physique*, *10*, 113–121.

Water Environment Federation. (1999). Standard Methods for the Examination of Water and Wastewater. *American Public Health Association, American Water Works Association, Water Environment Federation*, *1*, 1–6.

Winkler, M.-K. H., Boets, P., Hahne, B., Goethals, P., & Volcke, E. I. P. (2017). Effect of the dilution rate on microbial competition: r-strategist can win over k-strategist at low substrate concentration. *PLOS ONE*, *12*(3), e0172785. https://doi.org/10.1371/journal.pone.0172785

Wraight, C. A., & Clayton, R. K. (1974). The absolute quantum efficiency of bacteriochlorophyll photooxidation in reaction centres of Rhodopseudomonas spheroides. *BBA - Bioenergetics*, *333*(2), 246–260. https://doi.org/10.1016/0005-2728(74)90009-7

Xia, B., Luo, J., Li, Y., Yang, B., Zhang, S., & Jiang, B. (2017). Preparation of sponge-like porous SiO2 antireflective coatings with excellent environment-resistance by an acid-catalysed sol-gel method. *RSC Advances*, *7*(43), 26834–26838. https://doi.org/10.1039/c7ra00622e

Yen, H. C., & Marrs, B. (1977). Growth of Rhodopseudomonas capsulata under anaerobic dark conditions with dimethyl sulfoxide. *Archives of Biochemistry and Biophysics*, *181*(2), 411–418. https://doi.org/10.1016/0003-9861(77)90246-6

Yurkov, V. V., & Beatty, J. T. (1998). Aerobic Anoxygenic Phototrophic Bacteria. *Microbiol. Mol. Biol. Rev.*, *62*(3), 695–724. https://doi.org/10.1038/415630a.

Zavala, N., Baeza, L., Gonzalez, S., & Choudhary, M. (2019). The Effects of Different Carbon Sources on the Growth of Rhodobacter sphaeroides. *Advances in Microbiology*, *09*(08), 737–749. https://doi.org/10.4236/aim.2019.98045

Supplementary materials

Supplementary material 1

Spectrum of the lamps with and without filter

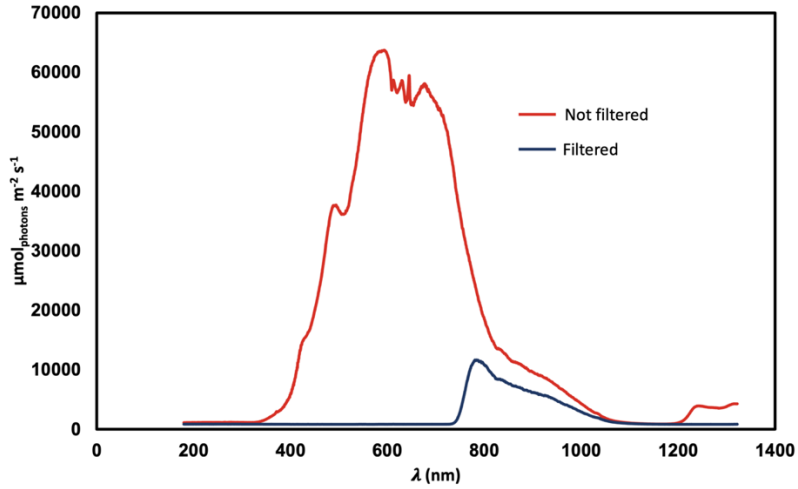

SI 1: **The light provided to the reactor was filtered with filter sheets. Only the wavelengths above 750nm were reaching the surface of the reactor.**

Supplementary material 2

Correlation between incident light and specific light supply rate

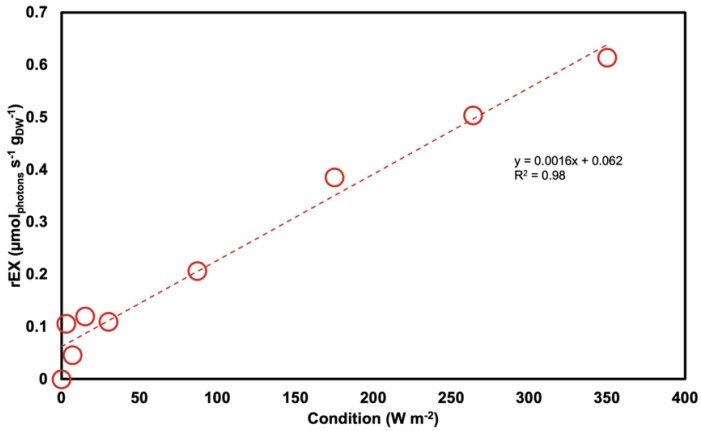

SI 2: **the incident light and the specific light supply rate (rEX) were linearly correlated. The rEX was calculated as in Material and Methods section of this chapter, and the average biomass concentration of all measured cycles under each condition was used.**

Supplementary material 3

Correlation between absorbance units and gVSS L^{-1}

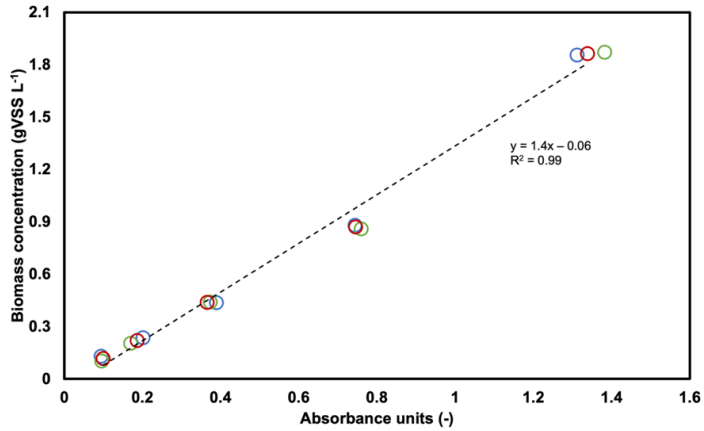

SI 3: **Correlation between the absorbance at 660 nm and the VSS concentration of the PPB-enriched biomass, based on dilution series of mixed liquor taken from the reactor (2×, 4×, 8×, 16× diluted). It displays the experimental data of three measurement series with the linear regression line. The linear regression of the triplicate measurement was y = 1.4x. For absorbance measurements, mixed-liquor samples were diluted to fit in the range from 0.2-1.0 absorbance units. On this absorbance window the correlation to VSS was considered as linear.**

Supplementary material 4

Amplicon sequencing analysis

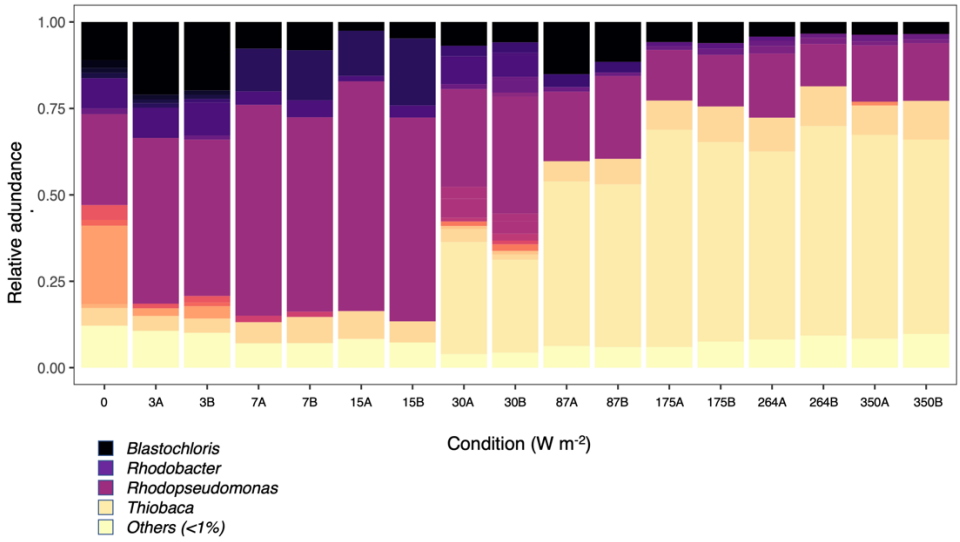

The microbial community analysis for each condition was analysed in duplicate. The results of the amplicon 16S rRNA gene sequencing are shown as relative abundance of the genera for each sample. An online-only version of the amplified reads is available

Supplementary material 5

Metaproteomic analysis, online version only

The results of the metaproteomic analysis are shown as the peak area for each identified protein. Only proteins with 2 or more peptides are here presented, to assure accuracy.

Chapter 6

General conclusions

Harnessing the metabolic versatility of purple bacteria

This thesis aimed to explore the metabolic versatility of purple phototrophic bacteria (PPB), with respect to the application of anaerobic, mixed-culture, photobioprocesses for wastewater treatment and valorization. PPB-based wastewater technologies are at their early stage of development, currently mostly relating to bench-scale ideas and technology readiness levels of 2-4. The metabolic insights on PPB gathered with pure-culture studies over the last 80 years are far to be translated into practice, for both axenic industrial biotechnologies or open environmental bioengineering processes. After early characterizations of purple bacteria and their metabolism(s) in Delft by van Niel, primary environmental applications of PPB take origin in sunlight-driven ponds used to passively treat sewage residues such as reported from Japan as early as the 1970's. By being able to combine multiple phototrophic and chemotrophic modes of growth, PPB are one of the most versatile guilds of microorganisms in nature. While growing preferentially by photoorganoheterotrophy – *e.g.*, using volatile fatty acids (VFAs) as electron donors and carbon sources, and infrared light (IR) wavelengths as energy source – their metabolism is impacted and tuned by dynamics in environmental conditions such as light / dark cycles, light intensity, substrates, and redox conditions. Understanding the mechanisms governing the microbial metabolisms and their interactions with other populations is crucial to develop and maintain mixed-culture processes for bio-based environmental and refinery services.

6.1 Excess electrons are first allocated toward PHA, and secondly toward H_2

Poly-β-hydroxyalkanoates (PHAs) and biohydrogen (H_2) are two of the major products that have been considered to be valorized from PPB process. Both compounds are an electron sink in the metabolism, implying that the production of one compound prevents the formation of the other one. Using the model PPB *Rhodopseudomonas palustris* that was isolated from an enrichment culture performed in this thesis, and applying quantitative biotechnology methods, we elucidated in **Chapter 2** the mechanisms of electron allocation between PHA and H_2. Light and dark cycles can indirectly influence the direction of the electron flux from their supply with acetate toward one or the other product, besides biomass. Under light-saturating conditions and continuous regime, the duration of the light or dark phases determines the achievement of a steady state in the photoorganoheterotrophic metabolism of *Rhodopsdeudomonas*. Long (16 h) light phases lead to complete substrate depletion and steady conditions. Short (8 h) light phases prevent substrate limitation. The excess of carbon accumulated during the dark periods is redirected toward PHA. In growing cells, H_2 results only as a minor electron sink, secondary to PHA production. The experimental results were backed up by a mathematical model that captured the metabolic dynamics of PPB under light/dark diel cycles.

6.2 PPB are enriched and aggregated in simple SBR systems

In **Chapter 3**, we investigated the possibility to enrich a PPB mixed culture in a simple and efficient way, and potentially stimulating their aggregation in a dense biomass. Continuous IR irradiation combined with acetate supply selectively enriched for PPB up to 90% of the bacterial community, regardless of the imposed sludge retention time (SRT). The PPB biomass was able to simultaneously remove nutrients (C, N, P) to levels complying to the current European regulation, by assimilation in the sludge in a single-stage reactor. The use of a sequencing batch reactor (SBR) operation strategy allowed to accumulate high biomass concentrations (as high as 3.8 g VSS L^{-1}, *i.e.*, about 10 times higher than generally reported) forming dense bioaggregates with relatively fast settling ability. The formation of aggregates was stimulated by substrate gradients generated under SBR operation, and facilitated the solid-liquid separation required for downstream processing (*i.e.*, suppressing the need for energy-expensive membranes). We showed the feasibility of a PPB-based SBR process for full biological nutrient removal, when fed with VFAs (*i.e.*, pre-fermented wastewater).

6.3 PPB and FCB form a syntrophic interaction

About 19% of the total aqueous wastes derive from food and agricultural sources. The chemical oxygen demand (COD) of these streams is substantially higher (up to 22 g_{COD} L^{1-}) compared to municipal wastewater (*ca.* 500 mg_{COD} L^{-1} (Asgharnejad et al., 2021; Roeleveld & van Loosdrecht, 2002). Food-industry wastewater, in particular derived from fruit and vegetable processing, is usually rich in sugars h-1. In this scenario, and without pH control, fermentative chemotrophic bacteria (FCB) outcompete PPB, thanks to higher growth and carbon assimilation rates. The choice of an appropriate reactor regime is crucial to establish an efficient syntrophic enrichment for the application of PPB for nutrient removal and valorization of carbohydrate-based wastewater feedstocks. In **Chapter 4** we evaluated the competitive and syntrophic mechanisms between FCB and PPB in mixed culture. PPB present slower growth rates (ca μ=0.2 h^{-1} (Conrad & Schlegel, 1977; T. Liu et al., 2014)) under glucose-fed conditions, even in pure cultures, and were therefore outcompeted by FCB (μ=0.5 h^{-1} (Rombouts et al., 2019a) in batch cultures. In continuous cultures an appropriate dilution rate of 0.04 h^{-1} and pH regulation to 7.0 allowed the enrichment of PPB (up to 30%) in glucose-rich environments by enabling their metabolic coupling with FCB. The combination of the fermentative metabolism of FCB and photoorganoheterotrophic metabolism of PPB can become attractive to treat and valorize fermentable agri-food wastewater. Different configurations of single-sludge or two-sludge processes can be designed depending on treatment and valorization targets. If the aim is to valorize PPB biomass and/or intracellular products like single-cell proteins or photopigments, a two-sludge process can be

efficient to first pre-ferment the carbohydrates into VFAs and feed them to a second SBR to produce a highly enriched PPB biomass.

6.4 Light intensity governs the physiology of PPB enrichments

PPB utilize light as energy source, and VFAs as electron donors and as carbon source to build biomass. The quantum requirements for PPB have been evaluated in pure cultures, but in mixed cultures the limits of irradiation in PPB ecophysiology had not been clarified. In **Chapter 5** we evaluated the robustness of a PPB enrichment in an acetate-fed (*ca* 1 g COD L^{-1}) SBR fed exposed to decreasing IR light intensities from 350 W m^{-2} to darkness. We concluded that PPB can still be highly enriched at about 80% of the community also at very low light intensities, close to 1 W m^{-2} (*i.e.*, highlighting the robustness of selective enrichments of PPB with VFAs and IR light), while the effective biomass growth is substantially lower (0.22 h^{-1} at high light intensities and 0.01 h^{-1} at low light intensities). Two different windows of operation were identified in function of IR light and substrate availabilities. Under incident irradiances higher than 87 W m^{-2} or 10 $\mu mol_{photons}$ s^{-1} g_{DW}^{-1}, the performance of the biosystem is governed by acetate limitation. Below this value, light limitation prevails. Under anaerobic conditions, PPB compete for acetate mainly with acetoclastic methanogenic organisms, but which present lower growth rates. PPB take advantage of the ability to derive energy from light, and compensate the lack of irradiation by increasing the production of photosynthetic complexes under low light intensities.

6.5 PPB are promising organisms for water resource recovery

From the extensive investigations performed on PPB ecology and ecophysiology from pure to mixed cultures in this thesis, the following six key conclusions can be drawn:

1) The selective enrichment of PPB is enhanced by anaerobic conditions, IR light, VFA supply: pre-fermenting wastewater feeds can be efficient to selectively produce a PPB biomass in mixed-culture process.
2) When enriched and stabilized under these conditions, PPB form an extremely robust and resilient community.

3) SBR operation helps densify PPB bioaggregates and produce a concentrated, dense fast-settling biomass that enhances volumetric conversion rates, drives full nutrient removal in a single-stage process, and facilitates solid/liquid separation and downstream processing.

4) Light management is crucial for PPB growth and simultaneous nutrient removal: below 10 μmol photons g_{DW}^{-1} PPB become light-limited, and growth is substantially limited.

5) PPB can establish syntrophic interactions with fermentative organisms for the conversion and valorization of carbohydrate-based wastewater feedstocks under careful operation of reactor regimes (*e.g.*, by tuning the dilution rate in a single-stage continuous-flow system or by separating the fermentation and photoorganoheterotrophic processes in two SBRs).

Overall, PPB are promising organisms for combined wastewater treatment and resource recovery.
Compared to other recovery schemes, PPB present some advantages: *i*) PPB get their energy from IR radiation, even at very low radiations. They assimilate almost all the carbon and electron sources for biomass growth. This is particularly important for bioproduct formation and recovery, where the biomass production needs to be maximized; *ii*) thanks to their hyper-versatile metabolism they can grow on numerous substrates. PPB grow preferentially as photoheterotrophs, and compared to microalgal processes, they do not require symbiosis with chemotrophic bacteria to produce CO_2. *Iii)* PPB are a robust community, that can easily be enriched and aggregated when fed with VFAs and under IR light irradiation. Under these conditions, contaminations and culture crashes are prevented, and a continuity of the enrichment is assured. Iv) The high nutrient removal abilities of PPB can be combined with the production of high-value compounds, like PHAs, H_2, single-cell proteins or photopigments.

Factually, PPB-based processes can be implemented for water resource recovery. In particular, they can be considered as a new-generation biophotoprocesses, that follows the principles of circular economy. They can be implemented for closed- loop biotechnology, allowing an efficient photo-based nutrient capture in wastewaters combined with a resource upcycle.

References

Asgharnejad, H., Khorshidi Nazloo, E., Madani Larijani, M., Hajinajaf, N., & Rashidi, H. (2021). Comprehensive review of water management and wastewater treatment in food processing industries in the framework of water–food–environment nexus. *Comprehensive Reviews in Food Science and Food Safety*, *20*(5), 4779–4815. https://doi.org/10.1111/1541-4337.12782

Conrad, R., & Schlegel, H. G. (1977). Different Degradation Pathways for Glucose and Fructose in Rhodopseudomonas capsulata. In *Arch. Microbiol* (Vol. 112).

Liu, T., Zhu, L., Wei, W., & Zhou, Z. (2014). Function of glucose catabolic pathways in hydrogen production from glucose in Rhodobacter sphaeroides 6016. *International Journal of Hydrogen Energy*, *39*(9), 4215–4221. https://doi.org/10.1016/j.ijhydene.2013.12.188

Roeleveld, P. J., & van Loosdrecht, M. C. M. (2002). Experience with guidelines for wastewater characterisation in The Netherlands. *Water Science and Technology*, *45*(6), 77–87. https://doi.org/10.2166/wst.2002.0095

Rombouts, J. L., Mos, G., Weissbrodt, D. G., Kleerebezem, R., & Van Loosdrecht, M. C. M. (2019). Diversity and metabolism of xylose and glucose fermenting microbial communities in sequencing batch or continuous culturing. *FEMS Microbiology Ecology*, *95*(2), 233. https://doi.org/10.1093/femsec/fiy233

Chapter 7

Outlook

The metabolic versatility of PPB confers them a substantial ecological advantage that has yet to be fully harnessed for environmental biotechnology and biorefinery services. While PPB-based wastewater treatment processes are promising, their development is still at their early stages. Some recent pilot-scale industrial applications exemplify a growing interest for PPB-based WWT and recovery. However, some considerations must be taken for up-scaling mixed-cultures processes, by making a strong link to the ecology and ecophysiology of PPB.

Considerations for scaling up PPB-based processes

1.1 Selection of the carbon and electron sources

Some considerations must be taken to efficiently exploit the extreme metabolic versatility of PPB and to enrich them. The supply of different carbon sources and electron donors is known to impact PPB biomass growth and yields. For example, a mixture of VFAs resulted in higher biomass yields and growth rates compared to the supply of only one compound (Alloul et al., 2019). On the other hand, the use of carbohydrates-rich waters resulted in a low PPB enrichment (30% *vs*. 90%) compared to VFAs feed, and a residual carbon concentration (*ca* 50 C-mmol L^{-1}) (Chapter 4). In sugar-rich streams, the use of PPB communities is probably not the most efficient process for total carbon and nutrient removal. To enrich a PPB biomass, is advisable to use two separate treatment units: one first fermentation tank enriched in FCB, and a second unit enriched in PPB, to achieve full nutrient removal and a high enrichment of high-value PPB biomass. The use of PPB in a secondary unit, following a pre-fermentation process can be very efficient to convert carbohydrates into VFAs and supply the latter to selectively foster PPB biomass growth and nutrient capture.

1.2 Selection of light

Light is arguably the foremost important parameter to grow phototrophic cultures, and a careful analysis of the light type and intensity must be considered in regard to an upscale process.

1.2.1 Homogenization of the units

Light can be described through photometric (illuminance), radiometric (irradiance) and quantum units (photons flux density). In literature, the selection of the unit depends on the discipline, tradition, instrument availability and publication. Some of the units can be directly converted into other units (*i.e.,* lux and lumen). In other cases, the conversion between units is dependent on the light wavelength and energy input of the photons (*i.e.*, W m^{-2} and mol phot m^{-2} s^{-1}), but the information about the light spectrum is often not provided. The problem of unit uniformity has been identified since the 1980's, and attempt

have been made to provide conversion tables (Thimijan & Heins, 1983). However, up to the present day, the scientific community has not yet agreed on a common unit to describe light supply in photobioprocesses. This complicates the comparison and the reproduction of the results.
To have a fast and efficient development of PPB-based and other phototrophic biotechnologies, it is necessary to harmonize the way to measure and report light inputs. One key parameter and unit for light should be set for scale up. Furthermore, light intensity is sometimes calculated to the source, without considering the biomass concentration in the biosystem. This way, attenuation phenomena are not evaluated, and the light available to the cultures is overestimated. For engineering practice, it is advisable to measure light as specific light supply rate ($\mu mol_{photons}\ s^{-1}\ g_{DW}^{-1}$), as light attenuation due to biomass concentration and light energy are considered. With this unit, it is not necessary to specify the type of light emission, and allows to directly link irradiance with microbial kinetic parameters.

1.2.2 Reactor geometry

Light attenuation in the photobioreactors is a crucial parameter to estimate. Several studies have evaluated light attenuation in phototrophic systems, and numerous models have been developed to describe phototrophic growth in function of light attenuation. Light penetration in a liquid medium is related to the path length, the biomass concentration and the photopigments content: at high biomass concentrations, such as achieved in bioreactors of this thesis, light penetrates only a few centimeters.
Under bench-scale conditions, an accurate control of light is possible, thanks to reactor geometry and operation (*i.e.* by using continuous cultures with high dilution rates, Chapter 4). In pilot and full-scale systems, reactor geometry might be a limiting factor for the development of PPB-based and phototrophic technologies in general.
Some bench-scale systems utilize membrane reactors (Hülsen et al., 2014), where PPB biofilm are grown attached to a surface. This allows an efficient solid/liquid separation, ideal for wastewater treatment. However, this type of system might not be efficient for biomass recovery, increasing the energy costs of the separation (Fasaei et al., 2018). In this thesis, we proposed the use of an anchor stirrer equipped with silicon blades to remove the biofilm on the reactor walls. It was efficient to clean-up wall biofilm formation simultaneous to stirred-tank reactor operation at bench scale. At pilot / full scale, such system might be too expensive.
Microalgae are often cultivated in tubular photobioreactors, to maximize the light penetration. A similar approach has been taken to cultivate PPB at bench-scale (Carlozzi et al., 2006). However, PPB aggregate and form thick biofilms on the reactor walls (Chapter 2). This can prevent light penetration, and consequently the development. In the present pilot plants, PPB are enriched in

tanks, ponds or raceway reactors (Deep Purple project; SEMiLLA). This operational condition maximizes the surface exposed to light compared to the reactor volume, therefore allowing a higher irradiation of the PPB biomass. Further studies on the ideal reactor geometry for PPB cultivation are needed, to combine light penetration with biomass growth and aggregation, while keeping an anaerobic or microaerophilic environment.

1.2.3 Light type

The type of wavelengths provided to the cultures is as important as the light intensity. PPB take advantage of low-energy photons irradiations, in the near and far infrared spectrum depending on the species.
Artificial LED irradiation in microalgal cultures can cost up to 11 \$ kg_{DW}^{-1}, factually decreasing the applicability of the process to larger scales (Blanken et al., 2013). For PPB, it has been calculated that the LED-lamps irradiation cost of \$ 1.9 g_{DW}^{-1} would still be higher than the potential revenues of PPB products (Capson-Tojo et al., 2020).
To selectively provide IR light to enrich for PPB, several options can be considered: i) Use of IR emitting lamps: expensive and with a very short half-life; *ii*) Use of LEDs: cheaper compared to IR lamps, LEDs emit only at specific wavelengths. In pure cultures, the choice of a specific wavelength will promote either growth either photopigments formation, depending on the species (Kuo et al., 2012; Zhou et al., 2015); in mixed cultures it will influence the community selection processes. With a combined use of different LEDs, it is possible to achieve almost a full light spectrum, potentially allowing the simultaneous enrichment of several PPB species. *iii*) Filter natural light: IR light account for almost 50% of the solar radiation. Selecting for long wavelengths would prevent the growth of green-blue phototrophs in PPB reactors. Using the filters to seal the reactor would also allow the creation of an anaerobic environment, promoting PPB growth. The use of light filters to seal ponds or raceway reactors should be further evaluated, especially in geographical areas naturally subjected to high solar radiation.

Bioproducts recovery

2.1 PPB bioproducts currently studied: H_2, PHA, proteins

In recent years, the quest for 'green' products has increased. Current research on the valorization of PPB biomass focusses mainly on the production of bioplastics (PHA), biogas (H_2), and single cell proteins.
PHAs are a promising substitute to oil-based plastics. They are recyclable and biodegradable. PHA-producing bacteria can store up to 90% of the cell weight as biopolymer, therefore being efficient biorefineries (Johnson et al., 2009). PHAs have found commercial use and are currently used also to produce fully

biodegradable plastic bottles and packaging systems (Bugnicourt et al., 2014). Nonetheless, the stability of the bioplastic depends on the form and purity of the compounds. Microbial metabolism can be engineered to tune the production of either poly-β-hydroxybutyrate or poly-β-hydroxyvalerate in axenic cultures, increasing the production costs due to sterility requirements (Chen & Jiang, 2017). Alternatives that do not require the separation of the two compounds are currently explored, e.g., for self-healing concrete (Vermeer et al., 2021).
PHA production in PPB pure cultures has been maximized to about 90% of the biomass dry weight (Montiel-Corona & Buitrón, 2021). In PPB mixed cultures, the highest PHA production reported was equivalent to only the 20% to the biomass dry weight (Luongo et al., 2017). The downstream process of extraction and purification is the limiting factor for a broad PHAs use, being laborious and expensive (Rodriguez-Perez et al., 2018). The relatively low PHA production from PPB mixed cultures reduce the interest in PPB for application.

H_2 is an energy carrier, that rose interest for its potential as biofuel. Biohydrogen production utilizes renewable resources, in a carbon-neutral process with low environmental impact (Wu et al., 2012). PPB produce hydrogen gas to dissipate electron excess via a non-growth-related processes. The H_2 production by PPB means achieved relatively high yield over substrate (up 78% of the theoretical yield, extensively reviewed in Akkerman et al., 2002). However, they have low volumetric production rates and require large volumes of substrates and large surface area photobioreactors (Hallenbeck, 2014). Despite the substantial research on photofermentation, the TLR for this process is still at level 1-3.

Single-cell protein designates microorganisms such as bacteria, fungi or microalgae with high-protein content that can be further used as feed for aquaculture, animal feed or even human consumption (Anupama & Ravindra, 2000; Daniel Puyol et al., 2017). PPB have a high protein content (up to 70% of the dry weight) compared to other bacteria (30-60%) (Honda et al., 2006; Nasseri et al., 2011). Combined with high biomass yields over substrate, a constitutive production of antioxidants, and lack of toxicity, PPB are an efficient source of protein for animals and fish feedstocks. Single-cell protein production is currently probably the most promising application of PPB mixed cultures, as it allows a direct use of the biomass.

2.2 Perspective applications: Carotenoids

Carotenoids are a class of photoactive molecules, present in almost all phototrophic organisms, from higher plants to bacteria. They are accessory pigments, harvesting light at 350-450 nm and transferring the energy to the reaction centres (Cerullo et al., 2003; Michael T. Madigan et al., 2015). Additionally, carotenoids protect the cells from photooxidation (Sipka & Maróti, 2018).

Carotenoids are currently used as food additives, in pharmaceutical preparations and the cosmetic industry (Barreiro & Barredo, 2018a). They are harnessed both for their antioxidant properties as well as for their intense yellow-red coloration, making them suitable as dyes (Cardoso et al., 2017). Carotenoids are remarkable not only for their role in light harvesting, but also for their structural importance, antioxidant properties, and action in preventing photo-damage. In humans, carotenoids reduce the risk of cardiovascular disfunctions and age-related diseases (Rao & Rao, 2007). It is estimated that the world carotenoid market will reach 6222.6 metric tons per year and a worth of $ 2.0 billions by 2022, with a yearly increase in the demand equal to 5.7 % from 2017 (Bogacz-Radomska et al., 2020).

Despite the growing demand, production and extraction of carotenoids remains a challenge. In 2019, 80-90% of the world carotenoid production was fulfilled by chemical synthesis (Saini & Keum, 2019). However, the demand for naturally produced compounds is increasing among the consumers. Natural carotenoids are primarily extracted from plants, flowers, fruits, and seeds. Due to the high costs, seasonality, and the geographic determinants of the plant production, microbial alternatives are explored (Bogacz-Radomska et al., 2020). Microbial platforms for carotenoids production are gaining interest due to the lower costs, linked to lower land requirements, year-round harvest and higher growth rate compared to plants (Barreiro & Barredo, 2018b). Only three microalgae genera are currently used for industrial carotenoid production, Dunaliella, Haematococcus, and Scenedesmus, but several other microorganisms, including fungi, are currently under examination as potential biofactories (Bonet et al., 2016).

Downstream processing is a bottleneck in the carotenoids production. Traditional extraction methods include the use of organic solvents, such as dichloromethane, hexane, methanol, ethanol, dimethyl ether, diethyl ether, toluene, 2-propanol, n-butanol, heptane, acetonitrile, tetradecane, dodecane, hexadecane, or tetrahydrofuran, some of them being problematic / forbidden for implementation at industrial scale (The European Parliament and the Council, 2018). Independently from the extraction yields, these compounds are often expensive, and considered unsafe for human health and the environment. Emerging technologies, such as ionic liquid extraction, enzyme-assisted extraction, and supercritical CO_2 (SC-CO_2) extraction gain interest as 'green' alternatives for carotenoids recovery (Richmond, 2003). SC-CO_2 extraction utilizes CO_2 at high pressure and constant temperature to extract lipophilic molecules. Its usage is advisable over organic solvents, as it is not environmentally toxic, and its disposal is safe. The density of the SC-CO_2, and therefore its polarity, can be controlled by tuning temperature and pressure conditions. This allows the extraction of different type of molecules (Baskar et al., 2019). The extraction at low temperatures (31 °C) avoids degradation and maintains the functional structure of thermosensitive compounds, like carotenoids (Shi et al., 2007). In algal systems, SC-CO_2 has been repeatedly

applied for the extraction of carotenoids and photopigments (Goto et al., 2015). CO_2 has been used pure, or in combination with co-solvents, like ethanol, to increase the extraction yields (Da Porto et al., 2014).

In the context of a circular economy, the use of PPB as wastewater biofactories for carotenoids production has not been extensively explored yet. Under anaerobic conditions, PPB naturally produce carotenoids as part of their photosynthetic machinery. In PPB, carotenoids extraction has been performed only through organic solvents. In collaboration with the Hanze University of Applied Sciences in Groningen, The Netherlands, we evaluated the feasibility of a SC-CO_2 extraction for PPB carotenoids. We cultivated Rhodopseudomonas palustris in an axenic, SBR system. We provided 0.9 g L^{-1} of sodium acetate as C-source, and high light intensities (300 W m^{-2}) as energy sources. High irradiation was chosen to promote biomass growth rather than photopigment production. PPB biomass was separated from the liquid phase by centrifugation, freeze-dried overnight, and grinded to powder. Two different extractions were attempted, with and without addition of ethanol as co-solvent (Table 1). The extract was then collected by vacuum evaporation. A 1% decrease in mass was reported after extraction with pure CO_2. The extraction yield of carotenoids from the PPB biomass (i.e., mass extracted / mass PPB (dry weight) before extraction * 100) was 1.57% m/m. An overall mass recovery of 100.67% was achieved. When ethanol was used as co-solvent, the extraction yield decreased to 0.5%. The mass of the PPB sample after extraction was higher than before the extraction, potentially indicating the presence of residual ethanol in the sample.

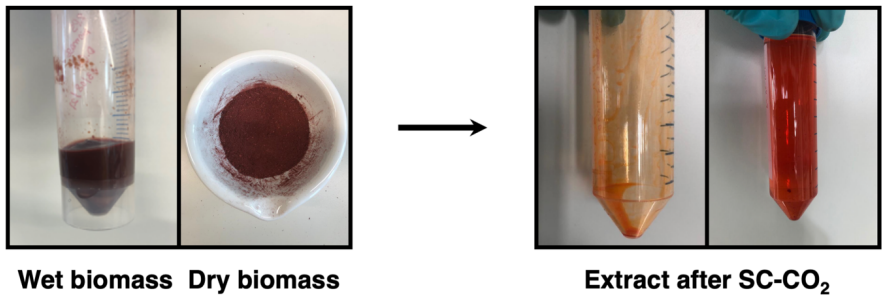

Figure 1: **Wet and dry biomass before extraction. Photopigment extracted with SC-CO_2 method**

Table 1: **SC-CO_2 extraction conditions for carotenoids recovery from PPB biomass**

	SC-CO_2 extraction 1	**SC-CO_2 extraction 2**
Pressure (bar)	300	300
Temperature (°C)	40	40
CO_2 flow rate (g min^{-1})	20	20
Extraction duration (h) Ethanol (cosolvent) flow rate (ml min^{-1})	3 -	3 0.2
Post-flushing under pressurization*	No	Yes
Post-flushing at ambient**	Yes	Yes

* flushing the extraction unit (in the absence of extractor) at 300 bar; 40 °C; 20 g/min CO_2; 0.2 ml/min EtOH; 30 min

** flushing the extraction unit (in the absence of extractor) at ambient condition; 2 ml/min EtOH; 30 min

Spectrophotometric analysis was used to qualitatively determine the extracted carotenoids. Volumes of 200 µL of extracted pigments dissolved in ethanol were used to perform a wavelengths scan, from 240 to 999 nm. Ethanol was used as measuring blank. One clear peak was visible at 470 nm (Figure 2). The absence of peaks in the 600-700 nm area indicated the absence of bacteriochlorophyll pigments, and therefore a selective extraction of carotenoids.

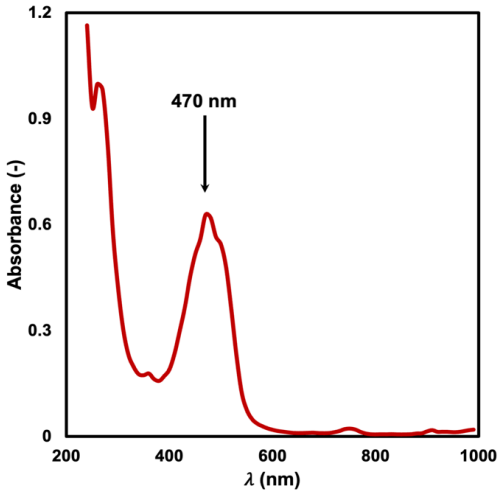

Figure 8: **Spectrophotometric analysis of the SC-CO2 extraction products. One clear peak is visible at 470 nm, but no peak is present in the 600-700 nm area, indicating the selective extraction of carotenoids.**
A precise determination of the main carotenoids extracted was not possible without HPLC or HPLC-MS analyses. In fact, the carotenoids absorption peaks are very close one to the other, and spectrophotometric analysis doesn't provide sufficient resolution (Clementson & Wojtasiewicz, 2019). As ethanol is a slightly polar compound, and the extract solution was homogeneous, we can hypnotize the presence of carotenoids with polar components.
Further and more in-depth analysis of the exact composition of the SC-CO_2 extract should be done, to assess the quality and quantity of the singular components.

The market for naturally produced carotenoids is continuously increasing. As an example, lycopene is one of the most commonly used food-grade pigments (Nigam & Luke, 2016).
Lycopene had a market worth of 107 million $ in 2020, and it is expected to grow to 187 million $ by 2030 (Bogacz-Radomska et al., 2020). The increasing demand for naturally produced compounds and additives can be filled by the microbial production of carotenoids without using plant-based technologies. In this regard, our results showed that PPB can produce almost 8 mg of carotenoids per gram of dry weight biomass (Chapter 6). As a comparison, tomato produce about 24.1 mg of carotenoids per 100 g of fresh product. Considering that the water percentage in tomatoes is 95% of the fresh product weight, the carotenoids content corresponds to 4.8 mg per g of dry product weight. With a carotenoids production almost 2 times higher than tomato, PPB are promising candidates as carotenoids biofactories.
Coupling carotenoids production with residual streams treatment has the potential to recover high-value products while recovering natural resources. European authorities have defined a framework to reclassify waste streams as secondary raw materials. As stated, waste can be re-converted into resources if: " *i) the substance or object is commonly used for specific purposes*;
there is an existing market or demand for the substance; *ii) the use is lawful (the substance or object fulfils the technical requirements for the specific purposes and meets the existing legislation and standards applicable to products)*; *iii) its use will not lead to overall adverse environmental or human health impacts* ".

In this framework and as emerged from this thesis, PPB can be used to treat VFA-rich aqueous waste streams. The high biomass concentration, and their natural propension to aggregate can be advantageous for intracellular high-value product formation and separation. Light sources and intensity of irradiation should be carefully considered for process design, specifically for carotenoids production, when biomass formation and photopigment content in the cells have a tradeoff.

References

Akkerman, I., Janssen, M., Rocha, J., & Wijffels, R. H. (2002). Photobiological hydrogen production: photochemical efficiency and bioreactor design. *International Journal of Hydrogen Energy*, *27*(11–12), 1195–1208. https://doi.org/10.1016/S0360-3199(02)00071-X

Alloul, A., Wuyts, S., Lebeer, S., & Vlaeminck, S. E. (2019). Volatile fatty acids impacting phototrophic growth kinetics of purple bacteria: Paving the way for protein production on fermented wastewater. *Water Research*, *152*, 138–147. https://doi.org/10.1016/j.watres.2018.12.025

Anupama, & Ravindra, P. (2000). Value-added food: Single cell protein. *Biotechnology Advances*, *18*(6), 459–479. https://doi.org/10.1016/S0734-9750(00)00045-8

Barreiro, C., & Barredo, J.-L. (2018a). Carotenoids Production: A Healthy and Profitable Industry. In *Methods in Molecular Biology* (Vol. 1852, pp. 45–55). https://doi.org/10.1007/978-1-4939-8742-9_2

Barreiro, C., & Barredo, J.-L. (2018b). *Microbial Carotenoids* (C. Barreiro & J.-L. Barredo (Eds.); Vol. 1852). Springer New York. https://doi.org/10.1007/978-1-4939-8742-9

Baskar, G., Kalavathy, G., Aiswarya, R., & Abarnaebenezer Selvakumari, I. (2019). Advances in bio-oil extraction from nonedible oil seeds and algal biomass. In *Advances in Eco-Fuels for a Sustainable Environment* (pp. 187–210). https://doi.org/10.1016/b978-0-08-102728-8.00007-3

Blanken, W., Cuaresma, M., Wijffels, R. H., & Janssen, M. (2013). Cultivation of microalgae on artificial light comes at a cost. In *Algal Research* (Vol. 2, Issue 4, pp. 333–340). https://doi.org/10.1016/j.algal.2013.09.004

Bogacz-Radomska, L., Harasym, J., & Piwowar, A. (2020). Commercialization aspects of carotenoids. In *Carotenoids: Properties, Processing and Applications*. Elsevier Inc. https://doi.org/10.1016/b978-0-12-817067-0.00010-5

Bonet, M. L., Canas, J. A., Ribot, J., & Palou, A. (2016). Carotenoids in Nature. In *Carotenoids in nature: biosynthesis, regulation, and function* (Vol. 79). https://doi.org/10.1007/978-3-319-39126-7

Bugnicourt, E., Cinelli, P., Lazzeri, A., & Alvarez, V. (2014). Polyhydroxyalkanoate (PHA): Review of synthesis, characteristics, processing and potential applications in packaging. *Express Polymer Letters*. https://doi.org/10.3144/expresspolymlett.2014.82

Capson-Tojo, G., Batstone, D. J., Grassino, M., Vlaeminck, S. E., Puyol, D., Verstraete, W., Kleerebezem, R., Oehmen, A., Ghimire, A., Pikaar, I., Lema, J. M., & Hülsen, T. (2020). Purple phototrophic bacteria for resource recovery: Challenges and opportunities. *Biotechnology Advances*, *43*(March), 107567. https://doi.org/10.1016/j.biotechadv.2020.107567

Cardoso, L. A. C., Karp, S. G., Vendruscolo, F., Kanno, K. Y. F., Zoz, L. I. C., & Carvalho, J. C. (2017). Biotechnological Production of Carotenoids and Their Applications in Food and Pharmaceutical Products. *Carotenoids*. https://doi.org/10.5772/67725

Carlozzi, P., Pushparaj, B., Degl'Innocenti, A., & Capperucci, A. (2006). Growth characteristics of Rhodopseudomonas palustris cultured outdoors, in an underwater tubular photobioreactor, and investigation on photosynthetic efficiency. *Applied Microbiology and Biotechnology*, *73*(4), 789–795. https://doi.org/10.1007/s00253-006-0550-z

Cerullo, G., Polli, D., Lanzani, G., De Silvestri, S., Hashimoto, H., & Cogdell, R. J. (2003). Photosynthetic light-harvesting by carotenoids: detection of an intermediate excited state. *2003 European Quantum Electronics Conference. EQEC 2003 (IEEE Cat No.03TH8665)*, *298*(December), 169. https://doi.org/10.1109/EQEC.2003.1314026

Chen, G. Q., & Jiang, X. R. (2017). Engineering bacteria for enhanced polyhydroxyalkanoates (PHA) biosynthesis. *Synthetic and Systems Biotechnology*, *2*(3), 192–197. https://doi.org/10.1016/j.synbio.2017.09.001

Clementson, L. A., & Wojtasiewicz, B. (2019). Dataset on the absorption characteristics of extracted phytoplankton pigments. *Data in Brief*, *24*, 103875. https://doi.org/10.1016/j.dib.2019.103875

Da Porto, C., Decorti, D., & Natolino, A. (2014). Water and ethanol as co-solvent in supercritical fluid

extraction of proanthocyanidins from grape marc: A comparison and a proposal. In *Journal of Supercritical Fluids* (Vol. 87, pp. 1–8). https://doi.org/10.1016/j.supflu.2013.12.019

Deep-Purple project. *Https://deep-purple.eu/*.

Fasaei, F., Bitter, J. H., Slegers, P. M., & van Boxtel, A. J. B. (2018). Techno-economic evaluation of microalgae harvesting and dewatering systems. *Algal Research*, *31*(June 2017), 347–362. https://doi.org/10.1016/j.algal.2017.11.038

Goto, M., Kanda, H., Wahyudiono, & Machmudah, S. (2015). Extraction of carotenoids and lipids from algae by supercritical CO2 and subcritical dimethyl ether. In *Journal of Supercritical Fluids* (Vol. 96, pp. 245–251). https://doi.org/10.1016/j.supflu.2014.10.003

Hallenbeck, P. C. (2014). Bioenergy from Microorganisms: An Overview. In D. Zannoni & R. De Philippis (Eds.), *Microbial BioEnergy: Hydrogen Production* (pp. 3–21). Springer Netherlands. https://doi.org/10.1007/978-94-017-8554-9_1

Honda, R., Fukushi, K., & Yamamoto, K. (2006). Optimization of wastewater feeding for single-cell protein production in an anaerobic wastewater treatment process utilizing purple non-sulfur bacteria in mixed culture condition. *Journal of Biotechnology*, *125*, 565–573. https://doi.org/10.1016/j.jbiotec.2006.03.022

Hülsen, T., Batstone, D. J., & Keller, J. (2014). Phototrophic bacteria for nutrient recovery from domestic wastewater. *Water Research*, *50*, 18–26. https://doi.org/10.1016/j.watres.2013.10.051

Johnson, K., Jiang, Y., Kleerebezem, R., Muyzer, G., & Van Loosdrecht, M. C. M. (2009). Enrichment of a mixed bacterial culture with a high polyhydroxyalkanoate storage capacity. *Biomacromolecules*, *10*(4), 670–676. https://doi.org/10.1021/bm8013796

Kuo, F. S., Chien, Y. H., & Chen, C. J. (2012). Effects of light sources on growth and carotenoid content of photosynthetic bacteria Rhodopseudomonas palustris. *Bioresource Technology*, *113*, 315–318. https://doi.org/10.1016/j.biortech.2012.01.087

Luongo, V., Ghimire, A., Frunzo, L., Fabbricino, M., d'Antonio, G., Pirozzi, F., & Esposito, G. (2017). Photofermentative production of hydrogen and poly-B-hydroxybutyrate from dark fermentation products. *Bioresource Technology*, *228*, 171–175. https://doi.org/10.1016/j.biortech.2016.12.079

Madigan, M. T., Bender, K., Buckley, D., Sattley, M., & Stahl, D. (2015). Brock Biology of Microorganisms. In *Pearson* (Fourtheen, Vol. 1). Pearson. https://doi.org/10.1017/cbo9780511549984.016

Montiel-Corona, V., & Buitrón, G. (2021). Polyhydroxyalkanoates from organic waste streams using purple non-sulfur bacteria. In *Bioresource Technology* (Vol. 323, p. 124610). Elsevier Ltd. https://doi.org/10.1016/j.biortech.2020.124610

Nasseri, A. T., Rasoul-Ami, S., Morowvat, M. H., & Ghasemi, Y. (2011). Single Cell Protein: Production and Process. *American Journal of Food Technology*, *6*(2), 103–116. https://doi.org/10.3923/ajft.2011.103.116

Nigam, P. S., & Luke, J. S. (2016). Food additives: Production of microbial pigments and their antioxidant properties. In *Current Opinion in Food Science*. https://doi.org/10.1016/j.cofs.2016.02.004

Puyol, D., Batstone, D. J., Hülsen, T., Astals, S., Peces, M., & Krömer, J. O. (2017). Resource recovery from wastewater by biological technologies: Opportunities, challenges, and prospects. *Frontiers in Microbiology*, *7*(JAN), 1–23. https://doi.org/10.3389/fmicb.2016.02106

Rao, A. V., & Rao, L. G. (2007). Carotenoids and human health. *Pharmacological Research*, *55*(3), 207–216. https://doi.org/10.1016/j.phrs.2007.01.012

Richmond, A. (2003). Handbook of Microalgal Culture. In A. Richmond (Ed.), *Handbook of Microalgal Culture*. Blackwell Publishing Ltd. https://doi.org/10.1002/9780470995280

Rodriguez-Perez, S., Serrano, A., Pantión, A. A., & Alonso-Fariñas, B. (2018). Challenges of scaling-up PHA production from waste streams. A review. In *Journal of Environmental Management* (Vol. 205, pp. 215–230). https://doi.org/10.1016/j.jenvman.2017.09.083

Saini, R. K., & Keum, Y. S. (2019). Microbial platforms to produce commercially vital carotenoids at industrial scale: an updated review of critical issues. *Journal of Industrial Microbiology and Biotechnology*, *46*(5), 657–674. https://doi.org/10.1007/s10295-018-2104-7

SEMiLLA.*https://www.uantwerpen.be/en/research-groups/sustainable-energy/news-and-events/purperbacterie/*.

Shi, J., Mittal, G., Kim, E., & Xue, S. J. (2007). Solubility of carotenoids in supercritical CO2. In *Food Reviews International* (Vol. 23, Issue 4, pp. 341–371). https://doi.org/10.1080/87559120701593806

Sipka, G., & Maróti, P. (2018). Photoprotection in intact cells of photosynthetic bacteria: quenching of bacteriochlorophyll fluorescence by carotenoid triplets. *Photosynthesis Research*, *136*(1), 17–30. https://doi.org/10.1007/s11120-017-0434-3

The European Parliament and the Council. (2018). REACH Regulation. *Sustainaspeak*, 219–219. https://doi.org/10.4324/9781315270326-156

Thimijan, R., & Heins, R. (1983). Photometric, radiometric, and quantum light units of measure: a review of procedures for interconversion. *HortScience*, *18*(6), 818–822.

Vermeer, C. M., Rossi, E., Tamis, J., Jonkers, H. M., & Kleerebezem, R. (2021). From waste to self-healing concrete: A proof-of-concept of a new application for polyhydroxyalkanoate. *Resources, Conservation and Recycling*, *164*. https://doi.org/10.1016/j.resconrec.2020.105206

Wu, T. Y., Hay, J. X. W., Kong, L. B., Juan, J. C., & Jahim, J. M. (2012). Recent advances in reuse of waste material as substrate to produce biohydrogen by purple non-sulfur (PNS) bacteria. In *Renewable and Sustainable Energy Reviews*. https://doi.org/10.1016/j.rser.2012.02.002

Zhou, Q., Zhang, P., Zhang, G., & Peng, M. (2015). Biomass and pigments production in photosynthetic bacteria wastewater treatment: Effects of photoperiod. *Bioresource Technology*, *190*, 196–200. https://doi.org/10.1016/j.biortech.2015.04.092

Acknowledgments

It is a common metaphor to describe a Ph.D. as a rollercoaster.
Looking back, I would rather describe it as a journey through a jungle: challenging, and impossible to undertake alone.
For this reason, I would like to warmly thank all the people that accompanied me during these four years of scientific and personal growth.

My first and biggest 'thank you' goes to my promotors, David and Mark, for giving me the opportunity to work in your group.
David, thank you for believing in me when I was nothing but a scared shy student. For all you thaught me. For your guidance, but most of all, thank you for all the freedom you gave me to develop my project.
Mark, thank you for all the scientific discussions we had. I learnt a lot from you, and there is nothing more important in life than keep learning. Aside from science, thank you for opening my eyes on the importance of being curious and passionate while doing research. I took it for granted, but it is not.

Secondly, thanks to all the students that worked with me in this project. To the students that I had the pleasure to directly supervise, **Heleen**, **Jeong Hoon**, **Guillaume**, **Mythili**, **Viktor**, **Daniela**, **Casper**, and to the students I have interacted with, **Berber**, **Charlotte**, **Reetu**, **Luuk, Wesley**. You challenged me to do the best I could to be a good mentor. You thaught me a lot, and this thesis would have been very different without your help. Thank you.

Thank you to all the incredible scientists that I had the pleasure to interact with and learn from during these years: **Abbas**, **Bing**, **Cristian**, **Daniel**, **Dimitry**, **Gijs**, **Meng**, **Martin**, **Merle**, **Pascale**, **Robbert**, **Siegfried**, **Sirous**, **Yuemei**. Your expertise and your advice have been precious.

Thanks to the whole EBT team.
In particular, to our technicians' team: **Rob**, **Dirk** and **Marcel** for the incredibly useful assistance in reactor setup, and for your endless patience when I was asking for the impossible. **Apilena**, **Astrid**, **Ben**, **Cor**, **Jannie**, **Marcel**, **Max**, **Miranda**, **Patricia**, **Zita**: thank you so much for the technical support.

To all the EBT fellows, **Aina**, **Ali**, **Ana-Maria**, **Chris**, **Dana**, **Danny**, **Diana**, **Felipe**, **Francesc**, **Gerben** (and thanks a lot for all your help!), **Hugo**, **Jure**, **Laura**, **Lemin**, **Leonor**, **Marissa**, **Maxim**, **Monica**, **Morez**, **Nina**, **Rodoula**, **Sam**, **Simon**, **Stefan**, **Timmy**, **Viktor**, **Vojtech**, for making EBT an eclectic, dynamic, and fun place to work in. It has been great sharing the labs with you.

To the BT-PhD committee members: **Albert**, **Anna**, **Britte**, **Chema**, **Florence**, **Stefan**: what a team we were! It has been incredibly fun organizing with you serious and less serious events.

My office mates. **Michele** and **Jules**: from the moment I arrived, you guys took me under your wings, and you have been my mentors ever since. Thank you for all the discussions we had, you have been an inspiration for me. **Andres**, **Rhodi**, **Maria-Paula**, **Ruben**, **Ahmed**, thanks for making our office a fun place to be.

Being an expat made me realize the importance of having a solid network of friends you can count on at any time. The memories we created together will forever remain with me. I am not good with words, and I know that this short paragraph is not enough to express all the affection, gratitude and love I have for you. You are a piece of my hearth.

A special acknowledgment to my paranymphs, David and Alexandra.
David, you have been a happiness pillar for me during these years, and I can't imagine going through the PhD without you. You have been the most amazing friend, housemate, and colleague. We shared the best and the worst moment, and I couldn't be more grateful for all the time together. Gracias, primo.
Alexandra, from the first time we talked, I've always found funny to see how different yet similar we are. I am just lucky to have met you, because I found a wonderful human, a great friend, and an incredible force of nature. You rock girl.

To my Delft family, because with you I always felt at home. **Daniel**, **Fabio**, **Florence**, **Georg**, **Ingrid**, **Maria-Paula**, **Mariana**, **Marina**, **Michele**, **Sergio**: I couldn't be more grateful for meeting you. We have been 'partners in crime', and I cherish every moment together. Words can't properly describe how much I love you all, so I will just say 'thank you people, lots of love'.

Mamma e **Papà**, grazie per avermi sempre supportata, a distanza, in qualsiasi parte del mondo io fossi e qualsiasi cosa decidessi di fare. Spero di avervi resi fieri di me, e spero di continuare a farlo sempre.

Andrea, you have always been by my side, even while houndreds of km apart. You supported me during the darkest moments, and you were there in the happiest times. You challenged me. You made me grow. I am extremely grateful for having you in my life. Grazie Amore, ti amo.

Biography

Marta Cerruti was born in Venice, Italy, on June 19th 1992.

In 2013 she completed her Bachelor's degree in Biotechnology from University of Torino, Italy.
Passionate about environmental preservation, she started her MSc degree program in Plant Biotechnology, from University of Turin, Italy.

During her studies, she discovered a particular curiosity for microbial processes, that she explored first during an internship in plant-microbe interactions at INRA Institute, France, and then during her MSc end-project on a model organism found in wastewater treatment plants, at EPFL, Switzerland.

In 2017 she started her PhD program at TU Delft, the Netherlands, on purple bacteria for wastewater treatment, combining her interest in phototrophic systems, microbial communities and environmental preservation.
The four years of work are summarized in this book.

After the PhD, she started working at ETH Zurich, Switzerland, as a post-doctoral researcher on gut microbial ecology.

List of publications

2021 **Synthrophy between fermentative and purple phototrophic bacteria for carbohydrate-based wastewater treatment**; bioRxiv
https://doi.org/10.1101/2021.05.13.444055
M.Cerruti, G. Crosset-Perrotin, M. Ananth, J. Rombouts, D. Weissbrodt

Plant-Wide Systems Microbiology for the Wastewater Industry;
Environmental Science: Water Research & Technology
https://doi.org/10.1039/D1EW00231G
M. Cerruti, B. Guo, R. Delatolla, N. de Jonge, A. Hommes - de Vos van Steenwijk, P. Kadota, C. Lawson, T. Mao, M. Oosterkamp, F. Sabba, M. Stokholm-Bjerregaard, I. Watson, D. Frigon, D. Weissbrodt

Control tools to selectively produce purple bacteria for microbial protein in raceway reactors; Environmental Science and Technology
https://doi.org/10.1021/acs.est.0c08204
A. Alloul, M.Cerruti, D. Adamczyk, D. Weissbrodt, S. Vlaeminck

2020 **Enrichment and Aggregation of Purple Non-sulfur Bacteria in a Mixed-Culture Sequencing-Batch Photobioreactor for Biological Nutrient Removal From Wastewater**; Frontiers in Bioengineering and Biotechnology
https://doi.org/10.3389/fbioe.2020.557234
M. Cerruti, B. Stevens, S. Ebrahimi, A. Alloul, S.E. Vlaeminck, D. Weissbrodt

Effects of light/dark diel cycles on the photoorganoheterotrophic metabolism of *Rhodopseudomonas palustris* for differential electron allocation to PHAs and H_2;
bioRxiv https://doi.org/10.1101/2020.08.19.258533
M. Cerruti, H. Ouboter, V. Chasna, M. van Loosdrecht, C. Picioreanu, D.Weissbrodt

2019 **Drivers of Bioaggregation from flocs to biofilms and granular sludge**;
Environmental Science: Water Research & Technology
https://doi.org/10.1039/C9EW00450E
H.Aqeel, D.Weissbrodt, M. Cerruti, G. Wolfaardt, B.M. Wilén, S.N. Liss

Conference contributions

2020: **IWA Biofilms,** Indiana, USA (online conference) – oral presentation
Tracking metabolic versatility in biofilms: modelling photoorganoheterotrophic and photolithoauttrophic niches of a single purple phototrophic bacterium

2019 **KNWM Microbial Ecology Fall Meeting,** Wageningen, the Netherlands – oral presentation
Purple non-sulfur phototrophic bacteria: role of reactor regime and light intensities in the association with fermenters for sugar-based wastewater treatment

IWA MEWE Hiroshima, Japan – poster presentation
Substrate and light impacts on novel anaerobic associations of fermenters and purple non-sulfur bacteria for waste-based carbohydrate valorization

IWAlgae Valladolid, Spain – oral presentation
Purple non-sulfur bacteria: can we drive association with fermenters to treat sugar-based aqueous waste?

IWA Anaerobic digestion, Delft, the Netherlands – poster presentation
How does light intensity effect the physiology of purple bacteria and nutrient removal prom wastewater under anaerobic sequencing batch reactor regime?

Swiss Microbial Ecology Meeting, Lausanne, Switzerland – oral presentation
Effects of light / dark diel cycles on the versatile metabolism of purple non-sulfur phototrophic bacteria and their translation for water resource recovery

2018 **IWA EcoSTP,** London, Canada – oral presentations
Sequencing batch enrichment and metabolic drivers for water resource recovery using purple non-sulfur bacteria'

Introduction to ecogenomics and ecophysiology data and their integration with engineering

2017 **Swiss Society for Microbiology annual joint meeting,** Basel, Switzerland – poster presentation
Tetrasphaera japonica, a model to study the metabolism of polyphosphate-accumulating organisms in real wastewater treatment plants?